# Preliminary Cruise Report, TicoFlux II Expedition

# R/V *Melville,* VANC02, 7 September – 9 October 2002

# The thermal state of 20-25 Ma lithosphere subducting at the Costa Rica Margin: implications for hydrogeology, fluxes, and the seismogenic zone

Scientific Participants: A. Fisher[1], E. Silver[1], G. Wheat[2], R. Harris[3], C. Stein[4], M. Underwood[5], M. Bautier[6], P. Costa[1], G. Spinelli[7], C. Moser[8], M. Hutnak[1], P. Friedmann[1], D. Hasterok[3], C. Ellsworth[9], B. MacKnight[1], B. Hernandez[1], M. Jones[10], W. Parsons[2]

[1] University of California, Santa Cruz
[2] University of Alaska Fairbanks
[3] University of Utah
[4] University of Illinois at Chicago
[5] University of Missouri
[6] Universite de Franche Comt
[7] University of Michigan
[8] Oregon State University
[9] University of Victoria
[10] University of Minnesota, Duluth

Supported by NSF grants OCE-0001892 (Fisher and Silver), OCE-0001944 (Harris), OCE-0001941 (Stein), and OCE-0002031 (Wheat).

## I. Introduction

This report provides an operational and scientific overview of the TicoFlux II expedition (R/V *Melville* cruise VANC02) to the incoming plate along the Costa Rica margin, eastern equatorial Pacific Ocean. This report was prepared during and at the end of scientific operations, so all analyses are preliminary. Greater detail regarding background, motivation and strategy is presented in the NSF proposal that funded this work, along with references to previous work in this area. Results from TicoFlux I are summarized below. The TicoFlux II expedition was highly successful both operationally and scientifically. We had some initial difficulties with equipment, but these were mostly resolved and we achieved our primary objectives.

### A. Scientific Objectives

The TicoFlux II expedition was the second cruise of a field, lab, and modeling program to investigate the nature of hydrothermal activity and its influence on lithospheric and subduction processes offshore of the Nicoya Peninsula, Costa Rica margin. We focused observational efforts on a 120 nmi x 120 nmi (2° x 2°) region largely seaward of the trench (Figures I-1 and I-2) because this area contains fundamental transitions in the structural, thermal, and hydrogeologic state of the incoming plate. Part of the plate in this region formed at the East Pacific Rise and has unusually low heat flow, but the adjacent crust formed at the Cocos-Nazca Spreading Center has heat flow consistent with conductive models of lithospheric cooling. Field components of our experiment include seismic, swath-mapping, heat flow, coring, and geochemistry programs on 18-24 Ma lithosphere seaward of the Middle America Trench. This work will be followed up with additional laboratory analyses and modeling. Collectively, these efforts are intended to address the following questions:

(1) What is the thermal state of the lithosphere being subducted below the Nicoya Peninsula?

(2) What are characteristic heat and fluid fluxes responsible for this thermal state, how does water enter and exit the crust in this area, and what are the characteristic length scales of flow?

(3) How do the thermal state, water content, sediment composition, and diagenetic state of the incoming plate influence the mechanics of the subduction zone?

(4) What are the chemical implications of extensive fluid circulation within the incoming plate, both to the subduction zone and to the overlying ocean, and how can these data be used to understand global fluxes?

B. Regional Setting

The Cocos plate has a complex tectonic history in our work area, comprising seafloor generated at the East Pacific Rise (EPR) at a fast spreading rate, and at the Cocos-Nazca Spreading Center (CNS) at an intermediate spreading rate (Figs. I-1 and I-2). The plate is being subducted into the Mid American Trench along the eastern side of our study region. The area of EPR-generated seafloor offshore of the northern Nicoya Peninsula has magnetic anomalies that strike approximately N40W, subparallel to the trench. Towards the middle of the Nicoya Peninsula there is a boundary across which the magnetic anomalies abruptly switch orientation by ~90°, to N45E. This boundary is thought to separate crust formed at the EPR from that formed at the CNS, making it the trace of the triple junction or fracture zone, and also corresponds (at least, in part) to an abrupt difference in the relief of upper basement, known regionally as the "rough-smooth boundary" (RSB). Continuing to the southeast, there is another, more subtle, realignment of magnetic anomalies, which corresponds near the trench to the Fisher Ridge. The crust between the RSB and Fisher Ridge is sometimes referred to as the "smooth segment," while crust south of the Fisher Ridge is referred to as the "seamount segment". As suggested by these names, seamounts are more common southeast of Fisher Ridge than northwest of the ridge. The passage of the Galapagos hot spot under CNS-generated lithosphere has contributed to its rough basement relief and the formation of the Cocos and Carnegie ridges to the south of the TicoFlux study area.

Heat flow data within and near the study area collected prior to TicoFlux I are sparse (typical spacing of 60-120 km), but there is a pattern to the distribution of these early values. North of the RSB, heat flow is generally low (average = 31 $mW/m^2$ ), whereas heat flow to the south of the RSB is generally higher (average = 110 $mW/m^2$ ). The age contrast across the RSB is too small to account for the observed transition in seafloor heat flow. The global average of measured heat flow for this crustal age (20-25 Ma) is about 72 $mW/m^2$, corresponding to a heat flow fraction ($q_{observed}$ /$q_{expected}$ ) of 0.67. This fraction indicates that, on average on a global basis, 1/3 of heat flow through oceanic lithosphere of this age is lost by advection. The heat flow fraction north of the RSB is generally <0.25, suggesting an even larger fraction of advective heat

loss, but the heat flow fraction south of the RSB is generally >1.0. Hence, heat flow north of the RSB is low compared to both lithospheric-conductive and global average values, whereas that south of the RSB is high compared to global average values. The latter situation is particularly unusual because most young-crust sites have heat flow significantly lower than that predicted by conductive lithosphere models, presumably because advected heat loss is not measured by heat flow probes.

C. Results from TicoFlux I

The TicoFlux I expedition April-May 2001 on the R/V *Maurice Ewing* (cruise EW0104) included regional and local goals. We mapped out regional crustal structures and define the various tectonic boundaries across the work area using a combination of seismic, thermal, coring, and geochemical tools. We examined the various tectonic boundaries (ridge jump, propagator trace, triple-junction trace, fracture zone, faults) to determine which were associated with thermal, chemical, seismic and hydrogeologic boundaries. We also wanted to establish the nature of thermal and chemical variations around basement outcrops, and evaluate directions and intensity of fluid flow within basement using thermal and chemical tracers. The last issue was the primary focus of the TicoFlux II cruise during September-October 2002.

1. Seismic reflection

Prior to TicoFlux I, little information was available on the basement relief and sediment thickness in our study region (except for immediately adjacent to the trench). Older single channel data was available mainly in analog form and was of very poor quality. Interpretation of local tectonics, heat flow, and fluid flow required acquisition of a modern seismic reflection data set. We knew prior to TicoFlux I that exchange between crustal fluids with the overlying ocean was most likely to occur either where basement outcrops at the sea floor or where the sediment cover is thin. Seismic data are essential for mapping out basement and sediment geometries. We collected 1800 km of seismic data from a 10-gun array and a 6-km long hydrophone streamer array with 480 channels. Hydrosweep bathymetric data were collected during the multichannel seismic work and often as we transited between heat flow and/or coring sites. A low-angle reflection, possibly a crustal-penetrating fault, ~30 km from the trench axis and a number of seamounts, outcrops, and buried basement highs were found, significantly increasing the number of potential targets for coring and heat flow work. The seismic data indicate that there is regional sediment coverage on the order of 300-400 m thick above a highly reflective basement. Drilling

results from ODP Site 1039 documented that the upper 150 m of sediments are composed of hemipelagic mudstone and the lower section is largely pelagic nannofossil ooze. Seismic lines revealed the influence of magnetic and tectonic activity within the survey area, including high-angle faults that penetrate basement rocks and sediments, common sills defining the top of acoustic basement, and local basement highs, some of which penetrate seafloor sediments. Many basement ridges and seamounts show evidence for post depositional or syndepositional deformation. In some cases the lowermost 0.15 s of strata appear to be deformed after they were deposited. The well-layered middle part (pelagic ooze) appears to be deformed during deposition, and the upper hemipelagic layer generally covers the deformation. However, there are many examples of deformation extending through to the surface and clearly affecting the hemipelagic sediments. Away from local basement highs and faults, basement is remarkably flat.

2. Heat flow

We collected 127 measurements with a 3.5 m, 11-thermistor, violin-bow heat flow system leased from Earl Davis and colleagues at the Pacific Geosciences Center. These data were collected during 13 transects ("stations") with measurements generally spaced 1 nm (~1.8 km) apart. In addition, fourteen measurements were made with outrigger probes attached to the sediment core barrels. These tools were developed collabotratively by Antares (Berlin, Germany) and Heiner Villinger and colleagues from the University of Bremen.

Heat flow data collected during TicoFlux I helped to define an extreme contrast in thermal conditions on the Cocos Plate seaward of the Middle America trench. Heat flow values measured on seafloor created at the EPR were anomalously low (generally only 20-40 $mW/m^2$, about 20-40% of that predicted by conductive cooling models). In contrast, heat flow values measured on seafloor generated at the CNS was about equal to that predicted by conductive models. We crossed the thermal transition from low heat flow to high heat flow in four places, on HF-01, HF-08, HF-10, and HF-12. In all cases, the transition from cool to warm conditions occurs across a distance of 5 km, often with most of change between adjacent measurements <2 km apart. The width of the thermal transition should scale with the depth to the "source" of the transition; a shallow, hydrothermal cause should cause a narrow transition, whereas a deeper origin due to lithospheric thermal differences should give rise to broader transition. The remarkably abrupt transitions between thermal regimes is consistent with models of shallow hydrothermal circulation in EPR-generated basement.

Surprisingly only one on the four transitions (HF-08, nearest to the trench) coincided with a tectonic boundary, in this case the triple junction/fracture zone trace between EPR-generated and CNS-generated seafloor. The transitions along HF-10, HF-12, and HF-01 are offset to the northwest of the crustal change by about 40, 30, and 30 km, respectively and are much closer to basement outcrops than to tectonic boundaries. These basement outcrops, common on EPR-generated seafloor by conspicuously absent on CNS-generated seafloor immediately south of the triple junction/fracture zone trace, appear to allow water to bypass regionally thick sediments and move rapidly between the crust and ocean.

3. Pore Water Chemistry and Sedimentology:

Forty-four sediment cores were taken from 10 different regions in the TicoFlux study area during the first cruise. There were primary sediment lithologies identified in these cores: hemipelagic mud, nannofossil chalk, mixed sediment, variegated clay, and volcanic ash. By extracting pore waters from the sediments for geochemical analyses, our goals were to understand both fluid flow in the TicoFlux area and the significance of ridge-flank hydrothermal circulation on the global solute fluxes. Most core sites were situated on basement highs with relatively thin (< about 75 m) sediment to increase the chance of detecting water flow. Geochemical measurements at sea included pH, alkalinity, chlorinity, fluoride, calcium, magnesium, and phosphate. The geochemisty of the pore waters indicated fluid seepage in three areas, with rates up to 1 cm/yr, including a small basement high within the EPR crust (GC09), a shallow dipping reflector near the trench (GC18,19,38, 39) within EPR crust, and a local basement high on the propagator trace within CNS crust (GC23). The site over the basement fault had heat flow over 600 $mW/m^2$ and an unusually high calcium concentration indicating a deep source for the fluids. Work during the TicoFlux II expedition was intended to sample these and other sites of fluid seepage, and to determine the chemistry of fluids within the basement reservoir(s) below seepage sites.

## II. TicoFlux II Operational Summary

Operations during TicoFlux II are listed in Table II-1. The ship reached the dock in Puerto Caldera prior to TicoFlux II on schedule, but could remain at the dock only for one day before moving to anchorage. This complicated cruise preparations somewhat, but fortunately all equipment and most supplies had been preloaded in San Diego before the prior cruise. Port call was busy with considerable time spent preparing the seismic, coring, heat flow, and survey gear.

We left port as scheduled at 1600 on 9/7/02. We completed a 14 hour transit to the southern edge of our work area and put equipment into the water to run a test of the seismic gear. No useful data was collected during this initial test, but it provided an opportunity to get the guns and data acquisition system working properly, and the test was considered to be a success. The seismic system generally worked throughout the cruise, although there was noise in one of the streamer channels, we sometimes could not always keep the guns synchronized, and we had difficulty at first maintaining sufficient power in the batteries used to power the system. This last problem was solved when a larger-capacity was delivered to the ship.

We transited to the first coring station, a basement high (La Misma) located on the slope of the trench, and three cores were collected. Coring operations (gravity and piston) were run from the starboard rail using the trawl wire and winch. A 12-kHz pinger was attached to the wire for all gravity coring operations and was used for determining corer locations relative to the bottom. Coring stations typically lasted 9-14 hours, the time required to collect 3-4 gravity cores, or a combination of gravity and piston cores. Some coring time was also used to complete two hydrocasts to collect bottom water samples later during the cruise. The tension meter for the trawl wire required repair early in the cruise, but once this was completed, we proceeded to the first heat flow station, located above the trace of a low-angle basement reflector apparent on a multichannel seismic line collected during TicoFlux I.

Multipenetration heat flow data were collected with the PGC probe using the stern A-frame. Multipenetration heat flow stations during TicoFlux II were generally 12 or 24-32 hours in length. Outrigger probes were also attached to most core barrels, allowing assessment of thermal gradients at the same time as cores were collected. Longer heat flow stations were "sandwiched" between shorter coring stations, allowing the coring crew to remain on a (nominally) regular shift schedule, and shorter heat flow stations (used mainly later in the cruise) alternated with coring stations of approximately equal length. We used six seismic surveys to break up the schedule to allow a rough balance between time dedicated to heat flow and coring operations, and to help keep the scientific crews on regular shifts. By the end of the cruise, seismic, heat flow and coring time consumed 18%, 35%, and 31% of the available time, respectively, with remaining time dedicated to transits and equipment repair. Operations switched between seismic, heat flow, and coring throughout TicoFlux II, and we returned to port after 31 days of scientific operations, arriving at 0700 on 10/9/02.

III. Seismic Reflection Surveys

We acquired 1200 km of seismic reflection data (Table III-1) during TicoFlux II. The source was two GI (generator injector) guns. On lines 1-13 we used 105/105 inch$^3$ chambers, and for all other lines 45/105 inch$^3$ chambers. The receiver cable consisted of four 50 m active sections of 50 phones each. Shooting speed was 11 km/hour (approximately 3 m/s) and the shot interval was 10.8 seconds or approximately 33.3 m, giving a nominal 3 fold stacking geometry. The primary purpose for collecting the seismic data was to provide an accurate indication of sediment thickness and basement relief for heat flow and coring programs. In addition, the GI-gun source provided high resolution images of the sedimentary section, allowing us to refine estimates of timing of tectonic and volcanic events within the Cocos plate, and to image mass wasting phenomena on seamounts.

The seismic data were recorded with an OYO DAS acquisition system onto Exabyte tapes. Data processing included quality control and editing, brute stack, deconvolution, and water bottom mute and f-k migration, using the SIOSEIS processing system written and maintained by Paul Henkart at Scripps Institution of Oceanography. Data are archived on DAT tapes and CD-ROMs. The locations of individual surveys are shown in Figs. III-2 to 7, and selected data are shown (with collocated heat flow values) in Figs. III-8 to 24.

The seismic lines provided useful images over a major fracture zone, the propagator trace, several seamounts, and numerous seaknolls. A few of the seamounts and most of the knolls were not known prior to this work. TicoFlux II Lines1, 5a, and 19 cross the fracture zone, which is on strike of the triple junction trace of Barckhausen et al. (2001). The fracture zone has a very steep south face, and a gentle north slope. Sediments onlapping the latter show two periods of debris apron formation, and a period of uplift during the middle part of the stratigraphic sequence. Lines 16, 17 and 18 cross the propagator trace and illustrate its complexity. Seamounts are crossed by Lines 26 and 23b, 27 and 38a. Tilting, unconformities, and onlap relationships of sediments adjacent to the seamounts give a history of activity. However, the seamounts all appear to have been formed early in the history of the plate. Knolls are crossed in Lines 6 and 8a, 21, 22, 24, 28, 29, 31, 32, 33, 35, 36, 37, and 38a. Some of the latter crop out at the sea floor whereas others are covered with sediment. While bathymetrically minor, these knolls play significant roles in modulating heat and fluid flow throughout the region.

One seamount, crossed by Line38a, has suffered a major collapse event. Layered strata on both the seamount and the collapsed fragment illustrate the slide occurred through rotational

slumping. The slump block is 2 km long, 3 km wide and at least 300 m thick. It has a heave of several hundred m and a throw of 300 m. In sufficiently shallow water depths such a slump could generate a major local tsunami, if the collapse were to happen all at once. The timing of the slump is unknown, except that it is likely to have happened in the past 3 Ma.

## IV. Heat Flow Surveys

The TicoFlux II seafloor heat flow program comprised two main components. Most measurements were made a 3.5-m, 11-thermistor, violin-bow heat flow system built and maintained at the Pacific Geoscience Center by Earl Davis and colleagues. This system provided real-time (analog) telemetry from four thermistors and in-situ thermal conductivity measurements. Internal power allowed stations to run 30+ hours when fully charged, and most stations consisted of 10-20 measurements separated by 100-1000 m (Fig. IV-1). The second part of the seafloor heat flow program was based measurements made with autonomous outrigger temperature probes banded to piston and gravity core barrels. The tools were modified versions of instruments run during TicoFlux I, built by Antares (Berlin, Germany) in collaboration with Heiner Villinger and colleagues (University of Bremen). Both kinds of probes featured a small, cylindrical pressure case (18.5 cm long, 1.5 cm diameter) powered by a single, 3.0 V lithium battery. Serial communication is accomplished through the pressure case, allowing the electronics to remain sealed within the pressure case through most of the expedition. We also deployed wireline MAPRs during TicoFlux II, tools leased from the NOAA/PMEL lab (developed and maintained by Ed Baker and Sharon Walker). These instruments comprise a data logger, rapid-response thermistor probe, pressure (depth) sensor, and nephelometer and are intended to allow rough assessment as to the presence and magnitude of hydrothermal plumes during coring, dredging, or other wireline operations. We generally ran a single MAPR tool, clamped to the wire 30-80 m above the gravity core weight, during stations in which there was a nearby basement outcrop.

### A. Multipenetration Heat Flow Stations

A summary of heat flow station targets, dates, and penetrations is presented in Table IV-1. Preliminary results of multipenetration heat flow measurements are listed in Table IV-2. Station locations are based on P-CODE GPS positions when the probe first penetrated, with corrections for the distance between the GPS antenna and the stern A-frame and ship heading.

There are errors associated with uncertainties in the location of the probe relative to the ship, but we generally waited for the wire angle to straighten and the 12-kHz pinger in the wire to indicate that the probe had swung to vertical before putting the probe in the seafloor.

Heat flow measurements were made by lowering the heat flow probe into the seafloor at 40-60 m/min (depending on winch capabilities, which varied throughout the cruise). The probe was left in place for 7 minutes to allow partial equilibration after penetration, and then a calibrated heat pulse was fired to determine thermal conductivity, and another 7 minutes of data were collected (see examples, Fig. IV-2). After a measurement was completed, the probe was raised to 50-200 m above the seafloor while the ship transited at 1-2 kts to the next site. Analog telemetry of tilt and four thermistor channels allowed real-time assessment of probe functioning and crude estimation of thermal gradients. Complete digital data records were downloaded from the probe following recovery.

Multipenetration heat flow data were parsed into individual penetration files and processed using SlugHeat, a Matlab program based largely on the hfred/hflow set of processing programs (processing example: Fig. IV-3). Additional analysis will be required to finalize the heat flow values listed in this report (Table IV-2), but values are unlikely to change by more than a few percent as a result of reanalysis. No corrections have been applied for at this stage for instrument tilt (generally less than 5°), sedimentation, or local topography.

B. Outrigger Temperature Loggers on Cores

We used outrigger probes with two different external and mount designs. One probe design included a "short" sensor tip extending 2 cm from the end of the pressure case (slightly shorter than the 2.5-cm tip of the original design), containing a 10-kOhm (nominal at 25 °C), high-precision thermistor. The second probe design had identical pressure case and electronic components, but a 35-cm-long probe tip, with the thermistor positioned 10 cm from the end of the tip.

Two kinds of probe mounts were designed and constructed at UCSC. The shorter probes were deployed in cylindrical cases welded to the ends of metal fins held 12 cm from the outside of the core barrel. The design of these assemblies was based on the University of Bremen design used during TicoFlux I, except that the new metals fins were somewhat thicker, and the mounts were held onto the core barrels with four stainless steel bands (rather than two). Unfortunately, the probe mounts were constructed with a diameter somewhat larger than the OD of the core

barrels, but rubber gasket material between the mounts and core barrels filled the gap in diameter and increased friction between the mounts and core barrels, helping them to remain fixed during deployment.

The second mount design was based on outriggers used during the early days of oceanic heat flow studies, with the probe tips run up and over the top of a grooved fin. The fins were constructed of Delrin and attached to core barrel mounts with metal screws, and banded to the core barrels. A gap in the fin corresponded to the location of the thermistor sensor. A clam-shell pressure case holder supported the electronics immediately above the core barrel mount. Each of these designs had advantages and disadvantages, and it was beneficial to run combinations of these instruments in several cases, as described later. On most deployments, separate bottom water and tilt sensors were run in the top of the core weight.

Outrigger temperature probes were attached to 57 gravity and piston cores, yielding useful estimates of in-situ temperatures on 42 deployments. The outrigger tool data comprised the equivalent of two-three multipenetration stations, including some of the highest heat flow values measured during TicoFlux II, and also helped to determine where to place (or not place) subsequent multipenetrations stations. Operator error accounted for a lack of data recovered during one deployment, and failure of the core barrel to penetrate or tipping of the core barrel led to the other deployments from which no useful data were derived. Prior to the cruise, we were sent small resistors that we were instructed to solder to the circuit boards of the tools, to prevent static discharge during use, but attachment of these resistors led to communication difficulties with several tools. Subsequent removal of these resistors allowed the tools to be run. Examples of outrigger probe data are shown in Figure IV-4, and preliminary results are listed in Table IV-3.

The short probes proved themselves to be particularly robust, as they tended to bang against the side of the ship during corer recovery but were unharmed by this. The greatest difficulty we had with the small tools was bending of the probe tips, which extended up to 12 mm in front of the mount housings, during penetration of lithified sediments. We ran some of these tools with a shorter tip extension, through use of spacers in the mounts, but shorter extension led to less ideal sensor response following penetration. In contrast, the long probes provided data that looked much more like multipenetration data from the PGC tool, with a smaller frictional disturbance due to the smaller upset on the long outrigger fin relative to that used with the short tools. But the Delrin fins used with the longer tools are more fragile, as are

the longer probe tips, and the clam shell that holds the electronics on the long tools can get caught by the wire run down the core barrel to assist with corer recovery. In addition, the longer tools occupied a substantially larger footprint on the core barrels. In fact, when running a single-pipe gravity core, it was not possible to put more than two long probes and one short probe on the barrel, and still leave sufficient clearance below the cradle that holds the coring weight.

C. Heat flow results

Heat flow work was focused mainly around outcrops, where hydrothermal fluids were thought to be entering or leaving basement, and over buried basement highs. Some additional stations were intended to resolve thermal transitions well away from basement outcrops. In this brief, preliminary summary, we group stations by target type and area. Station and penetration locations are shown in Figures IV-5 to IV-16, and collocated heat flow and seismic data are shown in Figures III-8 to III-24.

Heat flow stations HF01 and HF02 were located across and near the area of high heat flow just seaward of the trench, in the northern end of our field area (Figs. IV-5 and IV-6). These stations were intended to help define the extent of the high heat flow region. HF01 was run along seismic TF1-Line 11, where a bright, continuous, low-angle reflector was observed. This was thought to be the seaward extension of a less resolved reflector on seismic line TF1-Line 5, above which we found the highest heat flow values. However, the heat flow along HF01 was not particularly elevated, so if this reflector is a fault or other feature that hosts hydrothermal circulation along TF1-Line 5, it is considerably less hydrothermally active along TF1-Line 11. HF02, oriented perpendicular to the trench, crossed a buried basement high seaward of the high heat flow area identified during TicoFluxI. The heat flow over the new feature was also elevated, up to 637 $mW/m^2$, but the continuation of this heat flow station towards the trench did not reveal additional values above 600 $mW/m^2$, and values drop to 50 $mW/m^2$ as the trench is approached.

Heat flow stations HF03 and HF04 were located along the propagator trace in the eastern survey area (Figs. IV-7 and IV-8), and were designed mainly to find coring targets and delineate the local hydrologic significance of outcrops. HF03 has the typical "high" values of the CNS crust ranging from 93 to 144 $mW/m^2$. HF04 is located between the topographic high of the propagator trace and a small basement outcrop to the west. The first measurement on the thinly sedimented slope of the propagator was 199 $mW/m^2$, but heat flow rapidly decreases to the single digits in the thickly sedimented area towards the outcrop and remains low as the outcrop is

approached, suggesting that the propagator ridge may be a site of hydrologic discharge and the seamount a site of local recharge. These observations, along with values determined during coring, confirm that there are patches within the CNS crust where vigorous water flow occurs, and that there are closely-spaced variations in heat flow, as apparent from scattered pre-TicoFlux measurements in this region..

Heat flow stations HF05, HF07, HF11 and HF16 were located close to the largest outcrop studied during TicoFlux II, Tengosed Seamount, near the center of our work area (Figs. IV-9, IV-11, and IV-13). This feature is approximately 5 nmi in diameter and rises 1100 m above the surrounding seafloor (and 1500 m above the surrounding top of basement). Station HF05 revealed very low values immediately adjacent to the seamount, while values were elevated adjacent to the seamount along HF16. Measurements somewhat farther from the seamount on HF07 and HF11 were uniformally low, except where basement rose close to the seafloor (HF07) or a large-scale thermal transition was crossed between cooler and warmer parts of the Cocos Plate (HF11) indicating that Tengosed is likely a site of regional recharge for the plate.

Four heat flow stations were extended radially away from Fuerte outcrop, about 25 nmi southwest of Tengosed Seamount (Fig. IV-10). Stations HF06, 09, 12, and 13 extend in the southwest, northeast, northwest, and southeast directions, respectively. On all but the southeastern flank (HF13) heat flow is high on the thinly sedimented slopes adjacent to the outcrop, 130-340 $mW/m^2$, but values decrease rapidly as sediment thickness increases away from the slopes, reaching lows near 30 $mW/m^2$. Heat flow from gravity cores on the upper flanks on the northeast side (GC 52-54) and on the southwest side (GC 55), ranges from 200 to 1160 $mW/m^2$. Collectively, these results suggest that Fuerte outcrop is a site of (relatively low-temperature) hydrothermal discharge. An exception to the pattern cited was found with GC56 on the southwest side, where heat flow was only 36 $mW/m^2$. For HF13 to the southeast, values are low right up to the edge of basaltic exposure (<20 $mW/m^2$), indicating that this part of the seamount is not discharging warm fluid. On the southwest line (HF06) away from the steep slope, the heat flow increases to ~100 $mW/m^2$.

Heat flow stations HF07 and HF08 were located adjacent to Dorado outcrop (Fig. IV-11). Values from HF-07 are <10-55 $mW/m^2$, higher where basement shallows, suggesting that thermal conditions are dominated by recharge from Tengosed to the east. But multipenetration values from HF08 are as high as 389 $mW/m^2$ on the west flank of Dorado, and heat flow determined with outrigger probes on nearby gravity cores (GC 33-42 ,50,51) are relatively high,

between 100 and 1000 mW/m$^2$. Collectively, these results indicate that Dorado is another site of localized, low-temperature, hydrothermal discharge.

Heat flow data were collected over two buried basement highs on the western edge of our field area, HF14 and HF15 (Figs. IV-15 and IV-15). Heat flow was 55 mW/m$^2$ near the peak of the basement high along HF14, but decreased to 12 mW/m$^2$ on the flank. In contrast, heat flow was higher (essentially equal to that predicted by conductive lithospheric cooling models, based on seafloor age, about 100 mW/m$^2$) along HF15, suggesting that this may be a small area in an otherwise hydrothermally-active plate where there is no hydrothermal mining of lithospheric heat.

Station HF10 (Fig. IV-12) ran across Perdido outcrop and the triple junction trace that separates EPR-generated and CNS-generated seafloor. The EPR side of this survey includes some of the lowest heat flow values measured during the TicoFlux expeditions, including three values that are ≤4 mW/m$^2$ (approaching the resolution of the instruments and analytical methods). Values are low in the immediately vicinity of the exposed basement, but rise to conductive lithospheric values on the CNS side of the outcrop.

The final heat flow station of TicoFlux II, HF17, was intended to resolve the location of the warm-cool transition northwest of the triple-junciton trace (Fig. IV-16). But this survey revealed remarkably consistent values of 103-109 mW/m$^2$, indicating that we never found the transition, and that the geometry of the boundary between warm and cool areas is highly irregular. This finding is consistent with a strong dependence of hydrothermal cooling on proximity to seamounts, and on strong heterogeneity and/or anisotropy in basement permeability.

D. MAPR Deployments

Preliminary MAPR results are summarized in Figures IV-17 to IV-26. Locations of these stations can be found on the corresponding tables and figures in Section V on coring. One of the paradoxes of the hydrothermal surveys during TicoFlux II is that, although the fluid fluxes thought to be responsible for suppression of seafloor heat flow over vast areas of EPR-generated seafloor must be enormous, the temperatures of fluids existing basement are likely to be little different from bottom seawater. In addition, these hydrothermal fluids are likely to have interacted with basement at temperatures <10-15 °C, and thus are likely to have a chemistry little different from bottom seawater. Thus locating plumes in this region on the basis of either temperature anomalies or nephelometry is likely to be very difficult, despite the apparent vigor

of circulation (based on regional heat flow values). It seems that subtle thermal anomalies may be the most likely indicators of massive hydrothermal discharge, since low temperature fluid plumes are likely to contain few particles, and therefore we have plotted temperature versus water depth to get a first order indication as to the possibility of identifying plumes.

Deployments during GC01-07 (Figs. IV-17 and IV–18) illustrate typical temperature-depth relations in this area in places where there is no evidence for thermal anomalies. Bottom water is typically 0.05-0.10°C warmer than the thermal minimum, and variations in temperature with depth below the minimum are roughly linear. The following MAPR responses near the seafloor water *might* be anomalous, relative to this (admittedly arbitrary) standard: GC16, GC18 (Fig. IV-19), GC22, GC23 (Fig. IV-21), GC33-35 (Fig. IV-22), GC49-50 (Fig. IV-24), and GC-55 (Fig. IV-26). More work will be required to compare these MAPR responses to values determined during heat flow operations, assess proximity to outcrops, and determine whether there is any indication of hydrothermal plume activity in the TicoFlux II work area.

## V. Sedimentology and Stratigraphy

Figure V-1 and Table V-1 show the locations of cores collected during TicoFlux II. Core locations are also shown in greater detail on local bathymetric maps in Figs. V-2 to V-11. The sediment types found in each core are illustrated in Figs. V-12 to V-19, and summaries of core recovery are listed in Table V-1. We assigned the lithologies to the following basic categories: hemipelagic mud, carbonate ooze, mixed sediment, variegated clay, volcanic ash, debris-flow deposits, sand turbidites, and Mn-oxide. Gradations exist among most categories, and many of the contacts between lithologies are transitional. Each of these primary sediment types is described briefly in this section.

Hemipelagic Mud. This mixture of biogenic and siliciclastic debris (diatomaceous silty clay) is the most common lithology throughout the study area. The texture ranges from silty clay to clay, and the color is uniform dark olive gray. Terrigenous grains consist largely of clay minerals, silt-sized plagioclase, and minor quartz. Biogenic constituents include abundant diatoms and variable amounts of radiolarians, sponge spicules, and silica needles/spines. Carbonate content is low, consisting mostly of coccoliths. Other particles in minor to trace quantities include volcanic glass shards and opaque grains. The mud is typically homogeneous to mottled, with local trace fossils (Zoophycos).

Calcareous ooze. Fine-grained pelagic sediment is white to light gray or very pale brown in color and typically mottled. Coccoliths make up the primary grain type in most such deposits. Other biogenic particles include foraminifers, fragments of larger carbonate shells, diatoms, radiolarians, and discoasters. Foraminifers are unusually abundant in GC-24, and fragments of chalk in GC-58 contain large amounts of inorganic carbonate (micrite). The content of clay minerals is low to very low in the chalk. Locally, burrows are filled with greenish black Fe-Mn oxide. This lithology also tends to be very firm, which inhibited penetration of cores.

Mixed Sediment. The category of mixed sediment differs from the typical hemipelagic mud by its relatively high content of calcareous nannofossils, plus siliciclastic grains. Color ranges from gray to light olive brown and light yellowish brown. Primary constituents include clay minerals, quartz/plagioclase silt, coccoliths, and carbonate shell fragments, with lesser amounts of diatoms and radiolarians. This lithology typically occurs as a transition from calcareous ooze to hemipelagic mud.

Variegated Clay. The variegated clay lithology ranges in color from brown to light olive brown, very pale brown, olive, olive gray, olive brown, yellowish brown, dark yellowish brown, and dark grayish brown. Clay minerals make up the bulk of these deposits; the amount of quartz/plagioclase silt ranges from trace to minor. The biogenic content is also unusually low. Volcanic glass shards are common in some samples, and core GC-50 contains abundant zeolites within an interval of altered clay. Clay-rich sediments are common in close proximity to basalt-sediment contacts. In many cases, fragments of basalt and Mn-oxide were recovered together with the clay. Reasons for the variability in color could not be determined by smear-slide examination, but the colors may be related to subtle differences in clay mineralogy, microfossil content, and/or alteration.

Volcanic Ash. There are two basic types of volcanic ash. The first type ranges in color from white to light gray, and the particles consist almost exclusively of clear, unaltered glass shards. Some such samples also contain euhedral crystals of fresh plagioclase, pyroxene, and/or amphibole. The light-colored layers probably originated through primary ash falls. The second type of ash ranges in color from dark gray to black. Fresh glass shards within the dark ash beds are brown in color, but heavily altered and devitrified glass shards are also common. Other constituents include vitric rock fragments, plagioclase and pyroxene crystals, opaque grains, clay minerals, and biogenic debris. The abundance of heavily altered grains indicates that older volcanic rocks were incorporated into the ash clouds during explosive eruptions. The ash layers

range from less than 1 mm in thickness to more than 10 cm. Particle size ranges from medium sand to coarse silt. Most beds have sharp bases and sharp to diffuse tops. Normal size grading is common. In some cases, the ash deposits occur as irregular patches or as material filling vertical burrows.

Debris-flow deposits. Remobilized sediment was recovered in two cores: PC-45 and GC-58. The floor of the Middle America Trench contains two mass-flow deposits. The source of that debris is probably the upper trench slope on the landward side, which is incised by numerous slope gullies and small canyons. The older of the two deposits is 67 cm thick and consists largely of remobilized dark olive gray mud with sparse fragments of moderately indurated mudstone. The upper deposit is over 220 cm thick and contains abundant fragments of moderately to poorly indurated hemipelagic mudstone in a matrix of softer dark olive gray mud. Clast size ranges up to 18-20 cm and clast fabric is disorganized. Clast shape varies from subangular to rounded. The top of the upper debris-flow deposit grades into a turbidite sand. The debris from Buquito submarine slide, in contrast, contains angular fragments of indurated light gray carbonate ooze supported by a matrix of softer dark olive gray hemipelagic mud. Clast size ranges up to 5-10 cm and the fabric is disorganized. The brecciated chalk contains abundant inorganic carbonate, which probably formed through recrystallization of coccoliths. Debris recovered from the flank of Buquito measured only about 10 in thickness and was limited to the bottom of the core cutter. It indicates, however, that deeply buried sedimentary deposits were exposed along the failure surface of the submarine slide.

Sand turbidites. The only core to contain sand turbidites comes from the floor of Middle America Trench (PC-45). Bed thickness ranges from 50 to 67 cm. The larger sand-sized grains consist of moderately indurated pieces of mudstone (weak enough to crush with one's finger tips), but there is also abundant siliciclastic quartz, plagioclase, and carbonate debris in the fine-sand to silt fraction. The turbidites display normal size grading. In one case the sand rests immediately above a debris-flow deposit, which indicates that the grain support mechanism changed from matrix-strength and buoyancy to turbulent autosuspension as seawater was entrained into the flow.

Mn-oxide. This black hydogeneous sediment occurs routinely at or near core tops and/or the sediment-basalt interface where rates of hemipelagic sedimentation are low. The mode of occurrence ranges from indurated nodules to coatings on basalt and mudstone fragments, cm-thick crusts, scattered non-indurated patches, gravel-sized fragments, and mm-thin layers.

The sediment types described above vary spatially in response to distance from the continental margin and seafloor relief. Debris-flow deposits and sandy turbidites are dominant on the floor of the Middle America Trench, whereas the seaward trench slope is covered by diatom-rich hemipelagic mud with layers of light gray and black volcanic ash. Olive brown to dark olive brown clay covers the slopes of Perdido outcrop; these clay-rich sediments typically contain Mn-oxide nodules and fragments of basalt. The most common lithology in the warm crust area is dark olive gray hemipelagic mud, although grayish brown clay-rich sediment also occurs locally in association with altered basalt. The cold crust area displays greater lithologic variability due to the effects of seafloor topography, bottom currents, and greater distance from sources of terrigenous input. Caballito outcrop, located in the southwest part of the study area, is surrounded by calcareous ooze; Mn-oxide crusts are common near core tops. Tengosed seamount is surrounded largely by diatom-rich hemipelagic mud except on the southwest side, which contains olive brown clay. Dorado outcrop also shows lithologic variability, with hemipelagic mud along the base and southwest slope, and highly altered yellowish brown clay (locally zeolitic) and Mn-oxide on the northwest slope.

Two kinds of physical properties samples were collected form selected cores: 304 samples were collected from 13 gravity and piston cores for index properties determination. These samples were 30-50 cc in volume and were collected soon after the cores were split, generally at 10-cm spacing, placed in pre-weighted and pre-numbered vials, and sealed with parafilm in ziplock bags. These samples were stored with wet sponges (to help maintain humid conditions in the ziplock bags) in a refrigerator during the cruise, then hand-carried back to UCSC in coolers with blue ice for analysis. These samples will be analyzed for water content, grain density, porosity, and bulk density.

In addition, 13 whole round samples, 15-cm in length, were collected from 6 cores for geotechnical analysis to determine permeability and consolidation properties. These samples were capped, taped, waxed, and stored cooled and upright. They were also carries back to UCSC in coolers and are now in storage in a cold room awaiting testing in the lab.

## VI. Geochemistry

The geochemical portion of TicoFlux II consisted of 62 gravity cores, three piston cores, and two hydrocasts (Table V-1). These activities were conducted during 22 sessions that lasted from 3 to 15 hours with an average length of 11 hours. Twelve primary seafloor features were

targeted, chosen in part based on seismic images and heat flow data acquired during TicoFlux I and II. Locations such as elevated basement features with relatively thin sediment coverage, or within a tapering sediment section adjacent to seafloor topographical highs, were prime coring targets. In addition, features with an abrupt increase in heat flow near their perimeters were selected because these are likely sites where formation fluids may vent from basaltic basement.

Sediment from these cores were described and sampled. A portion of the sampling program was focused on the extraction of pore waters. Three to twelve sediment sections (each about 3 to 4 cm in length) from all of the cores that contained sediment were placed in 85 mL centrifuge bottles, cooled to 2 to 4°C by placing them in a freezer for 30 minutes, and centrifuged at 13,000 rpm for 5 minutes. Fluids were extracted from these centrifuged sediments, filtered and aliquoted into several different containers. Several chemical analyses were conducted at sea (pH, alkalinity, calcium, phosphate, chlorinity and fluoride) on both pore waters and seawater collected during the two hydrocasts, which provided a sample of bottom seawater. These particular seaboard analyses aided our decisions at sea. A more comprehensive analytical program will be performed ashore, including measurement of trace elements in seawater and $^{14}C$ dating.

Below we report preliminary results of the geochemical portion of the TicoFlux II coring and hydrocast programs. We divided the discussion into three geographic sections: Near Trench, Warm Crust, and Cold Crust. We also briefly describe the two hydrocasts.

A. Near Trench (five sites)

The first site that was cored was a La Misma outcrop, which is descending into the trench. This feature shows evidence of faulting, clearly visible in the seismic record. Three gravity cores (GC 01-03) were collected on this feature (Fig. V-2), but there was no sign of pore water seepage in these cores (e.g., alkalinity and $PO_4$ increase with depth). The Perdido outcrop and an adjacent outcrop, on the triple junction trace, were targed by GC 04-10 (Fig. V-3). Once again there was no sign of pore water seepage, but some basalt was recovered. The southeastern sides of these outcrops are likely exposed basalt and are very steep. Later in the cruise a heat flow survey was conducted near and on this feature. The results are consistent with bottom seawater entering into the feature, therefore it is not surprising that we did not observe pore water seepage at this site.

The third site that we cored is the "high heat high" site from last year (Fig. V-10). This site is located over and close to a deep basement reflector (fault?) that can be traced to the sediment-basalt interface, which is about 75 m below the seafloor. Here the composition of the formation fluids is highly altered and similar to formation fluids from Baby Bare and DSDP Hole 504B. Some distinct chemical differences exist between these fluids with the formation fluids at this site, having much higher Ca and Li concentrations and lower Na concentrations. Six gravity cores (GC 11, 12, 62-65) and one piston core (PC 44) sampled this site. One gravity core and the piston core were positioned on the heat flow high determined from the heat flow survey last year. Here pore waters seep upward at a rate of about 2.5 cm/yr, which is well above the rate (0.5 cm/yr) that was determined from samples collected during TicoFlux I (Figure VI-1). The six gravity cores in part define the extent of pore water seepage in this region. Six samples from the piston core were placed in a glove bag. An aliquot from the deepest of these samples was stored for $^{14}C$ analysis. This core provides the data needed to better constrain the composition of the fluid in basement, because of the faster seepage rate, in contrast to the cores from last year that showed signs of reaction with the sediment as the formation fluid ascends..

A neighboring topographical high to the west also was cored (GC13 and 14). These cores show signs of an altered fluid in basaltic basement; however, the seepage rate is too low for these samples to be of much use for constraining basement fluid composition.

A fifth site in this area was cored (PC45). This site is located in the trench. The core was positioned to determine if turbidites and volcanic ash are observed within the trench. The volcanic layers provide a measure of timing and the magnitude of turbidite flows that may be related to large seismic events. This core could help with a future proposal to examine the role of turbidites in this setting.

B. Warm Crust (two sites)

Several sites were cored on the warm crust during TicoFlux I (Fig. V-4). One site clearly showed evidence for pore water seepage through the sediment (TFI-GC23). This general area was targeted to see if we could find a site with faster pore water seepage. Two new cores (GC15 and 16) were placed further up the slope, but seepage is slower at these sites. Two other targets in the area were cored (GC 17 and 18), but neither site showed evidence for pore water seepage. We then cored the site where TFI-GC23 was taken (GC 19), but found that seepage was less vigorous. This indicates the extent of heterogeneity in seepage processes – the seafloor targets

are likely to be relatively small, perhaps only a few tens to hundreds of meters on a side. We then placed three more cores (GC20, 46, and 47) around GC 19 (TFI-GC 23 from last year) to try to locate a site with faster pore water seepage. We placed PC 48 where we thought seepage might be the most vigorous. Six sediment samples from this core were placed in a nitrogen atmosphere for sampling. Unfortunately this core did not have the fastest pore water seepage (Figure VI-2). Thus the best samples of formation fluids from this area that are least affected by reaction with sediment during ascent are those from TFI-GC23, which was collected last year.

C. Cold Crust (five sites)

The first two sites that were cored in the Cold Crust region were ones that were targeted last year, and both contain carbonate oozes. One of the cores from last year (TFI-GC09) was consistent with pore water seepage and thus this site was heavily cored during TicoFlux II. Ten cores were placed on this site (GC 21, 22, 25-32) including the site where TFI-GC09 was cored last year (Fig. V-6). What we believed was pore water seepage last year may have been a result of diagenetic reactions. These cores clearly show an increase in Ca with depth and a decrease in phosphate and alkalinity, which is consistent with a connection with basement fluids. However, none of the profiles are clearly ones with pore water seepage of more than several mm/yr. Similarly, results from the two cores (GC 23 and 24) collected on a nearby feature do not indicate the significant pore water seepage.

The Dorado outcrop, a feature similar in size to Baby Bare on the flank of the Juan de Fuca ridge, was targeted because of its size and elevated heat flow as one approaches the feature. Here we placed eleven cores (GC33-43) to locate sites of pore water egress (Fig. V-7). One of the cores hit a site where pore water seepage is evident, based on decreases in phosphate and alkalinity with depth (Figure VI-3). This site (GC40) was later targeted by three additional cores (GC 49-51), each with evidence for pore water seepage. Only one core (GC 50, heat flow of 1.0 $W/m^2$) was long enough to place a section of sediment into a glove-bag for sampling in a nitrogen atmosphere. A sample was collected and an aliquot was saved for $^{14}C$ dating. Two markers were deployed at this site to help guide future (potential) submersible or ROV operations. These markers consist of a 3-pound dive weight, a 3-foot length of line, a white bucket lid with a number engraved in it, and a block of syntactic foam, also with a number on it. We used marker 1 on GC50 and marker 2 on GC51.

The large Fuente outcrop was also targeted during TicoFlux II. Six cores were dropped on this site (GC 52-57). Even though a heat flow of more than 1.1 $W/m^2$ was measured at one of the core sites (GC54), there was no evidence found for seepage of a fluid significantly different from seawater.

A single gravity core (GC58) was taken on a sediment slump between a seamount and the section of the seamount that broke off. This core had carbonate ooze at the base that was overlain by green-colored clays. This ooze also contained green clay intermixed with the carbonates, presumably a product of the slide. No seepage was evident at this site.

Another small feature was targeted (GC 59-61). This feature was a buried basement high where the sediment thins to less than 75 m. To the north of this line is a topographic high that is 30 m higher. This site also was targeted. A heat flow transect reveals almost uniform values around 100 $mW/m^2$, indicating that this site does not likely have pore water seepage. None of these cores shows signs of pore water seepage.

D. Hydrocasts

Two hydrocasts were taken in the cold plate region. Two 5-L nisken bottles with internal plastic-coated springs were used. These bottles were positioned 85 and 100 m above the seafloor when they were tripped with a messenger. Four 125-ml bottles were filled and later filtered. These samples provide a measure of bottom water concentrations and a means for assessing quality control of chemical analyses.

## VII. Acknowledgements

The success of the TicoFlux II program is due, in large part, to the outstanding facilities, officers, technicians and crew on R/V *Melville*. This research was supported by NSF grants OCE-0001892 (Fisher and Silver), OCE-0001944 (Harris), OCE-0001941 (Stein), and OCE-0002031 (Wheat).

VII. Science Party Contact List

Andrew T. Fisher
Earth Sciences Department
University of California, Santa Cruz
1156 High Street
Santa Cruz, CA 95064
831-459-5598
831-459-3074 (fax)
afisher@es.ucsc.edu

Eli Silver
Earth Sciences Department
University of California, Santa Cruz
1156 High Street
Santa Cruz, CA 95064
831-459-2266
831-459-3074 (fax)
esilver@es.ucsc.edu

Carol Stein
Dept. of Earth and Environmental
Sciences (M/C 186)
University of Illinois at Chicago
845 West Taylor Street
Chicago, Illinois 60607-7059
(312) 996-9349
(312) 413-2279 (fax)
cstein@uic.edu

Rob Harris
Dept. of Geology and Geophysics
University of Utah
717 W. B. B.
Salt Lake City, UT 84112
(801) 587-9366
(801) 581-7065 (fax)
rnharris@mines.utah.edu

C. Geoff Wheat
West Coast and Polar Regions
Undersea Research Center
PO Box 475
Moss Landing, Ca 95039
(shipping)
NURP/MLML Marine Operations
7700 Sandholdt Road, Bldg D
Moss Landing, Ca 95039
(831) 633-7033
(831) 633-6872 (fax)
wheat@mbari.org

Martine Buatier
Lab. Geosciences- UFR Sciences
Université de Franche-Comté
16 route de gray
25030 Besançon
FRANCE
martine.buatier@univ.fcomte.fr

Patrizia Costa
Earth Sciences Department
University of California, Santa Cruz
1156 High Street
Santa Cruz, CA 95064
831-459-2830
pcosta@es.ucsc.edu

Heather Deshon
Earth Sciences Department
University of California, Santa Cruz
1156 High Street
Santa Cruz, CA 95064
831-459-4426
831-459-3074 (fax)
hdeshon@es.ucsc.edu

Cindy Ellsworth
Pacific Geoscience Center, GSC
9860 W. Saanich Road
Sydney, B.C. Canada V8L4B2
(250) 363-6565 (fax)
cindy.ellsworth@hotmail.com

Patrice Friedmann
Earth Sciences Department
University of California, Santa Cruz
1156 High Street
Santa Cruz, CA 95064
831-459-4090
831-459-3074 (fax)
p_friedmann@hotmail.com

Derrick Hasterok
Dept. of Geology and Geophysics
University of Utah
717 W. B. B.
Salt Lake City, UT 84112
(801) 581-3588
(801) 581-7065 (fax)
dhasterok@mines.utah.edu

Brian Hernandez
6821 Ridgewood Dr.
Oakland, CA 94611
(510) 339-4358
aquaaa@hotmail.com

Mike Hutnak
Earth Sciences Department
University of California, Santa Cruz
1156 High Street
Santa Cruz, CA 95064
831-459-2838
831-459-3074 (fax)
mhutnak@es.ucsc.edu

Melissa Jones
1708 Laurel Ave.
Hudson, WI 54016
715-386-1729
crazy4milk@mad.scientist.com

Bob MacKnight
Earth Sciences Department
University of California, Santa Cruz
1156 High Street
Santa Cruz, CA 95064
831-425-8568
bmac@cats.ucsc.edu
bmacknight@es.ucsc.edu

Chris Moser
Oregon State University - COAS
104 Ocean. Admin. Bldg.
Corvallis, OR 97331-5503
(541) 737-5217
(541) 737-2064 (fax)
cmoser@coas.oregonstate.edu

William Parsons
c/o Patrice Friedmann
Earth Sciences Department
University of California, Santa Cruz
1156 High Street
Santa Cruz, CA 95064
831-459-4090
831-459-3074 (fax)
p_friedmann@hotmail.com

Glenn Spinelli
Dept. of Geological Sciences
University of Michigan
1416 Arborview Blvd.
Ann Arbor, MI 48103
734-883-5855
spinelli@es.ucsc.edu
(After November 2002 at the
University of Missouri)

Michael B. Underwood
101 Geology Building
Department of Geological Sciences
University of Missouri
Columbia, MO 65211
573-882-4685
573-882-5458 (fax)
UnderwoodM@missouri.edu

Figures and Tables

Figure III-19. Heat flow station HF12, located on seismic TF2-Line 27.

Figure III-20. Heat flow station HF13, located on seismic TF2-Line 27.

Figure III-21. Heat flow station HF14, located on seismic TF2-Line 38a.

Figure III-22. Heat flow station HF15, located on seismic TF2-Line 33.

Figure III-23. Heat flow station HF16, located on seismic TF2-Line 26.

Figure III-24. Heat flow station HF17, located on seismic TF1-Line 03.

Table IV-1. Summary of multipenetration station targets, times and measurements.

Table IV-2. Summary of multipenetration heat flow positions, values and nearest seismic points. Heat flow values have not been corrected for instrument tilt, sedimentation or local bathymetry.

Table IV-3. Summary of autonomous temperature logger deployments and results.

Figure IV-1. TicoFlux I heat flow station locations. Individual station maps are drawn for regions indicated with boxes.

Figure IV-2. Examples of data collected during four penetrations with PGC multipenetration heat flow probe. Measurement interval is 10 s. There are 11 sediment thermistors and one bottom water thermistor (value of latter remains relatively constant through penetration). Initial period of temperature rise and equilibration follows penetration of the seafloor by the probe. Heat pulse is fired after seven minutes in bottom with no change in elevation of probe. The instrument is left to equilibrate for about 7 minutes after firing heat pulse, then is removed the seafloor. These four examples illustrate a range of instrument responses. A. HF02, Penetration 3. Relatively high heat flow (637 $mW/m^2$) and homogeneous sedimentary thermal properties. B. HF10, Penetration 4. Extremely low heat flow (<4 $mW/m^2$) and homogeneous thermal properties. C. HF06, Penetration 3. Hard sediments lead to partial penetration, with the shallowest thermistor exposed to bottom water (note rapid re-equilibration following heat pulse) and the second shallowest thermistor being positioned close to the seafloor. Variable sedimentary thermal properties. D. HF08, Penetration 2, moderate heat flow and homogeneous thermal properties.

Figure IV-3. Example of processed, multipenetration probe data. A. Estimated equilibrium temperatures versus depth. All temperatures are relative to bottom water. Open symbols indicate depths for temperatures based on assumption that shallowest measurement is at seafloor. Solid symbols show apparent depths after requiring that thermal gradient pass through bottom water temperature at the seafloor. B. Sediment thermal conductivity versus depth. Solid lines indicate depth intervals over which conductivites are assumed to apply in calculating thermal resistances, half way between successive measurements, except for the shallowest value, which is assumed to apply up to the seafloor. Dashed line indicates thermal conductivity of shallow sediments required to make best-fitting straight line in part C pass through zero. This is the effective conductivity of the shallow sediment section, assuming that other conductivities and depth

intervals are correct. C. Temperature versus cumulated thermal resistance (depth corrected for differences in thermal conductivity). The slope of the best-fitting straight line that passes through the data is the conductive heat flow.

Figure IV-4. Examples of data collected during four deployments of Antares outrigger probes. Measurement interval is 5 s. There are various numbers of sediment thermistors and one bottom water thermistor, the latter mounted along with a tilt sensor in the core weight. Initial period of temperature rise and equilibration follows penetration of the seafloor by the core barrel and sensors. There is no heat pulse, so data are interpreted based on thermal conductivities of surrounding sediments as determined with the PGC tool, or from needle-probe analysis of recovered core material. The instrument is left to equilibrate for about 7 minutes after firing heat pulse, then is removed the seafloor. A. GC13. Relatively high heat flow (665 $mW/m^2$), as determined with four short probes. Note initial cooling followed by reheating by several probes. B. GC37. Temperatures measured with two short probes and one long probe. The former have much greater frictional heating upon penetration, while the latter has a thermal response more consistent with a line source. C. GC54. This deployment included two long probes (deep) and one short probe (shallow), but the latter did not penetrate the seafloor. Final estimated heat flow, 1.16 $W/m^2$, is the highest determined during either TicoFlux I or TicoFlux II. D. PC44. Four long probes delineate heat flow of 633 $mW/m^2$.,

Figure IV-5. Contoured hydrosweep bathymetry with HF01 measurement locations.

Figure IV-6. Contoured hydrosweep bathymetry with HF02 measurement locations.

Figure IV-7. Contoured hydrosweep bathymetry with HF03 measurement locations.

Figure IV-8. Contoured hydrosweep bathymetry with HF04 measurement locations.

Figure IV-9. Contoured hydrosweep bathymetry with HF05 and 16 measurement locations.

Figure IV-10. Contoured hydrosweep bathymetry with HF06, 09, 12, and 13 measurement locations.

Figure IV-11. Contoured hydrosweep bathymetry with HF07 and 08 measurement locations.

Figure IV-12. Contoured hydrosweep bathymetry with HF10 measurement locations.

Figure IV-13. Contoured hydrosweep bathymetry with HF11 measurement locations.

Figure IV-14. Contoured hydrosweep bathymetry with HF14 measurement locations.

Figure IV-15. Contoured hydrosweep bathymetry with HF15 measurement locations.

Figure IV-16. Contoured hydrosweep bathymetry with HF17 measurement locations.

Figure IV-17. MAPR data from GC01-03.

Figure V-15. Lithological logs of cores GC30-39.

Figure V-16. Lithological logs of cores GC40-49.

Figure V-17. Lithological logs of cores PC44, 45, 48.

Figure V-18. Lithological logs of cores GC50-59.

Figure V-19. Lithological logs of cores GC60-65.

Figure IV-1. Calcium concentrations in pore waters from cores that surround the "high heat flow area" located in 2001 are shown as a function of depth. Several modeled profiles are included to illustrate the range of pore water seepage rates through the sediment. Note the high Ca concentrations at depth consistent with a highly altered seawater in the basaltic basement below.

Figure IV-2. Calcium concentrations in pore waters from cores that surround Core 23, collected in 2001, are shown as a function of depth. These cores were collected on the warm crust. Several modeled profiles are included to illustrate the range of pore water seepage rates through the sediment. Note the high Ca concentrations at depth relative to the seawater concentration, but the concentrations are much less than that observed in the "high heat flow area". The fluids in basement however are still highly evolved seawater. The best samples, with the fastest upwelling seepage speeds, are from 2001. We could not duplicate this result during TicoFlux II.

Figure IV-3. Phosphate concentrations in pore waters from cores on the Baby Bare-sized feature in the cold crust region are shown as a function of depth. Modeled profiles indicating seepage are not included because of the complexities of adding a reaction term to the advection-diffusion equation. This will be completed ashore. The cores with upward seepage are those with phosphate concentrations less than the seawater value (about 2.9 μmol/kg). These fluids have Ca concentrations that are identical to bottom seawater and alkalinities that are equal to or slightly less than the bottom seawater value.

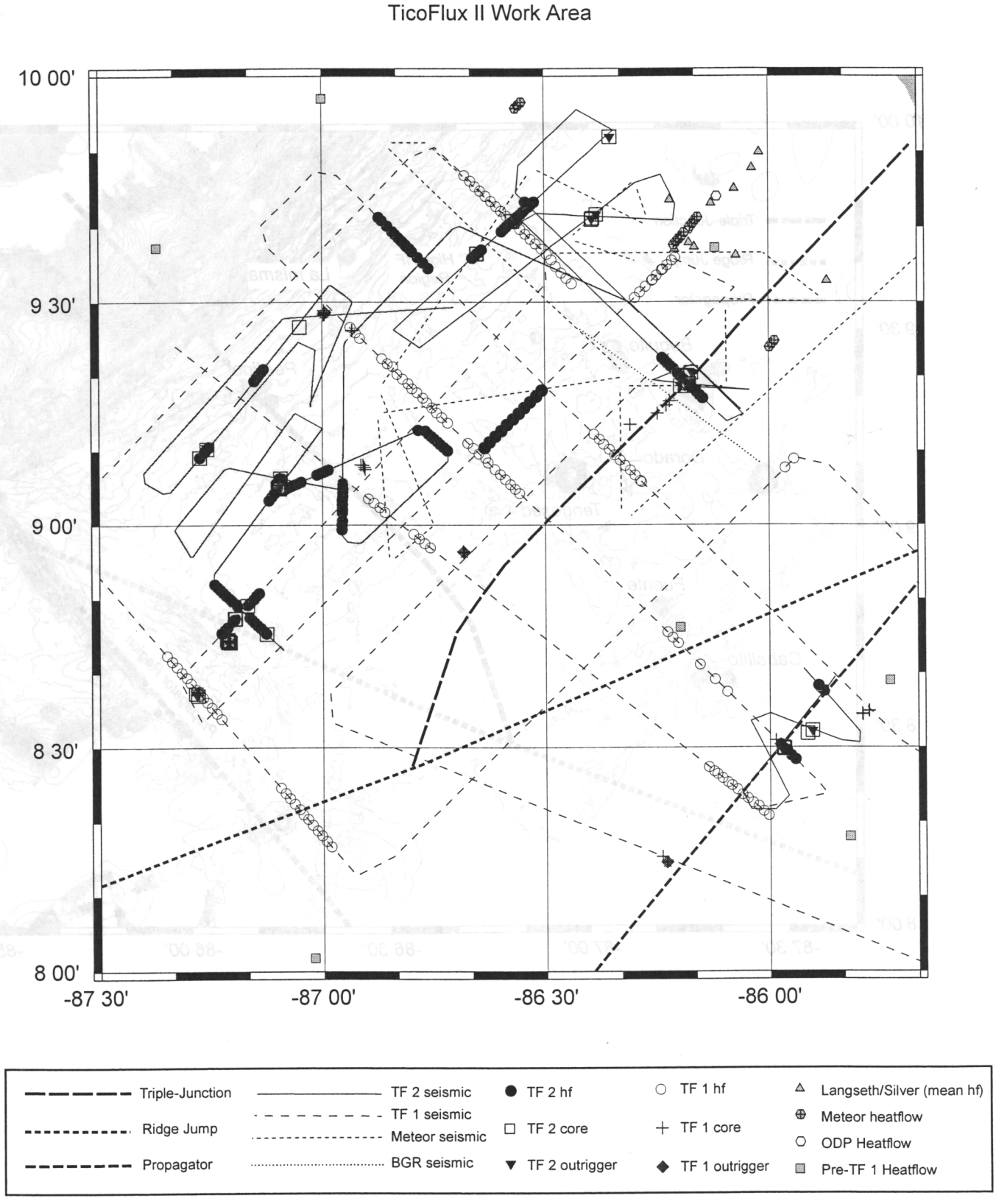
TicoFlux II Work Area
10 00'
9 30'
9 00'
8 30'
8 00'
-87 30'
-87 00'
-86 30'
-86 00'
Triple-Junction
Ridge Jump
Propagator
TF 2 seismic
TF 1 seismic
Meteor seismic
BGR seismic
TF 2 hf
TF 2 core
TF 2 outrigger
TF 1 hf
TF 1 core
TF 1 outrigger
Langseth/Silver (mean hf)
Meteor heatflow
ODP Heatflow
Pre-TF 1 Heatflow

Figure I-1

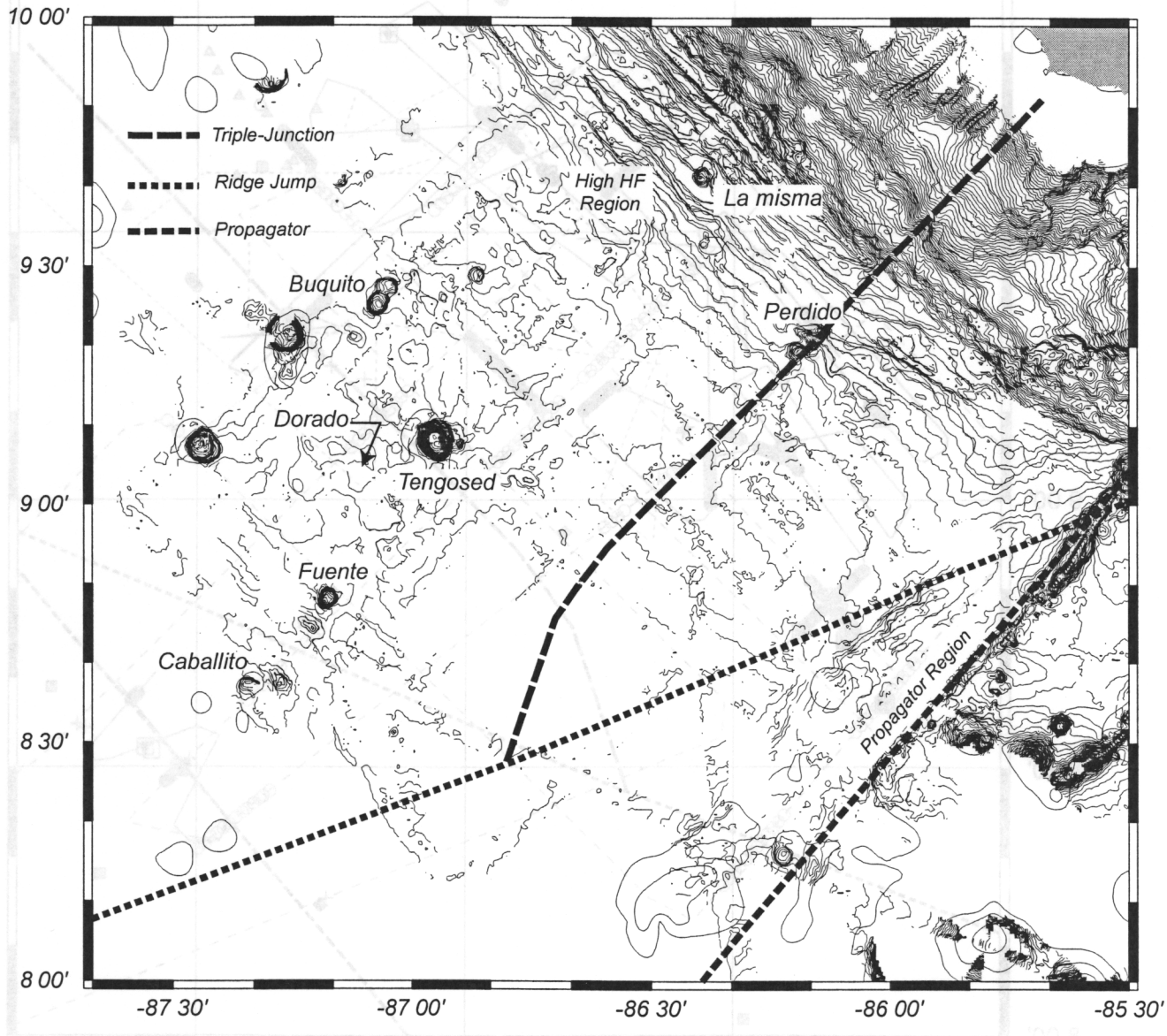
10 00'
9 30'
9 00'
8 30'
8 00'
-87 30'
-87 00'
-86 30'
-86 00'
-85 30'
Triple-Junction
Ridge Jump
Propagator
High HF Region
La misma
Perdido
Buquito
Dorado
Tengosed
Fuente
Caballito
Propagator Region

Figure I-2

Table II-1. Summary of TicoFlux II operations.

| Date and Time (starting, local) | Date and Time (starting, GMT) | Event | Duration (hrs) | Duration (days) | Running (days) | Comments |
|---|---|---|---|---|---|---|
| 9/2/02 8:00 | 9/2/02 14:00 | Ship reaches Puerto Caldera | **128.0** | 5.33 | 0.00 | |
| 9/7/02 16:00 | 9/7/02 22:00 | Ship leaves for TicoFlux II | **12.0** | 0.50 | 0.50 | |
| 9/8/02 4:00 | 9/8/02 10:00 | DP/seismic test | **9.0** | 0.38 | 0.88 | |
| 9/8/02 13:00 | 9/8/02 19:00 | Transit to TF2-core 1 | **1.0** | 0.04 | 0.92 | |
| 9/8/02 14:00 | 9/8/02 20:00 | TF2-Core 1 | **14.5** | 0.60 | 1.52 | GC-01, 02, 03: subducting seamount (La misma) |
| 9/9/02 4:30 | 9/9/02 10:30 | Transit | **2.0** | 0.08 | 1.60 | |
| 9/9/02 6:30 | 9/9/02 12:30 | Tension meter repair | **6.0** | 0.25 | 1.85 | |
| 9/9/02 12:30 | 9/9/02 18:30 | TF2-HF1 | **24.0** | 1.00 | 2.85 | Dipping reflector near area of high heat flow, close to tr |
| 9/10/02 12:30 | 9/10/02 18:30 | Transit | **4.0** | 0.17 | 3.02 | |
| 9/10/02 16:30 | 9/10/02 22:30 | TF2-Core 2 | **14.0** | 0.58 | 3.60 | GC-04, 05, 06, 07, outcrops at TJT (Perdido) |
| 9/11/02 6:30 | 9/11/02 12:30 | Seismic 1 - HF high | **48.0** | 2.00 | 5.60 | Lines 1-12 around trench, HF high area, outcrops |
| 9/13/02 6:30 | 9/13/02 12:30 | Transit | **1.0** | 0.04 | 5.65 | |
| 9/13/02 7:30 | 9/13/02 13:30 | TF2-Core 3 | **12.5** | 0.52 | 6.17 | GC-08, 09, 10 outcrops at TJT (Perdida) |
| 9/13/02 20:00 | 9/14/02 2:00 | Transit | **3.5** | 0.15 | 6.31 | |
| 9/13/02 23:30 | 9/14/02 5:30 | TF2-HF2 | **31.0** | 1.29 | 7.60 | Heat flow high area near trench |
| 9/15/02 6:30 | 9/15/02 12:30 | Transit | **2.0** | 0.08 | 7.69 | |
| 9/15/02 8:30 | 9/15/02 14:30 | TF2-Core 4 | **14.0** | 0.58 | 8.27 | GC-11, 12, 13, 14: heat flow high area |
| 9/15/02 22:30 | 9/16/02 4:30 | Transit to seismic | **6.0** | 0.25 | 8.52 | |
| 9/16/02 4:30 | 9/16/02 10:30 | Seismic 2 - propagator | **13.0** | 0.54 | 9.06 | Lines 13-18, Across propagator trace |
| 9/16/02 17:30 | 9/16/02 23:30 | Transit to core site | **2.0** | 0.08 | 9.15 | |
| 9/16/02 19:30 | 9/17/02 1:30 | TF2-Core 5 | **3.5** | 0.15 | 9.29 | GC-15, near propagator trace |
| 9/16/02 23:00 | 9/17/02 5:00 | Transit to heat flow | **1.0** | 0.04 | 9.33 | |
| 9/17/02 0:00 | 9/17/02 6:00 | TF2-HF3 | **11.5** | 0.48 | 9.81 | Near propagator trace |
| 9/17/02 11:30 | 9/17/02 17:30 | TF2-Core 6 | **13.5** | 0.56 | 10.38 | GC-16, 17, 18, 19: near propagator trace |
| 9/18/02 1:00 | 9/18/02 7:00 | Wait for La Launcha, get batteries | **7.0** | 0.29 | 10.67 | acquire batteries for seismic system |
| 9/18/02 8:00 | 9/18/02 14:00 | TF2-HF4 | **14.0** | 0.58 | 11.25 | Near propagator trace |
| 9/18/02 22:00 | 9/19/02 4:00 | Transit and TF2-Core 7 | **4.0** | 0.17 | 11.42 | GC-20: near propagator trace |
| 9/19/02 2:00 | 9/19/02 8:00 | Transit for Seismic #3 | **4.0** | 0.17 | 11.58 | |
| 9/19/02 6:00 | 9/19/02 12:00 | Seismic 3 - outcrops | **28.0** | 1.17 | 12.75 | Lines 19-26: across TJT, outcrops |
| 9/20/02 10:00 | 9/20/02 16:00 | Transit to core site | **3.0** | 0.13 | 12.88 | |

Table II-1. Summary of TicoFlux II operations.

| Date and Time (starting, local) | Date and Time (starting, GMT) | Event | Duration (hrs) | Duration (days) | Running (days) | Comments |
|---|---|---|---|---|---|---|
| 9/20/02 13:00 | 9/20/02 19:00 | TF2-Core 8 | **14.0** | 0.58 | 13.46 | GC-21, 22, 23, 24: buried basement high (near Fuente), |
| 9/21/02 3:00 | 9/21/02 9:00 | Transit | **2.5** | 0.10 | 13.56 | |
| 9/21/02 5:30 | 9/21/02 11:30 | TF2-HF5 | **24.5** | 1.02 | 14.58 | Adjacent to large seamount (Tengosed) |
| 9/22/02 6:00 | 9/22/02 12:00 | Transit and seabeam | **2.0** | 0.08 | 14.67 | |
| 9/22/02 8:00 | 9/22/02 14:00 | TF2-Core 9 | **12.0** | 0.50 | 15.17 | GC25, 26, 27, 28: buried basement high (near Fuente) |
| 9/22/02 20:00 | 9/23/02 2:00 | TF2-HF6 | **12.0** | 0.50 | 15.67 | Fuente outcrop |
| 9/23/02 8:00 | 9/23/02 14:00 | TF2-Core 10 | **12.0** | 0.50 | 16.17 | GC25, 26, 27, 28: buried basement high (near Fuente) |
| 9/23/02 20:00 | 9/24/02 2:00 | Seismic 4: outcrops | **24.0** | 1.00 | 17.17 | |
| 9/24/02 20:00 | 9/25/02 2:00 | TF2-HF7 | **12.0** | 0.50 | 17.67 | approaching small outcrop (Dorado) |
| 9/25/02 8:00 | 9/25/02 14:00 | TF2-Core 11 | **12.0** | 0.50 | 18.17 | GC 33, 34, 35, 36: near outcrop Dorado |
| 9/25/02 20:00 | 9/26/02 2:00 | TF2-HF8 | **11.0** | 0.46 | 18.63 | approaching small outcrop (Dorado) |
| 9/26/02 7:00 | 9/26/02 13:00 | TF2-Core 12 | **12.0** | 0.50 | 19.13 | GC 37, 38, 38, 40: near outcrop Dorado |
| 9/26/02 19:00 | 9/27/02 1:00 | TF2-HF9 | **12.0** | 0.50 | 19.63 | Adjacent to ourcrop Fuente |
| 9/27/02 7:00 | 9/27/02 13:00 | TF2-Core 13 | **12.0** | 0.50 | 20.13 | GC 41, 42, 43: near outcrop Dorado |
| 9/27/02 19:00 | 9/28/02 1:00 | Seismic 5: outcrops, heat flow high | **18.0** | 0.75 | 20.88 | |
| 9/28/02 13:00 | 9/28/02 19:00 | TF2-Core 14 | **15.5** | 0.65 | 21.52 | PC 44,45: heat flow high, trench |
| 9/29/02 4:30 | 9/29/02 10:30 | transit to TJT/outcrop | **3.0** | 0.13 | 21.65 | |
| 9/29/02 7:30 | 9/29/02 13:30 | TF2-HF10 | **24.5** | 1.02 | 22.67 | HF10: Outcrop perdido |
| 9/30/02 8:00 | 9/30/02 14:00 | Transit to warm crust | **6.0** | 0.25 | 22.92 | |
| 9/30/02 14:00 | 9/30/02 20:00 | TF2-Core 15 | **11.5** | 0.48 | 23.40 | GC 46, 47 PC 48: outcrop Dorado |
| 10/1/02 1:30 | 10/1/02 7:30 | Transit to outcrop area | **8.0** | 0.33 | 23.73 | |
| 10/1/02 9:30 | 10/1/02 15:30 | Seismic 6: outcrops | **8.0** | 0.33 | 24.06 | |
| 10/1/02 17:30 | 10/1/02 23:30 | Transit to heat flow | **2.5** | 0.10 | 24.17 | |
| 10/1/02 20:00 | 10/2/02 2:00 | TF2-HF11 | **14.5** | 0.60 | 24.77 | transition east of seamount Tengosed |
| 10/2/02 10:30 | 10/2/02 16:30 | Transit to core site | **2.0** | 0.08 | 24.85 | |
| 10/2/02 12:30 | 10/2/02 18:30 | TF2-Core 16 | **8.5** | 0.35 | 25.21 | GC 49, 50, 51: outcrop Dorado |
| 10/2/02 21:00 | 10/3/02 3:00 | Transit to heat flow | **2.0** | 0.08 | 25.29 | |
| 10/2/02 23:00 | 10/3/02 5:00 | TF2-HF12 | **13.0** | 0.54 | 25.83 | west of outcrop Fuente |
| 10/3/02 12:00 | 10/3/02 18:00 | Broken wire | **3.0** | 0.13 | 25.96 | repair broken trawl wire |
| 10/3/02 15:00 | 10/3/02 21:00 | TF2-Core 17 | **9.0** | 0.38 | 26.33 | adjacent to outcrop Fuente |

Table II-1. Summary of TicoFlux II operations.

| Date and Time (starting, local) | Date and Time (starting, GMT) | Event | Duration (hrs) | Duration (days) | Running (days) | Comments |
|---|---|---|---|---|---|---|
| 10/4/02 0:00 | 10/4/02 6:00 | TF2-HF13 | **11.0** | 0.46 | 26.79 | adjacent to outcrop Fuente |
| 10/4/02 11:00 | 10/4/02 17:00 | Hydrocast and TF2-Core 18 | **12.5** | 0.52 | 27.31 | H1, GC 55, 56, 57: basement high near Fuente |
| 10/4/02 23:30 | 10/5/02 5:30 | Transit to heat flow | **3.5** | 0.15 | 27.46 | |
| 10/5/02 3:00 | 10/5/02 9:00 | TF2-HF14 | **8.5** | 0.35 | 27.81 | buried basement high near outcrop Buquito |
| 10/5/02 11:30 | 10/5/02 17:30 | TF2-Core 19 | **3.0** | 0.13 | 27.94 | GC 58: adjacent to Buquito |
| 10/5/02 14:30 | 10/5/02 20:30 | Transit | **3.0** | 0.13 | 28.06 | |
| 10/5/02 17:30 | 10/5/02 23:30 | TF2-Core 20 and Hydrocast | **6.0** | 0.25 | 28.31 | HC2, GC 59: buried basement high west of Dorado |
| 10/5/02 23:30 | 10/6/02 5:30 | TF2-HF15 | **9.0** | 0.38 | 28.69 | buried basement high west of Dorado |
| 10/6/02 8:30 | 10/6/02 14:30 | TF2-Core 21 | **6.0** | 0.25 | 28.94 | GC 60, 61: buried basement high west of Dorado |
| 10/6/02 14:30 | 10/6/02 20:30 | transit to heat flow | **1.5** | 0.06 | 29.00 | |
| 10/6/02 16:00 | 10/6/02 22:00 | TF2-HF16 | **10.0** | 0.42 | 29.42 | HF 16: between Tengosed and Dorado |
| 10/7/02 2:00 | 10/7/02 8:00 | transit to coring | **4.5** | 0.19 | 29.60 | |
| 10/7/02 6:30 | 10/7/02 12:30 | TF2-Core 22 | **12.0** | 0.50 | 30.10 | GC 62, 63, 64, 65: area of high heat flow near trench |
| 10/7/02 18:30 | 10/8/02 0:30 | transit to heat flow | **2.5** | 0.10 | 30.21 | |
| 10/7/02 21:00 | 10/8/02 3:00 | TF2-HF17 | **22.0** | 0.92 | 31.13 | Looking for another transition, missed it! |
| 10/8/02 19:00 | 10/9/02 1:00 | Transit to Puerta Caldera | **12.0** | 0.50 | 31.63 | |
| 10/9/02 7:00 | 10/9/02 13:00 | Arrive in port | | | | |

Table III-1. Ticoflux 2 Seismic Lines: Start and End points of each line.

Line 1

| SHOT | TR | RP | TR ID | RANGE | DELAY | NSAMPS | SI | YR | DAY | HR | MIN | SEC |
|---|---|---|---|---|---|---|---|---|---|---|---|---|
| 1 | 1 | 1 | 0 1 | 0 | 0 | 7000 | 1000 | 2002 | 255 | 17 | 4 | 49 |
| 883 | 4 | 883 | 0 1 | 0 | 0 | 7000 | 1000 | 2002 | 255 | 19 | 32 | 52 |

Line 3

| SHOT | TR | RP | TR ID | RANGE | DELAY | NSAMPS | SI | YR | DAY | HR | MIN | SEC |
|---|---|---|---|---|---|---|---|---|---|---|---|---|
| 884 | 1 | 884 | 1 1 | 0 | 0 | 7000 | 1000 | 2002 | 255 | 21 | 5 | 10 |
| 1408 | 4 | 1408 | 4 1 | 0 | 0 | 7000 | 1000 | 2002 | 255 | 22 | 55 | 10 |

Line 5a

| SHOT | TR | RP | TR ID | RANGE | DELAY | NSAMPS | SI | YR | DAY | HR | MIN | SEC |
|---|---|---|---|---|---|---|---|---|---|---|---|---|
| 1409 | 1 | 1409 | 1 1 | 0 | 0 | 7000 | 1000 | 2002 | 255 | 22 | 55 | 56 |
| 3759 | 4 | 3759 | 4 1 | 0 | 0 | 7000 | 1000 | 2002 | 256 | 5 | 55 | 44 |

Line 5b

| SHOT | TR | RP | TR ID | RANGE | DELAY | NSAMPS | SI | YR | DAY | HR | MIN | SEC |
|---|---|---|---|---|---|---|---|---|---|---|---|---|
| 3760 | 1 | 3760 | 0 1 | 0 | 0 | 7000 | 1000 | 2002 | 256 | 6 | 17 | 41 |
| 3970 | 4 | 3970 | 0 1 | 0 | 0 | 7000 | 1000 | 2002 | 256 | 6 | 52 | 41 |

Line 6

| SHOT | TR | RP | TR ID | RANGE | DELAY | NSAMPS | SI | YR | DAY | HR | MIN | SEC |
|---|---|---|---|---|---|---|---|---|---|---|---|---|
| 3971 | 1 | 3971 | 0 1 | 0 | 0 | 7000 | 1000 | 2002 | 256 | 6 | 52 | 51 |
| 5046 | 4 | 5046 | 0 1 | 0 | 0 | 7000 | 1000 | 2002 | 256 | 10 | 9 | 35 |

Line 7

| SHOT | TR | RP | TR ID | RANGE | DELAY | NSAMPS | SI | YR | DAY | HR | MIN | SEC |
|---|---|---|---|---|---|---|---|---|---|---|---|---|
| 5047 | 1 | 5047 | 0 1 | 0 | 0 | 7000 | 1000 | 2002 | 256 | 10 | 9 | 45 |
| 5438 | 4 | 5438 | 0 1 | 0 | 0 | 7000 | 1000 | 2002 | 256 | 11 | 32 | 9 |

Line 8

| SHOT | TR | RP | TR ID | RANGE | DELAY | NSAMPS | SI | YR | DAY | HR | MIN | SEC |
|---|---|---|---|---|---|---|---|---|---|---|---|---|
| 5439 | 1 | 5439 | 1 1 | 0 | 0 | 7000 | 1000 | 2002 | 256 | 12 | 8 | 43 |
| 7713 | 4 | 7713 | 4 1 | 0 | 0 | 7000 | 1000 | 2002 | 256 | 18 | 37 | 37 |

Line 10

| SHOT | TR | RP | TR ID | RANGE | DELAY | NSAMPS | SI | YR | DAY | HR | MIN | SEC |
|---|---|---|---|---|---|---|---|---|---|---|---|---|
| 7714 | 1 | 7714 | 1 1 | 0 | 0 | 7000 | 1000 | 2002 | 256 | 19 | 27 | 27 |
| 10271 | 4 | 10271 | 4 1 | 0 | 0 | 7000 | 1000 | 2002 | 257 | 2 | 34 | 38 |

Line 12

| SHOT | TR | RP | TR ID | RANGE | DELAY | NSAMPS | SI | YR | DAY | HR | MIN | SEC |
|---|---|---|---|---|---|---|---|---|---|---|---|---|
| 10273 | 1 | 10273 | 1 1 | 0 | 0 | 7000 | 1000 | 2002 | 256 | 3 | 44 | 13 |
| 10977 | 4 | 10977 | 4 1 | 0 | 0 | 7000 | 1000 | 2002 | 256 | 5 | 41 | 33 |

Line 13

| SHOT | TR | RP | TR ID | RANGE | DELAY | NSAMPS | SI | YR | DAY | HR | MIN | SEC |
|---|---|---|---|---|---|---|---|---|---|---|---|---|

Table III-1. Ticoflux 2 Seismic Lines: Start and End points of each line.

| | | | | | | | | | | | | | | |
|---|---|---|---|---|---|---|---|---|---|---|---|---|---|---|
| 10978 | 1 | 10978 | 1 | 1 | 0 | 0 | 7000 | 1000 | 2002 | 256 | 5 | 41 | 43 |
| 12119 | 4 | 12119 | 4 | 1 | 0 | 0 | 7000 | 1000 | 2002 | 256 | 10 | 26 | 16 |

Line 14

| SHOT | TR | RP | TR | ID | RANGE | DELAY | NSAMPS | SI | YR | DAY | HR | MIN | SEC |
|---|---|---|---|---|---|---|---|---|---|---|---|---|---|
| 1 | 1 | 1 | 0 | 1 | 0 | 0 | 7000 | 1000 | 2002 | 259 | 10 | 38 | 55 |
| 1151 | 4 | 1151 | 0 | 1 | 0 | 0 | 7000 | 1000 | 2002 | 259 | 13 | 55 | 48 |

Line 15

| SHOT | TR | RP | TR | ID | RANGE | DELAY | NSAMPS | SI | YR | DAY | HR | MIN | SEC |
|---|---|---|---|---|---|---|---|---|---|---|---|---|---|
| 1159 | 1 | 2388 | 1 | 1 | -127 | 3000 | 4001 | 1000 | 2002 | 259 | 14 | 17 | 13 |
| 1408 | 4 | 2690 | 1 | 1 | 23 | 3000 | 4001 | 1000 | 2002 | 259 | 14 | 58 | 43 |

Line 16

| SHOT | TR | RP | TR | ID | RANGE | DELAY | NSAMPS | SI | YR | DAY | HR | MIN | SEC |
|---|---|---|---|---|---|---|---|---|---|---|---|---|---|
| 1471 | 1 | 2763 | 1 | 1 | -127 | 3000 | 4001 | 1000 | 2002 | 259 | 15 | 29 | 42 |
| 2204 | 4 | 3646 | 1 | 1 | 23 | 3000 | 4001 | 1000 | 2002 | 259 | 17 | 31 | 51 |

Line 17

| SHOT | TR | RP | TR | ID | RANGE | DELAY | NSAMPS | SI | YR | DAY | HR | MIN | SEC |
|---|---|---|---|---|---|---|---|---|---|---|---|---|---|
| 2205 | 1 | 3643 | 1 | 1 | -127 | 1000 | 6001 | 1000 | 2002 | 259 | 17 | 54 | 26 |
| 2991 | 4 | 4589 | 1 | 1 | 23 | 1000 | 6001 | 1000 | 2002 | 259 | 20 | 5 | 26 |

Line 18

| SHOT | TR | RP | TR | ID | RANGE | DELAY | NSAMPS | SI | YR | DAY | HR | MIN | SEC |
|---|---|---|---|---|---|---|---|---|---|---|---|---|---|
| 2992 | 1 | 4588 | 1 | 1 | -127 | 2000 | 4001 | 1000 | 2002 | 259 | 20 | 14 | 42 |
| 3794 | 4 | 5553 | 1 | 1 | 23 | 2000 | 4001 | 1000 | 2002 | 259 | 22 | 29 | 1 |

Line 19

| SHOT | TR | RP | TR | ID | RANGE | DELAY | NSAMPS | SI | YR | DAY | HR | MIN | SEC |
|---|---|---|---|---|---|---|---|---|---|---|---|---|---|
| 1 | 1 | 996 | 1 | 1 | -271 | 1000 | 6001 | 1000 | 2002 | 262 | 12 | 34 | 21 |
| 1016 | 4 | 2352 | 1 | 1 | -121 | 1000 | 6001 | 1000 | 2002 | 262 | 15 | 42 | 7 |

Line 21

| SHOT | TR | RP | TR | ID | RANGE | DELAY | NSAMPS | SI | YR | DAY | HR | MIN | SEC |
|---|---|---|---|---|---|---|---|---|---|---|---|---|---|
| 1117 | 1 | 3229 | 1 | 1 | -271 | 1000 | 6001 | 1000 | 2002 | 262 | 16 | 6 | 33 |
| 2523 | 4 | 6044 | 1 | 1 | -121 | 1000 | 6001 | 1000 | 2002 | 262 | 20 | 26 | 39 |

Line 22

| SHOT | TR | RP | TR | ID | RANGE | DELAY | NSAMPS | SI | YR | DAY | HR | MIN | SEC |
|---|---|---|---|---|---|---|---|---|---|---|---|---|---|
| 2524 | 1 | 4360 | 1 | 1 | -271 | 4000 | 3001 | 1000 | 2002 | 262 | 20 | 36 | 19 |
| 3690 | 4 | 5918 | 1 | 1 | -121 | 4000 | 3001 | 1000 | 2002 | 263 | 0 | 6 | 11 |

Line 23a

| SHOT | TR | RP | TR | ID | RANGE | DELAY | NSAMPS | SI | YR | DAY | HR | MIN | SEC |
|---|---|---|---|---|---|---|---|---|---|---|---|---|---|
| 3691 | 1 | 5915 | 1 | 1 | -271 | 1000 | 6001 | 1000 | 2002 | 263 | 0 | 6 | 22 |
| 4457 | 4 | 6939 | 1 | 1 | -121 | 1000 | 6001 | 1000 | 2002 | 263 | 2 | 24 | 14 |

Table III-1. Ticoflux 2 Seismic Lines: Start and End points of each line.

Line 23b

| SHOT | TR | RP | TR ID | RANGE | DELAY | NSAMPS | SI | YR | DAY | HR | MIN | SEC |
|---|---|---|---|---|---|---|---|---|---|---|---|---|
| 4459 | 1 | 6939 | 1 1 | -271 | 2500 | 4001 | 1000 | 2002 | 263 | 4 | 56 | 41 |
| 5275 | 4 | 8030 | 1 1 | -121 | 2500 | 4001 | 1000 | 2002 | 263 | 7 | 23 | 32 |

Line 24

| SHOT | TR | RP | TR ID | RANGE | DELAY | NSAMPS | SI | YR | DAY | HR | MIN | SEC |
|---|---|---|---|---|---|---|---|---|---|---|---|---|
| 5276 | 1 | 8029 | 1 1 | -271 | 3000 | 4001 | 1000 | 2002 | 263 | 7 | 34 | 48 |
| 6268 | 4 | 9355 | 1 1 | -121 | 3000 | 4001 | 1000 | 2002 | 263 | 10 | 33 | 21 |

Line 25

| SHOT | TR | RP | TR ID | RANGE | DELAY | NSAMPS | SI | YR | DAY | HR | MIN | SEC |
|---|---|---|---|---|---|---|---|---|---|---|---|---|
| 6269 | 1 | 9352 | 1 1 | -271 | 3000 | 4001 | 1000 | 2002 | 263 | 10 | 47 | 4 |
| 6491 | 4 | 9651 | 1 1 | -121 | 3000 | 4001 | 1000 | 2002 | 263 | 11 | 27 | 1 |

Line 26

| SHOT | TR | RP | TR ID | RANGE | DELAY | NSAMPS | SI | YR | DAY | HR | MIN | SEC |
|---|---|---|---|---|---|---|---|---|---|---|---|---|
| 6492 | 1 | 9651 | 1 1 | -271 | 1000 | 6001 | 1000 | 2002 | 263 | 11 | 37 | 3 |
| 7577 | 4 | 11100 | 1 1 | -121 | 1000 | 6001 | 1000 | 2002 | 263 | 14 | 52 | 20 |

Line 27

| SHOT | TR | RP | TR ID | RANGE | DELAY | NSAMPS | SI | YR | DAY | HR | MIN | SEC |
|---|---|---|---|---|---|---|---|---|---|---|---|---|
| 70 | 1 | 1088 | 1 1 | -271 | 1000 | 6001 | 1000 | 2002 | 267 | 4 | 48 | 10 |
| 693 | 4 | 1922 | 1 1 | -121 | 1000 | 6001 | 1000 | 2002 | 267 | 6 | 40 | 19 |

Line 28

| SHOT | TR | RP | TR ID | RANGE | DELAY | NSAMPS | SI | YR | DAY | HR | MIN | SEC |
|---|---|---|---|---|---|---|---|---|---|---|---|---|
| 694 | 1 | 1920 | 1 1 | -271 | 1000 | 6001 | 1000 | 2002 | 267 | 6 | 54 | 44 |
| 2056 | 4 | 3739 | 1 1 | -121 | 1000 | 6001 | 1000 | 2002 | 267 | 10 | 59 | 53 |

Line 29

| SHOT | TR | RP | TR ID | RANGE | DELAY | NSAMPS | SI | YR | DAY | HR | MIN | SEC |
|---|---|---|---|---|---|---|---|---|---|---|---|---|
| 2057 | 1 | 3737 | 1 1 | -271 | 3000 | 4001 | 1000 | 2002 | 267 | 11 | 46 | 7 |
| 3611 | 4 | 5812 | 1 1 | -121 | 3000 | 4001 | 1000 | 2002 | 267 | 16 | 25 | 49 |

Line 30

| SHOT | TR | RP | TR ID | RANGE | DELAY | NSAMPS | SI | YR | DAY | HR | MIN | SEC |
|---|---|---|---|---|---|---|---|---|---|---|---|---|
| 3612 | 1 | 5810 | 1 1 | -271 | 3000 | 4001 | 1000 | 2002 | 267 | 16 | 32 | 10 |
| 4159 | 4 | 6542 | 1 1 | -121 | 3000 | 4001 | 1000 | 2002 | 267 | 18 | 10 | 37 |

Line 31

| SHOT | TR | RP | TR ID | RANGE | DELAY | NSAMPS | SI | YR | DAY | HR | MIN | SEC |
|---|---|---|---|---|---|---|---|---|---|---|---|---|
| 4160 | 1 | 6541 | 1 1 | -271 | 1000 | 6001 | 1000 | 2002 | 267 | 18 | 16 | 36 |
| 4942 | 4 | 7587 | 1 1 | -121 | 1000 | 6001 | 1000 | 2002 | 267 | 20 | 37 | 21 |

Line 32

Table III-1. Ticoflux 2 Seismic Lines: Start and End points of each line.

| SHOT | TR | RP | TR ID | RANGE | DELAY | NSAMPS | SI | YR | DAY | HR | MIN | SEC |
|---|---|---|---|---|---|---|---|---|---|---|---|---|
| 1 | 1 | 996 | 1 1 | -271 | 1000 | 6001 | 1000 | 2002 | 271 | 2 | 28 | 47 |
| 489 | 4 | 1650 | 1 1 | -121 | 1000 | 6001 | 1000 | 2002 | 271 | 3 | 56 | 37 |

Line 33

| SHOT | TR | RP | TR ID | RANGE | DELAY | NSAMPS | SI | YR | DAY | HR | MIN | SEC |
|---|---|---|---|---|---|---|---|---|---|---|---|---|
| 490 | 1 | 1648 | 1 1 | -271 | 1000 | 6001 | 1000 | 2002 | 271 | 4 | 26 | 52 |
| 1940 | 4 | 3584 | 1 1 | -121 | 1000 | 6001 | 1000 | 2002 | 271 | 8 | 47 | 51 |

Line 34

| SHOT | TR | RP | TR ID | RANGE | DELAY | NSAMPS | SI | YR | DAY | HR | MIN | SEC |
|---|---|---|---|---|---|---|---|---|---|---|---|---|
| 1941 | 1 | 3582 | 1 1 | -271 | 3000 | 4001 | 1000 | 2002 | 271 | 8 | 59 | 48 |
| 2093 | 4 | 3788 | 1 1 | -121 | 3000 | 4001 | 1000 | 2002 | 271 | 9 | 27 | 10 |

Line 35

| SHOT | TR | RP | TR ID | RANGE | DELAY | NSAMPS | SI | YR | DAY | HR | MIN | SEC |
|---|---|---|---|---|---|---|---|---|---|---|---|---|
| 2094 | 1 | 3786 | 1 1 | -271 | 4000 | 3001 | 1000 | 2002 | 271 | 9 | 41 | 24 |
| 3607 | 4 | 5806 | 1 1 | -121 | 4000 | 3001 | 1000 | 2002 | 271 | 14 | 13 | 44 |

Line 36

| SHOT | TR | RP | TR ID | RANGE | DELAY | NSAMPS | SI | YR | DAY | HR | MIN | SEC |
|---|---|---|---|---|---|---|---|---|---|---|---|---|
| 3608 | 1 | 5805 | 1 1 | -271 | 3500 | 3001 | 1000 | 2002 | 271 | 14 | 16 | 54 |
| 4862 | 4 | 7480 | 1 1 | -121 | 3500 | 3001 | 1000 | 2002 | 271 | 18 | 2 | 47 |

Line 37

| SHOT | TR | RP | TR ID | RANGE | DELAY | NSAMPS | SI | YR | DAY | HR | MIN | SEC |
|---|---|---|---|---|---|---|---|---|---|---|---|---|
| 1 | 1 | 996 | 1 1 | -271 | 4000 | 3001 | 1000 | 2002 | 274 | 15 | 11 | 4 |
| 816 | 4 | 2086 | 1 1 | -121 | 4000 | 3001 | 1000 | 2002 | 274 | 17 | 38 | 29 |

Line 38a

| SHOT | TR | RP | TR ID | RANGE | DELAY | NSAMPS | SI | YR | DAY | HR | MIN | SEC |
|---|---|---|---|---|---|---|---|---|---|---|---|---|
| 1036 | 1 | 2376 | 1 1 | -271 | 1000 | 6001 | 1000 | 2002 | 274 | 18 | 21 | 4 |
| 1990 | 4 | 3651 | 1 1 | -121 | 1000 | 6001 | 1000 | 2002 | 274 | 21 | 12 | 57 |

Line 38b

| SHOT | TR | RP | TR ID | RANGE | DELAY | NSAMPS | SI | YR | DAY | HR | MIN | SEC |
|---|---|---|---|---|---|---|---|---|---|---|---|---|
| 1991 | 1 | 3649 | 1 1 | -271 | 1000 | 6001 | 1000 | 2002 | 274 | 21 | 17 | 11 |
| 2145 | 4 | 3857 | 1 1 | -121 | 1000 | 6001 | 1000 | 2002 | 274 | 21 | 44 | 54 |

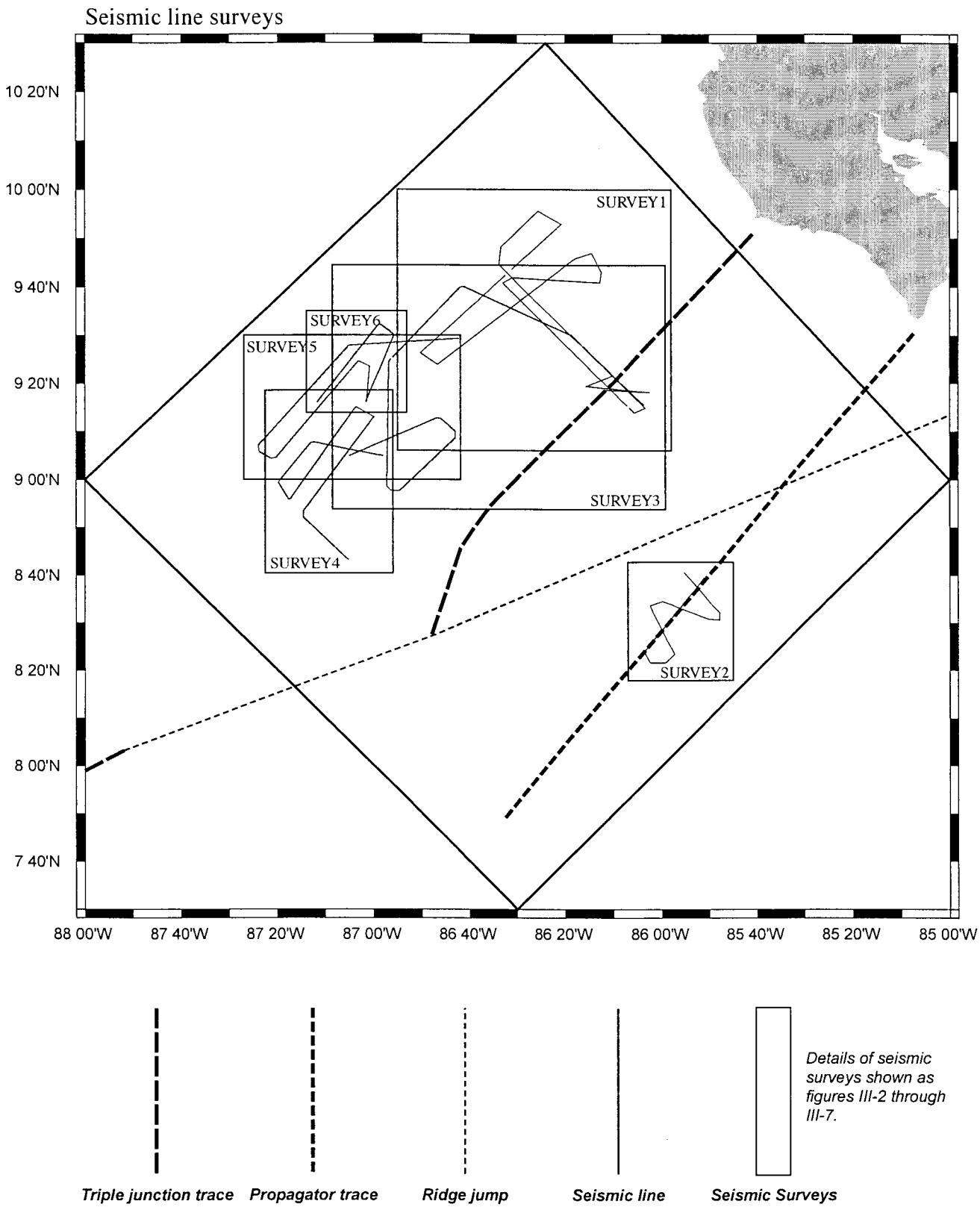
Seismic line surveys
10 20'N
10 00'N
9 40'N
9 20'N
9 00'N
8 40'N
8 20'N
8 00'N
7 40'N
88 00'W
87 40'W
87 20'W
87 00'W
86 40'W
86 20'W
86 00'W
85 40'W
85 20'W
85 00'W
SURVEY1
SURVEY2
SURVEY3
SURVEY4
SURVEY5
SURVEY6
Triple junction trace
Propagator trace
Ridge jump
Seismic line
Seismic Surveys
Details of seismic surveys shown as figures III-2 through III-7.

Figure III-1

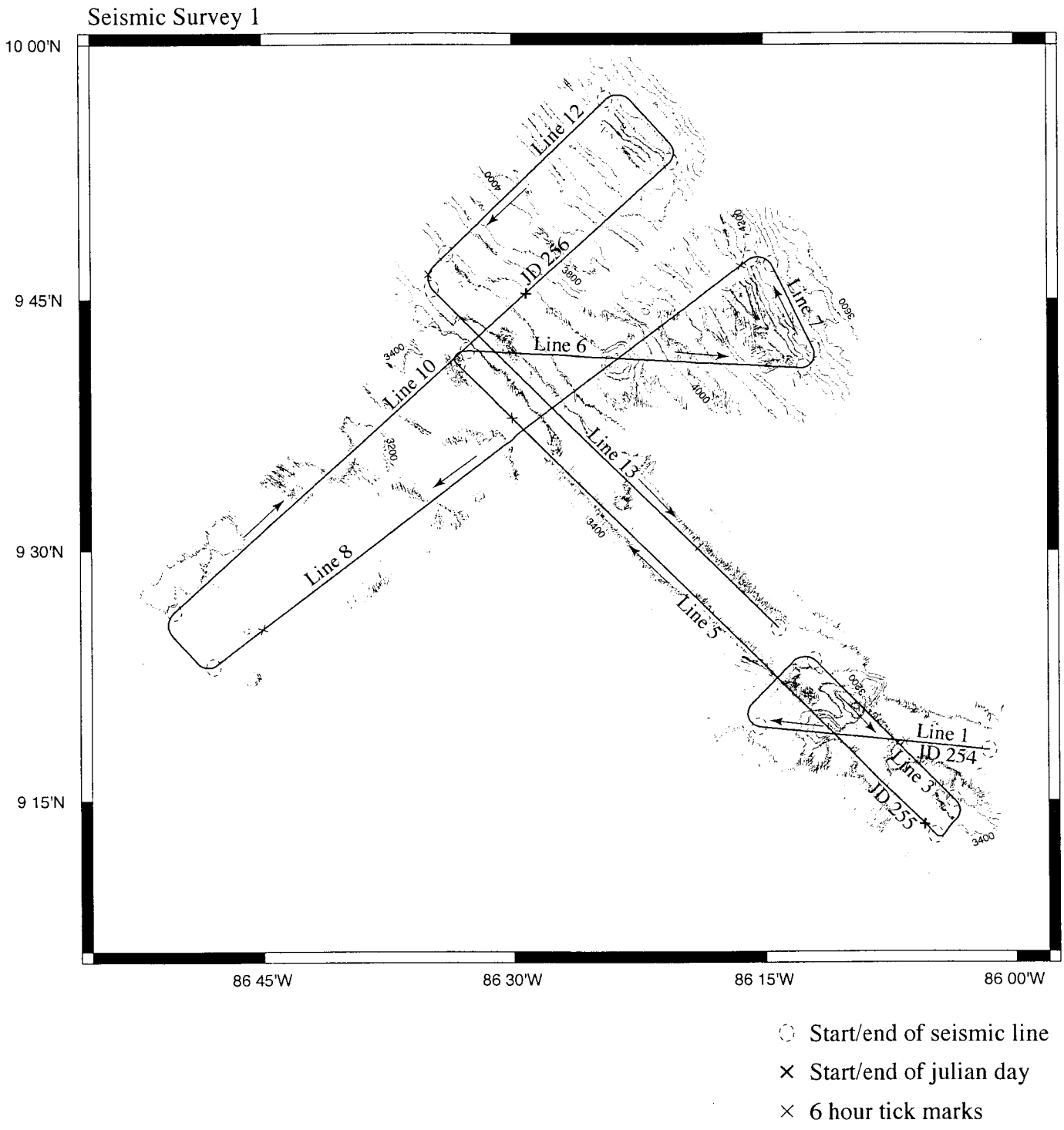
Seismic Survey 1
10 00'N
9 45'N
9 30'N
9 15'N
86 45'W
86 30'W
86 15'W
86 00'W
Line 12
JD 256
Line 6
Line 7
Line 10
Line 13
Line 8
Line 5
Line 1
JD 254
Line 3
JD 255
4000
3900
3600
3400
3200
Start/end of seismic line
Start/end of julian day
6 hour tick marks

Figure III-2

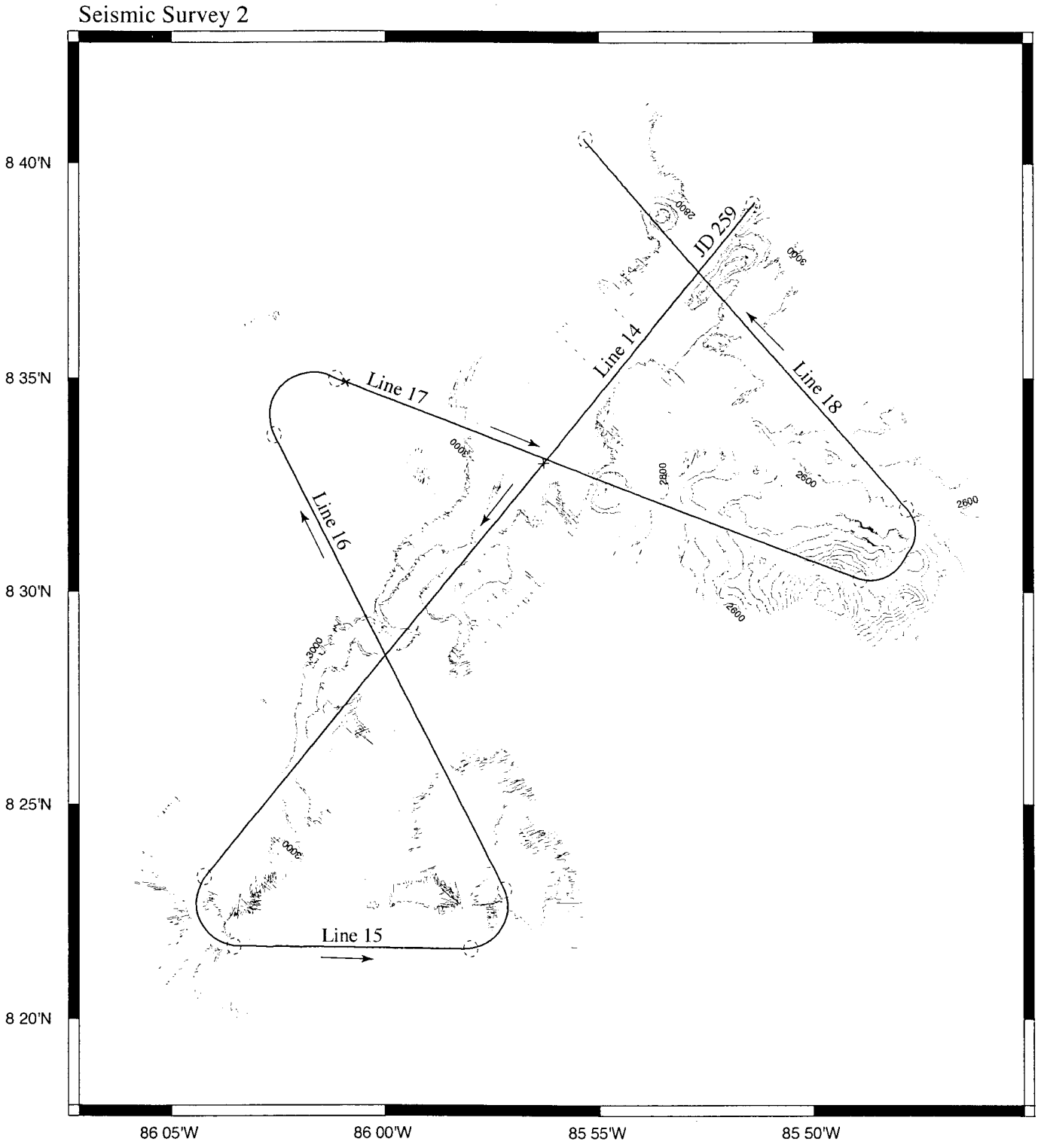
Seismic Survey 2
8 40'N
8 35'N
8 30'N
8 25'N
8 20'N
86 05'W
86 00'W
85 55'W
85 50'W
JD 259
Line 14
Line 15
Line 16
Line 17
Line 18
2800
3000
2600
Start/end of seismic line
Start/end of julian day
6 hour tick marks

Figure III-3

Seismic Survey 3

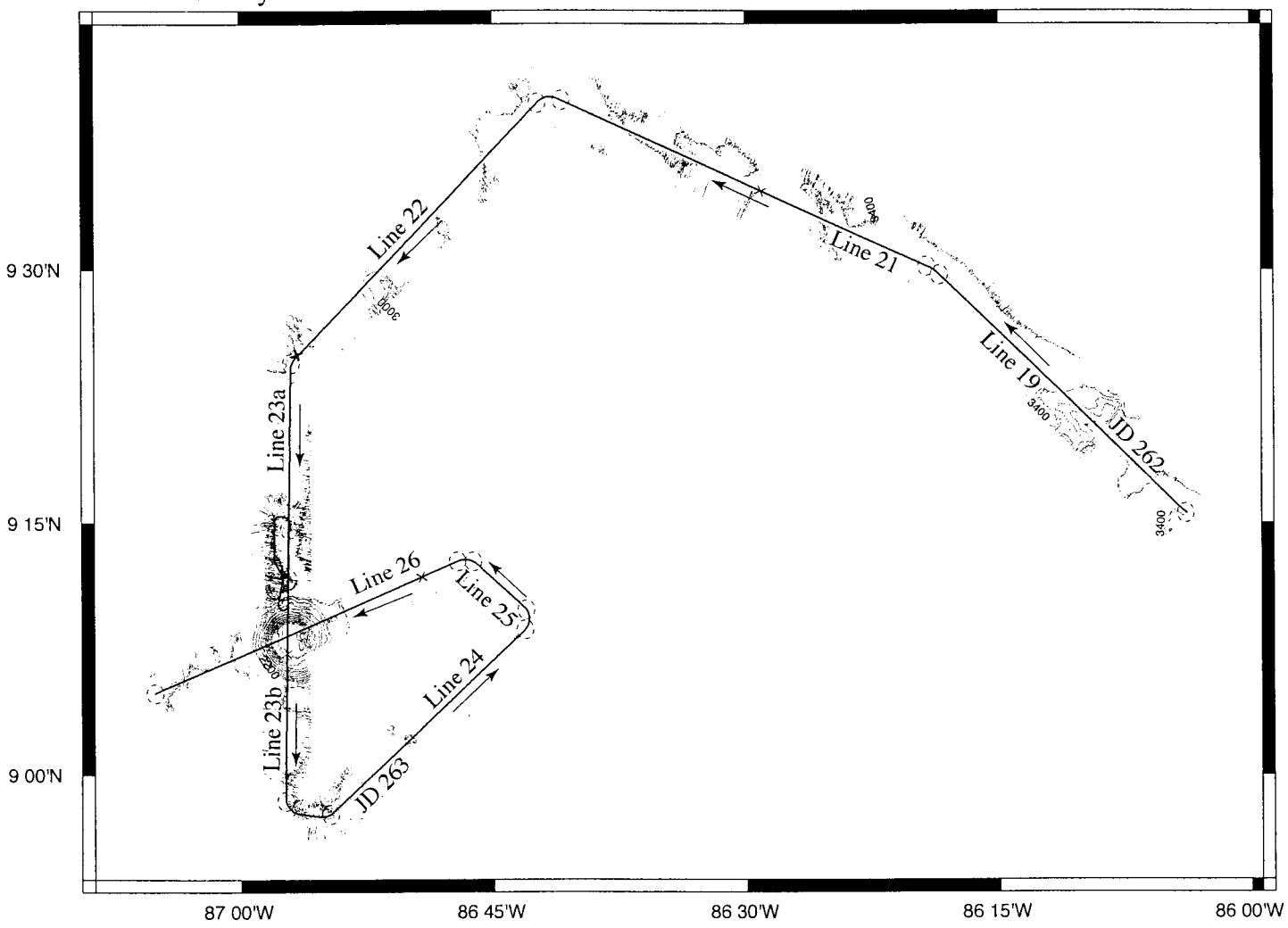


Start/end of seismic line

× Start/end of julian day

× 6 hour tick marks

Figure III-4

Seismic Survey 4

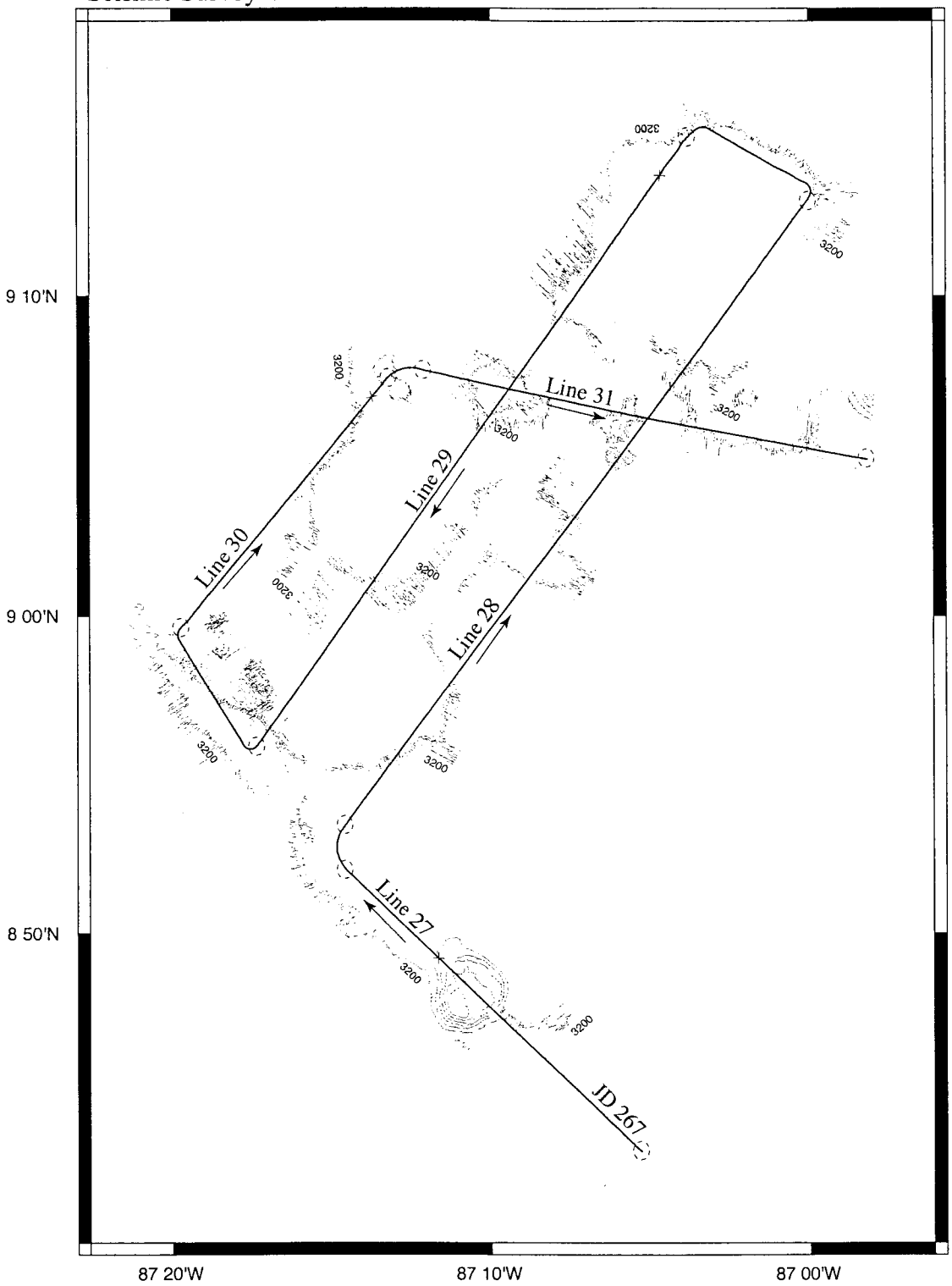


○ Start/end of seismic line

× Start/end of julian day

× 6 hour tick marks

Figure III-5

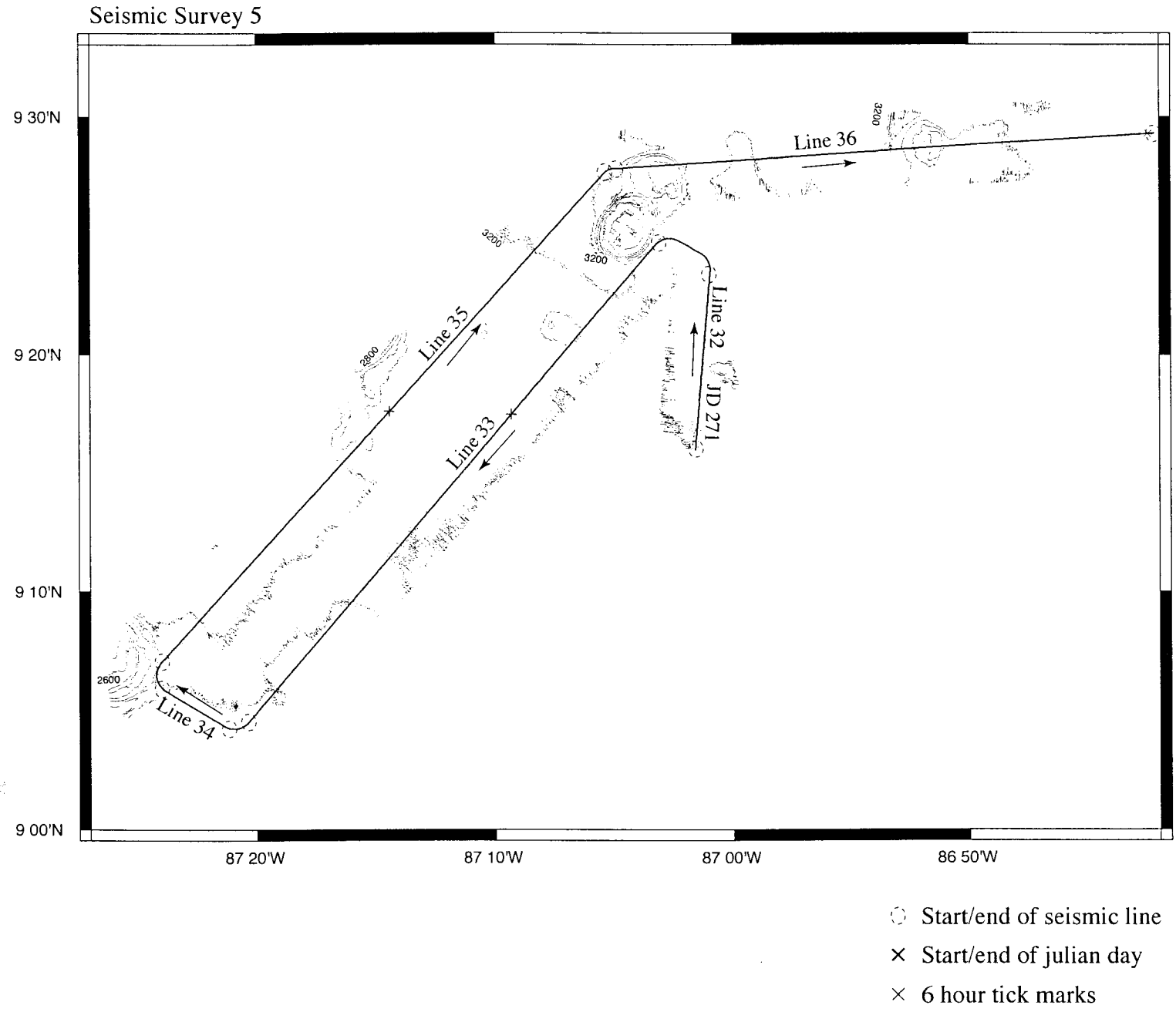
Seismic Survey 5
9 30'N
9 20'N
9 10'N
9 00'N
87 20'W
87 10'W
87 00'W
86 50'W
Line 36
Line 35
Line 33
Line 32
JD 271
Line 34
3200
3200
3200
2800
2600
Start/end of seismic line
Start/end of julian day
6 hour tick marks

Figure III-6

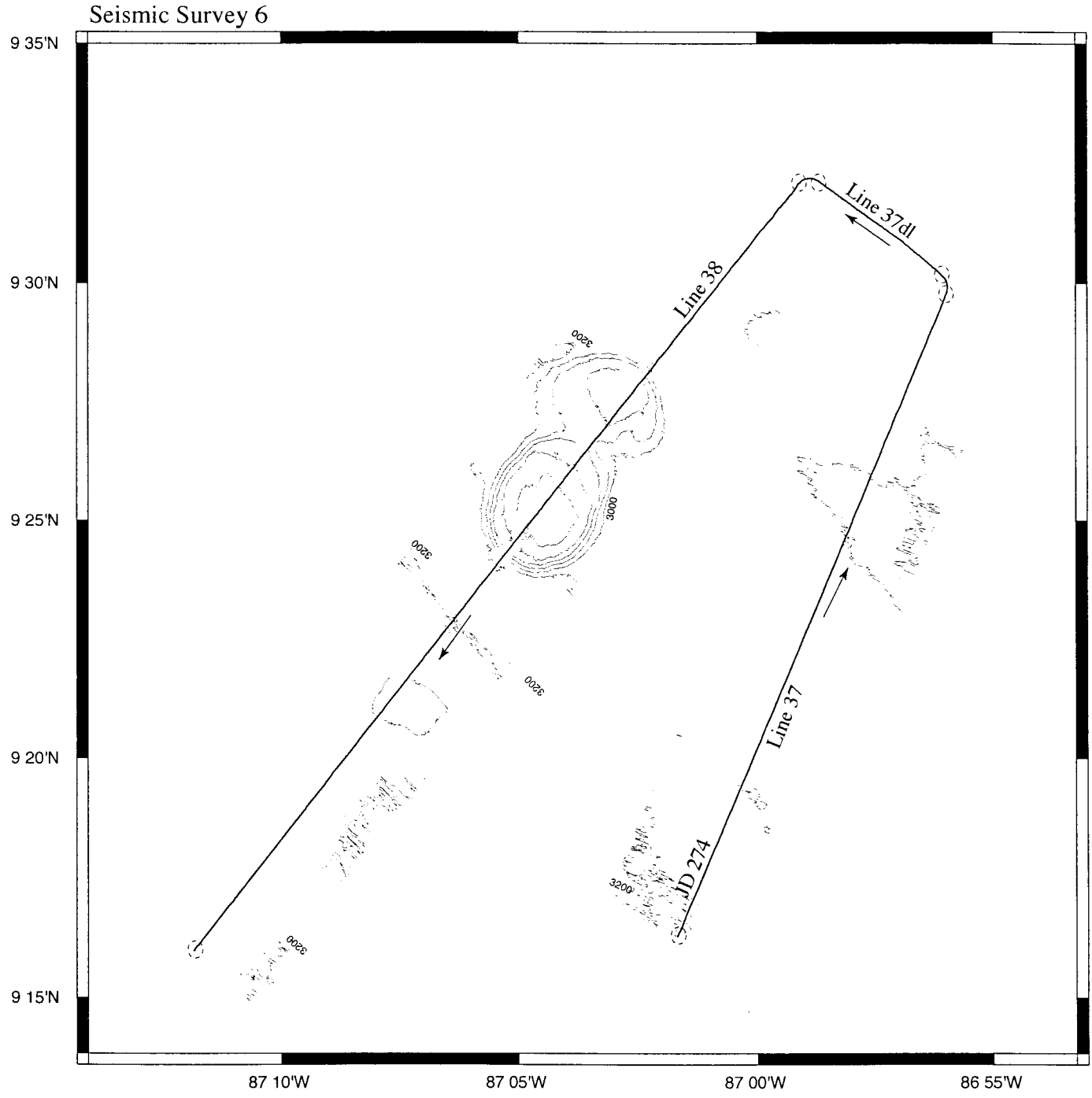
Seismic Survey 6
9 35'N
9 30'N
9 25'N
9 20'N
9 15'N
87 10'W
87 05'W
87 00'W
86 55'W
Line 37dl
Line 38
Line 37
JD 274
3200
3000
Start/end of seismic line
Start/end of julian day
6 hour tick marks

Figure III-7

Seismic Line TF1-11
Heat Flow TF2-01

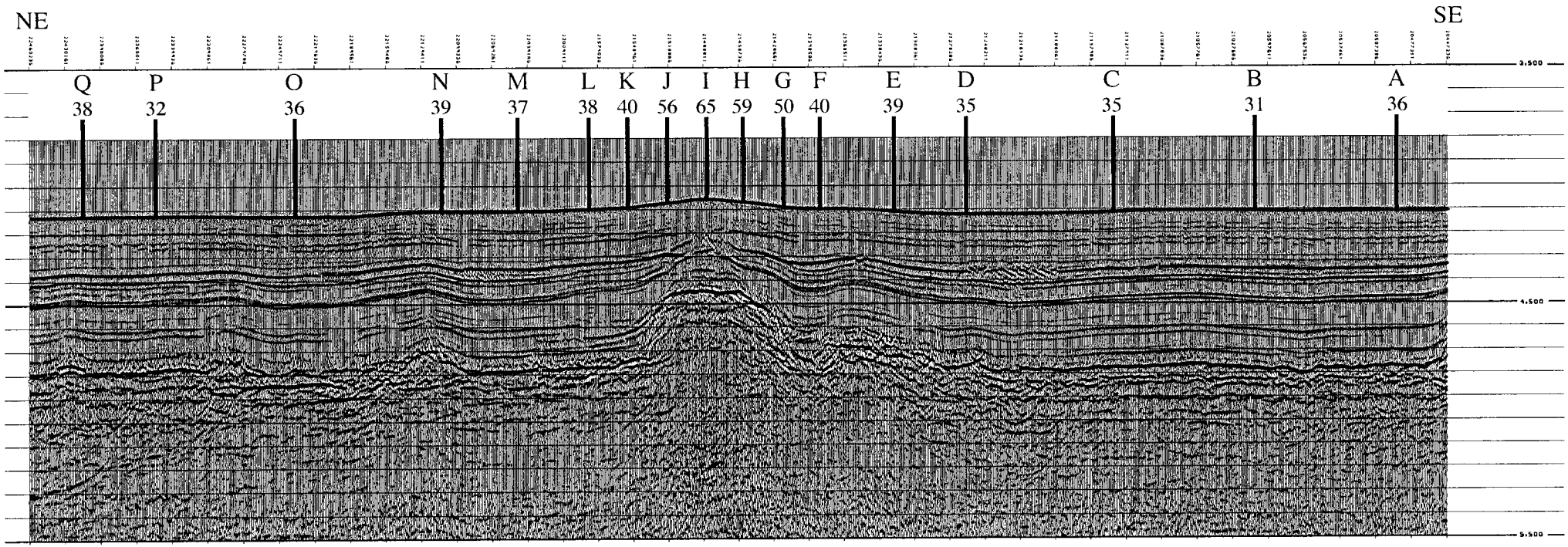


*(Seismic Line annotation GMT HHMM, RP # - 20000)*
*(Heat Flow Q values in mW/m²)*

Figure III-8

Seismic Line TF2-10
Heat Flow TF2-02

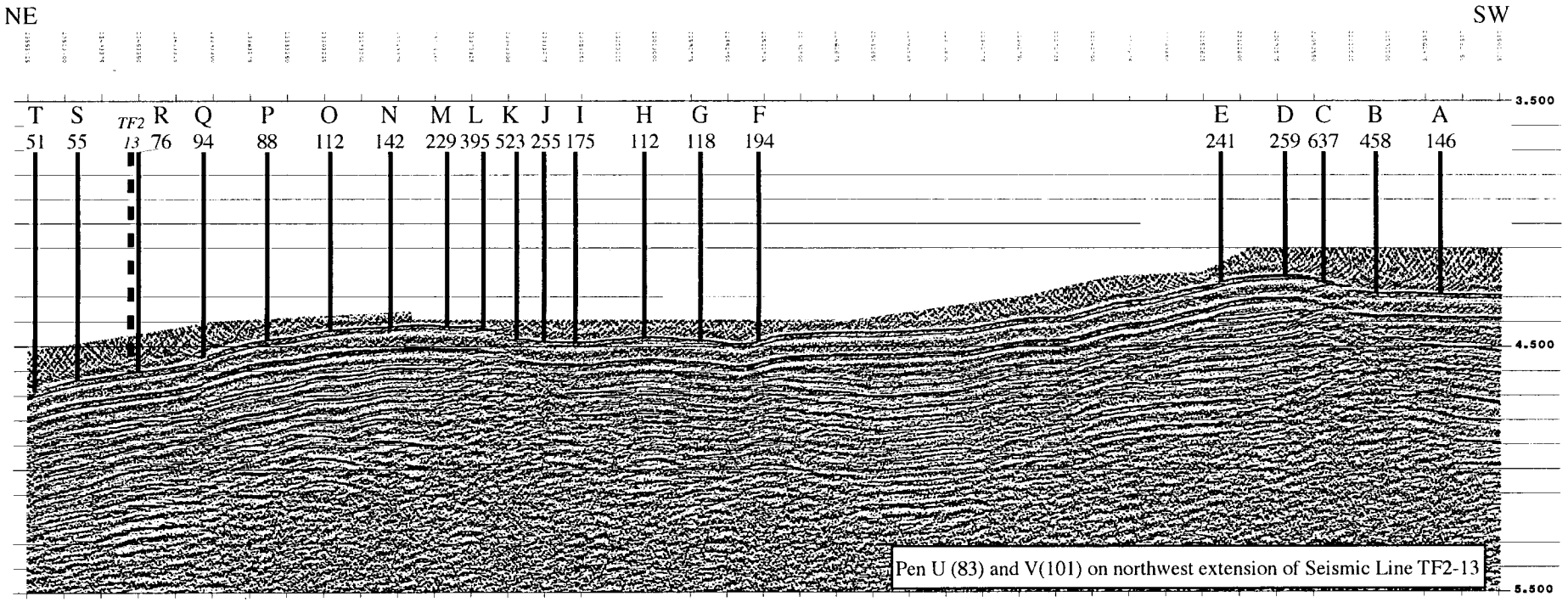


*(Seismic Line annotation GMT HHMM, RP # - 10000)*
*(Heat Flow Q values in mW/m²)*

Figure III-9

Seismic Line TF1-13
Heat Flow TF2-03

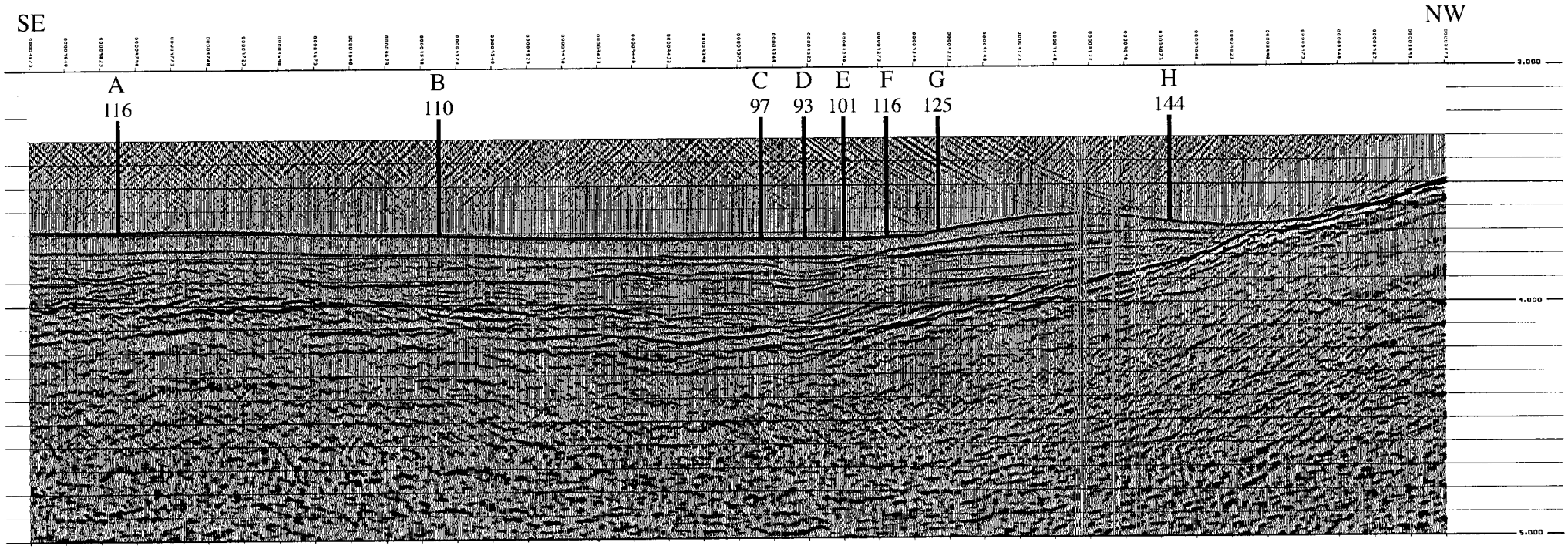


*(Seismic Line annotation RP # - 20000)*
*(Heat Flow Q values in mW/m²)*

Figure III-10

Seismic Line TF2-18
Heat Flow TF2-04

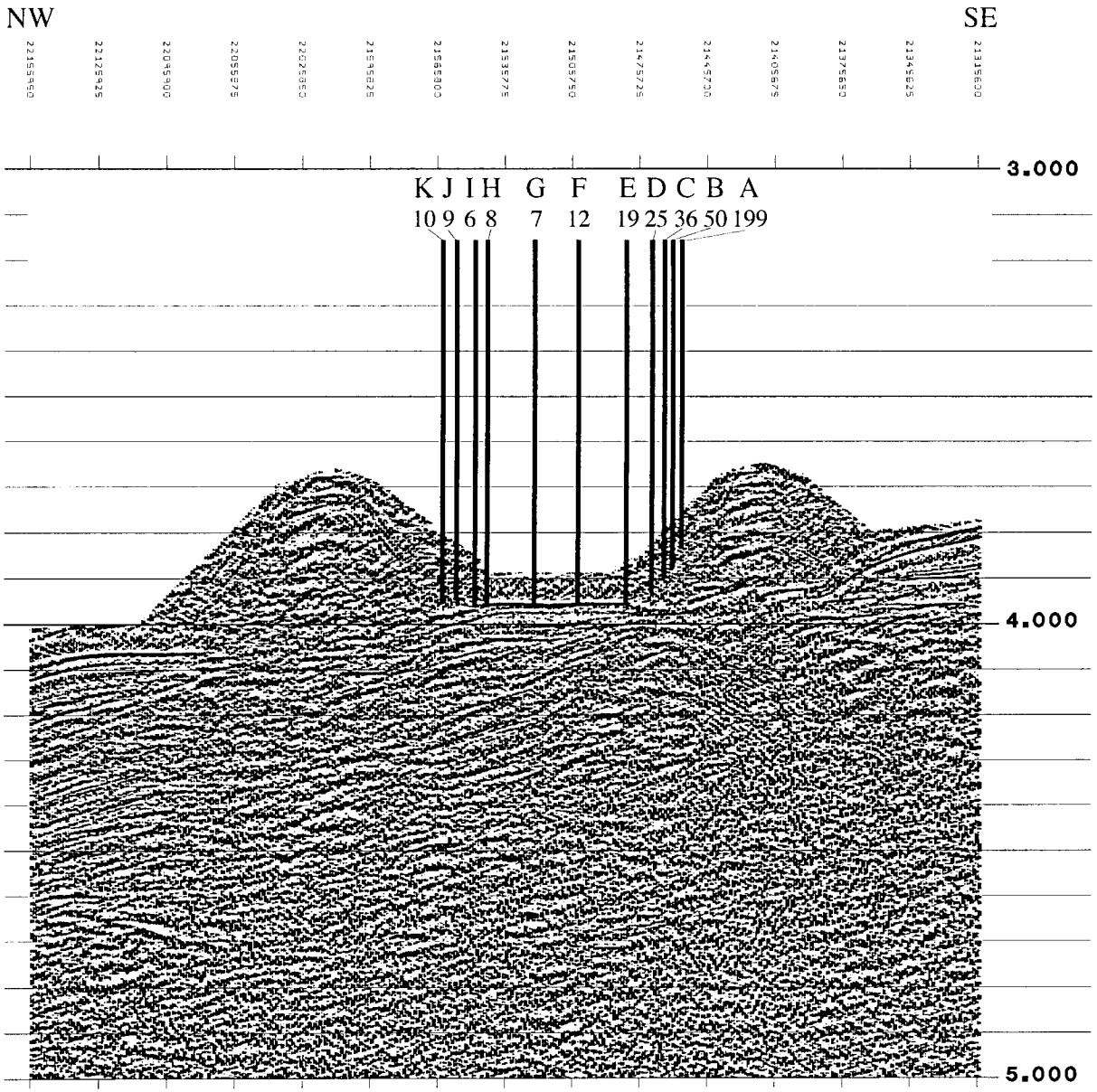


*(Seismic Line annotation GMT HHMM, RP #)*
*(Heat Flow Q values in mW/m²)*

Figure III-11

Seismic Line TF2-23b
Heat Flow TF2-05

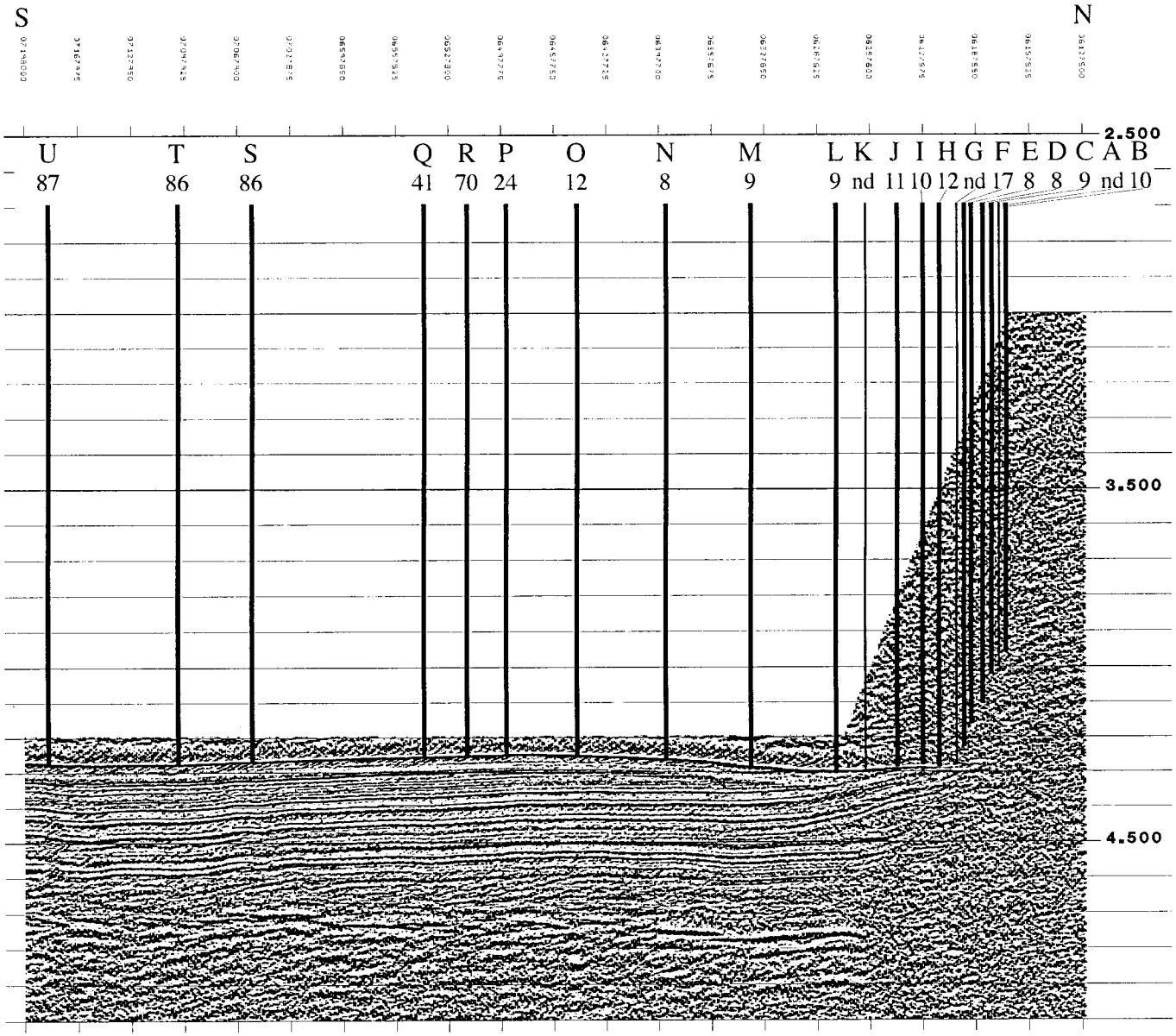


*(Seismic Line annotation GMT HHMM, RP #)*
*(Heat Flow Q values in mW/m² or no data)*

Figure III-12

Seismic Line TF1-04
Heat Flow TF2-06

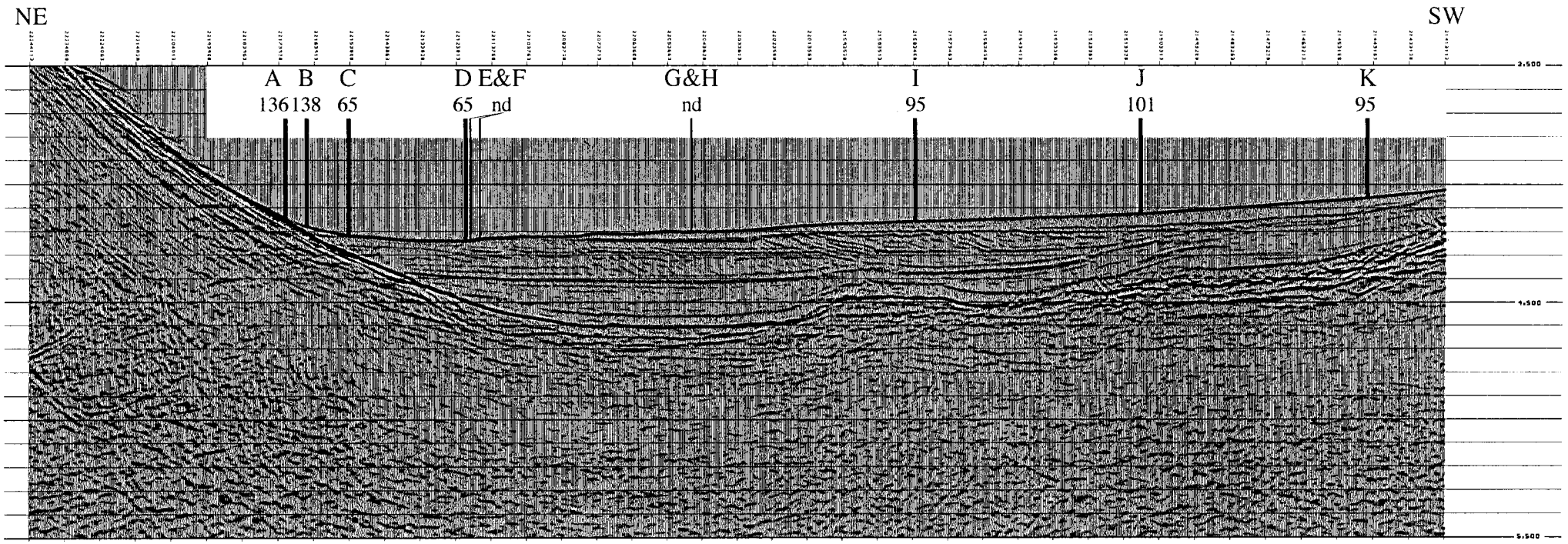


*(Seismic Line annotation GMT HHMM, RP #)*
*(Heat Flow Q values in mW/m² or no data )*

Figure III-13

Seismic Line TF2-26 & TF2-31
Heat Flow TF2-07

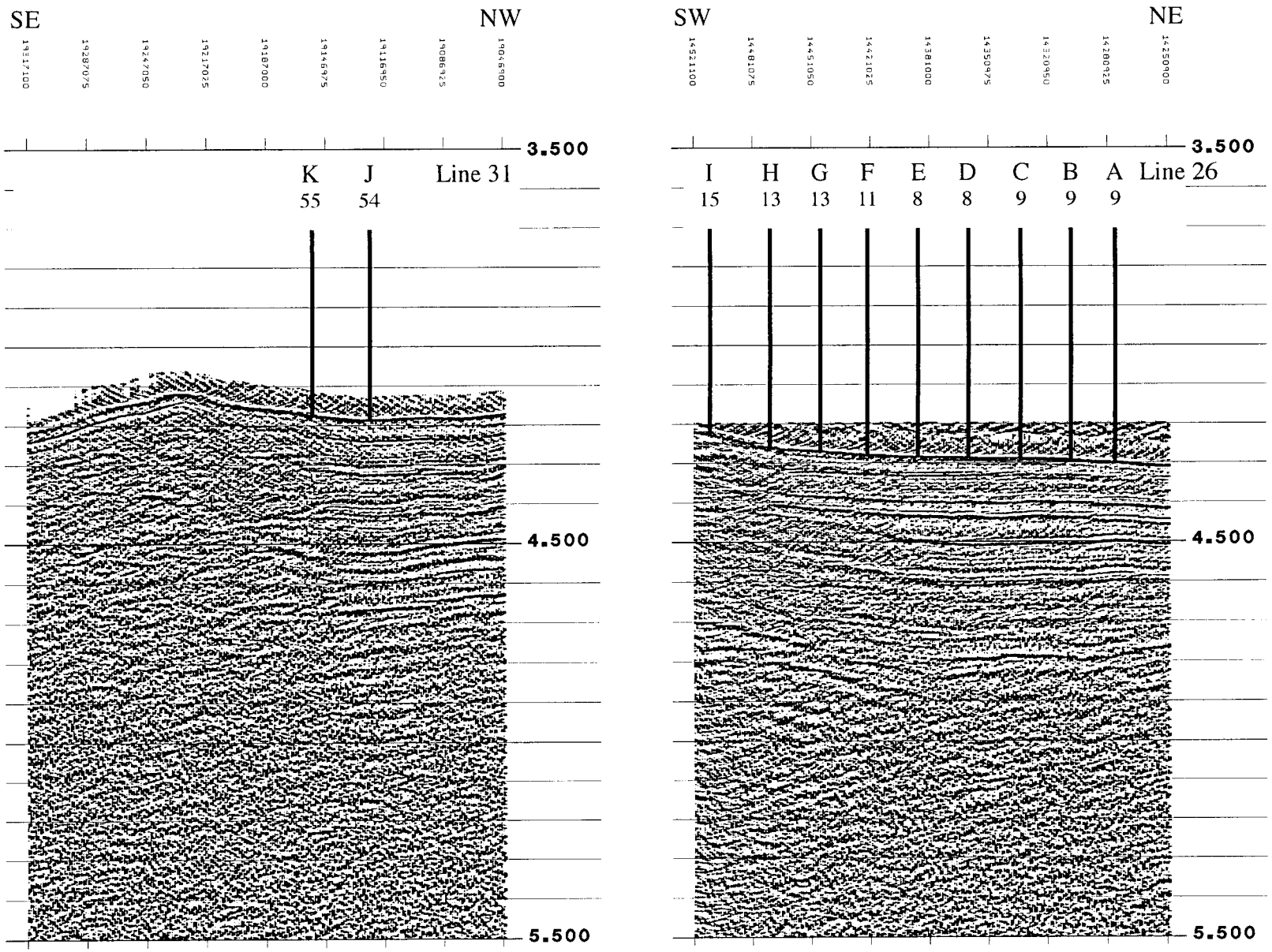


*(Seismic Line annotation GMT HHMM, RP #)*
*(Heat Flow Q values in mW/m²)*

*(Seismic Line annotation GMT HHMM, RP # - 10000)*
*(Heat Flow Q values in mW/m²)*

Figure III-14

Seismic Line TF2-28
Heat Flow TF2-08

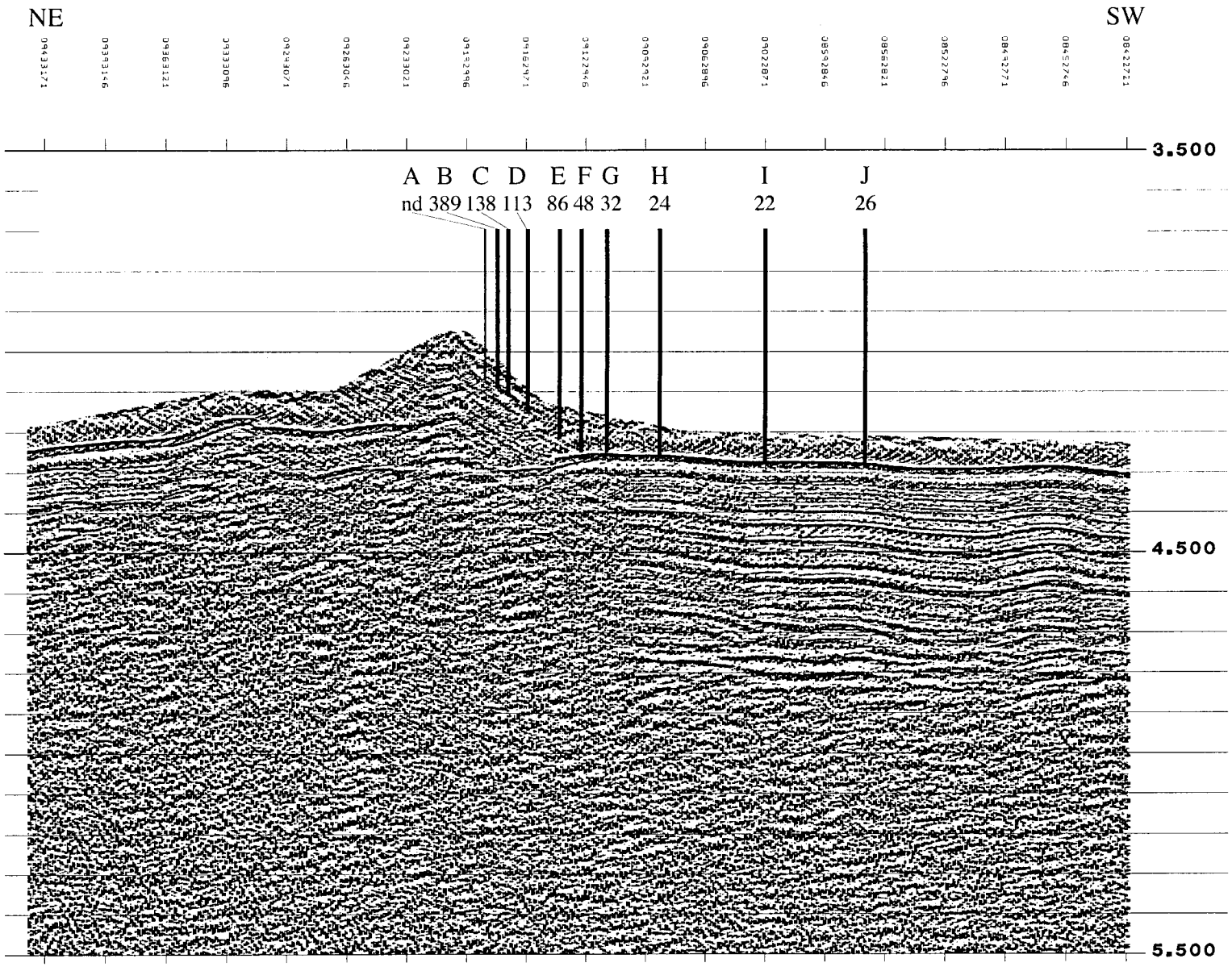


*(Seismic Line annotation GMT HHMM, RP #)*
*(Heat Flow Q values in mW/m² or no data)*

Figure III-15

Seismic Line TF1-04
Heat Flow TF2-09

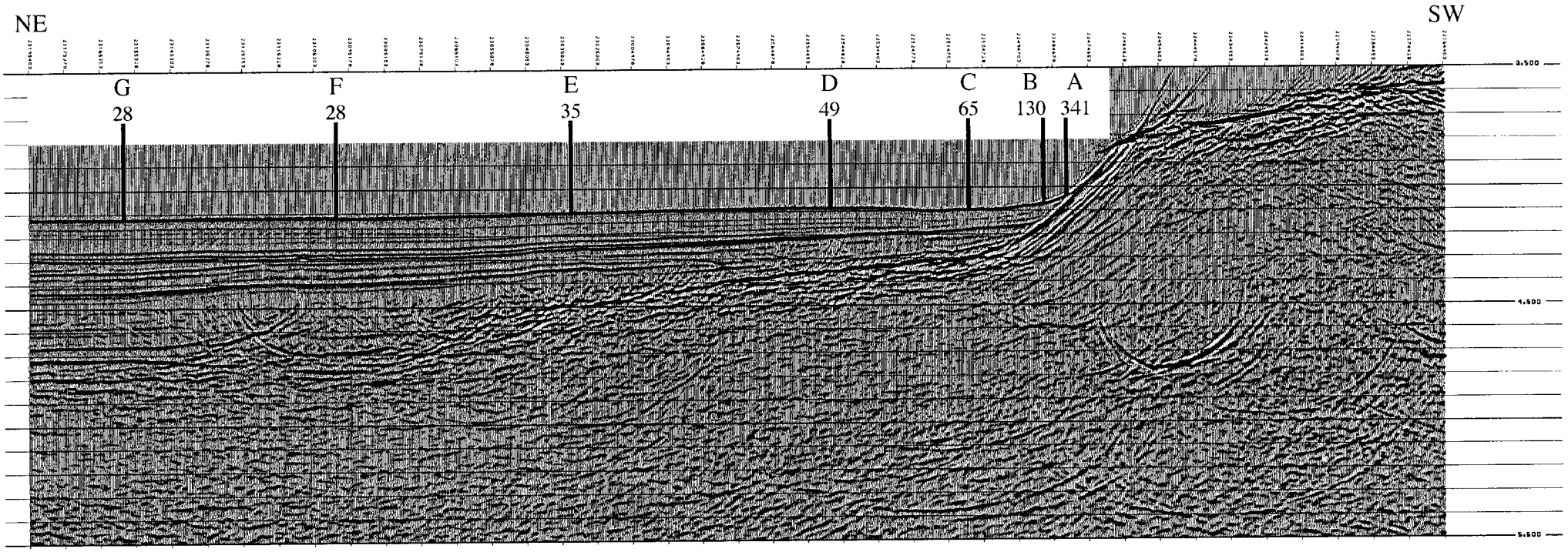


*(Seismic Line annotation GMT HHMM, RP #)*
*(Heat Flow Q values in mW/m²)*

Figure III-16

Seismic Line TF2-5a
Heat Flow TF2-10

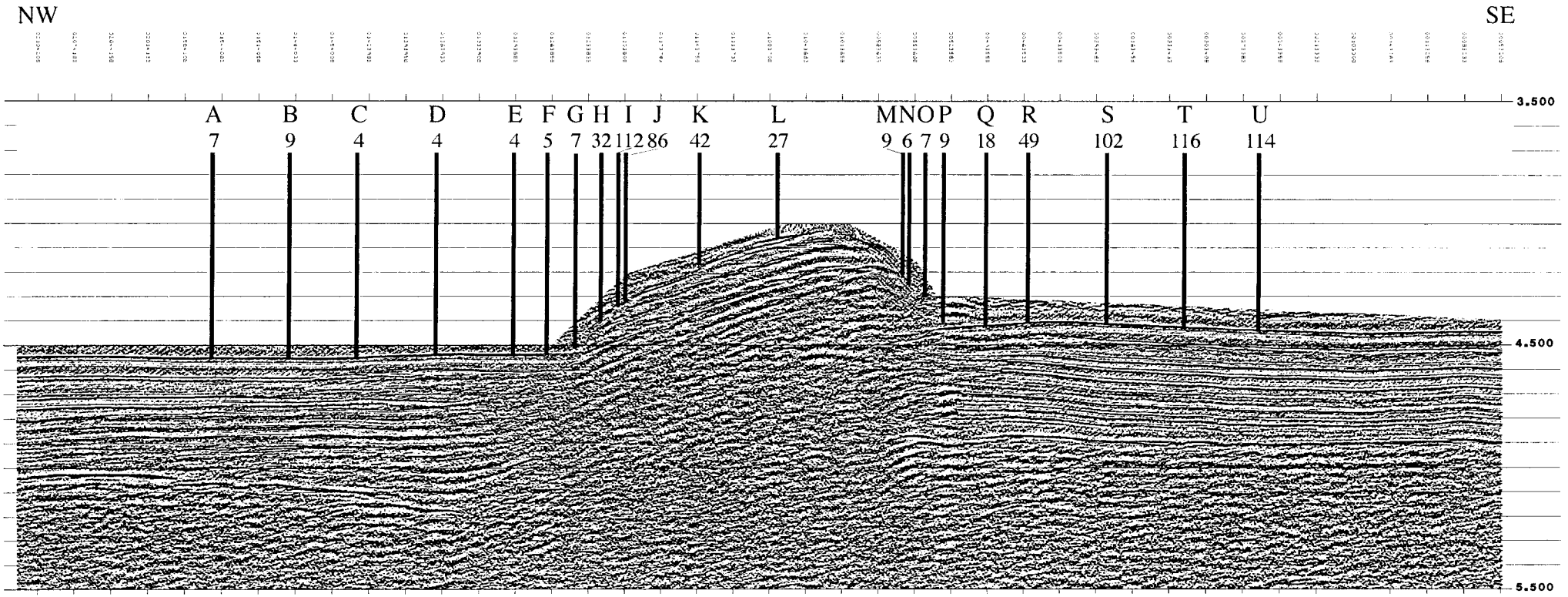


*(Seismic Line annotation GMT HHMM, RP #)*
*(Heat Flow Q values in mW/m²)*

Figure III-17

Seismic Line TF2-25
Heat Flow TF2-11

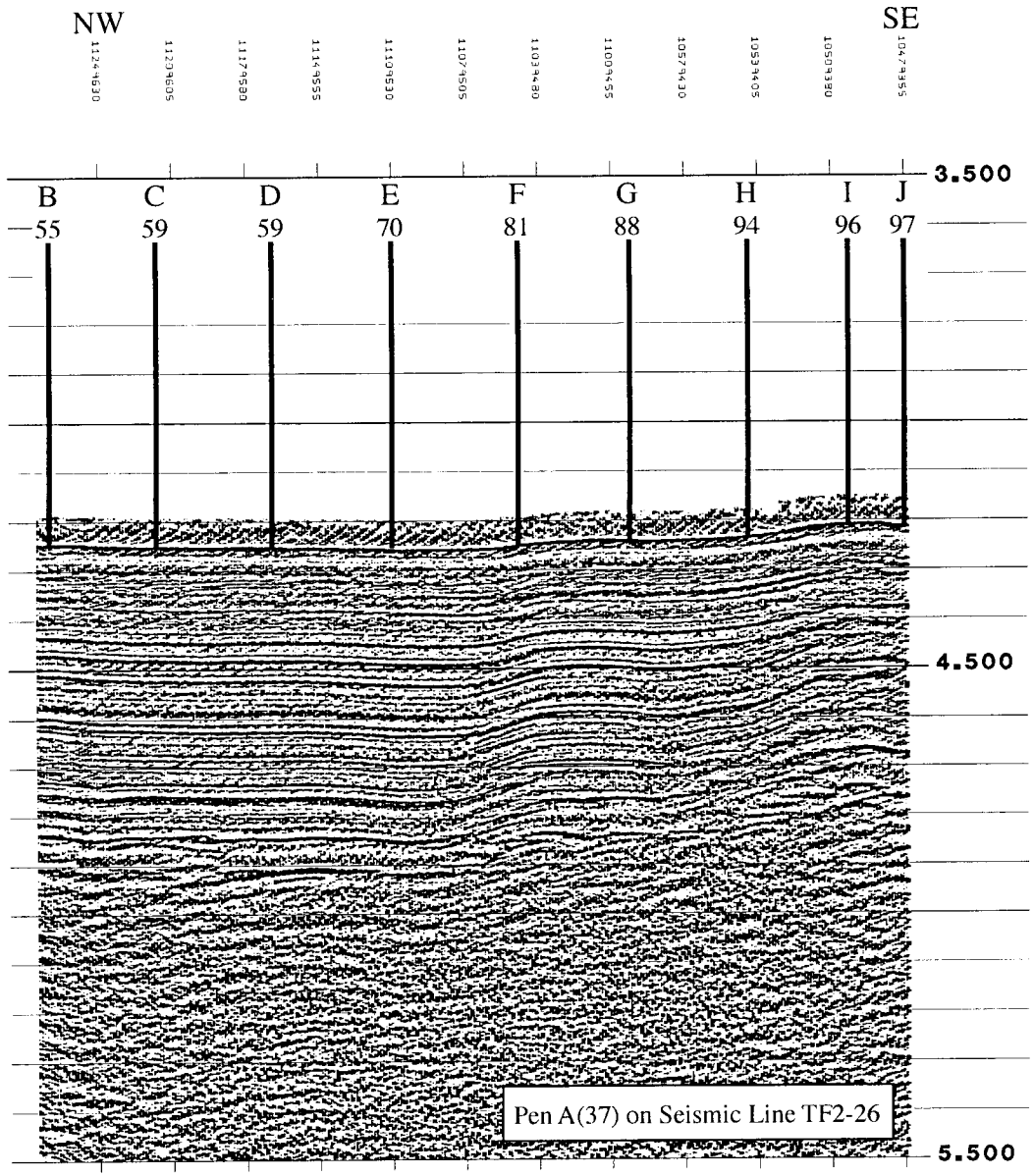


*(Seismic Line annotation RP #)*
*(Heat Flow Q values in mW/m²)*

Figure III-18

Seismic Line TF2-27
Heat Flow TF2-12

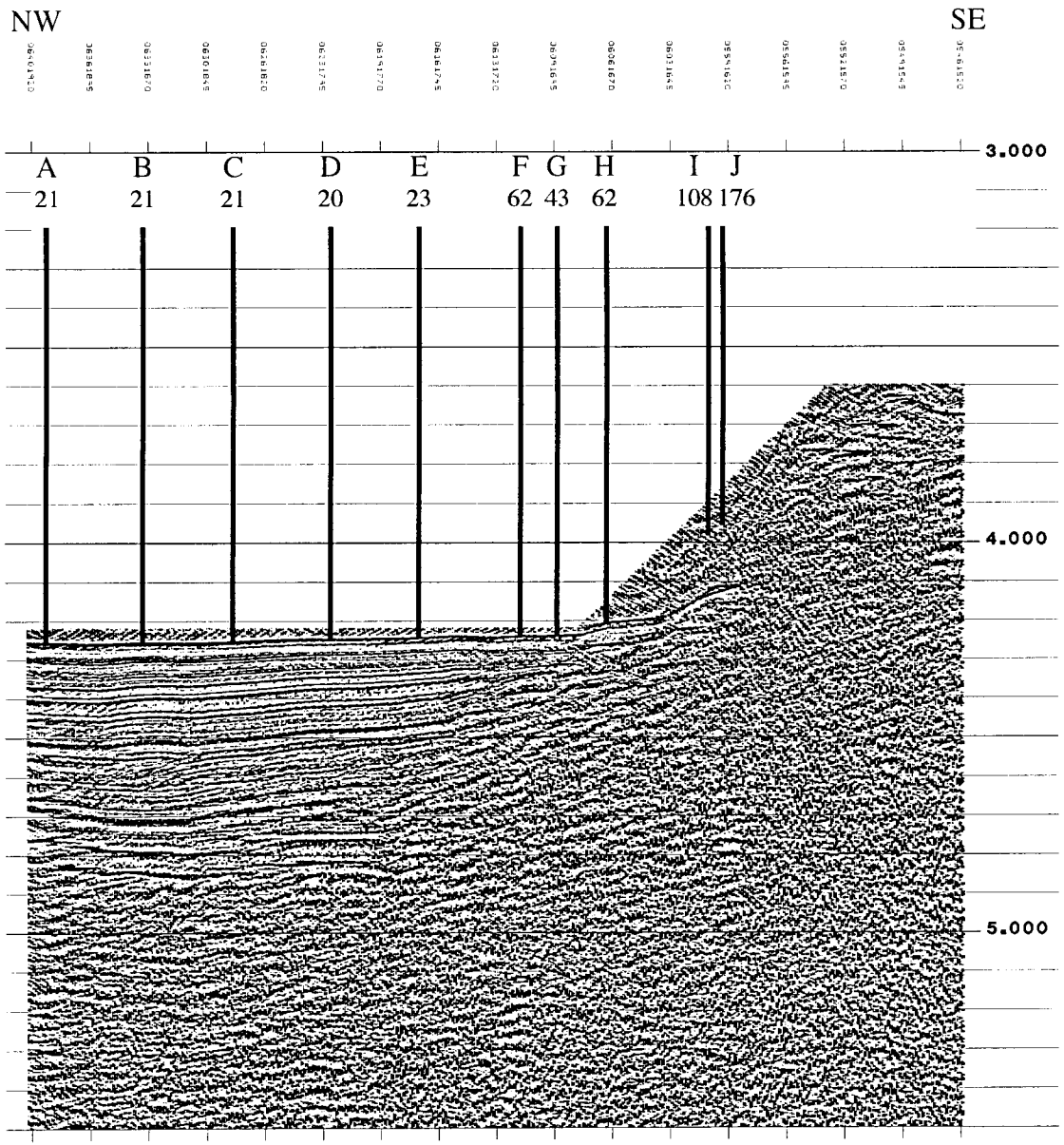


*(Seismic Line annotation GMT HHMM, RP #)*
*(Heat Flow Q values in mW/m²)*

Figure III-19

Seismic Line TF2-27
Heat Flow TF2-13

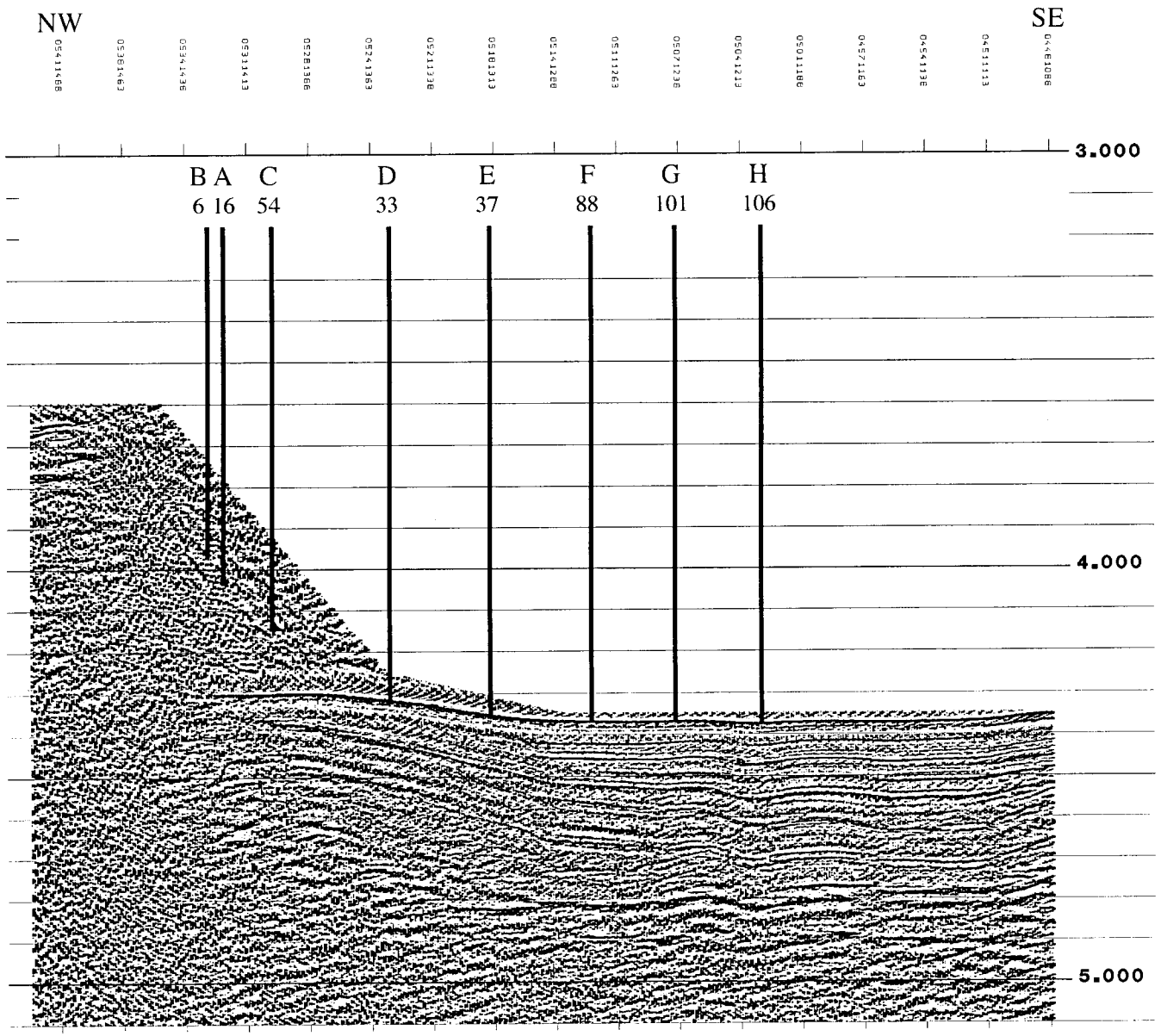


*(Seismic Line annotation GMT HHMM, RP #)*
*(Heat Flow Q values in mW/m²)*

Figure III-20

Seismic Line TF2-38a
Heat Flow TF2-14

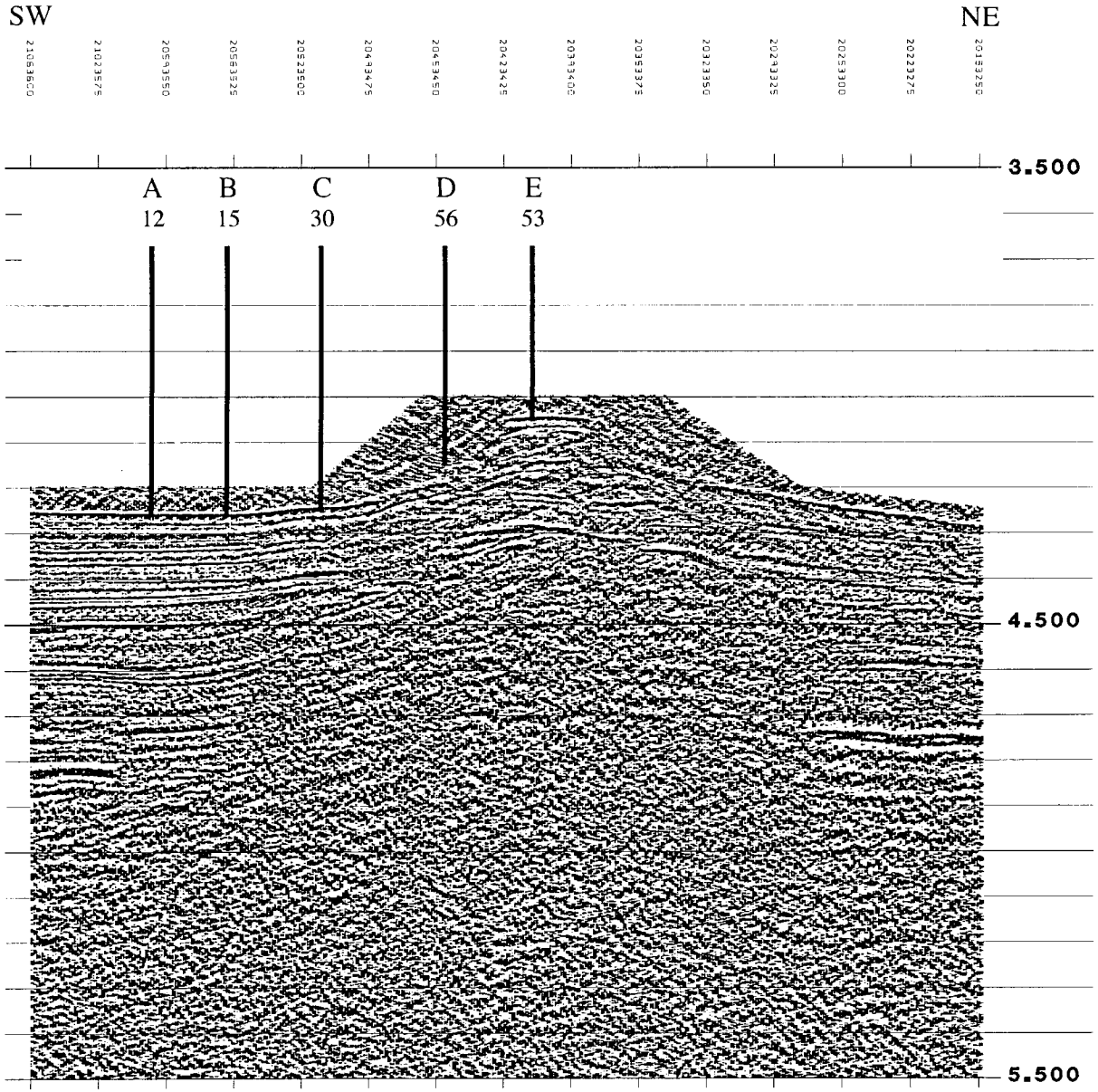


*(Seismic Line annotation GMT HHMM, RP #)*
*(Heat Flow Q values in mW/m²)*

Figure III-21

Seismic Line TF2-33
Heat Flow TF2-15

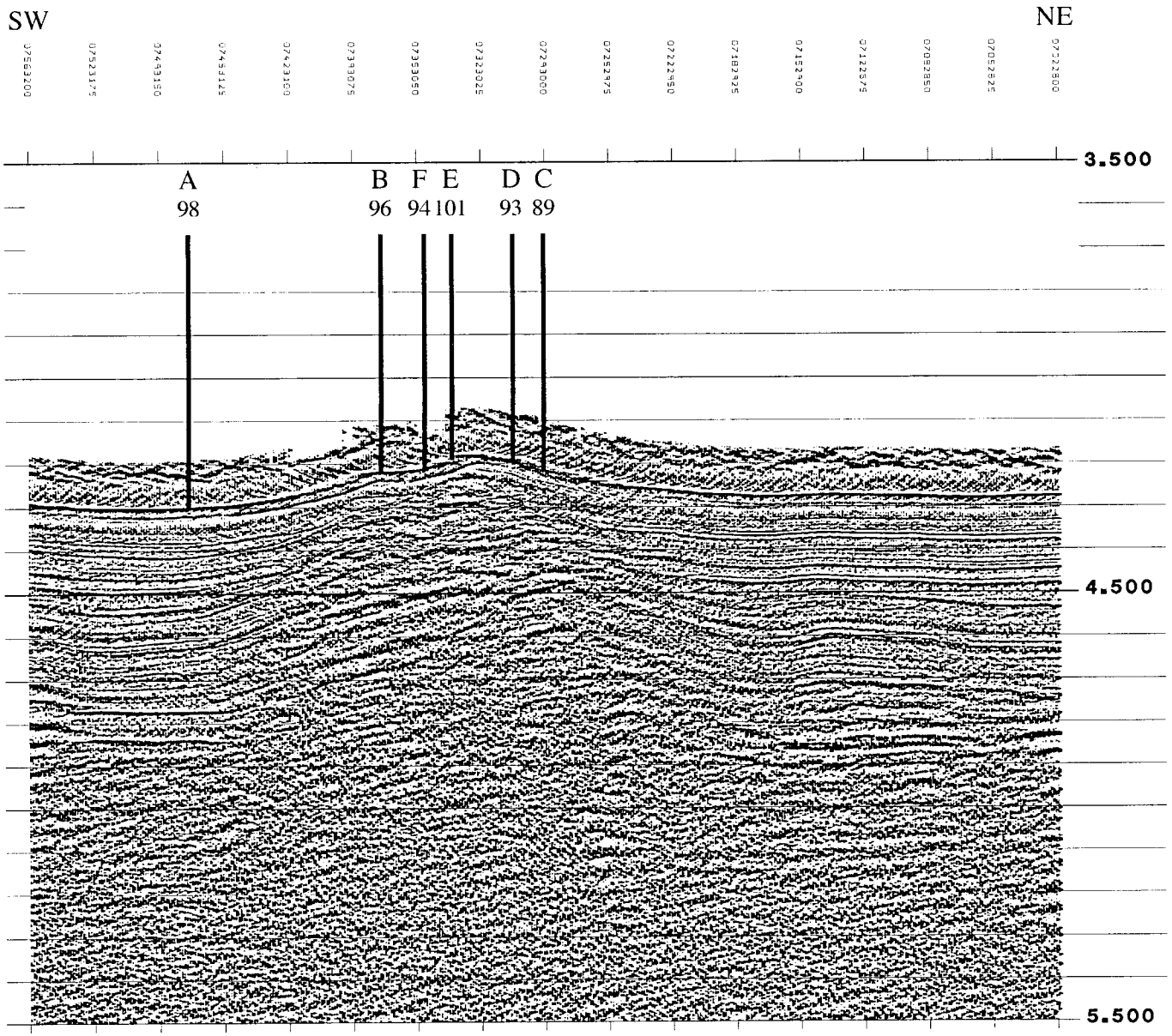


*(Seismic Line annotation GMT HHMM, RP #)*
*(Heat Flow Q values in mW/m²)*

Figure III-22

Seismic Line TF2-26
Heat Flow TF2-16

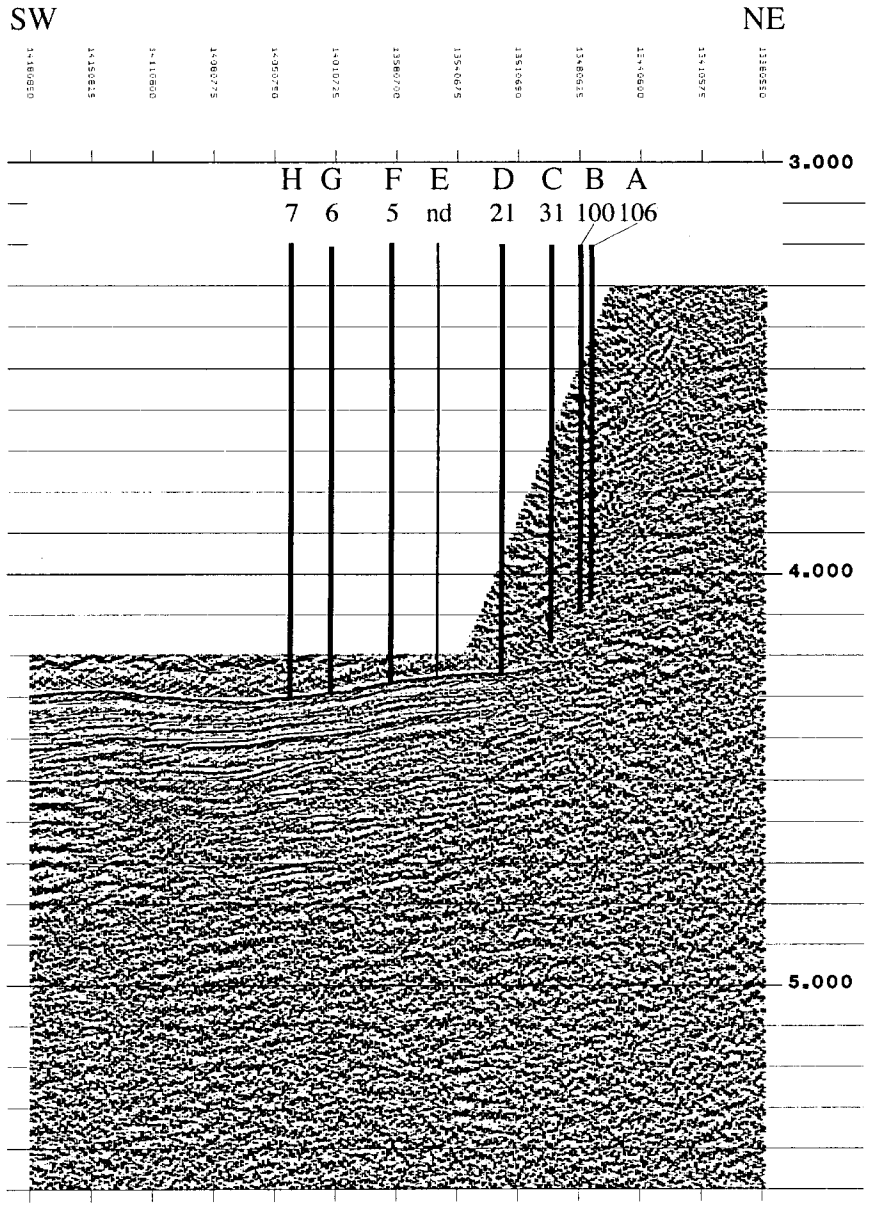


*(Seismic Line annotation GMT HHMM, RP # - 10,000)*
*(Heat Flow Q values in mW/m )*

Figure III-23

Seismic Line TF1-03
Heat Flow TF2-17

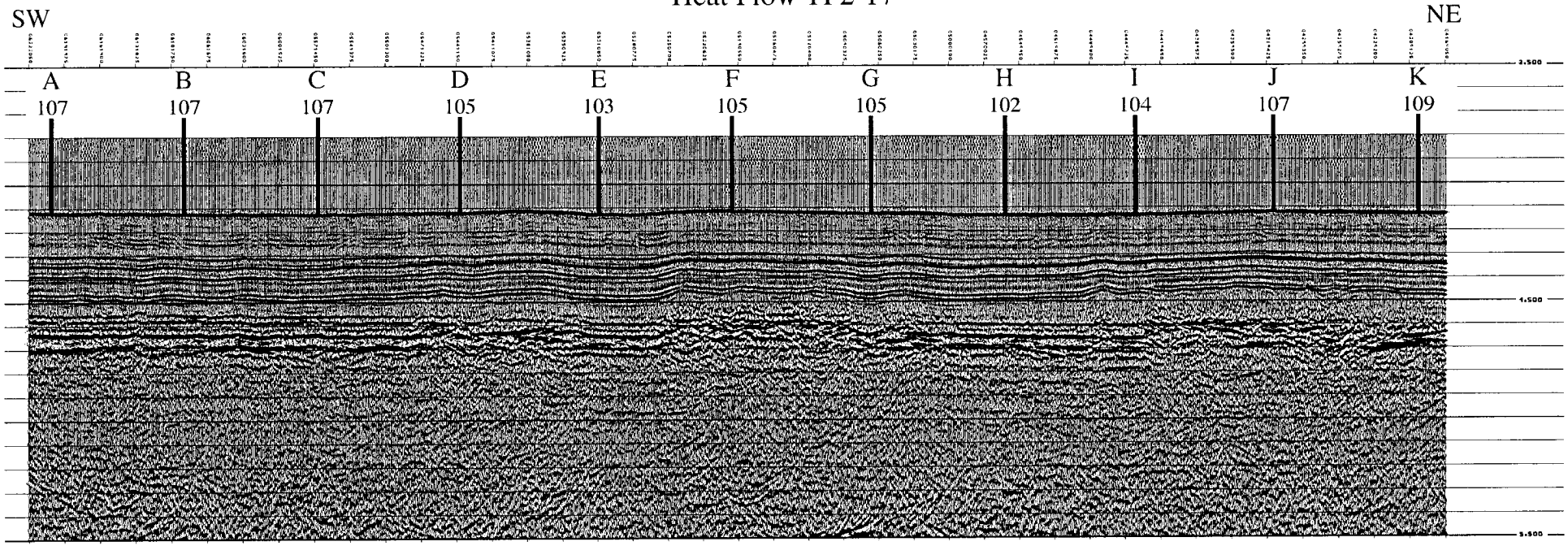


*(Seismic Line annotation GMT HHMM, RP # or RP# - 10,000)*
*(Heat Flow Q values in mW/m )*

Figure III-24

Table IV-1. Summary of multipenetration heat flow station information.

| Station | General area | Seismic coverage | Date/GMT | JD/GMT | N attempted | N successful |
|---|---|---|---|---|---|---|
| TF2HF01 | Above low-angle reflector, near high heat flow region close to trench, parallel to trench, to define size of region | TF1, Line 11 | 9/9 to 9/10 | 252 to 253 | 17 | 17 |
| TF2HF02 | Perpendicular to region of high heat flow documented during TicoFlux I, perpendicular to trench, includes one additional basement high, to define size of region | TF2, Line 10 | 9/14 to 9/15 | 257 to 258 | 22 | 22 |
| TF2HF03 | Approaching basement outcrop on propagator trace, mainly in support of geochemical goals | TF1, Line 13 | 9/17 | 260 | 8 | 8 |
| TF2HF04 | Across small basin, west of propagator, approaching basement outcrop | TF2, Line 18 | 9/18 to 9/19 | 261 to 262 | 11 | 11 |
| TF2HF05 | South of large Tengosed Seamount in middle of cool area | TF2, Line 23 | 9/21 to 9/22 | 264 to 265 | 21 | 19 |
| TF2HF06 | Southwest of Fuente Seamount, into sediment moat. | TF1, Line 4 | 9/23 | 266 | 11 | 7 |
| TF2HF07 | West-southwest of Tengosed Seamount, towards Dorado outcrop. Last two measurements over buried basement high | TF2, Line 26 (main proile); TF2 Line 31 (last 2 points0 | 9/25 | 268 | 7 | 7 |
| TF2HF08 | Southwest of Dorado outcrop, in cool area | TF2, Line 28 | 9/26 | 269 | 10 | 9 |
| TF2HF09 | Northeast of Fuente Seamount, near high heat flow determined with outriggers | TF2, Line 4 | 9/27 | 270 | 7 | 7 |
| TF2HF10 | Across Perdido outcrop on trace of triple junction | TF2, Line 5 | 9/29 to 9/30 | 272 to 273 | 21 | 21 |
| TF2HF11 | In cool area, between large seamount and TJT, parallel to TF1 Line 13 | TF2, Line 25 | 10/2 | 275 | 10 | 10 |
| TF2HF12 | Northwest of Fuente Seamount | TF2, Line 27 | 10/3 | 276 | 10 | 10 |
| TF2HF13 | Southeast of Fuente Seamount, heading towards warm plate, crosses transition | TF2, Line 27 | 10/4 | 277 | 8 | 8 |

Table IV-1. Summary of multipenetration heat flow station information.

| Station | General area | Seismic coverage | Date/GMT | JD/GMT | N attempted | N successful |
|---|---|---|---|---|---|---|
| TF2HF14 | Above buried basement high, in western part of cool area, southwest of Buquito Seamount | TF2, Line 38 | 10/5 | 278 | 5 | 5 |
| TF2HF15 | Above buried basement high in western part of cool area, near two large, unexplored seamounts | TF2, Line 33 | 10/6 | 279 | 6 | 6 |
| TF2HF16 | West-southwest of large Tengosed Seamount and east of Dorado outcrop. | TF2, Line 26 | 10/7 | 280 | 8 | 7 |
| TF2HF17 | Parallel to triple junction trace in warm area, looking for thermal transition, but never found it. | TF1, Line 3 | 10/8 to 10/9 | 281 to 282 | 20 | 20 |
| | | | | **Totals:** | **202** | **194** |

Table IV-2. Summary of multipenetration heat flow locations, preliminary values, and nearest seismic line and reflection point

| Station | Pen | Date | JD | GMT | CBD (m) | Latitude (N) | | Longitude (W) | | Q (mW/m$^2$) | Seismic Line | RP |
|---|---|---|---|---|---|---|---|---|---|---|---|---|
| | | | | | | Deg | Min | Deg | Min | | | |
| TF2HF01 | A | 9/9/02 | 252 | 2007 | 3175 | 09 | 34.467 | 086 | 45.645 | 36 | TF1 - 11 | 27338 |
| TF2HF01 | B | 9/9/02 | 252 | 2229 | 3175 | 09 | 35.194 | 086 | 46.345 | 31 | TF1 - 11 | 27633 |
| TF2HF01 | C | 9/10/02 | 253 | 0002 | 3170 | 09 | 35.931 | 086 | 47.073 | 35 | TF1 - 11 | 27938 |
| TF2HF01 | D | 9/10/02 | 253 | 0129 | 3180 | 09 | 36.671 | 086 | 47.812 | 35 | TF1 - 11 | 28245 |
| TF2HF01 | E | 9/10/02 | 253 | 0234 | 3165 | 09 | 37.059 | 086 | 48.189 | 39 | TF1 - 11 | 28403 |
| TF2HF01 | F | 9/10/02 | 253 | 0342 | 3160 | 09 | 37.445 | 086 | 48.561 | 40 | TF1 - 11 | 28560 |
| TF2HF01 | G | 9/10/02 | 253 | 0441 | 3150 | 09 | 37.654 | 086 | 48.758 | 50 | TF1 - 11 | 28645 |
| TF2HF01 | H | 9/10/02 | 253 | 0540 | 3135 | 09 | 37.865 | 086 | 48.953 | 59 | TF1 - 11 | 28730 |
| TF2HF01 | I | 9/10/02 | 253 | 0653 | 3125 | 09 | 38.046 | 086 | 49.138 | 65 | TF1 - 11 | 28806 |
| TF2HF01 | J | 9/10/02 | 253 | 0805 | 3150 | 09 | 38.236 | 086 | 49.335 | 56 | TF1 - 11 | 28886 |
| TF2HF01 | K | 9/10/02 | 253 | 0944 | 3160 | 09 | 38.433 | 086 | 49.543 | 40 | TF1 - 11 | 28970 |
| TF2HF01 | L | 9/10/02 | 253 | 1034 | 3165 | 09 | 38.625 | 086 | 49.740 | 38 | TF1 - 11 | 29051 |
| TF2HF01 | M | 9/10/02 | 253 | 1131 | 3170 | 09 | 39.009 | 086 | 50.123 | 37 | TF1 - 11 | 29211 |
| TF2HF01 | N | 9/10/02 | 253 | 1240 | 3170 | 09 | 39.401 | 086 | 50.506 | 39 | TF1 - 11 | 29372 |
| TF2HF01 | O | 9/10/02 | 253 | 1400 | 3180 | 09 | 40.130 | 086 | 51.223 | 36 | TF1 - 11 | 29672 |
| TF2HF01 | P | 9/10/02 | 253 | 1526 | 3180 | 09 | 40.860 | 086 | 51.960 | 32 | TF1 - 11 | 29976 |
| TF2HF01 | Q | 9/10/02 | 253 | 1633 | 3180 | 09 | 41.270 | 086 | 52.333 | 38 | TF1 - 11 | 30139 |
| TF2HF02 | A | 9/14/02 | 257 | 0733 | 3200 | 09 | 35.835 | 086 | 39.715 | 146 | TF2 - 10 | 12465 |
| TF2HF02 | B | 9/14/02 | 257 | 0851 | 3180 | 09 | 36.173 | 086 | 39.343 | 458 | TF2 - 10 | 12509 |
| TF2HF02 | C | 9/14/02 | 257 | 0948 | 3150 | 09 | 36.430 | 086 | 39.061 | 637 | TF2 - 10 | 12541 |
| TF2HF02 | D | 9/14/02 | 257 | 1040 | 3135 | 09 | 36.641 | 086 | 38.813 | 259 | TF2 - 10 | 12569 |
| TF2HF02 | E | 9/14/02 | 257 | 1152 | 3155 | 09 | 36.977 | 086 | 38.439 | 241 | TF2 - 10 | 12613 |
| TF2HF02 | F | 9/14/02 | 257 | 1510 | 3340 | 09 | 39.410 | 086 | 35.739 | 194 | TF2 - 10 | 12927 |
| TF2HF02 | G | 9/14/02 | 257 | 1617 | 3335 | 09 | 39.739 | 086 | 35.375 | 118 | TF2 - 10 | 12968 |
| TF2HF02 | H | 9/14/02 | 257 | 1723 | 3330 | 09 | 40.064 | 086 | 35.016 | 112 | TF2 - 10 | 13010 |
| TF2HF02 | I | 9/14/02 | 257 | 1842 | 3340 | 09 | 40.404 | 086 | 34.636 | 175 | TF2 - 10 | 13054 |
| TF2HF02 | J | 9/14/02 | 257 | 1941 | 3340 | 09 | 40.563 | 086 | 34.454 | 255 | TF2 - 10 | 13075 |
| TF2HF02 | K | 9/14/02 | 257 | 2042 | 3300 | 09 | 40.737 | 086 | 34.264 | 523 | TF2 - 10 | 13096 |
| TF2HF02 | L | 9/14/02 | 257 | 2156 | 3290 | 09 | 40.905 | 086 | 34.082 | 395 | TF2 - 10 | 13118 |
| TF2HF02 | M | 9/14/02 | 257 | 2302 | 3290 | 09 | 41.090 | 086 | 33.878 | 229 | TF2 - 10 | 13142 |
| TF2HF02 | N | 9/15/02 | 258 | 0010 | 3290 | 09 | 41.392 | 086 | 33.528 | 142 | TF2 - 10 | 13182 |
| TF2HF02 | O | 9/15/02 | 258 | 0124 | 3315 | 09 | 41.720 | 086 | 33.168 | 112 | TF2 - 10 | 13223 |

Notes:
ND = no data (no penetration or excessive probe motion)

Table IV-2. Summary of multipenetration heat flow locations, preliminary values, and nearest seismic line and reflection point

| | | | | | | Latitude (N) | | Longitude (W) | | | | |
|---|---|---|---|---|---|---|---|---|---|---|---|---|
| Station | Pen | Date | JD | GMT | CBD (m) | Deg | Min | Deg | Min | Q (mW/m$^2$) | Seismic Line | RP |
| TF2HF02 | P | 9/15/02 | 258 | 0236 | 3340 | 09 | 42.059 | 086 | 32.800 | 88 | TF2 - 10 | 13266 |
| TF2HF02 | Q | 9/15/02 | 258 | 0351 | 3390 | 09 | 42.386 | 086 | 32.436 | 94 | TF2 - 10 | 13308 |
| TF2HF02 | R | 9/15/02 | 258 | 0505 | 3435 | 09 | 42.713 | 086 | 32.070 | 76 | TF2 - 10 | 13351 |
| TF2HF02 | S | 9/15/02 | 258 | 0629 | 3460 | 09 | 43.026 | 086 | 31.709 | 55 | TF2 - 10 | 13392 |
| TF2HF02 | T | 9/15/02 | 258 | 0747 | 3505 | 09 | 43.343 | 086 | 31.365 | 51 | TF2 - 10 | 13422 |
| TF2HF02 | U | 9/15/02 | 258 | 0934 | 3435 | 09 | 42.983 | 086 | 32.210 | 83 | TF2 - 13 | 13358 |
| TF2HF02 | V | 9/15/02 | 258 | 1045 | 3440 | 09 | 43.331 | 086 | 32.547 | 101 | TF2 - 13 | 13354 |
| TF2HF03 | A | 9/17/02 | 260 | 0658 | 2875 | 08 | 28.324 | 085 | 56.508 | 116 | TF1 - 13 | 29811 |
| TF2HF03 | B | 9/17/02 | 260 | 0827 | 2885 | 08 | 28.855 | 085 | 57.060 | 110 | TF1 - 13 | 29586 |
| TF2HF03 | C | 9/17/02 | 260 | 0953 | 2805 | 08 | 29.407 | 085 | 57.609 | 97 | TF1 - 13 | 29356 |
| TF2HF03 | D | 9/17/02 | 260 | 1038 | 2810 | 08 | 29.472 | 085 | 57.689 | 93 | TF1 - 13 | 29326 |
| TF2HF03 | E | 9/17/02 | 260 | 1117 | 2815 | 08 | 29.547 | 085 | 57.758 | 101 | TF1 - 13 | 29298 |
| TF2HF03 | F | 9/17/02 | 260 | 1200 | 2825 | 08 | 29.618 | 085 | 57.829 | 116 | TF1 - 13 | 29268 |
| TF2HF03 | G | 9/17/02 | 260 | 1240 | 2820 | 08 | 29.704 | 085 | 57.920 | 125 | TF1 - 13 | 29230 |
| TF2HF03 | H | 9/17/02 | 260 | 1435 | 2745 | 08 | 30.349 | 085 | 58.542 | 144 | TF1 - 13 | 28966 |
| TF2HF04 | A | 9/18/02 | 261 | 1627 | 2875 | 08 | 37.490 | 085 | 52.640 | 199 | TF2 - 18 | 5710 |
| TF2HF04 | B | 9/18/02 | 261 | 1709 | 2860 | 08 | 37.539 | 085 | 52.679 | 50 | TF2 - 18 | 5715 |
| TF2HF04 | C | 9/18/02 | 261 | 1758 | 2880 | 08 | 37.576 | 085 | 52.709 | 36 | TF2 - 18 | 5718 |
| TF2HF04 | D | 9/18/02 | 261 | 1851 | 2950 | 08 | 37.625 | 085 | 52.746 | 25 | TF2 - 18 | 5723 |
| TF2HF04 | E | 9/18/02 | 261 | 1941 | 2950 | 08 | 37.709 | 085 | 52.822 | 19 | TF2 - 18 | 5732 |
| TF2HF04 | F | 9/18/02 | 261 | 2044 | 2950 | 08 | 37.862 | 085 | 52.970 | 12 | TF2 - 18 | 5748 |
| TF2HF04 | G | 9/18/02 | 261 | 2139 | 2950 | 08 | 38.035 | 085 | 53.120 | 7 | TF2 - 18 | 5766 |
| TF2HF04 | H | 9/18/02 | 261 | 2230 | 2960 | 08 | 38.198 | 085 | 53.264 | 8 | TF2 - 18 | 5783 |
| TF2HF04 | I | 9/18/02 | 261 | 2324 | 2970 | 08 | 38.255 | 085 | 53.305 | 6 | TF2 - 18 | 5790 |
| TF2HF04 | J | 9/19/02 | 262 | 0009 | 2970 | 08 | 38.291 | 085 | 53.345 | 9 | TF2 - 18 | 5794 |
| TF2HF04 | K | 9/19/02 | 262 | 0050 | 2930 | 08 | 38.332 | 085 | 53.382 | 10 | TF2 - 18 | 5799 |
| TF2HF05 | A | 9/21/02 | 264 | 1310 | 3125 | 09 | 05.513 | 086 | 57.263 | ND | TF2 - 23b | 7539 |
| TF2HF05 | B | 9/21/02 | 264 | 1348 | 3100 | 09 | 05.556 | 086 | 57.264 | 10 | TF2 - 23b | 7537 |
| TF2HF05 | C | 9/21/02 | 264 | 1438 | 3150 | 09 | 05.457 | 086 | 57.259 | 9 | TF2 - 23b | 7543 |
| TF2HF05 | D | 9/21/02 | 264 | 1525 | 3165 | 09 | 05.397 | 086 | 57.262 | 8 | TF2 - 23b | 7547 |

Notes:
ND = no data (no penetration or excessive probe motion)

Table IV-2. Summary of multipenetration heat flow locations, preliminary values, and nearest seismic line and reflection point

| Station | Pen | Date | JD | GMT | CBD (m) | Latitude (N) Deg | Latitude (N) Min | Longitude (W) Deg | Longitude (W) Min | Q (mW/m$^2$) | Seismic Line | RP |
|---|---|---|---|---|---|---|---|---|---|---|---|---|
| TF2HF05 | E | 9/21/02 | 264 | 1603 | 3170 | 09 | 05.342 | 086 | 57.259 | 8 | TF2 - 23b | 7551 |
| TF2HF05 | F | 9/21/02 | 264 | 1649 | 3170 | 09 | 05.286 | 086 | 57.264 | 17 | TF2 - 23b | 7555 |
| TF2HF05 | G | 9/21/02 | 264 | 1725 | 3170 | 09 | 05.235 | 086 | 57.259 | ND | TF2 - 23b | 7559 |
| TF2HF05 | H | 9/21/02 | 264 | 1813 | 3170 | 09 | 05.131 | 086 | 57.257 | 12 | TF2 - 23b | 7567 |
| TF2HF05 | I | 9/21/02 | 264 | 1859 | 3170 | 09 | 05.023 | 086 | 57.264 | 10 | TF2 - 23b | 7575 |
| TF2HF05 | J | 9/21/02 | 264 | 1956 | 3170 | 09 | 04.851 | 086 | 57.275 | 11 | TF2 - 23b | 7587 |
| TF2HF05 | K | 9/21/02 | 264 | 2055 | 3170 | 09 | 04.629 | 086 | 57.279 | ND | TF2 - 23b | 7603 |
| TF2HF05 | L | 9/21/02 | 264 | 2138 | 3200 | 09 | 04.407 | 086 | 57.271 | 9 | TF2 - 23b | 7618 |
| TF2HF05 | M | 9/21/02 | 264 | 2250 | 3190 | 09 | 03.857 | 086 | 57.280 | 9 | TF2 - 23b | 7657 |
| TF2HF05 | N | 9/22/02 | 265 | 0010 | 3190 | 09 | 03.293 | 086 | 57.292 | 8 | TF2 - 23b | 7697 |
| TF2HF05 | O | 9/22/02 | 265 | 0130 | 3190 | 09 | 02.747 | 086 | 57.301 | 12 | TF2 - 23b | 7735 |
| TF2HF05 | P | 9/22/02 | 265 | 0243 | 3190 | 09 | 02.196 | 086 | 57.312 | 24 | TF2 - 23b | 7774 |
| TF2HF05 | Q | 9/22/02 | 265 | 0357 | 3190 | 09 | 01.637 | 086 | 57.318 | 41 | TF2 - 23b | 7813 |
| TF2HF05 | R | 9/22/02 | 265 | 0514 | 3200 | 09 | 01.937 | 086 | 57.324 | 70 | TF2 - 23b | 7791 |
| TF2HF05 | S | 9/22/02 | 265 | 0628 | 3200 | 09 | 00.544 | 086 | 57.329 | 86 | TF2 - 23b | 7889 |
| TF2HF05 | T | 9/22/02 | 265 | 0749 | 3200 | 08 | 60.001 | 086 | 57.346 | 86 | TF2 - 23b | 7927 |
| TF2HF05 | U | 9/22/02 | 265 | 0913 | 3205 | 08 | 59.410 | 086 | 57.356 | 87 | TF2 - 23b | 7969 |
| TF2HF06 | A | 9/23/02 | 266 | 0401 | 3200 | 08 | 47.335 | 087 | 11.797 | 136 | TF1 - 04 | 3934 |
| TF2HF06 | B | 9/23/02 | 266 | 0439 | 3210 | 08 | 47.302 | 087 | 11.832 | 138 | TF1 - 04 | 3920 |
| TF2HF06 | C | 9/23/02 | 266 | 0517 | 3225 | 08 | 47.222 | 087 | 11.907 | 65 | TF1 - 04 | 3888 |
| TF2HF06 | D | 9/23/02 | 266 | 0611 | 3225 | 08 | 47.018 | 087 | 12.092 | 65 | TF1 - 04 | 3807 |
| TF2HF06 | E | 9/23/02 | 266 | 0623 | 3225 | 08 | 47.017 | 087 | 12.091 | ND | TF1 - 04 | 3806 |
| TF2HF06 | F | 9/23/02 | 266 | 0647 | 3260 | 08 | 46.977 | 087 | 12.128 | ND | TF1 - 04 | 3799 |
| TF2HF06 | G | 9/23/02 | 266 | 0758 | 3240 | 08 | 46.620 | 087 | 12.461 | ND | TF1 - 04 | 3647 |
| TF2HF06 | H | 9/23/02 | 266 | 0818 | 3240 | 08 | 46.620 | 087 | 12.459 | ND | TF1 - 04 | 3647 |
| TF2HF06 | I | 9/23/02 | 266 | 0926 | 3210 | 08 | 46.222 | 087 | 12.828 | 95 | TF1 - 04 | 3487 |
| TF2HF06 | J | 9/23/02 | 266 | 1036 | 3180 | 08 | 45.818 | 087 | 13.201 | 101 | TF1 - 04 | 3326 |
| TF2HF06 | K | 9/23/02 | 266 | 1149 | 3130 | 08 | 45.427 | 087 | 13.577 | 95 | TF1 - 04 | 3166 |
| TF2HF07 | A | 9/25/02 | 268 | 0024 | 3200 | 09 | 05.795 | 087 | 02.937 | 9 | TF2 - 26 | 10922 |
| TF2HF07 | B | 9/25/02 | 268 | 0126 | 3200 | 09 | 05.686 | 087 | 03.177 | 9 | TF2 - 26 | 10940 |
| TF2HF07 | C | 9/25/02 | 268 | 0227 | 3200 | 09 | 05.573 | 087 | 03.443 | 9 | TF2 - 26 | 10962 |

Notes:
ND = no data (no penetration or excessive probe motion)

Table IV-2. Summary of multipenetration heat flow locations, preliminary values, and nearest seismic line and reflection point

| Station | Pen | Date | JD | GMT | CBD (m) | Latitude (N) Deg | Latitude (N) Min | Longitude (W) Deg | Longitude (W) Min | Q (mW/m²) | Seismic Line | RP |
|---|---|---|---|---|---|---|---|---|---|---|---|---|
| TF2HF07 | D | 9/25/02 | 268 | 0324 | 3200 | 09 | 05.471 | 087 | 03.707 | 8 | TF2 - 26 | 10983 |
| TF2HF07 | E | 9/25/02 | 268 | 0421 | 3200 | 09 | 05.342 | 087 | 03.983 | 8 | TF2 - 26 | 11004 |
| TF2HF07 | F | 9/25/02 | 268 | 0516 | 3190 | 09 | 05.220 | 087 | 04.254 | 11 | TF2 - 26 | 11026 |
| TF2HF07 | G | 9/25/02 | 268 | 0614 | 3180 | 09 | 05.102 | 087 | 04.527 | 13 | TF2 - 26 | 11047 |
| TF2HF07 | H | 9/25/02 | 268 | 0715 | 3160 | 09 | 04.981 | 087 | 04.800 | 13 | TF2 - 26 | 11068 |
| TF2HF07 | I | 9/25/02 | 268 | 0806 | 3140 | 09 | 04.868 | 087 | 05.034 | 15 | TF2 - 26 | 11095 |
| TF2HF07 | J | 9/25/02 | 268 | 1009 | 3085 | 09 | 06.255 | 087 | 05.436 | 54 | TF2 - 31 | 7044 |
| TF2HF07 | K | 9/25/02 | 268 | 1058 | 3075 | 09 | 06.329 | 087 | 05.791 | 55 | TF2 - 31 | 7019 |
| TF2HF08 | A | 9/26/02 | 269 | 0401 | 3155 | 09 | 04.997 | 087 | 05.937 | ND | TF2 - 28 | 2987 |
| TF2HF08 | B | 9/26/02 | 269 | 0425 | 3200 | 09 | 04.958 | 087 | 05.968 | 389 | TF2 - 28 | 2983 |
| TF2HF08 | C | 9/26/02 | 269 | 0501 | 3207 | 09 | 04.916 | 087 | 05.998 | 138 | TF2 - 28 | 2979 |
| TF2HF08 | D | 9/26/02 | 269 | 0546 | 3200 | 09 | 04.804 | 087 | 06.086 | 113 | TF2 - 28 | 2968 |
| TF2HF08 | E | 9/26/02 | 269 | 0637 | 3190 | 09 | 04.689 | 087 | 06.170 | 86 | TF2 - 28 | 2958 |
| TF2HF08 | F | 9/26/02 | 269 | 0718 | 3175 | 09 | 04.571 | 087 | 06.252 | 48 | TF2 - 28 | 2947 |
| TF2HF08 | G | 9/26/02 | 269 | 0801 | 3170 | 09 | 04.458 | 087 | 06.336 | 32 | TF2 - 28 | 2936 |
| TF2HF08 | H | 9/26/02 | 269 | 0857 | 3175 | 09 | 04.230 | 087 | 06.510 | 24 | TF2 - 28 | 2915 |
| TF2HF08 | I | 9/26/02 | 269 | 1018 | 3180 | 09 | 03.771 | 087 | 06.848 | 22 | TF2 - 28 | 2872 |
| TF2HF08 | J | 9/26/02 | 269 | 1124 | 3190 | 09 | 03.309 | 087 | 07.196 | 26 | TF2 - 28 | 2830 |
| TF2HF09 | A | 9/27/02 | 270 | 0553 | 3125 | 08 | 49.161 | 087 | 10.085 | 341 | TF1 - 04 | 4669 |
| TF2HF09 | B | 9/27/02 | 270 | 0629 | 3150 | 08 | 49.196 | 087 | 10.054 | 130 | TF1 - 04 | 4683 |
| TF2HF09 | C | 9/27/02 | 270 | 0714 | 3160 | 08 | 49.331 | 087 | 09.932 | 65 | TF1 - 04 | 4737 |
| TF2HF09 | D | 9/27/02 | 270 | 0808 | 3155 | 08 | 49.586 | 087 | 09.694 | 49 | TF1 - 04 | 4839 |
| TF2HF09 | E | 9/27/02 | 270 | 0924 | 3170 | 08 | 50.038 | 087 | 09.278 | 35 | TF1 - 04 | 5020 |
| TF2HF09 | F | 9/27/02 | 270 | 1043 | 3180 | 08 | 50.456 | 087 | 08.895 | 28 | TF1 - 04 | 5186 |
| TF2HF09 | G | 9/27/02 | 270 | 1150 | 3185 | 08 | 50.831 | 087 | 08.558 | 28 | TF1 - 04 | 5336 |
| TF2HF10 | A | 9/29/02 | 272 | 1559 | 3395 | 09 | 22.472 | 086 | 14.373 | 7 | TF2 - 5a | 4087 |
| TF2HF10 | B | 9/29/02 | 272 | 1709 | 3395 | 09 | 22.079 | 086 | 13.992 | 9 | TF2 - 5a | 4036 |
| TF2HF10 | C | 9/29/02 | 272 | 1826 | 3390 | 09 | 21.695 | 086 | 13.615 | <4 | TF2 - 5a | 3987 |
| TF2HF10 | D | 9/29/02 | 272 | 1942 | 3380 | 09 | 21.315 | 086 | 13.220 | <4 | TF2 - 5a | 3936 |
| TF2HF10 | E | 9/29/02 | 272 | 2050 | 3380 | 09 | 20.942 | 086 | 12.807 | <4 | TF2 - 5a | 3883 |

Notes:
ND = no data (no penetration or excessive probe motion)

Table IV-2. Summary of multipenetration heat flow locations, preliminary values, and nearest seismic line and reflection point

| Station | Pen | Date | JD | GMT | CBD (m) | Latitude (N) | | Longitude (W) | | Q (mW/m²) | Seismic Line | RP |
|---|---|---|---|---|---|---|---|---|---|---|---|---|
| | | | | | | Deg | Min | Deg | Min | | | |
| TF2HF10 | F | 9/29/02 | 272 | 2144 | 3380 | 09 | 20.748 | 086 | 12.615 | 5 | TF2 - 5a | 3859 |
| TF2HF10 | G | 9/29/02 | 272 | 2240 | 3375 | 09 | 20.588 | 086 | 12.455 | 7 | TF2 - 5a | 3839 |
| TF2HF10 | H | 9/29/02 | 272 | 2333 | 3325 | 09 | 20.472 | 086 | 12.343 | 32 | TF2 - 5a | 3824 |
| TF2HF10 | I | 9/30/02 | 273 | 0025 | 3330 | 09 | 20.385 | 086 | 12.260 | 112 | TF2 - 5a | 3812 |
| TF2HF10 | J | 9/30/02 | 273 | 0109 | 3310 | 09 | 20.352 | 086 | 12.223 | 86 | TF2 - 5a | 3808 |
| TF2HF10 | K | 9/30/02 | 273 | 0224 | 3125 | 09 | 19.952 | 086 | 11.824 | 42 | TF2 - 5a | 3755 |
| TF2HF10 | L | 9/30/02 | 273 | 0336 | 3010 | 09 | 19.552 | 086 | 11.419 | 27 | TF2 - 5a | 3701 |
| TF2HF10 | M | 9/30/02 | 273 | 0525 | 3335 | 09 | 18.926 | 086 | 10.785 | 9 | TF2 - 5a | 3616 |
| TF2HF10 | N | 9/30/02 | 273 | 0601 | 3325 | 09 | 18.888 | 086 | 10.745 | 6 | TF2 - 5a | 3611 |
| TF2HF10 | O | 9/30/02 | 273 | 0646 | 3325 | 09 | 18.812 | 086 | 10.667 | 7 | TF2 - 5a | 3600 |
| TF2HF10 | P | 9/30/02 | 273 | 0724 | 3300 | 09 | 18.694 | 086 | 10.548 | 9 | TF2 - 5a | 3584 |
| TF2HF10 | Q | 9/30/02 | 273 | 0805 | 3295 | 09 | 18.497 | 086 | 10.348 | 18 | TF2 - 5a | 3557 |
| TF2HF10 | R | 9/30/02 | 273 | 0857 | 3290 | 09 | 18.277 | 086 | 10.135 | 49 | TF2 - 5a | 3528 |
| TF2HF10 | S | 9/30/02 | 273 | 1010 | 3285 | 09 | 17.869 | 086 | 09.731 | 102 | TF2 - 5a | 3475 |
| TF2HF10 | T | 9/30/02 | 273 | 1119 | 3295 | 09 | 17.463 | 086 | 09.333 | 116 | TF2 - 5a | 3423 |
| TF2HF10 | U | 9/30/02 | 273 | 1227 | 3305 | 09 | 17.063 | 086 | 08.936 | 114 | TF2 - 5a | 3372 |
| TF2HF11 | A | 10/2/02 | 275 | 0226 | 3155 | 09 | 12.767 | 086 | 47.096 | 37 | TF2 - 26 | 60 |
| TF2HF11 | B | 10/2/02 | 275 | 0416 | 3160 | 09 | 12.660 | 086 | 46.117 | 55 | TF2 - 25 | 9650 |
| TF2HF11 | C | 10/2/02 | 275 | 0531 | 3160 | 09 | 12.305 | 086 | 45.709 | 59 | TF2 - 25 | 9611 |
| TF2HF11 | D | 10/2/02 | 275 | 0645 | 3160 | 09 | 11.948 | 086 | 45.312 | 59 | TF2 - 25 | 9571 |
| TF2HF11 | E | 10/2/02 | 275 | 0758 | 3175 | 09 | 11.578 | 086 | 44.909 | 70 | TF2 - 25 | 9530 |
| TF2HF11 | F | 10/2/02 | 275 | 0916 | 3170 | 09 | 11.210 | 086 | 44.483 | 81 | TF2 - 25 | 9488 |
| TF2HF11 | G | 10/2/02 | 275 | 1028 | 3160 | 09 | 10.849 | 086 | 44.089 | 88 | TF2 - 25 | 9448 |
| TF2HF11 | H | 10/2/02 | 275 | 1140 | 3155 | 09 | 10.485 | 086 | 43.680 | 94 | TF2 - 25 | 9408 |
| TF2HF11 | I | 10/2/02 | 275 | 1250 | 3135 | 09 | 10.118 | 086 | 43.281 | 96 | TF2 - 25 | 9370 |
| TF2HF11 | J | 10/2/02 | 275 | 1333 | 3135 | 09 | 09.985 | 086 | 43.135 | 97 | TF2 - 25 | 9355 |
| TF2HF12 | A | 10/3/02 | 276 | 0611 | 3170 | 08 | 51.994 | 087 | 14.531 | 21 | TF2 - 27 | 1912 |
| TF2HF12 | B | 10/3/02 | 276 | 0728 | 3170 | 08 | 51.622 | 087 | 14.136 | 21 | TF2 - 27 | 1872 |
| TF2HF12 | C | 10/3/02 | 276 | 0844 | 3170 | 08 | 51.243 | 087 | 13.744 | 21 | TF2 - 27 | 1832 |
| TF2HF12 | D | 10/3/02 | 276 | 0953 | 3165 | 08 | 50.860 | 087 | 13.344 | 20 | TF2 - 27 | 1792 |
| TF2HF12 | E | 10/3/02 | 276 | 1103 | 3160 | 08 | 50.491 | 087 | 12.952 | 23 | TF2 - 27 | 1754 |

Notes:
ND = no data (no penetration or excessive probe motion)

Table IV-2. Summary of multipenetration heat flow locations, preliminary values, and nearest seismic line and reflection point

| Station | Pen | Date | JD | GMT | CBD (m) | Latitude (N) Deg | Latitude (N) Min | Longitude (W) Deg | Longitude (W) Min | Q (mW/m$^2$) | Seismic Line | RP |
|---|---|---|---|---|---|---|---|---|---|---|---|---|
| TF2HF12 | F | 10/3/02 | 276 | 1211 | 3160 | 08 | 50.088 | 087 | 12.533 | 62 | TF2 - 27 | 1714 |
| TF2HF12 | G | 10/3/02 | 276 | 1302 | 3155 | 08 | 49.895 | 087 | 12.323 | 43 | TF2 - 27 | 1694 |
| TF2HF12 | H | 10/3/02 | 276 | 1406 | 3140 | 08 | 49.695 | 087 | 12.118 | 62 | TF2 - 27 | 1674 |
| TF2HF12 | I | 10/3/02 | 276 | 1520 | 3085 | 08 | 49.329 | 087 | 11.740 | 108 | TF2 - 27 | 1628 |
| TF2HF12 | J | 10/3/02 | 276 | 1620 | 3040 | 08 | 49.069 | 087 | 11.462 | 176 | TF2 - 27 | 1624 |
| TF2HF13 | A | 10/4/02 | 277 | 0808 | 3160 | 08 | 47.449 | 087 | 09.769 | 16 | TF2 - 27 | 1423 |
| TF2HF13 | B | 10/4/02 | 277 | 0848 | 3135 | 08 | 47.488 | 087 | 09.814 | 6 | TF2 - 27 | 1428 |
| TF2HF13 | C | 10/4/02 | 277 | 0956 | 3205 | 08 | 47.201 | 087 | 09.512 | 54 | TF2 - 27 | 1396 |
| TF2HF13 | D | 10/4/02 | 277 | 1104 | 3210 | 08 | 46.836 | 087 | 09.126 | 33 | TF2 - 27 | 1356 |
| TF2HF13 | E | 10/4/02 | 277 | 1209 | 3230 | 08 | 46.458 | 087 | 08.735 | 37 | TF2 - 27 | 1316 |
| TF2HF13 | F | 10/4/02 | 277 | 1316 | 3250 | 08 | 46.080 | 087 | 08.340 | 88 | TF2 - 27 | 1276 |
| TF2HF13 | G | 10/4/02 | 277 | 1422 | 3255 | 08 | 45.711 | 087 | 07.957 | 101 | TF2 - 27 | 1236 |
| TF2HF13 | H | 10/4/02 | 277 | 1532 | 3260 | 08 | 45.338 | 087 | 07.569 | 106 | TF2 - 27 | 1196 |
| TF2HF14 | A | 10/5/02 | 278 | 1047 | 3175 | 09 | 19.382 | 087 | 09.138 | 12 | TF2 - 38a | 3554 |
| TF2HF14 | B | 10/5/02 | 278 | 1155 | 3175 | 09 | 19.809 | 087 | 08.811 | 15 | TF2 - 38a | 3527 |
| TF2HF14 | C | 10/5/02 | 278 | 1301 | 3165 | 09 | 20.209 | 087 | 08.500 | 30 | TF2 - 38a | 3490 |
| TF2HF14 | D | 10/5/02 | 278 | 1414 | 3130 | 09 | 20.655 | 087 | 08.151 | 56 | TF2 - 38a | 3448 |
| TF2HF14 | E | 10/5/02 | 278 | 1530 | 3025 | 09 | 20.994 | 087 | 07.880 | 53 | TF2 - 38a | 3416 |
| TF2HF15 | A | 10/6/02 | 279 | 0719 | 3210 | 09 | 09.100 | 087 | 16.457 | 98 | TF2 - 33 | 3136 |
| TF2HF15 | B | 10/6/02 | 279 | 0917 | 3150 | 09 | 09.859 | 087 | 15.810 | 96 | TF2 - 33 | 3063 |
| TF2HF15 | C | 10/6/02 | 279 | 1106 | 3122 | 09 | 10.506 | 087 | 15.258 | 89 | TF2 - 33 | 3000 |
| TF2HF15 | D | 10/6/02 | 279 | 1148 | 3120 | 09 | 10.365 | 087 | 15.374 | 93 | TF2 - 33 | 3014 |
| TF2HF15 | E | 10/6/02 | 279 | 1236 | 3135 | 09 | 10.116 | 087 | 15.579 | 101 | TF2 - 33 | 3036 |
| TF2HF15 | F | 10/6/02 | 279 | 1311 | 3143 | 09 | 09.998 | 087 | 15.693 | 94 | TF2 - 33 | 3048 |
| TF2HF16 | A | 10/6/02 | 279 | 2348 | 3100 | 09 | 07.434 | 086 | 59.204 | 106 | TF2 - 26 | 10621 |
| TF2HF16 | B | 10/7/02 | 280 | 0030 | 3100 | 09 | 07.412 | 086 | 59.252 | 100 | TF2 - 26 | 10625 |
| TF2HF16 | C | 10/7/02 | 280 | 0129 | 3150 | 09 | 07.348 | 086 | 59.421 | 31 | TF2 - 26 | 10638 |
| TF2HF16 | D | 10/7/02 | 280 | 0235 | 3150 | 09 | 07.230 | 086 | 59.682 | 21 | TF2 - 26 | 10659 |
| TF2HF16 | E | 10/7/02 | 280 | 0341 | 3180 | 09 | 07.114 | 086 | 59.946 | ND | TF2 - 26 | 10681 |

Notes:
ND = no data (no penetration or excessive probe motion)

Table IV-2. Summary of multipenetration heat flow locations, preliminary values, and nearest seismic line and reflection point

| Station | Pen | Date | JD | GMT | CBD (m) | Latitude (N) Deg | Latitude (N) Min | Longitude (W) Deg | Longitude (W) Min | Q (mW/m$^2$) | Seismic Line | RP |
|---|---|---|---|---|---|---|---|---|---|---|---|---|
| TF2HF16 | F | 10/7/02 | 280 | 0437 | 3190 | 09 | 07.003 | 087 | 00.212 | 5 | TF2 - 26 | 10701 |
| TF2HF16 | G | 10/7/02 | 280 | 0536 | 3200 | 09 | 06.890 | 087 | 00.465 | 6 | TF2 - 26 | 10723 |
| TF2HF16 | H | 10/7/02 | 280 | 0633 | 3210 | 09 | 06.775 | 087 | 00.723 | 7 | TF2 - 26 | 10743 |
| TF2HF17 | A | 10/8/02 | 281 | 0504 | 3190 | 09 | 10.527 | 086 | 38.421 | 107 | TF1 - 03 | 12003 |
| TF2HF17 | B | 10/8/02 | 281 | 0640 | 3185 | 09 | 11.214 | 086 | 37.753 | 107 | TF1 - 03 | 11721 |
| TF2HF17 | C | 10/8/02 | 281 | 0820 | 3185 | 09 | 11.880 | 086 | 37.067 | 107 | TF1 - 03 | 11440 |
| TF2HF17 | D | 10/8/02 | 281 | 0958 | 3185 | 09 | 12.579 | 086 | 36.361 | 105 | TF1 - 03 | 11146 |
| TF2HF17 | E | 10/8/02 | 281 | 1134 | 3190 | 09 | 13.290 | 086 | 35.633 | 103 | TF1 - 03 | 10849 |
| TF2HF17 | F | 10/8/02 | 281 | 1304 | 3175 | 09 | 13.969 | 086 | 34.926 | 105 | TF1 - 03 | 10561 |
| TF2HF17 | G | 10/8/02 | 281 | 1441 | 3185 | 09 | 14.691 | 086 | 34.236 | 105 | TF1 - 03 | 10267 |
| TF2HF17 | H | 10/8/02 | 281 | 1634 | 3190 | 09 | 15.361 | 086 | 33.514 | 102 | TF1 - 03 | 9979 |
| TF2HF17 | I | 10/8/02 | 281 | 1810 | 3190 | 09 | 16.038 | 086 | 32.865 | 104 | TF1 - 03 | 9704 |
| TF2HF17 | J | 10/8/02 | 281 | 1941 | 3190 | 09 | 16.701 | 086 | 32.143 | 107 | TF1 - 03 | 9415 |
| TF2HF17 | K | 10/8/02 | 281 | 2115 | 3190 | 09 | 17.426 | 086 | 31.429 | 109 | TF1 - 03 | 9116 |

Notes:
ND = no data (no penetration or excessive probe motion)

Table IV-3. Antares (outrigger) heat flow stations, locations, preliminary results.

| Station | Date | JD | GMT | CBD (m) | Latitude (N) Deg | Latitude (N) Min | Longitude (W) Deg | Longitude (W) Min | $N_A$ | $N_T$ | K (W/m°C) | Q (mW/m²) |
|---|---|---|---|---|---|---|---|---|---|---|---|---|
| GC01 | 9/9/06 | 251 | 2236 | 3400 | 09 | 40.998 | 086 | 23.727 | 4S | 4S | 0.75 | 33-35 |
| GC02 | 9/10/06 | 252 | 0319 | 3400 | 09 | 41.129 | 086 | 23.605 | 4S | no data, probes not started | | |
| GC03 | 9/10/06 | 252 | 0757 | 3575 | 09 | 41.650 | 086 | 23.063 | 4S | 4S | 0.75 | 69 |
| GC04 | 9/11/06 | 253 | 0028 | 3114 | 09 | 18.663 | 086 | 11.880 | 4S | 4S | 0.75 | 107 |
| GC05 | 9/11/06 | 253 | 0414 | 3250 | 09 | 18.664 | 086 | 11.264 | 4S | 4S | 0.75 | 69 |
| GC06 | 9/11/06 | 253 | 0806 | 3250 | 09 | 18.665 | 086 | 11.102 | 4S | no data, tipped over | | |
| GC07 | 9/11/06 | 253 | 1202 | 3250 | 09 | 20.462 | 086 | 10.430 | 4S | 4S | 0.75 | 64 |
| GC08 | 9/14/06 | 256 | 1424 | 3250 | 09 | 20.039 | 086 | 10.995 | 4S | no data, tipped over | | |
| GC09 | 9/14/06 | 256 | 1835 | 3250 | 09 | 19.908 | 086 | 10.880 | 4S | no data, tipped over | | |
| GC10 | 9/14/06 | 256 | 2237 | 3330 | *09* | *18.955* | *086* | *10.728* | 4S | 2S | 0.75 | >28 |
| GC11 | 9/16/06 | 258 | 1438 | 3300 | 09 | 40.765 | 086 | 34.254 | 4S | 4S | 0.75 | 538 |
| GC12 | 9/16/06 | 258 | 1811 | 3300 | 09 | 40.793 | 086 | 34.296 | 4S | 4S | 0.75 | 556 |
| GC13 | 9/16/06 | 258 | 2219 | 3160 | 09 | 36.438 | 086 | 39.065 | 4S | 4S | 0.75 | 665 |
| GC14 | 9/17/06 | 259 | 0137 | 3160 | 09 | 36.394 | 086 | 39.130 | 4S | 4S | 0.75 | 539 |
| GC15 | 9/18/06 | 260 | 0237 | 2810 | 08 | 29.808 | 085 | 58.163 | 4S | no data, did not penetrate | | |
| GC16 | 9/18/06 | 260 | 1814 | 2755 | 08 | 29.837 | 085 | 56.045 | 4S | 4S | 0.75 | 121 |
| GC17 | 9/18/06 | 260 | 2155 | 2830 | 08 | 32.218 | 085 | 54.239 | 4S | 3S | 0.75 | 30 |
| GC18 | 9/19/06 | 261 | 0128 | 2844 | 08 | 31.864 | 085 | 54.883 | 4S | no data, tipped over | | |
| GC19 | 9/19/06 | 261 | 0502 | 2835 | 08 | 29.788 | 085 | 58.036 | 4S | 4S | 0.75 | 130 |
| GC20 | 9/20/06 | 262 | 0525 | 2780 | 08 | 29.749 | 085 | 58.064 | 4S | 4S | 0.75 | 141 |
| GC21 | 9/21/06 | 263 | 1916 | 3035 | 08 | 44.205 | 087 | 12.736 | 3S | 3S | 0.75 | >125 |
| GC22 | 9/21/06 | 263 | 2235 | 3020 | 08 | 44.337 | 087 | 12.650 | 3S | no data, tipped over | | |
| GC23 | 9/22/06 | 264 | 0240 | 2900 | 08 | 37.012 | 087 | 16.813 | 3S | no data, tipped over | | |
| GC24 | 9/22/06 | 264 | 0546 | 2860 | 08 | 37.251 | 087 | 17.057 | 3S | 3S | 0.75 | 181 |
| GC33 | 9/26/06 | 268 | 1437 | 3120 | 09 | 05.249 | 087 | 05.764 | 2S, 1L | 1S, 1L | 0.75 | 73 |
| GC34 | 9/26/06 | 268 | 1746 | 3100 | 09 | 05.196 | 087 | 05.831 | 2S, 1L | no data, did not penetrate | | |
| GC35 | 9/26/06 | 268 | 2057 | 3125 | 09 | 05.231 | 087 | 05.790 | 2S, 1L | 1S, 1L | 0.75 | 113 |
| GC36 | 9/27/06 | 269 | 0020 | 3075 | 09 | 06.300 | 087 | 05.637 | 2S, 1L | 1S, 1L | 0.75 | 56 |
| GC37 | 9/27/06 | 269 | 1518 | 3110 | 09 | 05.213 | 087 | 05.812 | 2S, 1L | 1S, 1L | 0.75 | 198 |
| GC38 | 9/27/06 | 269 | 1822 | 3207 | 09 | 04.969 | 087 | 05.979 | 2S, 1L | 1S, 1L | 0.75 | 288 |
| GC39 | 9/27/06 | 269 | 2132 | 3180 | 09 | 05.005 | 087 | 05.944 | 2S, 1L | 1S, 1L | 0.75 | 202 |
| GC40 | 9/28/06 | 270 | 0044 | 3140 | *09* | *05.046* | *087* | *05.931* | 2S, 1L | 1S, 1L | 0.75 | 611 |
| GC41 | 9/28/06 | 270 | 1641 | 3100 | 09 | 05.082 | 087 | 05.889 | 1S, 2L | no data, tipped over | | |
| GC42 | 9/28/06 | 270 | 1939 | 3160 | 09 | 04.848 | 087 | 05.780 | 1S, 2L | 1S, 2L | 0.75 | 522-540 |

Notes:
ND = no center beam depth recorded; NA = number of probes attempted; NT = number of useful equilibrium temperatures derived; S = short probe, L = long probe

Table IV-3. Antares (outrigger) heat flow stations, locations, preliminary results.

| Station | Date | JD | GMT | CBD (m) | Latitude (N) Deg | Latitude (N) Min | Longitude (W) Deg | Longitude (W) Min | $N_A$ | $N_T$ | K (W/m°C) | Q (mW/m²) |
|---|---|---|---|---|---|---|---|---|---|---|---|---|
| GC43 | 9/28/06 | 270 | 2248 | 3140 | 09 | 04.877 | 087 | 05.759 | 1S, 2L | no data, tipped over | | |
| PC44 | 9/29/06 | 271 | 2222 | ND | 09 | 40.782 | 086 | 34.296 | 4L | 4L | 0.75 | 633 |
| PC45 | 9/30/06 | 272 | 0634 | 4780 | 09 | 51.931 | 086 | 21.277 | 4L | 2L | 0.75 | 33 |
| GC46 | 10/1/06 | 273 | 2102 | 2840 | 08 | 29.828 | 085 | 58.011 | 1S, 2L | 1S, 2L | 0.75 | 153 |
| GC47 | 10/1/06 | 273 | 2335 | 2840 | 08 | 29.797 | 085 | 58.006 | 1S, 2L | 1S, 2L | 0.75 | 140 |
| PC48 | 10/2/06 | 274 | 0429 | 2840 | 08 | 29.805 | 085 | 58.023 | 4L | 4L | 0.75 | 127 |
| GC49 | 10/3/06 | 275 | 1922 | 3140 | 09 | 05.058 | 087 | 05.925 | 1S, 2L | 28° tilt, no useful data | | |
| GC50 | 10/3/06 | 275 | 2218 | 3140 | 09 | 05.052 | 087 | 05.926 | 1S, 2L | 2L | 0.75 | 997 |
| GC51 | 10/4/06 | 276 | 0103 | 3140 | 09 | 05.051 | 087 | 05.917 | 1S, 2L | 2L | 0.75 | 735 |
| GC52 | 10/4/06 | 276 | 2228 | 3150 | 08 | 49.189 | 087 | 10.103 | 1S, 2L | 1S, 2L | 0.75 | 315 |
| GC53 | 10/5/06 | 277 | 0131 | 3080 | 08 | 49.130 | 087 | 10.145 | 1S, 2L | 1L ıl penetration, >272 | | |
| GC54 | 10/5/06 | 277 | 0424 | 3125 | 08 | 49.158 | 087 | 10.121 | 1S, 2L | 2L | 0.75 | 1162 |
| GC55 | 10/5/06 | 277 | 2221 | 3213 | 08 | 47.353 | 087 | 11.825 | 1S, 2L | 1S, 2L | 0.75 | 215 |
| GC56 | 10/6/06 | 278 | 0110 | 3170 | 08 | 47.400 | 087 | 11.775 | 1S, 2L | 2L | 0.75 | 36 |
| GC57 | 10/6/06 | 278 | 0408 | 3130 | 08 | 47.431 | 087 | 11.742 | 1S, 2L | no data, tipped over | | |
| GC58 | 10/6/06 | 278 | 1921 | 2950 | 09 | 26.613 | 087 | 03.051 | 1S, 2L | no data, tipped over | | |
| GC59 | 10/7/06 | 279 | 0053 | 3140 | 09 | 10.232 | 087 | 15.498 | 1S, 2L | 1S, 2L | 0.75 | 129 |
| GC60 | 10/7/06 | 279 | 1620 | 3107 | 09 | 10.540 | 087 | 15.568 | 1S, 2L | 1S, 2L | 0.75 | 95 |
| GC61 | 10/7/06 | 279 | 1900 | 3115 | 09 | 10.483 | 087 | 15.614 | 1S, 2L | 1S, 2L | 0.75 | 103 |
| GC62 | 10/8/06 | 280 | 1352 | 3315 | 09 | 40.883 | 086 | 34.457 | 1S, 2L | 1S, 2L | 0.75 | 516 |
| GC63 | 10/8/06 | 280 | 1644 | 3340 | 09 | 40.916 | 086 | 34.329 | 1S, 2L | 1S, 2L | 0.75 | 503 |
| GC64 | 10/8/06 | 280 | 1932 | 3320 | 09 | 40.841 | 086 | 34.214 | 1S, 2L | 1S, 2L | 0.75 | 635 |
| GC65 | 10/8/06 | 280 | 2227 | 3340 | 09 | 40.674 | 086 | 34.386 | 1S, 2L | 1S, 2L | 0.75 | 406 |

Notes:
ND = no center beam depth recorded; NA = number of probes attempted; NT = number of useful equilibrium temperatures derived; S = short probe, L = long probe

Table IV-3. Antares (outrigger) heat flow stations, locations, preliminary results.

| Station | Date | JD | GMT | CBD (m) | Latitude (N) | | Longitude (W) | | $N_A$ | $N_T$ | K (W/m°C) | Q (mW/m²) |
|---|---|---|---|---|---|---|---|---|---|---|---|---|
| | | | | | Deg | Min | Deg | Min | | | | |
| GC01 | 9/9/02 | 251 | 2236 | 3400 | 09 | 40.998 | 086 | 23.727 | 4S | 4S | 0.75 | 33-35 |
| GC02 | 9/10/02 | 252 | 0319 | 3400 | 09 | 41.129 | 086 | 23.605 | 4S | no data, probes not started | | |
| GC03 | 9/10/02 | 252 | 0757 | 3575 | 09 | 41.650 | 086 | 23.063 | 4S | 4S | 0.75 | 69 |
| GC04 | 9/11/02 | 253 | 0028 | 3114 | 09 | 18.663 | 086 | 11.880 | 4S | 4S | 0.75 | 107 |
| GC05 | 9/11/02 | 253 | 0414 | 3250 | 09 | 18.664 | 086 | 11.264 | 4S | 4S | 0.75 | 69 |
| GC06 | 9/11/02 | 253 | 0806 | 3250 | 09 | 18.665 | 086 | 11.102 | 4S | no data, tipped over | | |
| GC07 | 9/11/02 | 253 | 1202 | 3250 | 09 | 20.462 | 086 | 10.430 | 4S | 4S | 0.75 | 64 |
| GC08 | 9/14/02 | 256 | 1424 | 3250 | 09 | 20.039 | 086 | 10.995 | 4S | no data, tipped over | | |
| GC09 | 9/14/02 | 256 | 1835 | 3250 | 09 | 19.908 | 086 | 10.880 | 4S | no data, tipped over | | |
| GC10 | 9/14/02 | 256 | 2237 | 3330 | *09* | *18.955* | *086* | *10.728* | 4S | 2S | 0.75 | >28 |
| GC11 | 9/16/02 | 258 | 1438 | 3300 | 09 | 40.765 | 086 | 34.254 | 4S | 4S | 0.75 | 538 |
| GC12 | 9/16/02 | 258 | 1811 | 3300 | 09 | 40.793 | 086 | 34.296 | 4S | 4S | 0.75 | 556 |
| GC13 | 9/16/02 | 258 | 2219 | 3160 | 09 | 36.438 | 086 | 39.065 | 4S | 4S | 0.75 | 665 |
| GC14 | 9/17/02 | 259 | 0137 | 3160 | 09 | 36.394 | 086 | 39.130 | 4S | 4S | 0.75 | 539 |
| GC15 | 9/18/02 | 260 | 0237 | 2810 | 08 | 29.808 | 085 | 58.163 | 4S | no data, did not penetrate | | |
| GC16 | 9/18/02 | 260 | 1814 | 2755 | 08 | 29.837 | 085 | 56.045 | 4S | 4S | 0.75 | 121 |
| GC17 | 9/18/02 | 260 | 2155 | 2830 | 08 | 32.218 | 085 | 54.239 | 4S | 3S | 0.75 | 30 |
| GC18 | 9/19/02 | 261 | 0128 | 2844 | 08 | 31.864 | 085 | 54.883 | 4S | no data, tipped over | | |
| GC19 | 9/19/02 | 261 | 0502 | 2835 | 08 | 29.788 | 085 | 58.036 | 4S | 4S | 0.75 | 130 |
| GC20 | 9/20/02 | 262 | 0525 | 2780 | 08 | 29.749 | 085 | 58.064 | 4S | 4S | 0.75 | 141 |
| GC21 | 9/21/02 | 263 | 1916 | 3035 | 08 | 44.205 | 087 | 12.736 | 3S | 3S | 0.75 | >125 |
| GC22 | 9/21/02 | 263 | 2235 | 3020 | 08 | 44.337 | 087 | 12.650 | 3S | no data, tipped over | | |
| GC23 | 9/22/02 | 264 | 0240 | 2900 | 08 | 37.012 | 087 | 16.813 | 3S | no data, tipped over | | |
| GC24 | 9/22/02 | 264 | 0546 | 2860 | 08 | 37.251 | 087 | 17.057 | 3S | 3S | 0.75 | 181 |
| GC33 | 9/26/02 | 268 | 1437 | 3120 | 09 | 05.249 | 087 | 05.764 | 2S, 1L | 1S, 1L | 0.75 | 73 |
| GC34 | 9/26/02 | 268 | 1746 | 3100 | 09 | 05.196 | 087 | 05.831 | 2S, 1L | no data, did not penetrate | | |
| GC35 | 9/26/02 | 268 | 2057 | 3125 | 09 | 05.231 | 087 | 05.790 | 2S, 1L | 1S, 1L | 0.75 | 113 |
| GC36 | 9/27/02 | 269 | 0020 | 3075 | 09 | 06.300 | 087 | 05.637 | 2S, 1L | 1S, 1L | 0.75 | 56 |
| GC37 | 9/27/02 | 269 | 1518 | 3110 | 09 | 05.213 | 087 | 05.812 | 2S, 1L | 1S, 1L | 0.75 | 198 |
| GC38 | 9/27/02 | 269 | 1822 | 3207 | 09 | 04.969 | 087 | 05.979 | 2S, 1L | 1S, 1L | 0.75 | 288 |
| GC39 | 9/27/02 | 269 | 2132 | 3180 | 09 | 05.005 | 087 | 05.944 | 2S, 1L | 1S, 1L | 0.75 | 202 |
| GC40 | 9/28/02 | 270 | 0044 | 3140 | *09* | *05.046* | *087* | *05.931* | 2S, 1L | 1S, 1L | 0.75 | 611 |
| GC41 | 9/28/02 | 270 | 1641 | 3100 | 09 | 05.082 | 087 | 05.889 | 1S, 2L | no data, tipped over | | |
| GC42 | 9/28/02 | 270 | 1939 | 3160 | 09 | 04.848 | 087 | 05.780 | 1S, 2L | 1S, 2L | 0.75 | 522-540 |

Notes:
ND = no center beam depth recorded; NA = number of probes attempted; NT = number of useful equilibrium temperatures derived; S = short probe, L = long probe

Table IV-3. Antares (outrigger) heat flow stations, locations, preliminary results.

| Station | Date | JD | GMT | CBD (m) | Latitude (N) Deg | Latitude (N) Min | Longitude (W) Deg | Longitude (W) Min | $N_A$ | $N_T$ | K (W/m°C) | Q (mW/m²) |
|---|---|---|---|---|---|---|---|---|---|---|---|---|
| GC43 | 9/28/02 | 270 | 2248 | 3140 | 09 | 04.877 | 087 | 05.759 | 1S, 2L | no data, tipped over | | |
| PC44 | 9/29/02 | 271 | 2222 | ND | 09 | 40.782 | 086 | 34.296 | 4L | 4L | 0.75 | 633 |
| PC45 | 9/30/02 | 272 | 0634 | 4780 | 09 | 51.931 | 086 | 21.277 | 4L | 2L | 0.75 | 33 |
| GC46 | 10/1/02 | 273 | 2102 | 2840 | 08 | 29.828 | 085 | 58.011 | 1S, 2L | 1S, 2L | 0.75 | 153 |
| GC47 | 10/1/02 | 273 | 2335 | 2840 | 08 | 29.797 | 085 | 58.006 | 1S, 2L | 1S, 2L | 0.75 | 140 |
| PC48 | 10/2/02 | 274 | 0429 | 2840 | 08 | 29.805 | 085 | 58.023 | 4L | 4L | 0.75 | 127 |
| GC49 | 10/3/02 | 275 | 1922 | 3140 | 09 | 05.058 | 087 | 05.925 | 1S, 2L | 28° tilt, no useful data | | |
| GC50 | 10/3/02 | 275 | 2218 | 3140 | 09 | 05.052 | 087 | 05.926 | 1S, 2L | 2L | 0.75 | 997 |
| GC51 | 10/4/02 | 276 | 0103 | 3140 | 09 | 05.051 | 087 | 05.917 | 1S, 2L | 2L | 0.75 | 735 |
| GC52 | 10/4/02 | 276 | 2228 | 3150 | 08 | 49.189 | 087 | 10.103 | 1S, 2L | 1S, 2L | 0.75 | 315 |
| GC53 | 10/5/02 | 277 | 0131 | 3080 | 08 | 49.130 | 087 | 10.145 | 1S, 2L | 1L ıl penetration, >272 | | |
| GC54 | 10/5/02 | 277 | 0424 | 3125 | 08 | 49.158 | 087 | 10.121 | 1S, 2L | 2L | 0.75 | 1162 |
| GC55 | 10/5/02 | 277 | 2221 | 3213 | 08 | 47.353 | 087 | 11.825 | 1S, 2L | 1S, 2L | 0.75 | 215 |
| GC56 | 10/6/02 | 278 | 0110 | 3170 | 08 | 47.400 | 087 | 11.775 | 1S, 2L | 2L | 0.75 | 36 |
| GC57 | 10/6/02 | 278 | 0408 | 3130 | 08 | 47.431 | 087 | 11.742 | 1S, 2L | no data, tipped over | | |
| GC58 | 10/6/02 | 278 | 1921 | 2950 | 09 | 26.613 | 087 | 03.051 | 1S, 2L | no data, tipped over | | |
| GC59 | 10/7/02 | 279 | 0053 | 3140 | 09 | 10.232 | 087 | 15.498 | 1S, 2L | 1S, 2L | 0.75 | 129 |
| GC60 | 10/7/02 | 279 | 1620 | 3107 | 09 | 10.540 | 087 | 15.568 | 1S, 2L | 1S, 2L | 0.75 | 95 |
| GC61 | 10/7/02 | 279 | 1900 | 3115 | 09 | 10.483 | 087 | 15.614 | 1S, 2L | 1S, 2L | 0.75 | 103 |
| GC62 | 10/8/02 | 280 | 1352 | 3315 | 09 | 40.883 | 086 | 34.457 | 1S, 2L | 1S, 2L | 0.75 | 516 |
| GC63 | 10/8/02 | 280 | 1644 | 3340 | 09 | 40.916 | 086 | 34.329 | 1S, 2L | 1S, 2L | 0.75 | 503 |
| GC64 | 10/8/02 | 280 | 1932 | 3320 | 09 | 40.841 | 086 | 34.214 | 1S, 2L | 1S, 2L | 0.75 | 635 |
| GC65 | 10/8/02 | 280 | 2227 | 3340 | 09 | 40.674 | 086 | 34.386 | 1S, 2L | 1S, 2L | 0.75 | 406 |

Notes:
ND = no center beam depth recorded; NA = number of probes attempted; NT = number of useful equilibrium temperatures derived; S = short probe, L = long probe

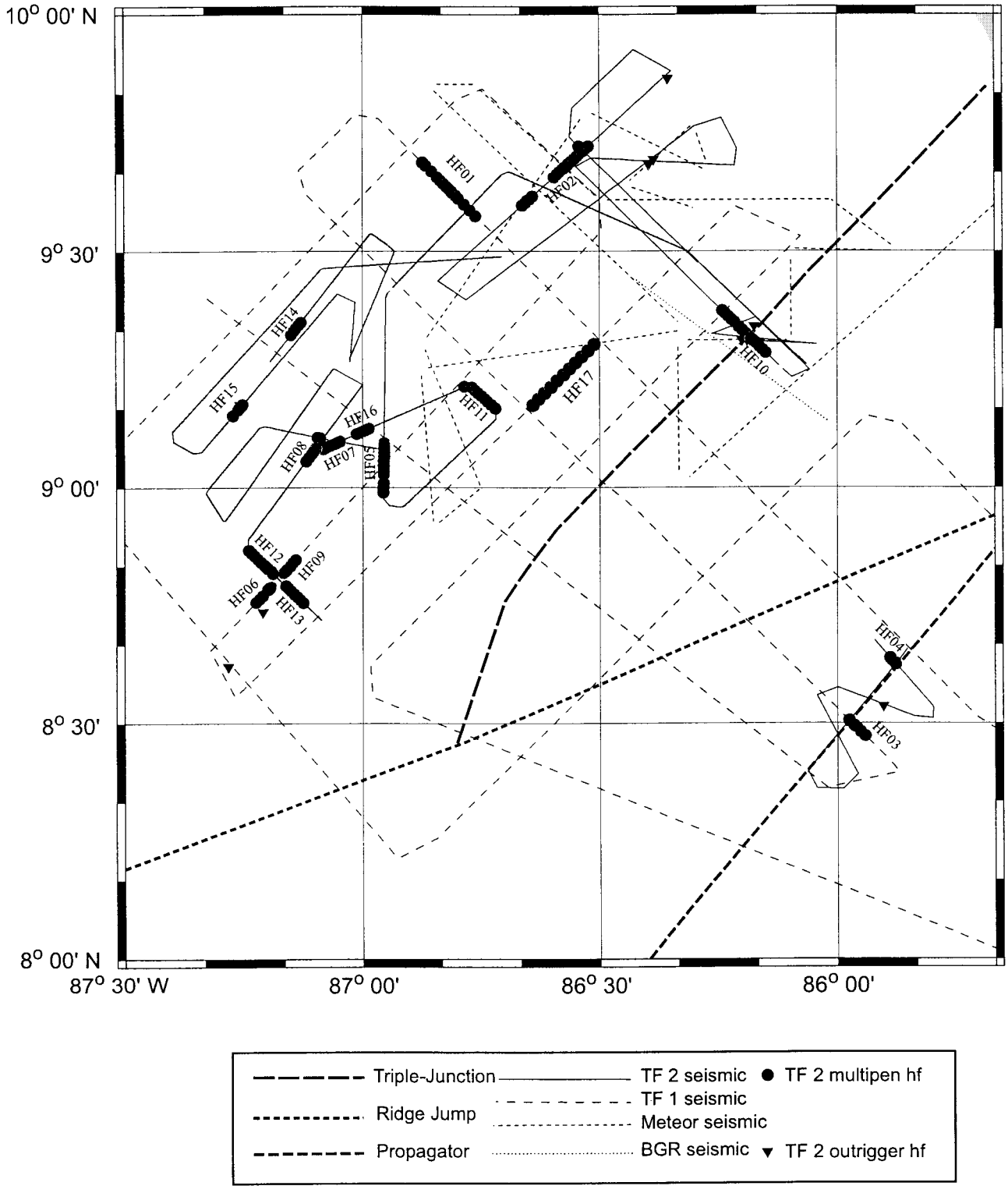
10° 00' N
9° 30'
9° 00'
8° 30'
8° 00' N
87° 30' W
87° 00'
86° 30'
86° 00'
HF01
HF02
HF03
HF04
HF06
HF07
HF08
HF09
HF10
HF11
HF12
HF13
HF14
HF15
HF16
HF17
Triple-Junction
Ridge Jump
Propagator
TF 2 seismic
TF 1 seismic
Meteor seismic
BGR seismic
TF 2 multipen hf
TF 2 outrigger hf

Figure IV-1

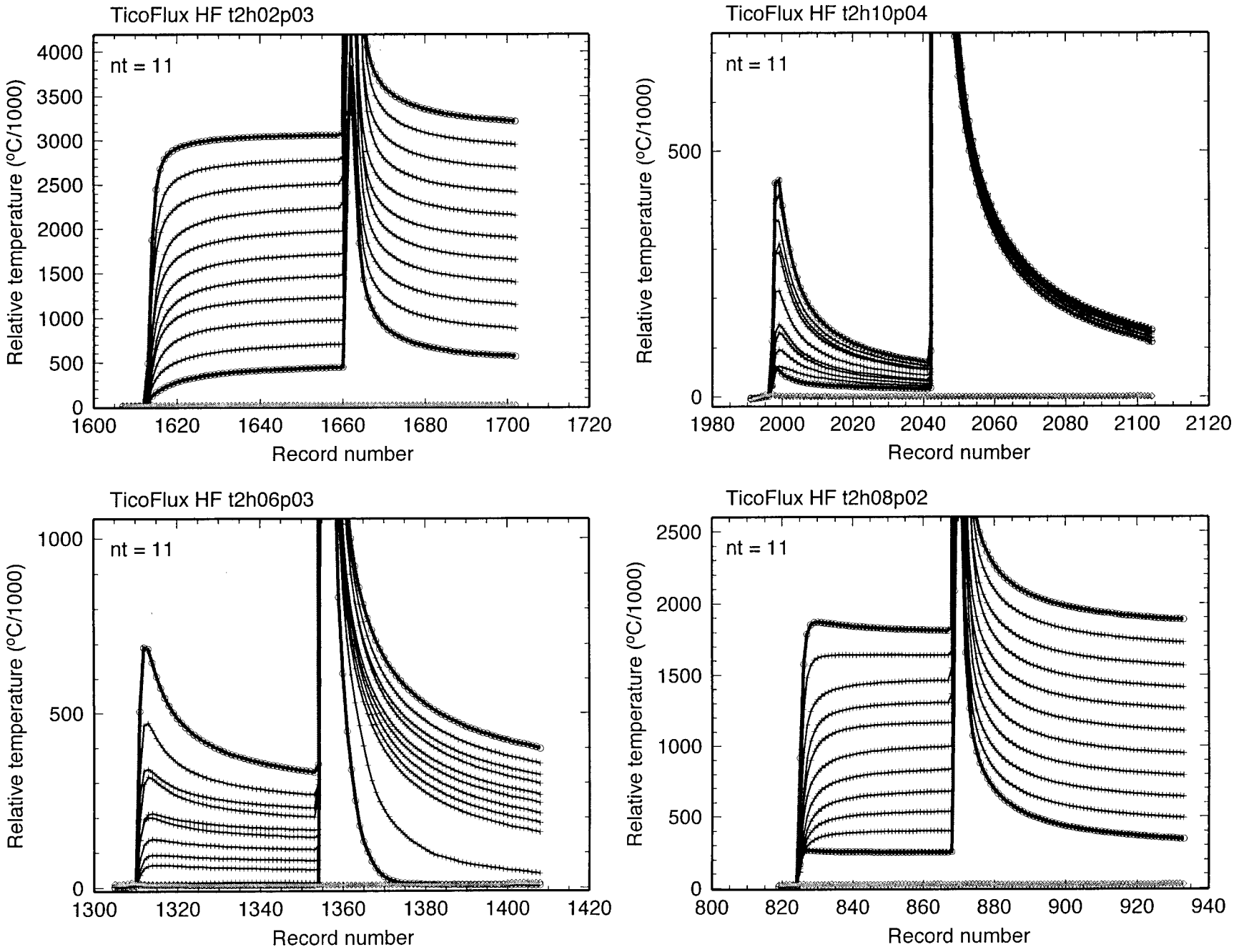
TicoFlux HF t2h02p03
nt = 11
Relative temperature (°C/1000)
Record number
TicoFlux HF t2h10p04
nt = 11
Relative temperature (°C/1000)
Record number
TicoFlux HF t2h06p03
nt = 11
Relative temperature (°C/1000)
Record number
TicoFlux HF t2h08p02
nt = 11
Relative temperature (°C/1000)
Record number

Figure IV-2

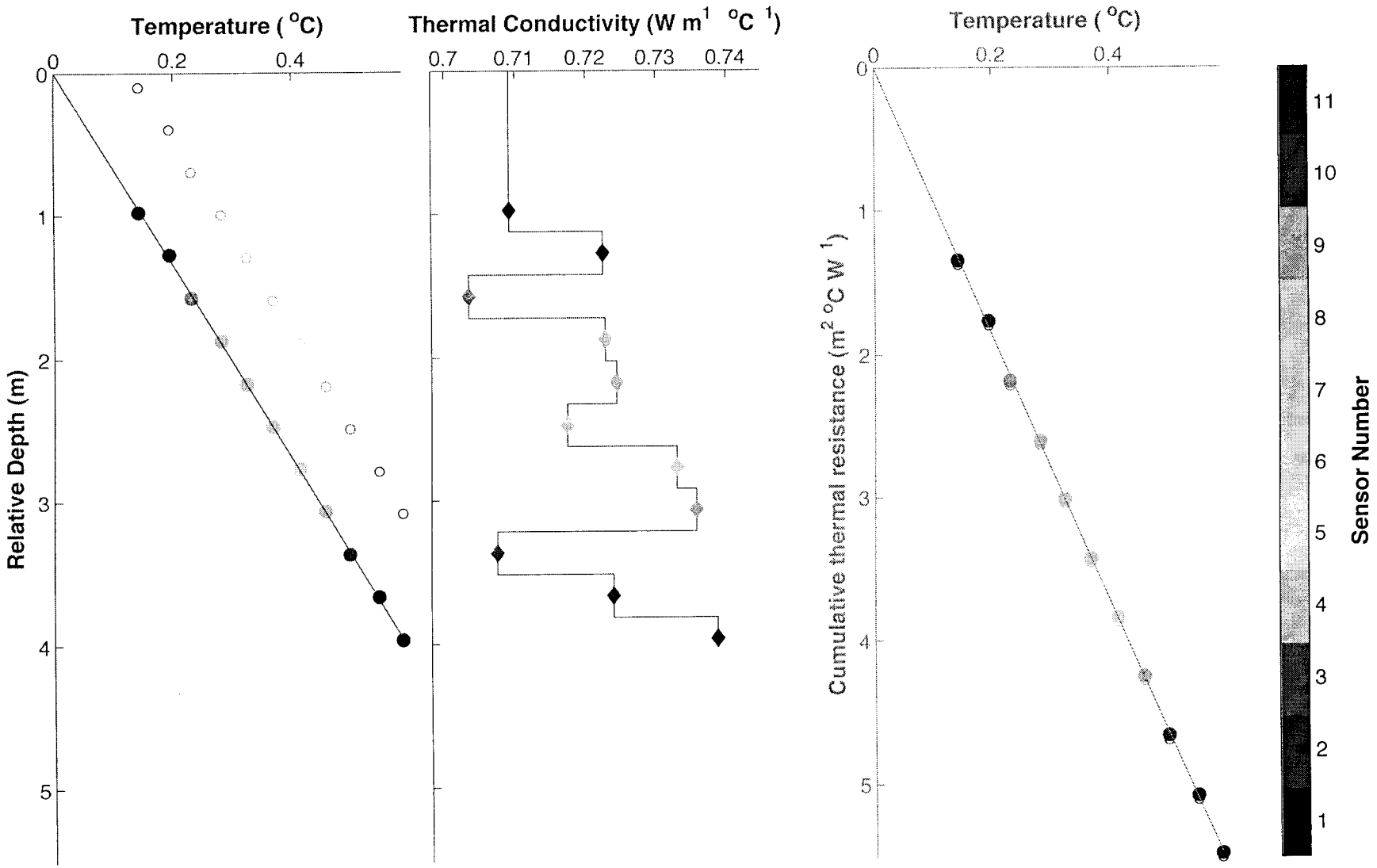


**t2h17p02**

Results: C:\Matlab\work\ticoflux\hf17/t2h17p02.res
Penetration: C:\Matlab\work\Ticoflux\hf17\t2h17p02.pen

Trial: 1 Iteration: 4
Processed: 09 Oct 2002 00:48:36

Figure IV-3

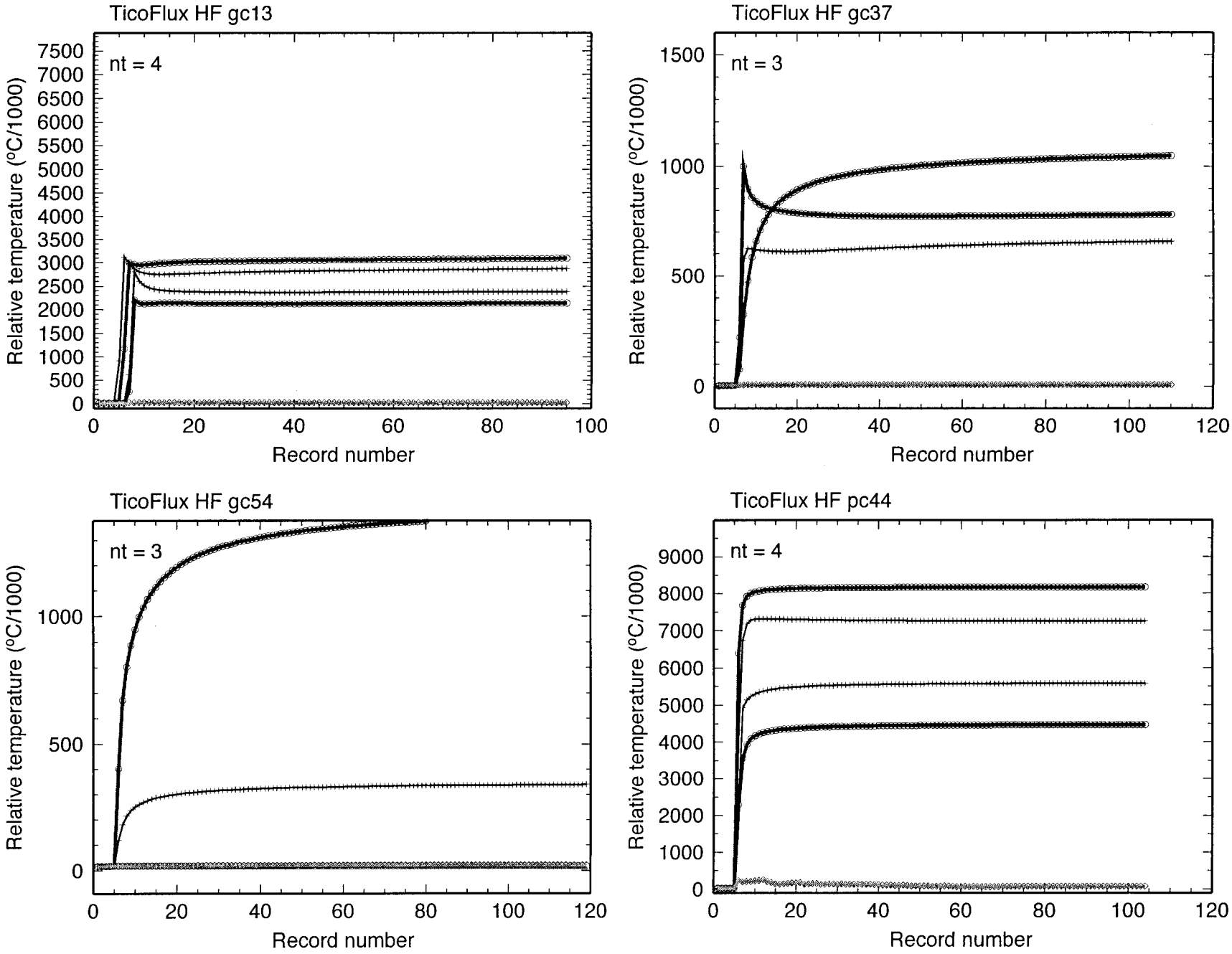
TicoFlux HF gc13
nt = 4
Relative temperature (°C/1000)
Record number
TicoFlux HF gc37
nt = 3
Relative temperature (°C/1000)
Record number
TicoFlux HF gc54
nt = 3
Relative temperature (°C/1000)
Record number
TicoFlux HF pc44
nt = 4
Relative temperature (°C/1000)
Record number

Figure IV-4

**TF2HF01**

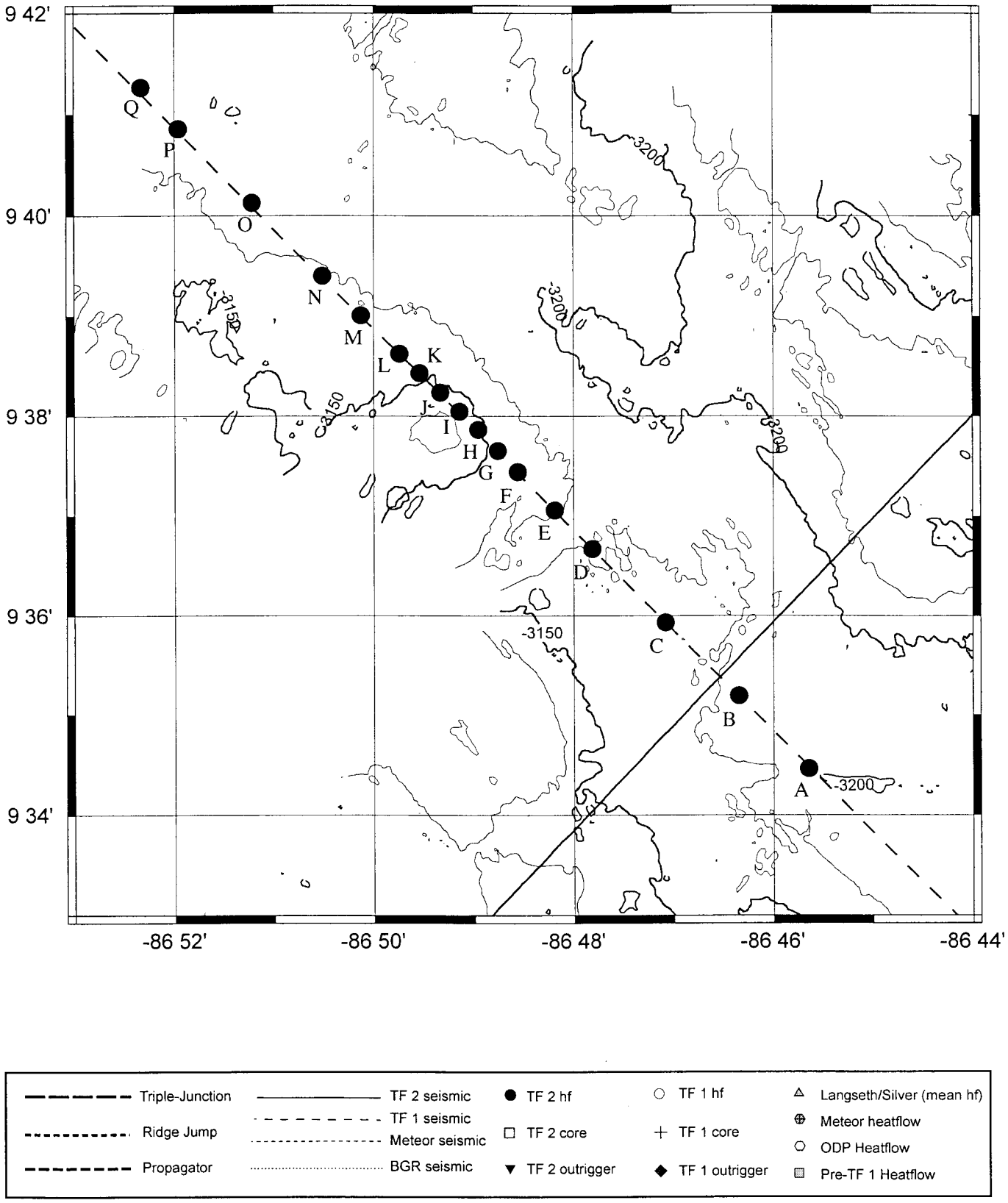


Figure IV-5

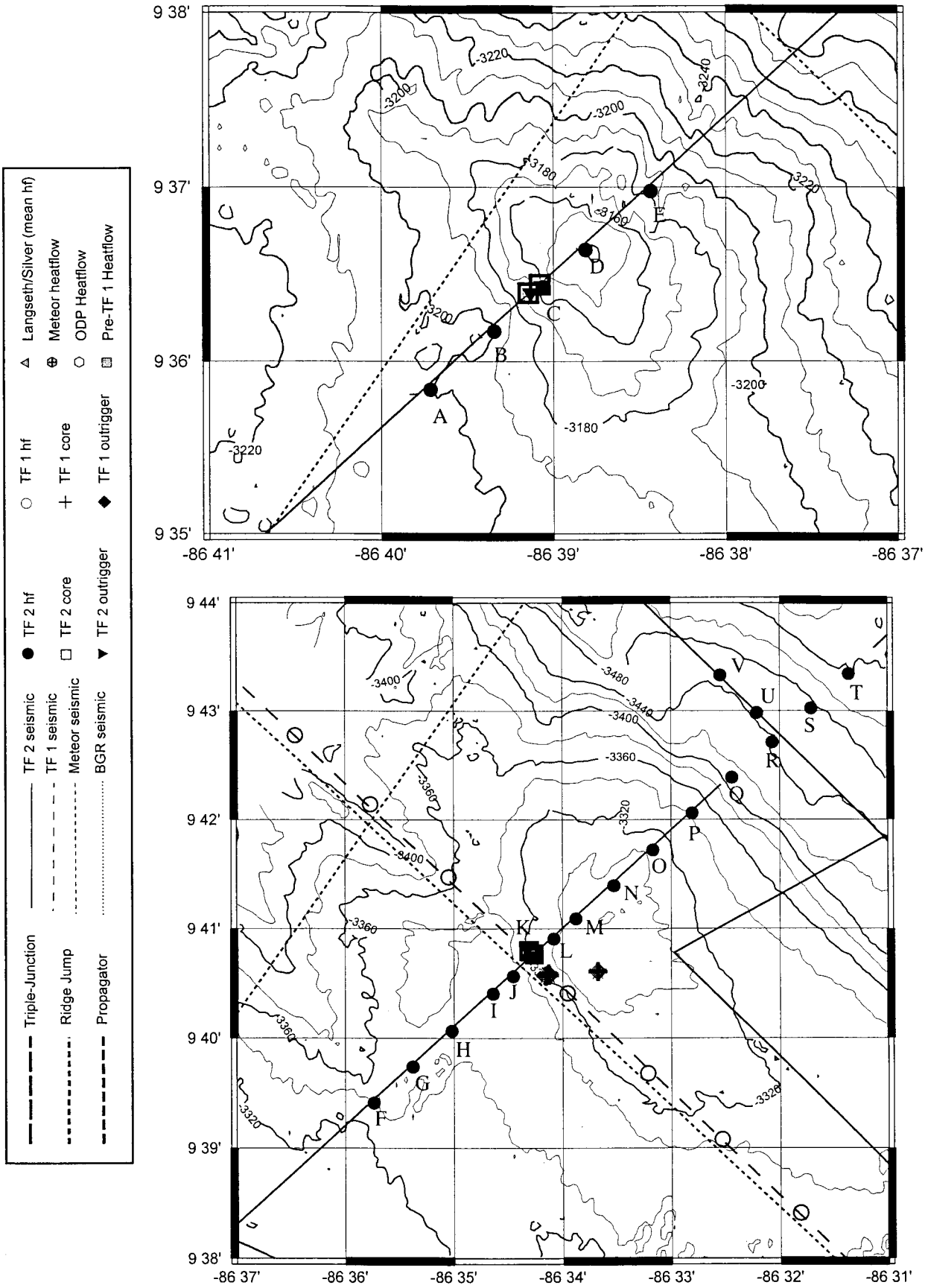
Triple-Junction
Ridge Jump
Propagator
TF 2 seismic
TF 1 seismic
Meteor seismic
BGR seismic
TF 2 hf
TF 2 core
TF 2 outrigger
TF 1 hf
TF 1 core
TF 1 outrigger
Langseth/Silver (mean hf)
Meteor heatflow
ODP Heatflow
Pre-TF 1 Heatflow
9 38'
9 37'
9 36'
9 35'
-86 41'
-86 40'
-86 39'
-86 38'
-86 37'
-3220
-3200
-3240
-3180
-3160
A
B
C
D
E
9 44'
9 43'
9 42'
9 41'
9 40'
9 39'
9 38'
-86 37'
-86 36'
-86 35'
-86 34'
-86 33'
-86 32'
-86 31'
-3400
-3480
-3440
-3360
-3320
F
G
H
I
J
K
L
M
N
O
P
Q
R
S
T
U
V

Figure IV-6

TF2HF03

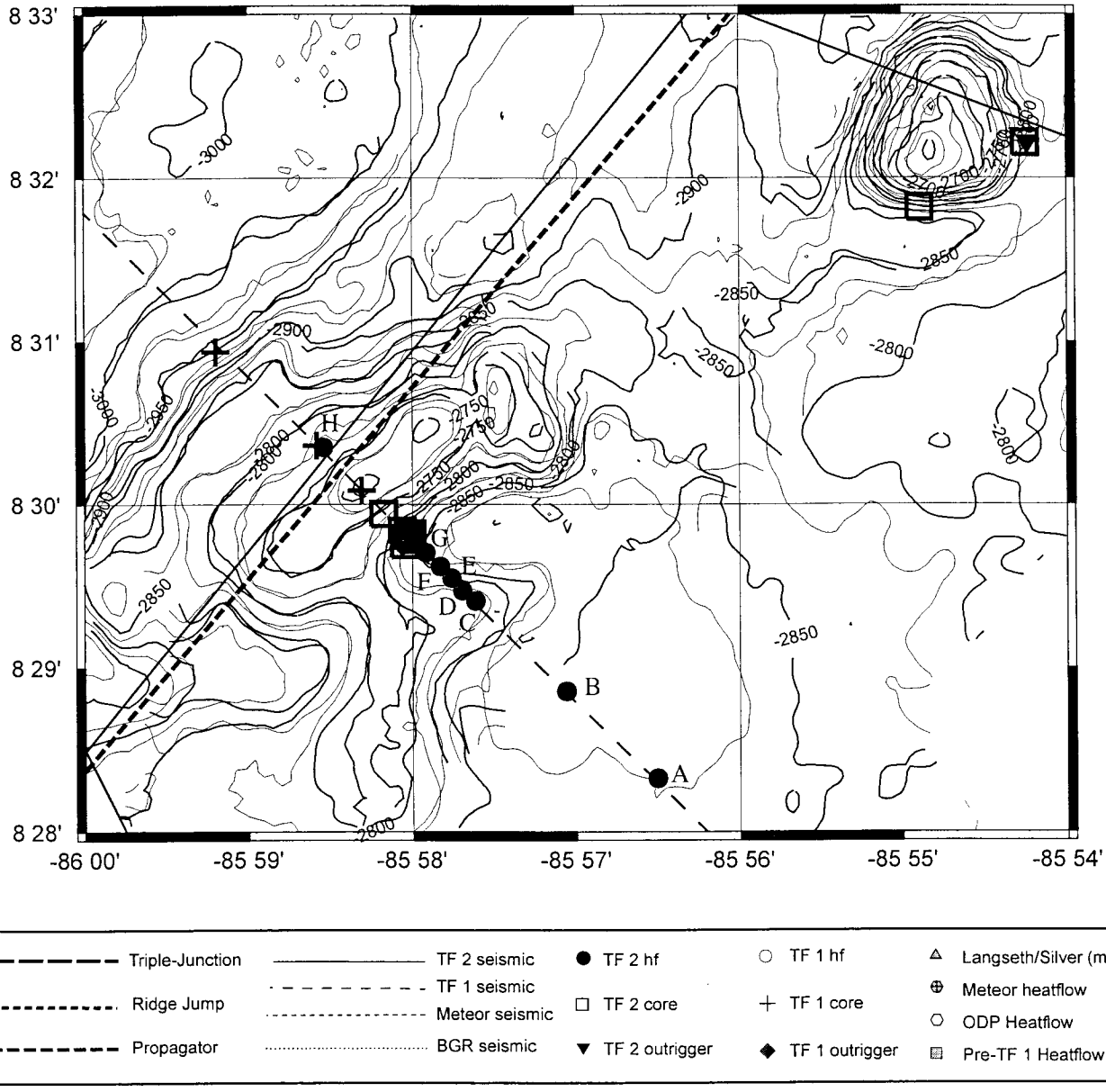


Figure IV-7

TF2HF04

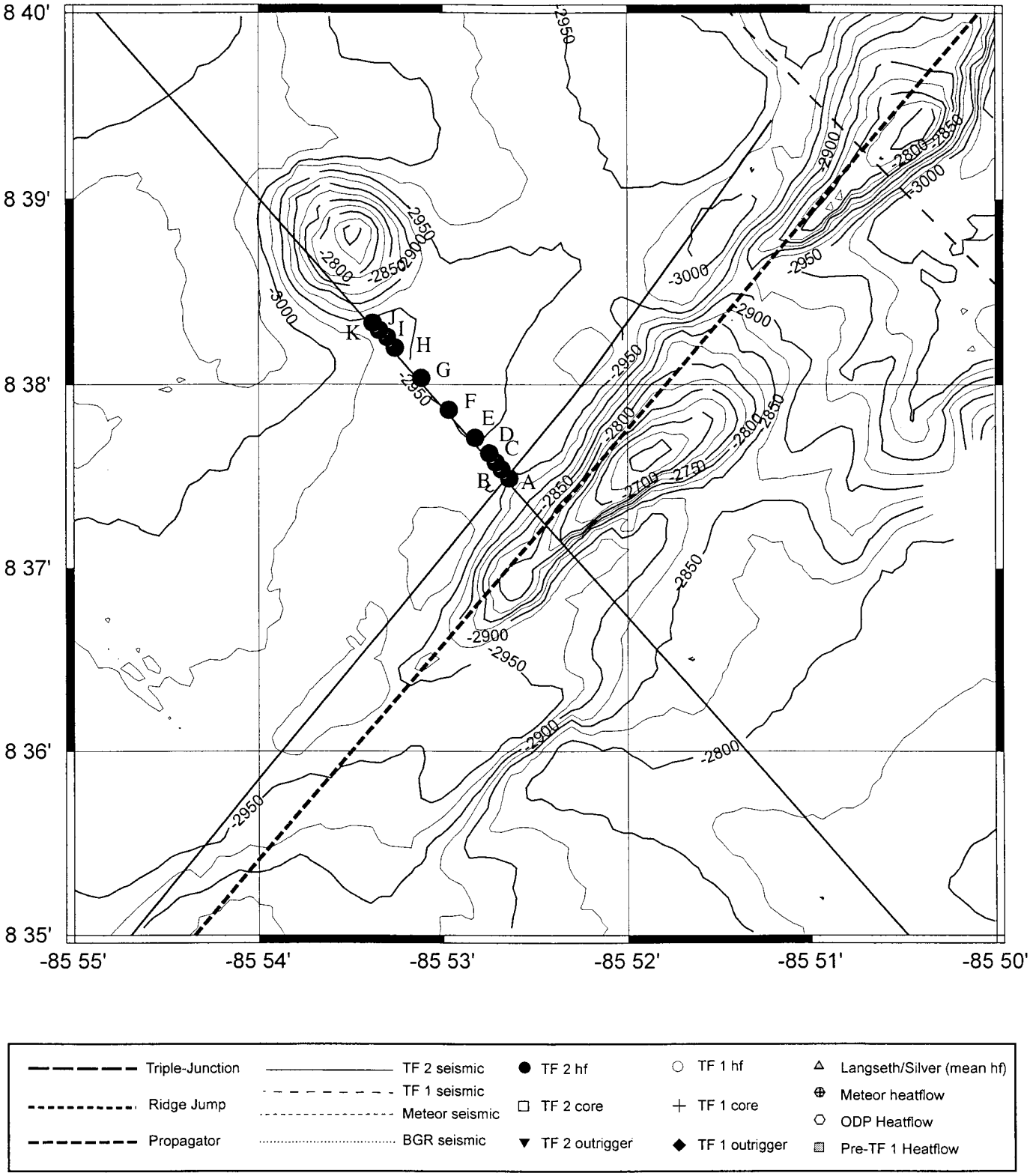


Figure IV-8

TF2HF05 TF2HF16

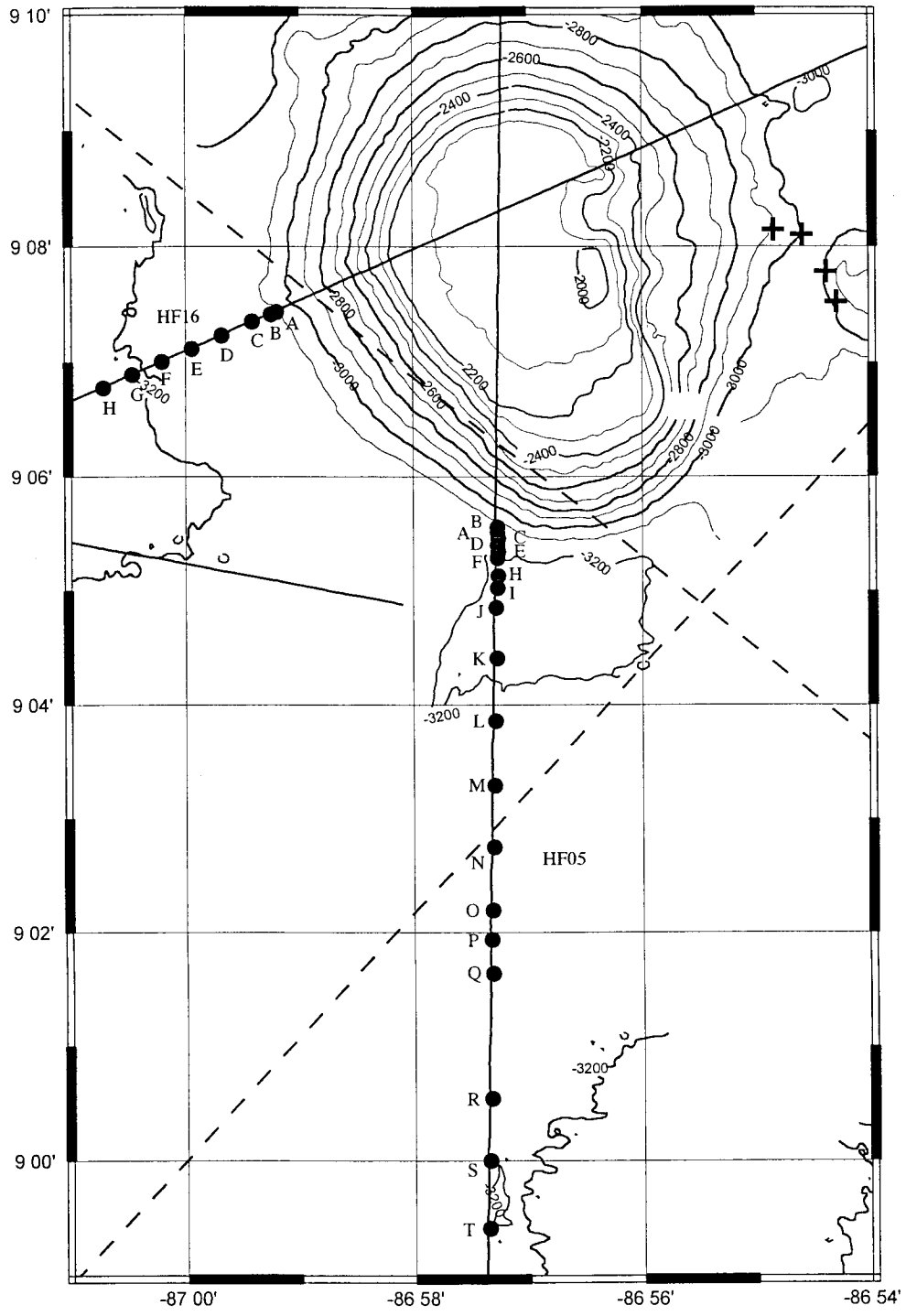


Triple-Junction
Ridge Jump
Propagator
TF 2 seismic
TF 1 seismic
Meteor seismic
BGR seismic
TF 2 hf
TF 2 core
TF 2 outrigger
TF 1 hf
TF 1 core
TF 1 outrigger
Langseth/Silver (mean hf)
Meteor heatflow
ODP Heatflow
Pre-TF 1 Heatflow

Figure IV-9

TF2HF06, 09, 12, 13

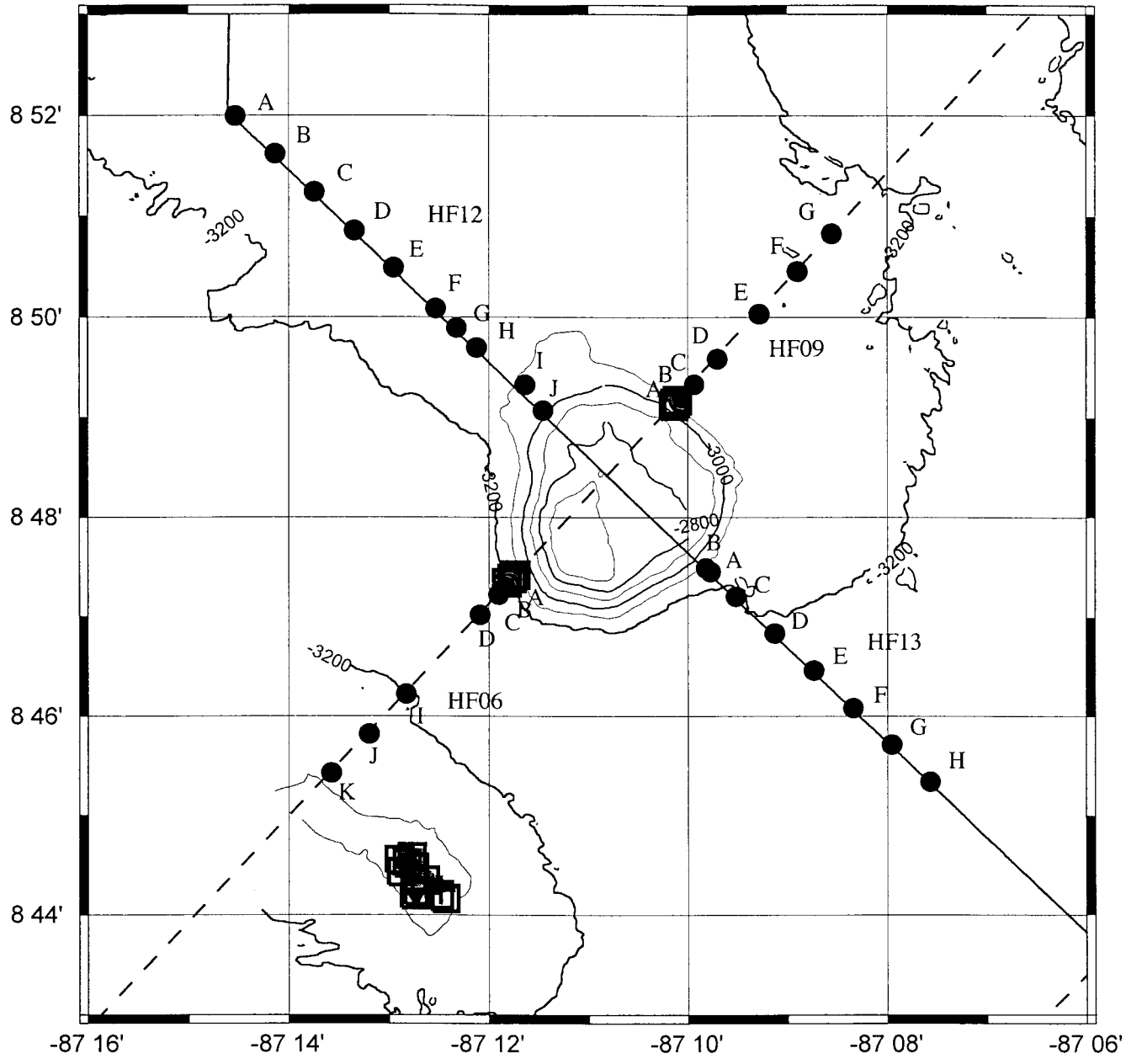


Triple-Junction
Ridge Jump
Propagator
TF 2 seismic
TF 1 seismic
Meteor seismic
BGR seismic
TF 2 hf
TF 2 core
TF 2 outrigger
TF 1 hf
TF 1 core
TF 1 outrigger
Langseth/Silver (mean hf)
Meteor heatflow
ODP Heatflow
Pre-TF 1 Heatflow

Figure IV-10

TF2HF07 TF2HF08

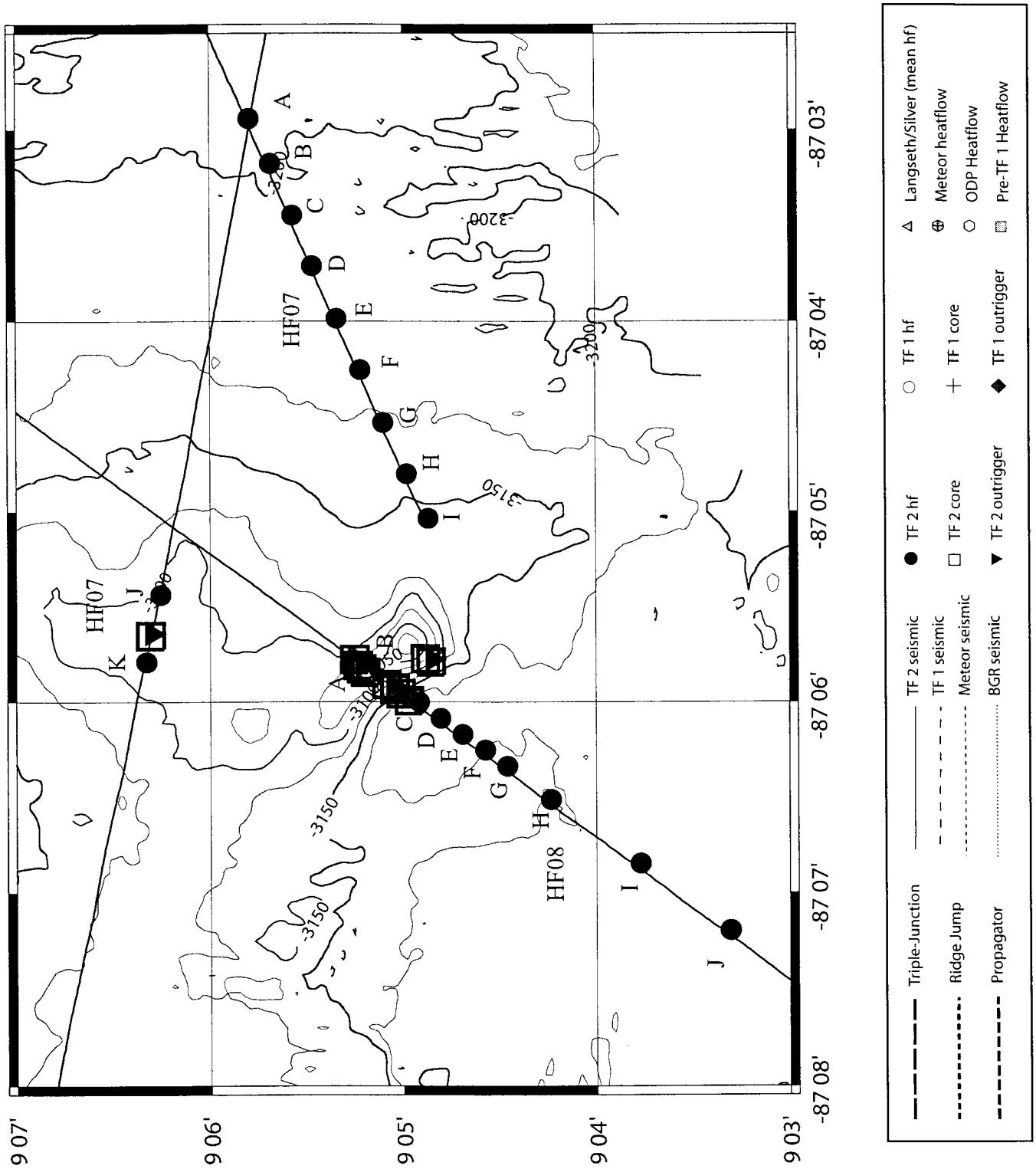


Figure IV-11

TF2HF10

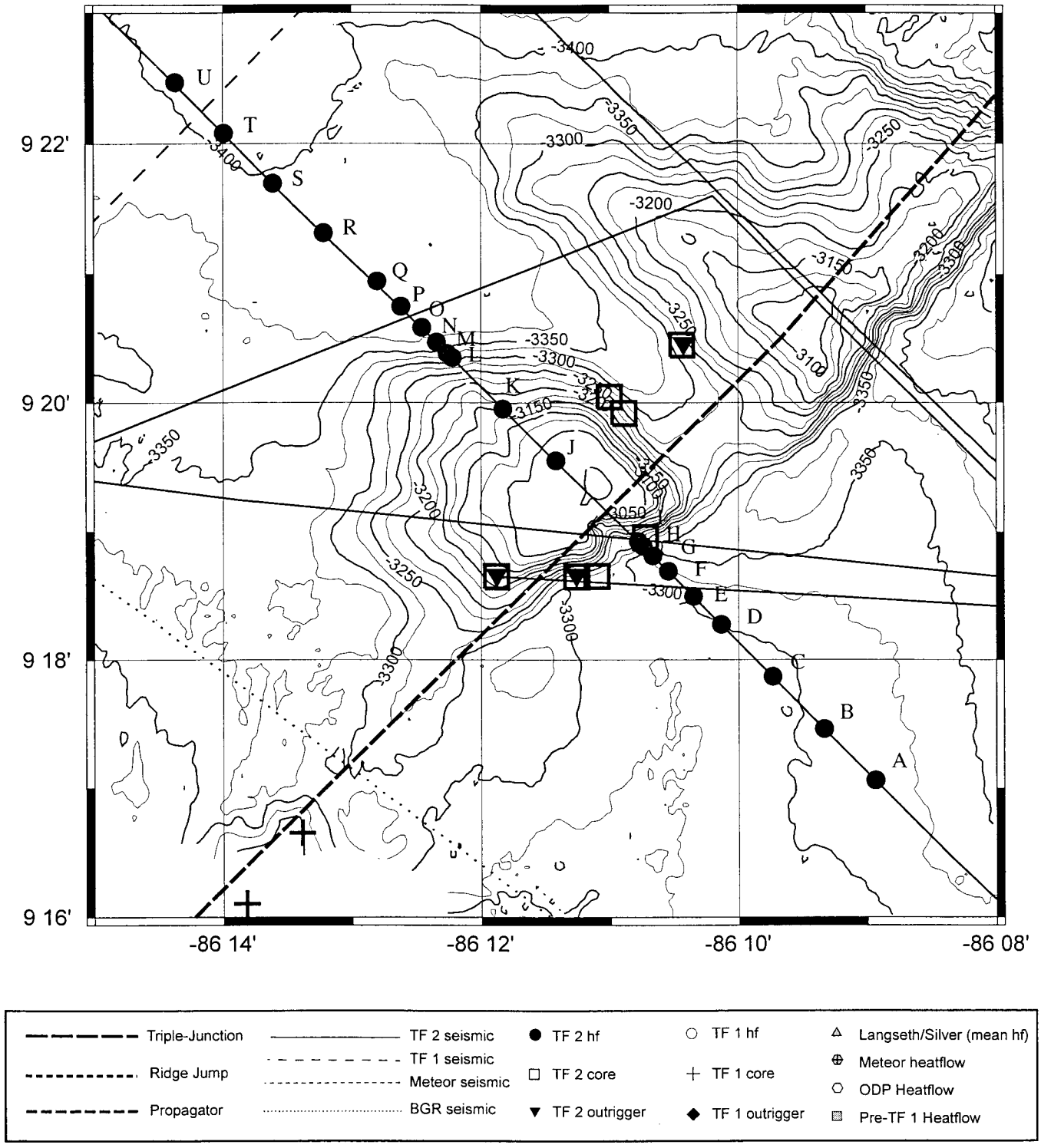


Figure IV-12

TF2HF11

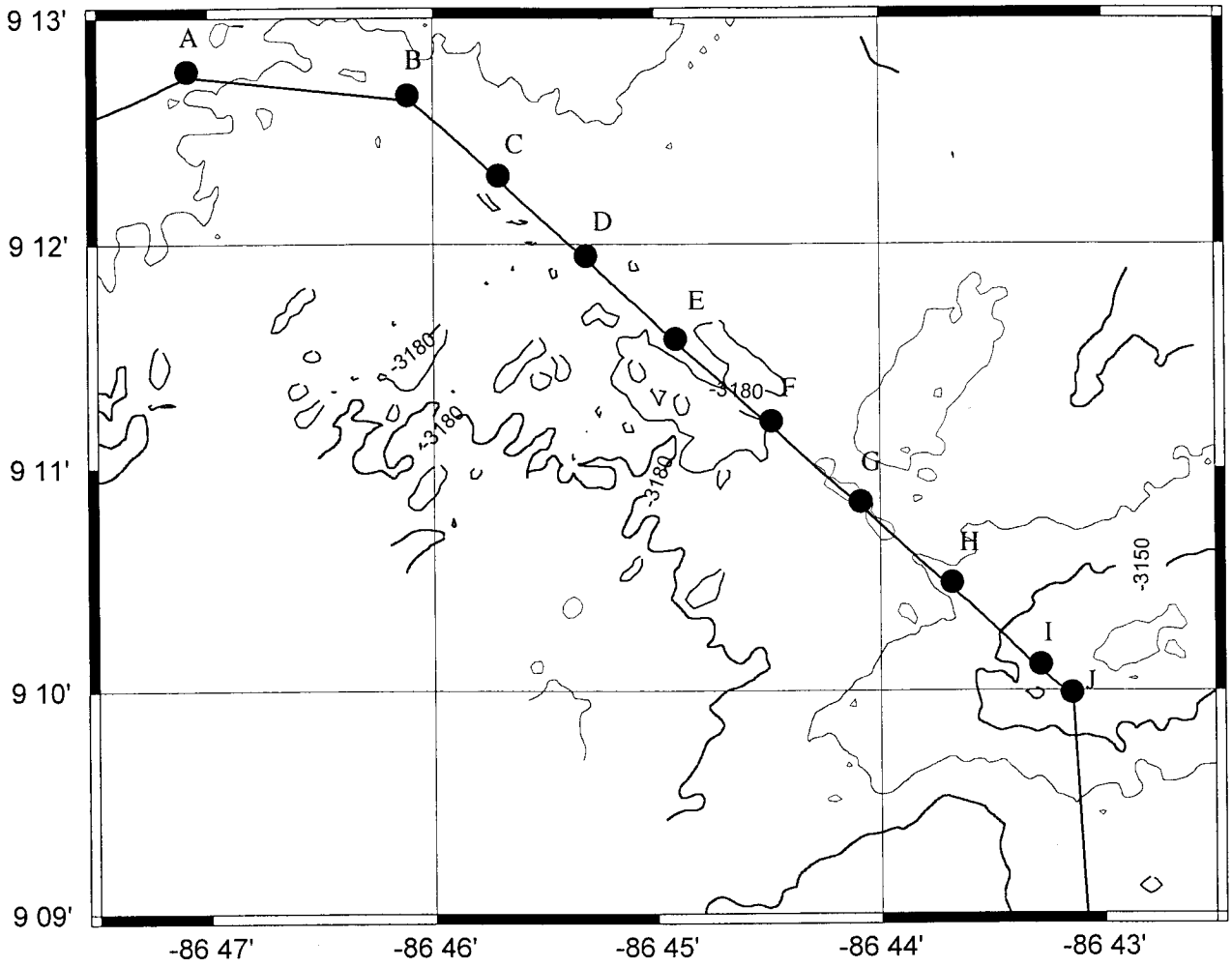


Triple-Junction
Ridge Jump
Propagator
TF 2 seismic
TF 1 seismic
Meteor seismic
BGR seismic
TF 2 hf
TF 2 core
TF 2 outrigger
TF 1 hf
TF 1 core
TF 1 outrigger
Langseth/Silver (mean hf)
Meteor heatflow
ODP Heatflow
Pre-TF 1 Heatflow

Figure IV-13

TF2HF14

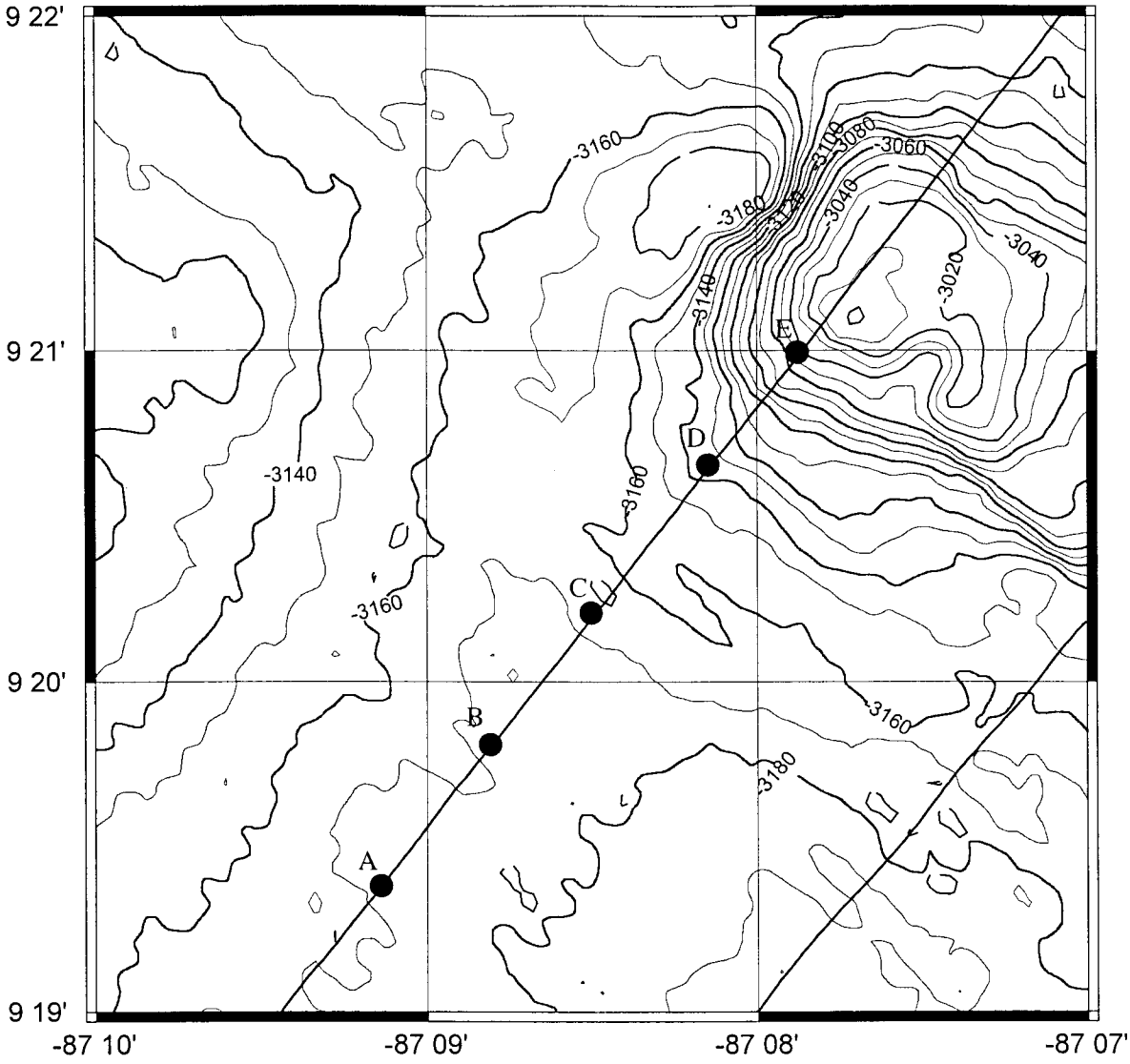


Triple-Junction
Ridge Jump
Propagator
TF 2 seismic
TF 1 seismic
Meteor seismic
BGR seismic
TF 2 hf
TF 2 core
TF 2 outrigger
TF 1 hf
TF 1 core
TF 1 outrigger
Langseth/Silver (mean hf)
Meteor heatflow
ODP Heatflow
Pre-TF 1 Heatflow

Figure IV-14

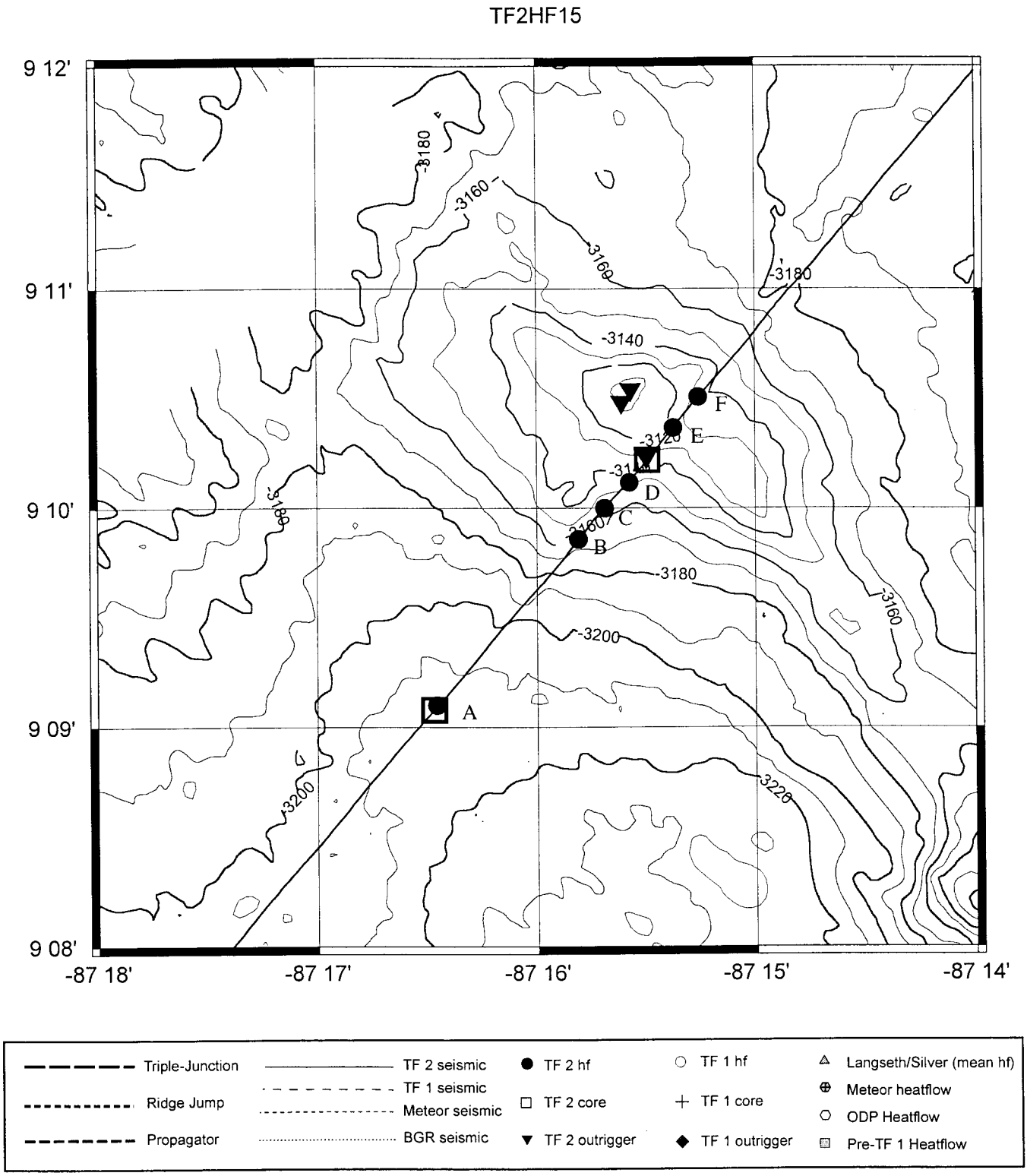
TF2HF15
9 12'
9 11'
9 10'
9 09'
9 08'
-87 18'
-87 17'
-87 16'
-87 15'
-87 14'
-3180
-3160
-3140
-3200
-3220
A
B
C
D
E
F
Triple-Junction
Ridge Jump
Propagator
TF 2 seismic
TF 1 seismic
Meteor seismic
BGR seismic
TF 2 hf
TF 2 core
TF 2 outrigger
TF 1 hf
TF 1 core
TF 1 outrigger
Langseth/Silver (mean hf)
Meteor heatflow
ODP Heatflow
Pre-TF 1 Heatflow

Figure IV-15

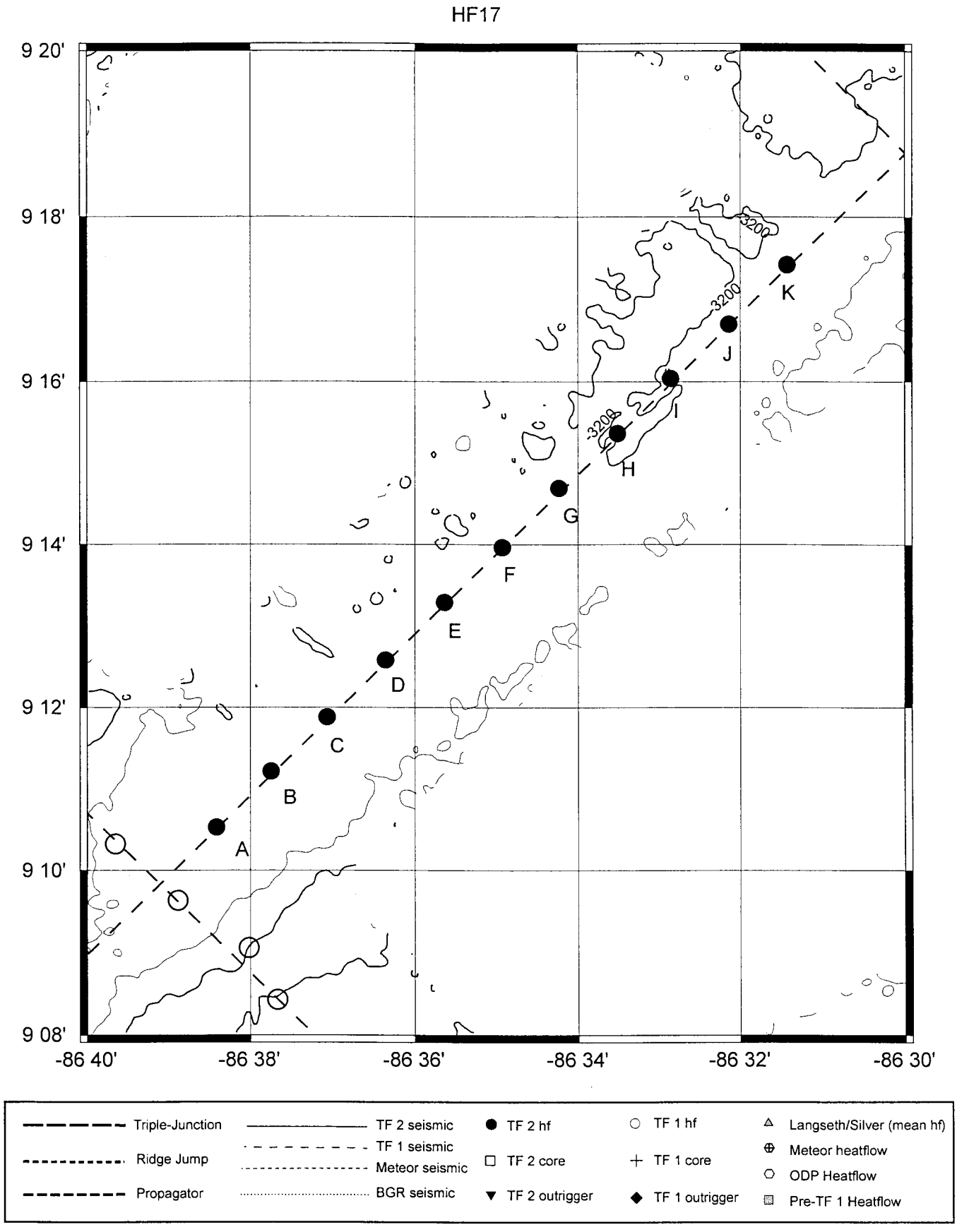
HF17
9 20'
9 18'
9 16'
9 14'
9 12'
9 10'
9 08'
-86 40'
-86 38'
-86 36'
-86 34'
-86 32'
-86 30'
-3200
-3200
-3200
A
B
C
D
E
F
G
H
I
J
K
Triple-Junction
Ridge Jump
Propagator
TF 2 seismic
TF 1 seismic
Meteor seismic
BGR seismic
TF 2 hf
TF 2 core
TF 2 outrigger
TF 1 hf
TF 1 core
TF 1 outrigger
Langseth/Silver (mean hf)
Meteor heatflow
ODP Heatflow
Pre-TF 1 Heatflow

Figure IV-16

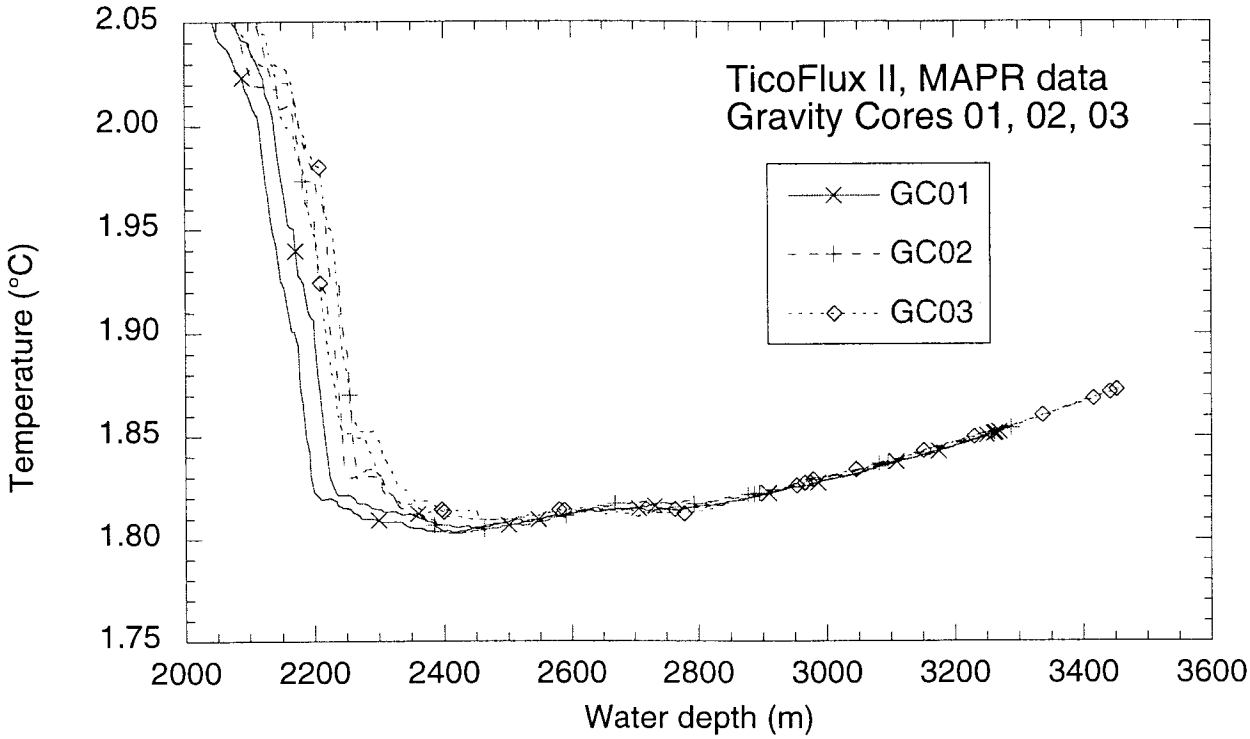
TicoFlux II, MAPR data
Gravity Cores 01, 02, 03
GC01
GC02
GC03
Temperature (°C)
Water depth (m)
2.05
2.00
1.95
1.90
1.85
1.80
1.75
2000
2200
2400
2600
2800
3000
3200
3400
3600

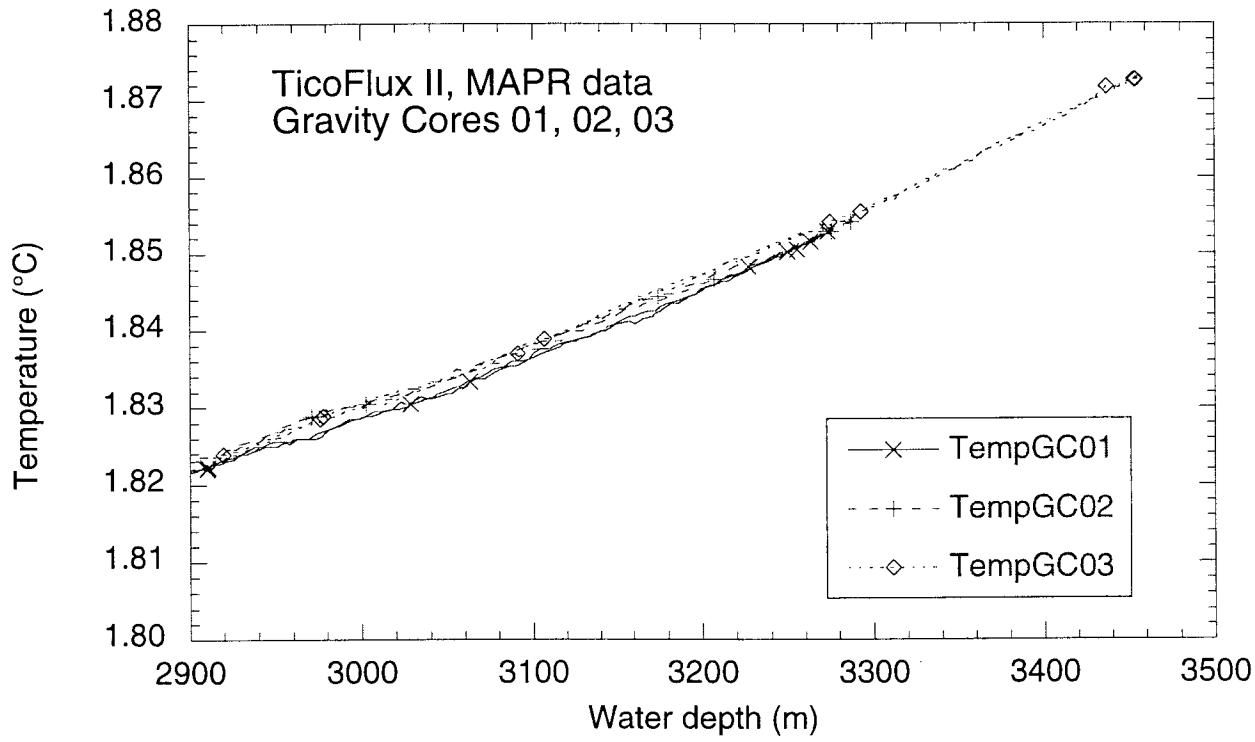
TicoFlux II, MAPR data
Gravity Cores 01, 02, 03
TempGC01
TempGC02
TempGC03
Temperature (°C)
Water depth (m)
1.88
1.87
1.86
1.85
1.84
1.83
1.82
1.81
1.80
2900
3000
3100
3200
3300
3400
3500

Figure IV-17

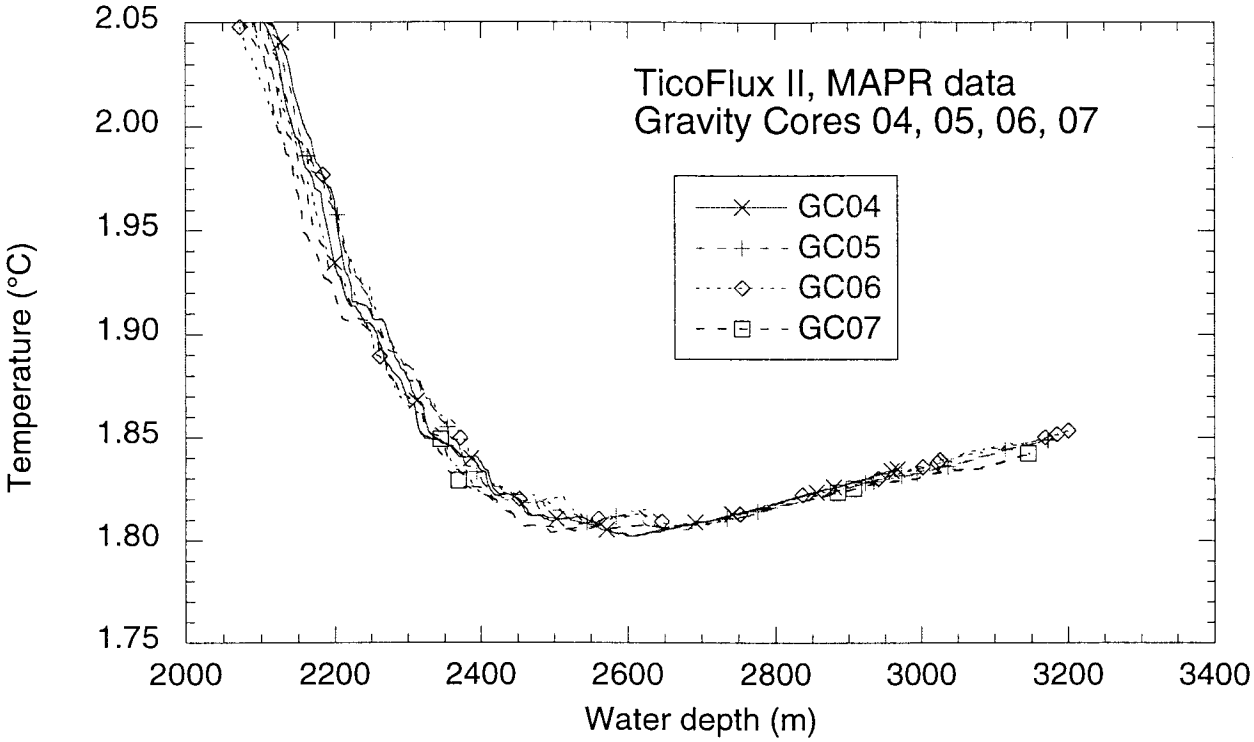
TicoFlux II, MAPR data
Gravity Cores 04, 05, 06, 07
GC04
GC05
GC06
GC07
Temperature (°C)
Water depth (m)
2.05
2.00
1.95
1.90
1.85
1.80
1.75
2000
2200
2400
2600
2800
3000
3200
3400

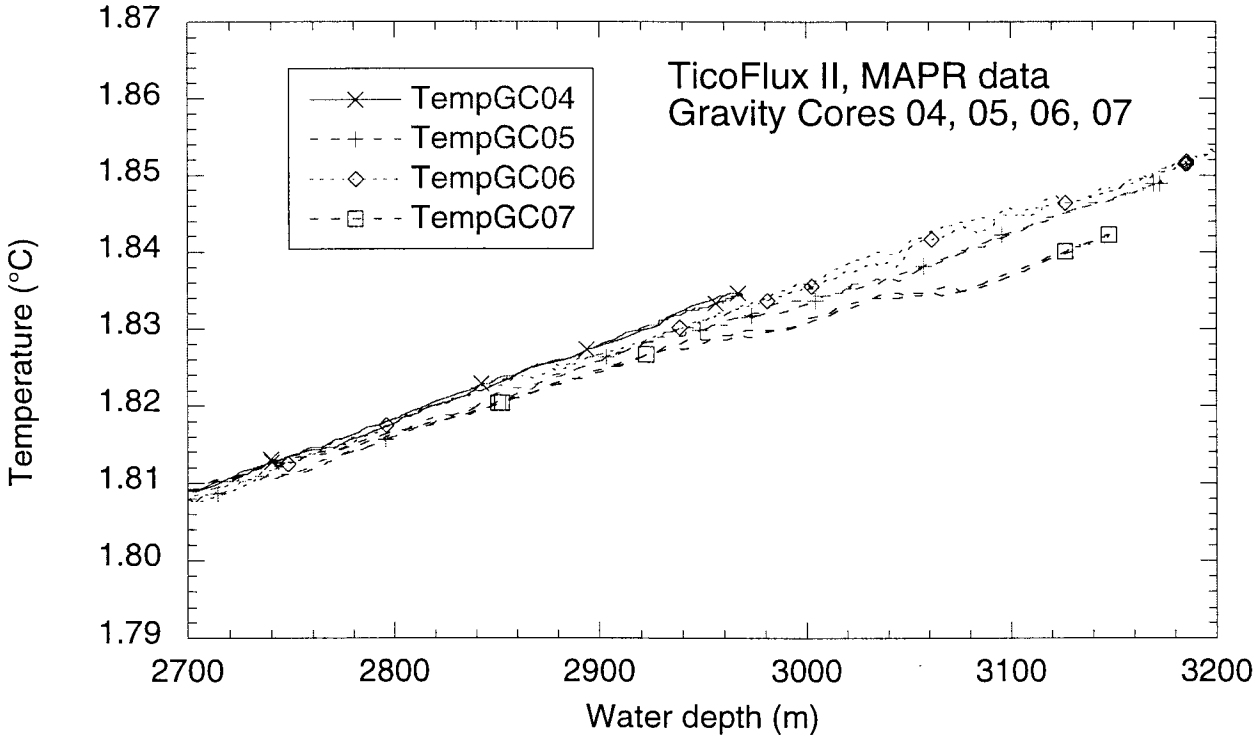
TicoFlux II, MAPR data
Gravity Cores 04, 05, 06, 07
TempGC04
TempGC05
TempGC06
TempGC07
Temperature (°C)
Water depth (m)
1.87
1.86
1.85
1.84
1.83
1.82
1.81
1.80
1.79
2700
2800
2900
3000
3100
3200

Figure IV-18

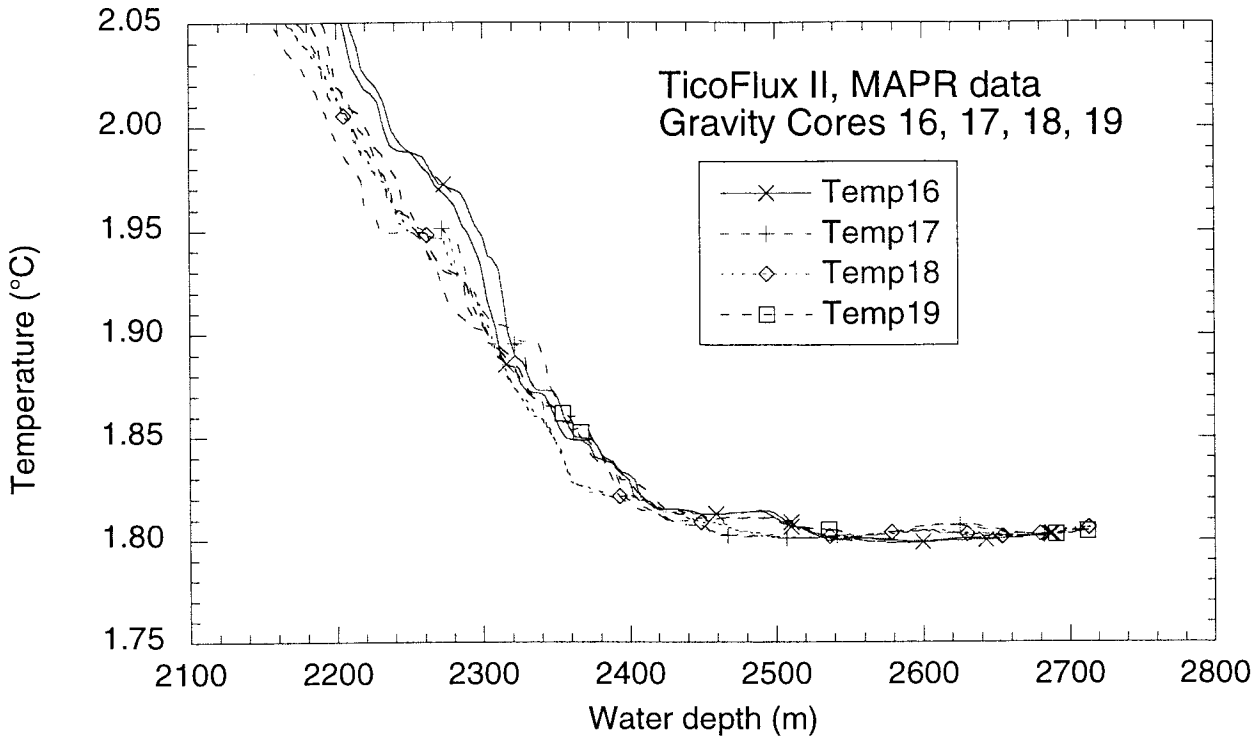
TicoFlux II, MAPR data
Gravity Cores 16, 17, 18, 19
Temp16
Temp17
Temp18
Temp19
Temperature (°C)
Water depth (m)
2.05
2.00
1.95
1.90
1.85
1.80
1.75
2100
2200
2300
2400
2500
2600
2700
2800

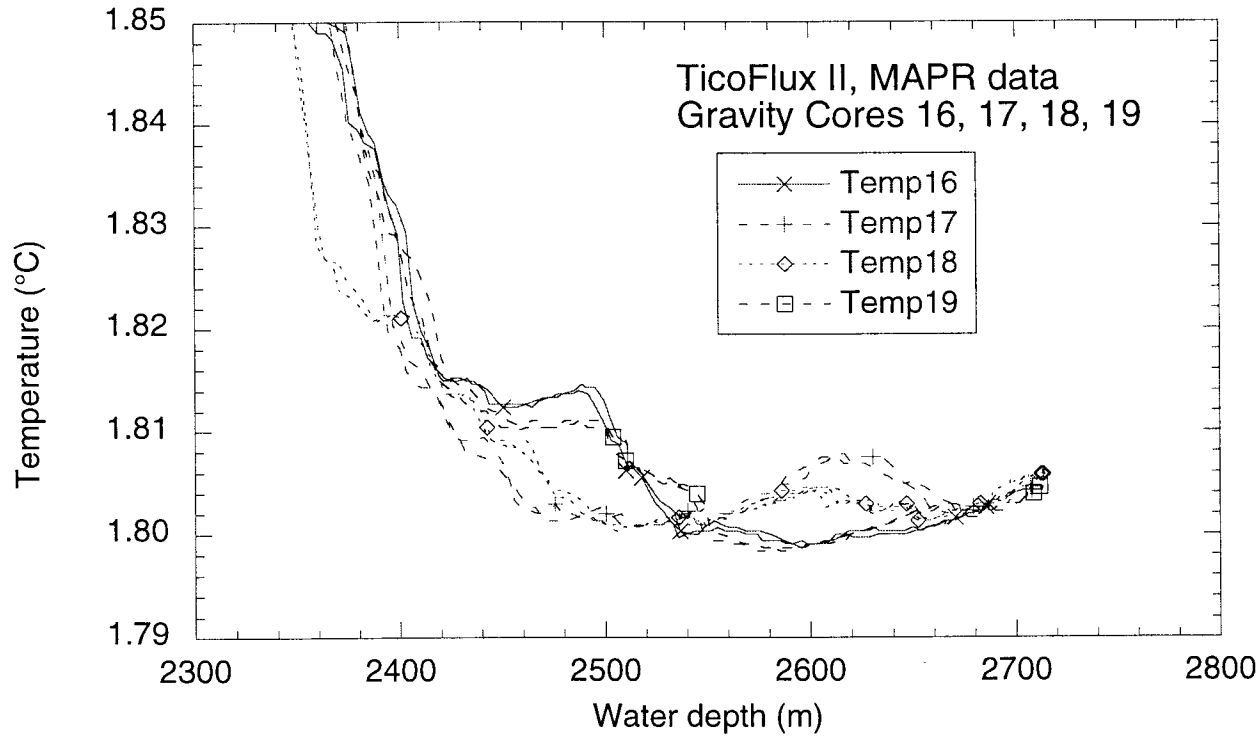
TicoFlux II, MAPR data
Gravity Cores 16, 17, 18, 19
Temp16
Temp17
Temp18
Temp19
Temperature (°C)
Water depth (m)
1.85
1.84
1.83
1.82
1.81
1.80
1.79
2300
2400
2500
2600
2700
2800

Figure IV-19

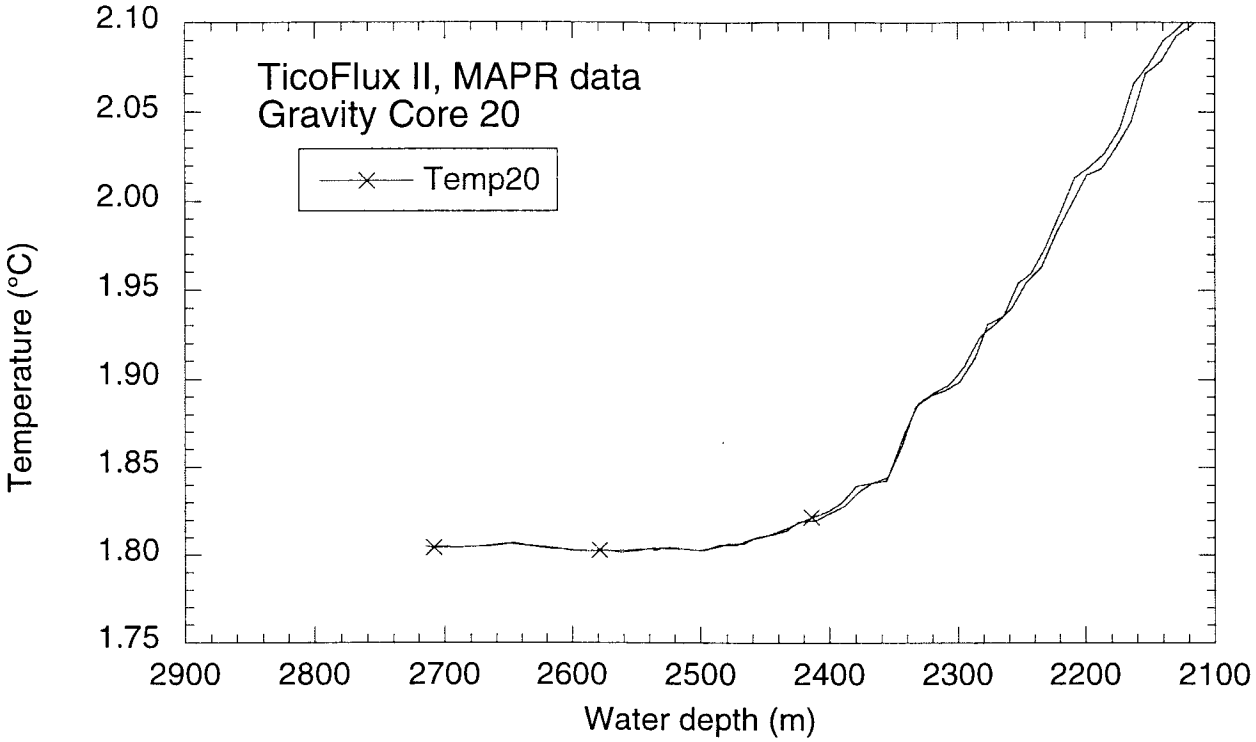
TicoFlux II, MAPR data
Gravity Core 20
Temp20
Temperature (°C)
2.10
2.05
2.00
1.95
1.90
1.85
1.80
1.75
2900
2800
2700
2600
2500
2400
2300
2200
2100
Water depth (m)

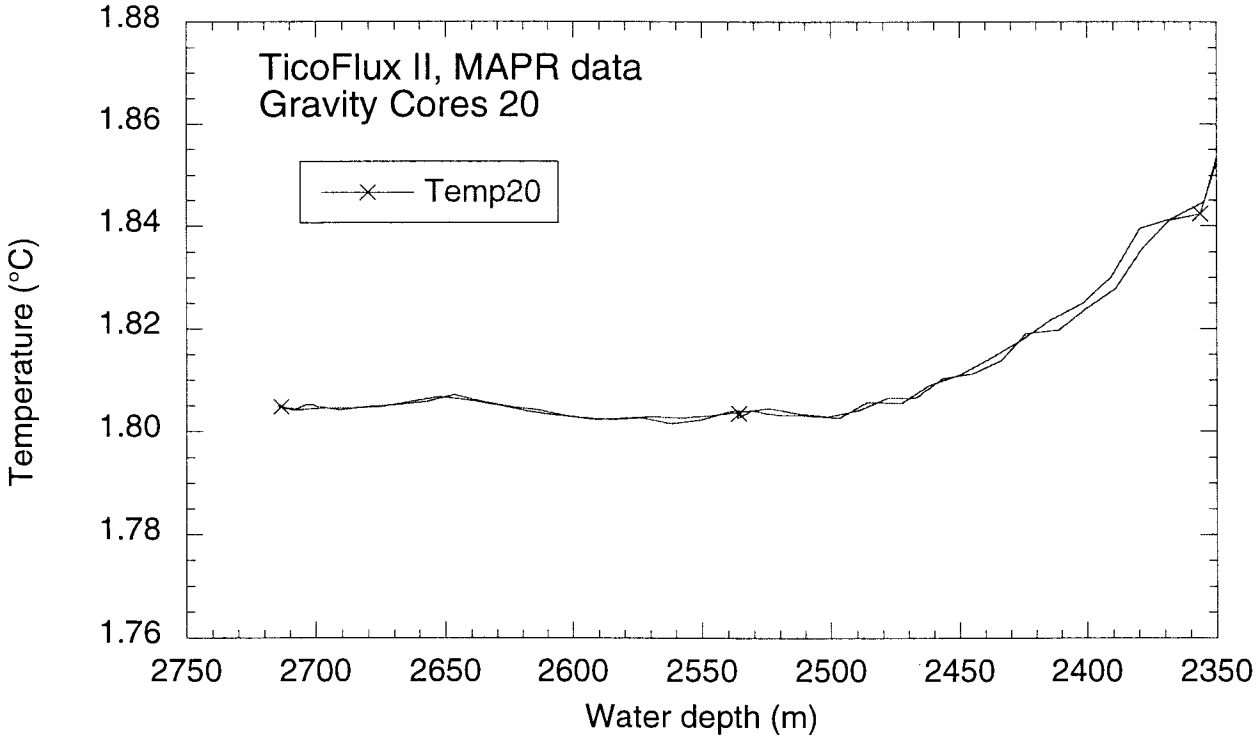
TicoFlux II, MAPR data
Gravity Cores 20
Temp20
Temperature (°C)
1.88
1.86
1.84
1.82
1.80
1.78
1.76
2750
2700
2650
2600
2550
2500
2450
2400
2350
Water depth (m)

Figure IV-20

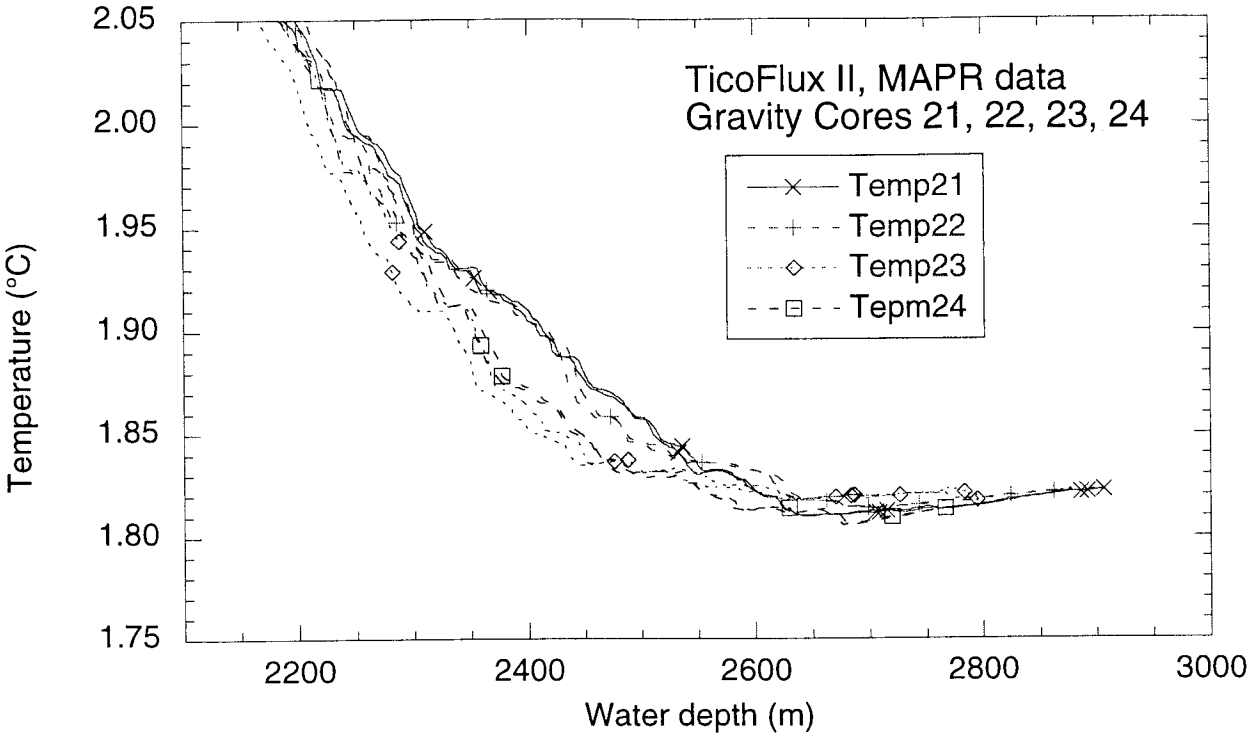
TicoFlux II, MAPR data
Gravity Cores 21, 22, 23, 24
Temp21
Temp22
Temp23
Tepm24
Temperature (°C)
Water depth (m)
2.05
2.00
1.95
1.90
1.85
1.80
1.75
2200
2400
2600
2800
3000

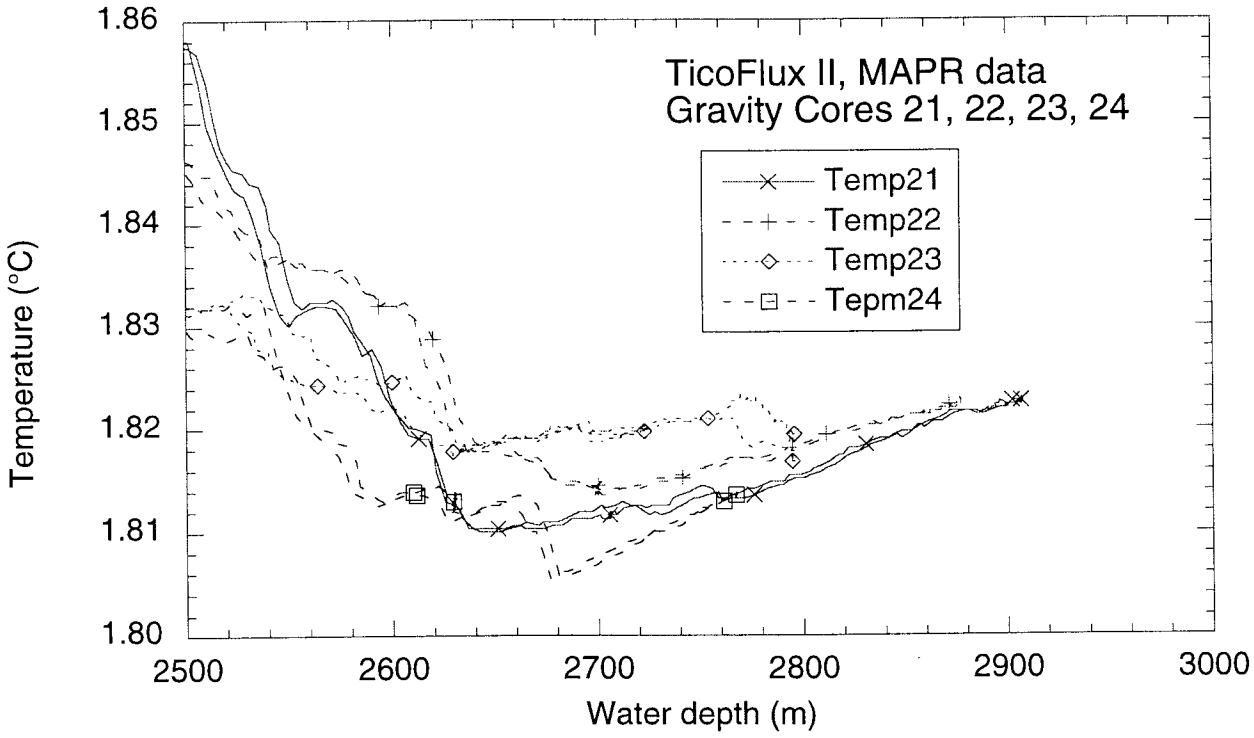
TicoFlux II, MAPR data
Gravity Cores 21, 22, 23, 24
Temp21
Temp22
Temp23
Tepm24
Temperature (°C)
Water depth (m)
1.86
1.85
1.84
1.83
1.82
1.81
1.80
2500
2600
2700
2800
2900
3000

Figure IV-21

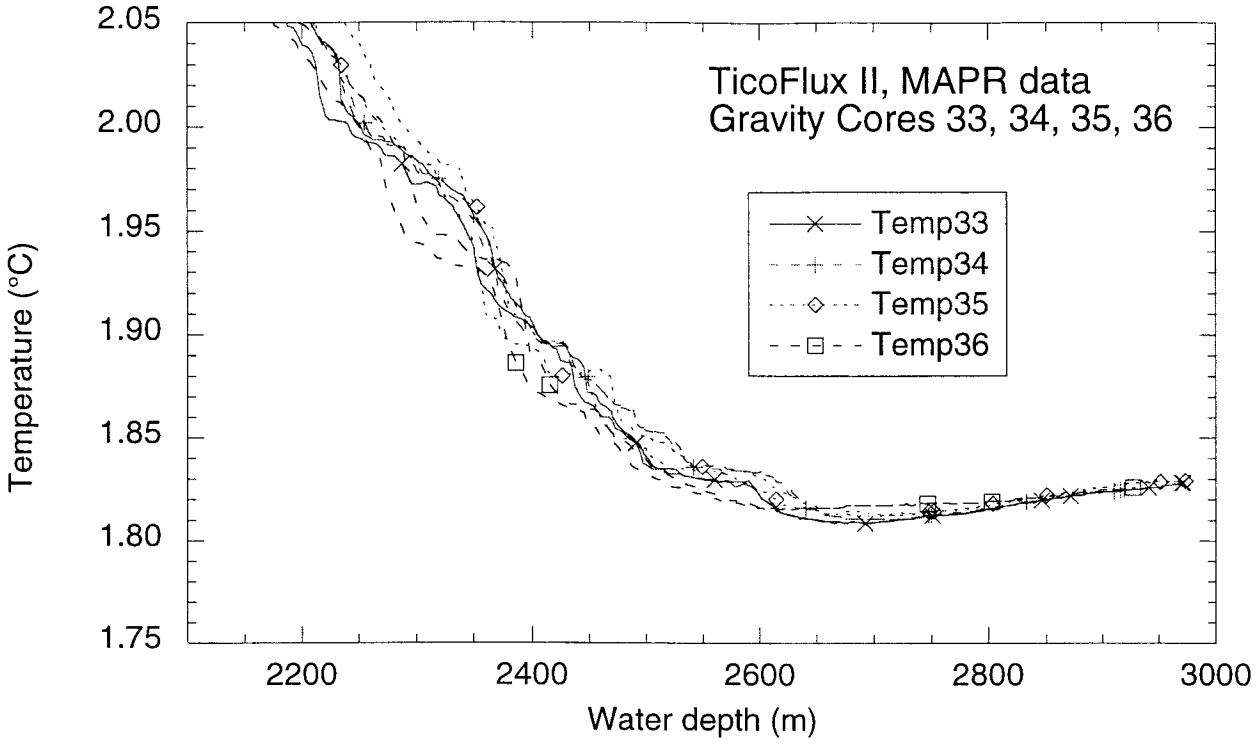
TicoFlux II, MAPR data
Gravity Cores 33, 34, 35, 36
Temp33
Temp34
Temp35
Temp36
Temperature (°C)
Water depth (m)
2.05
2.00
1.95
1.90
1.85
1.80
1.75
2200
2400
2600
2800
3000

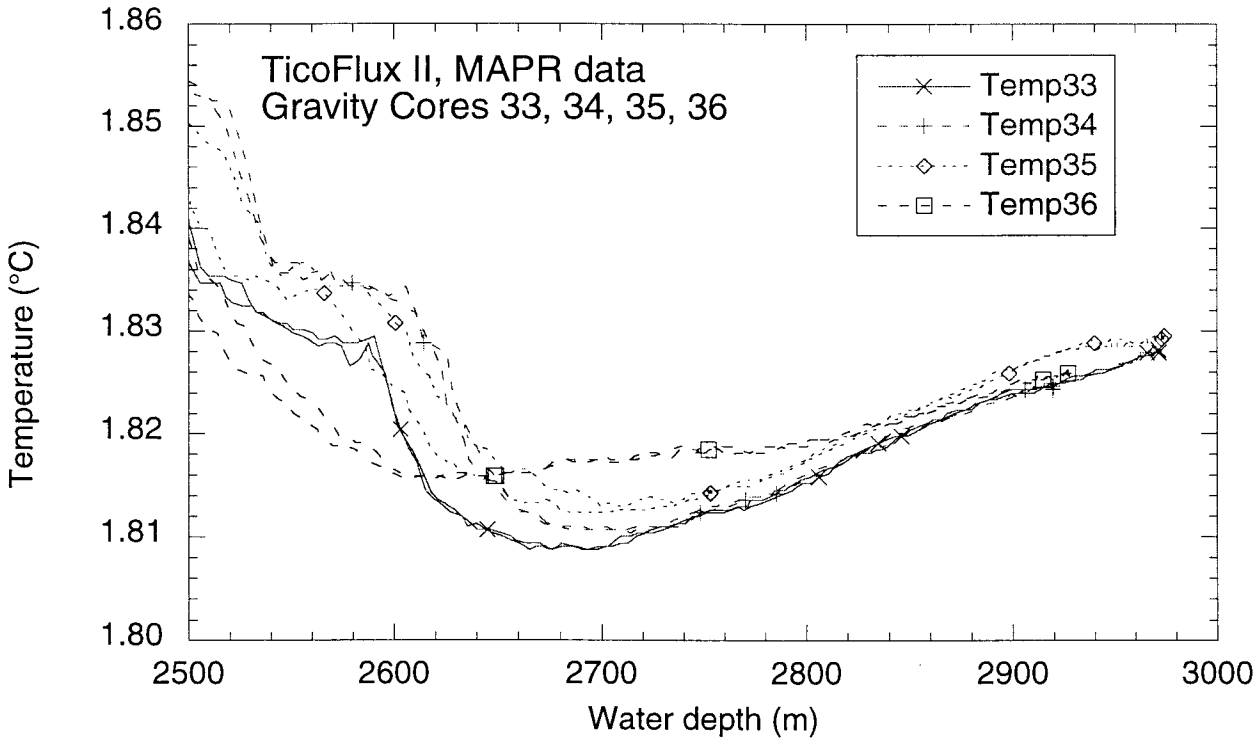
TicoFlux II, MAPR data
Gravity Cores 33, 34, 35, 36
Temp33
Temp34
Temp35
Temp36
Temperature (°C)
Water depth (m)
1.86
1.85
1.84
1.83
1.82
1.81
1.80
2500
2600
2700
2800
2900
3000

Figure IV-22

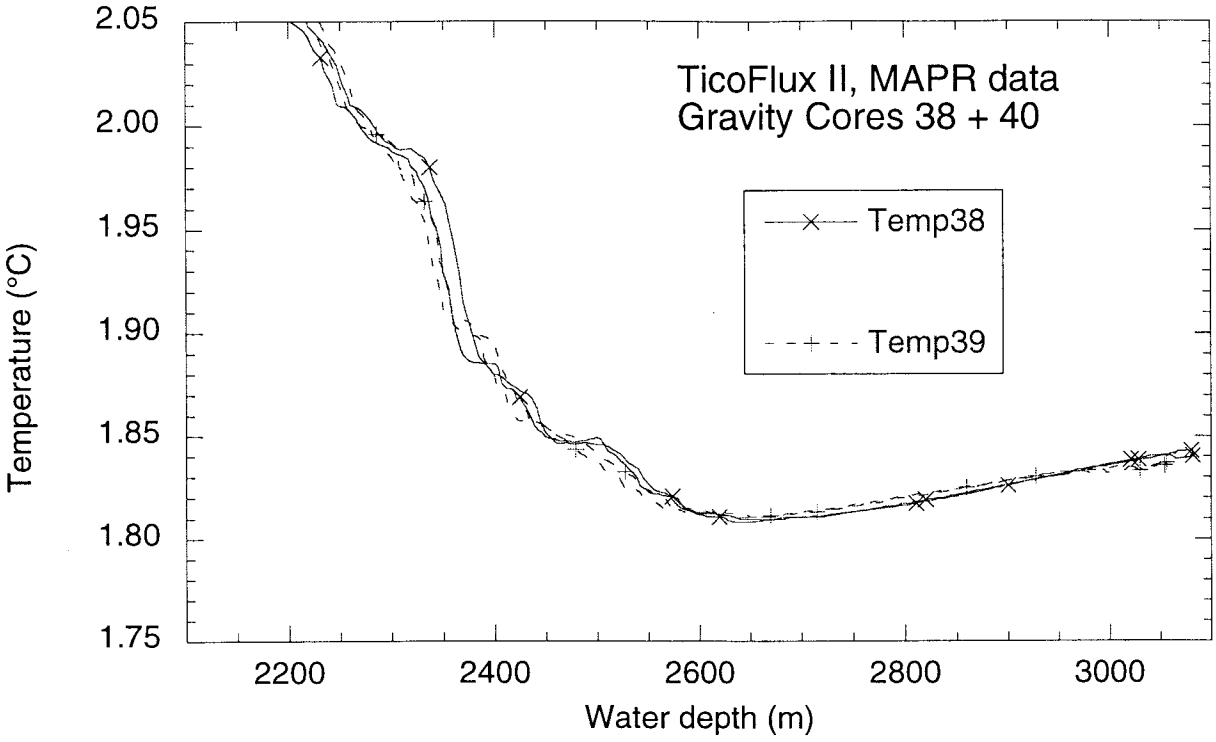
TicoFlux II, MAPR data
Gravity Cores 38 + 40
Temp38
Temp39
Temperature (°C)
Water depth (m)
2.05
2.00
1.95
1.90
1.85
1.80
1.75
2200
2400
2600
2800
3000

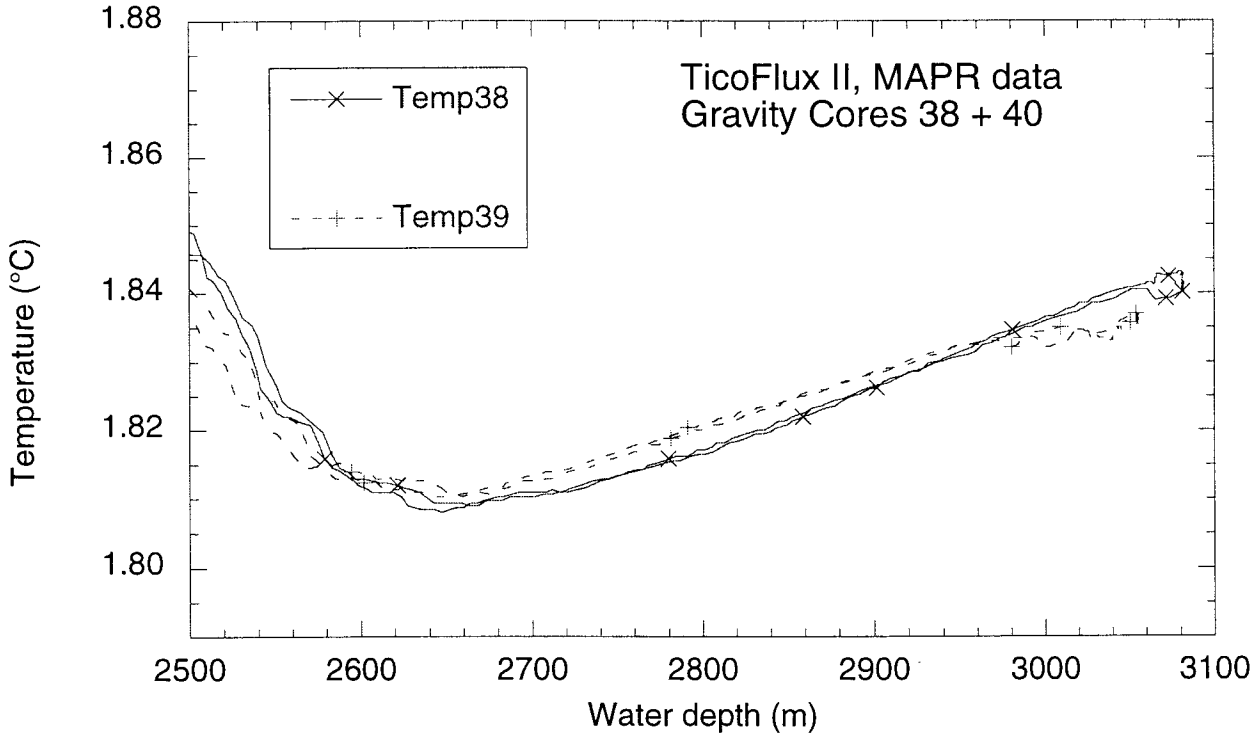
TicoFlux II, MAPR data
Gravity Cores 38 + 40
Temp38
Temp39
Temperature (°C)
Water depth (m)
1.88
1.86
1.84
1.82
1.80
2500
2600
2700
2800
2900
3000
3100

Figure IV-23

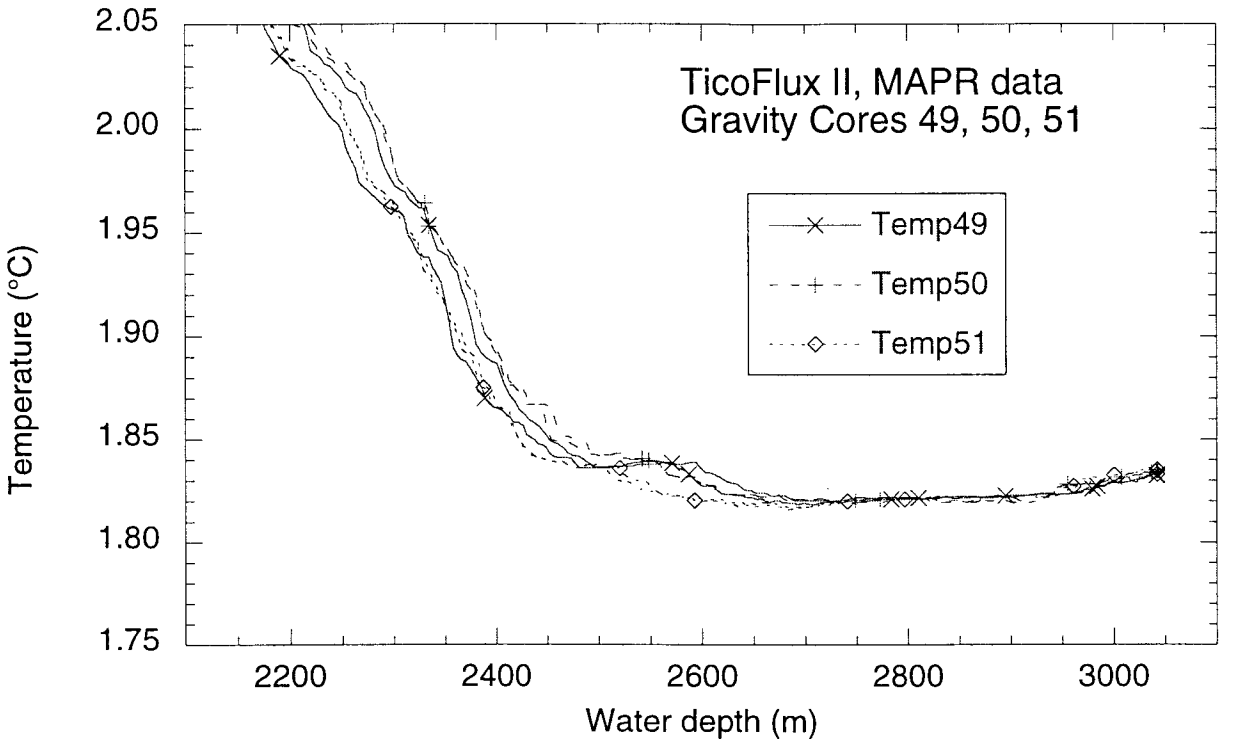
TicoFlux II, MAPR data
Gravity Cores 49, 50, 51
Temp49
Temp50
Temp51
Temperature (°C)
Water depth (m)
2.05
2.00
1.95
1.90
1.85
1.80
1.75
2200
2400
2600
2800
3000

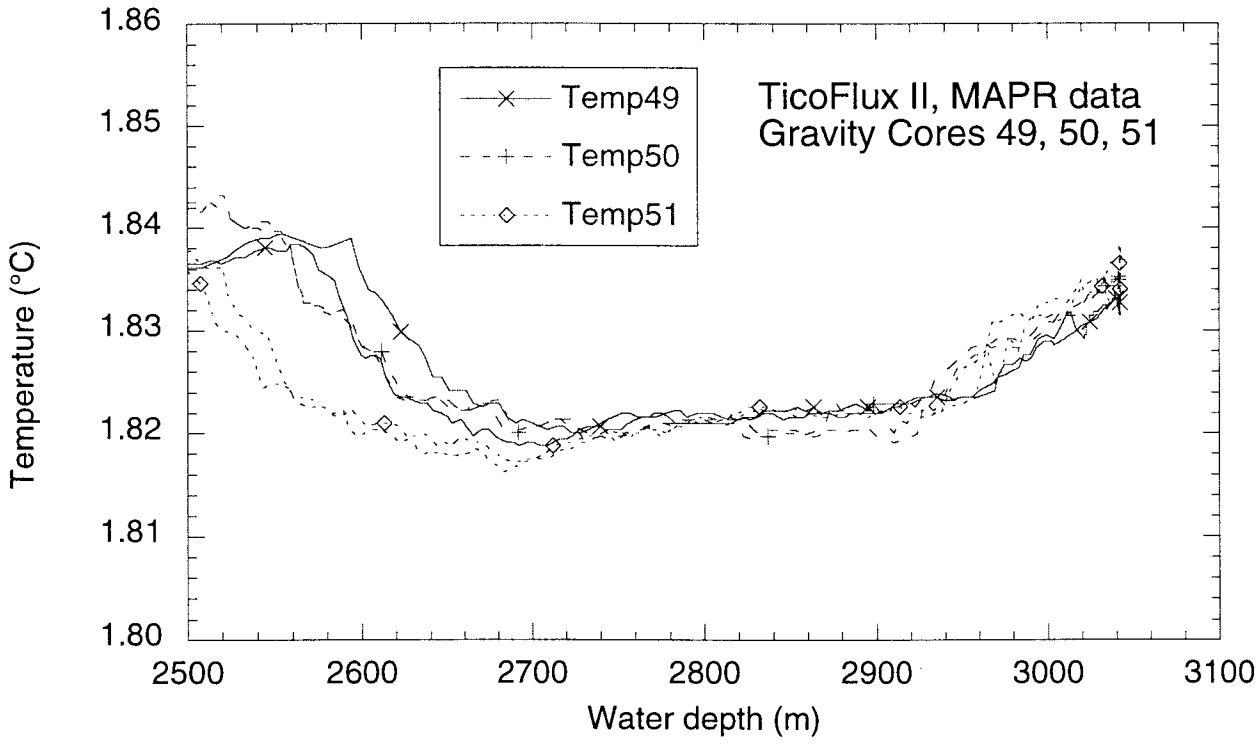
TicoFlux II, MAPR data
Gravity Cores 49, 50, 51
Temp49
Temp50
Temp51
Temperature (°C)
Water depth (m)
1.86
1.85
1.84
1.83
1.82
1.81
1.80
2500
2600
2700
2800
2900
3000
3100

Figure IV-24

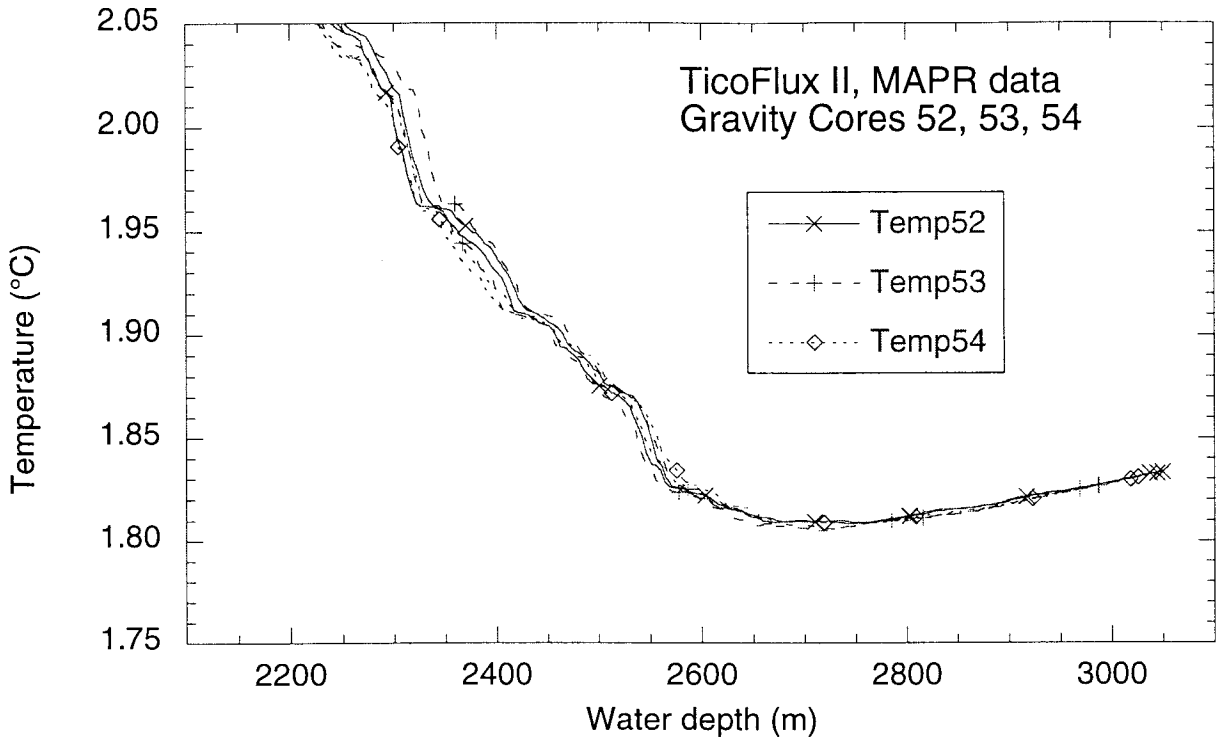
TicoFlux II, MAPR data
Gravity Cores 52, 53, 54
Temp52
Temp53
Temp54
Temperature (°C)
Water depth (m)
2.05
2.00
1.95
1.90
1.85
1.80
1.75
2200
2400
2600
2800
3000

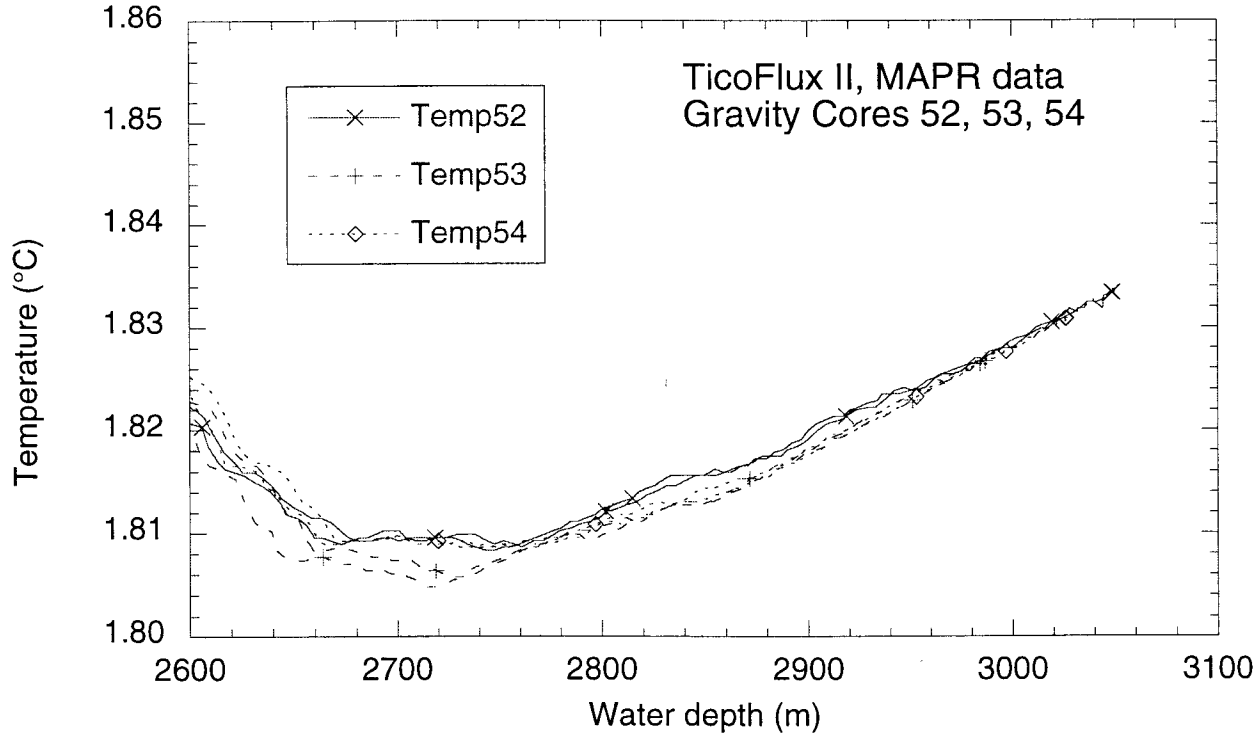
TicoFlux II, MAPR data
Gravity Cores 52, 53, 54
Temp52
Temp53
Temp54
Temperature (°C)
Water depth (m)
1.86
1.85
1.84
1.83
1.82
1.81
1.80
2600
2700
2800
2900
3000
3100

Figure IV-25

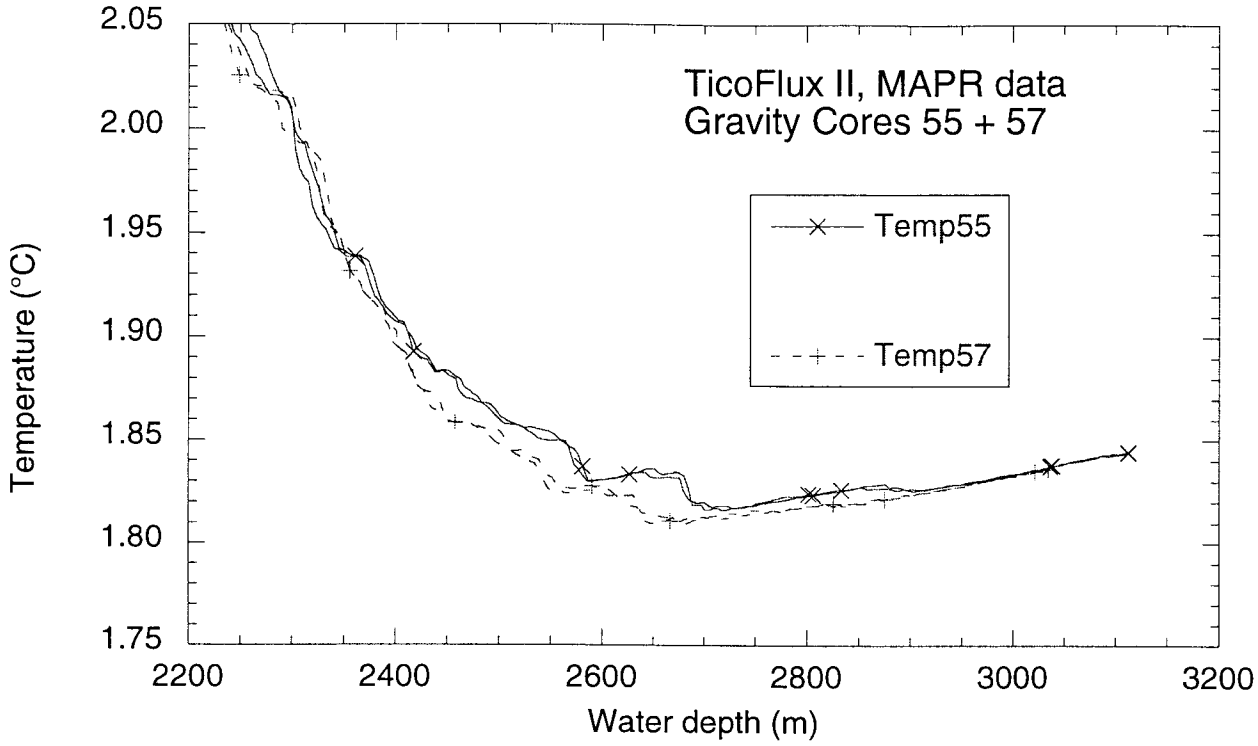
TicoFlux II, MAPR data
Gravity Cores 55 + 57
Temp55
Temp57
Temperature (°C)
Water depth (m)
2.05
2.00
1.95
1.90
1.85
1.80
1.75
2200
2400
2600
2800
3000
3200

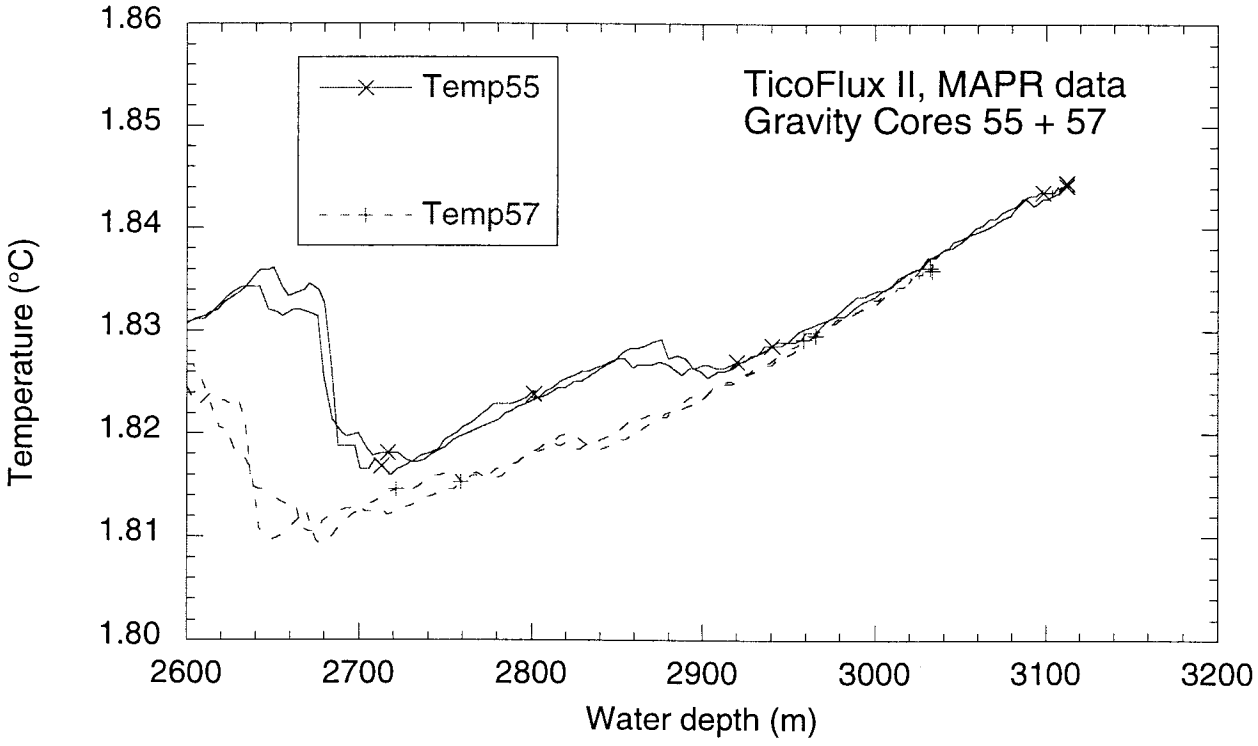
TicoFlux II, MAPR data
Gravity Cores 55 + 57
Temp55
Temp57
Temperature (°C)
Water depth (m)
1.86
1.85
1.84
1.83
1.82
1.81
1.80
2600
2700
2800
2900
3000
3100
3200

Figure IV-26

Table V-1. Core locations, recovery, and figure cross-reference.

| Core Identification | Depth (m) | Latitude (°N) | Longitude (°W) | Length (cm) | Lithologic Summary | Location map |
|---|---|---|---|---|---|---|
| MV0209-01GC | 3400 | 9°40.997 | 86°23.741 | 205 | Dark olive gray hemipelagic mud; homogeneous | Fig. V-2 |
| MV0209-02GC | 3400 | 9°41.130 | 86°23.620 | 358 | Dark olive gray hemipelagic mud; white ash bed (graded) at 115-120 cm; bioturbated black ash at 150-164 cm | Fig. V-2 |
| MV0209-03GC | 3575 | 9°41.646 | 86°23.027 | 353 | Dark olive gray hemipelagic mud; irregular lenses of ash at 65, 86, 120 cm; white ash layer at 253-256 cm; mud is unsually well compacted | Fig. V-2 |
| MV0209-04GC | 3114 | 9°18.640 | 84°11.881 | 355 | Dark olive gray hemipelagic mud; white ash layer at 292-303 cm | Fig. V-3 |
| MV0209-05GC | 3250 | 9°18.650 | 86°11.260 | 379 | Olive brown clay with pebbles and granules of basalt (0-62 cm); dark olive gray hemipelagic mud; lenses of black volcanic ash at 134, 275 cm | Fig. V-3 |
| MV0209-06GC | 3250 | 9°18.649 | 86°11.108 | 10 | Core catcher only: dark olive gray hemipelagic mud | Fig. V-3 |
| MV0209-07GC | 3250 | 9°20.451 | 86°10.439 | 353 | Dark olive gray hemipelagic mud; homogeneous | Fig. V-3 |
| MV0209-08GC | 3250 | 9°20.046 | 86°11.004 | 35 | Core catcher only: dark olive gray mud mixed with basalt and lithified mudstone fragments (0-6 cm); light olive brown clay (6-30 cm); very dark grayish brown mud mixed with basalt fragments (30-35 cm) | Fig. V-3 |
| MV0209-09GC | 3250 | 9°19.920 | 86°10.888 | 10 | Core catcher only: gravel of indurated mudstone, Mn-oxide, altered basalt | Fig. V-3 |
| MV0209-10GC | 3250 | 9°18.955 | 86°10.847 | 113 | Olive to olive-gray clay (20-31, 90-113 cm); dark olive gray hemipelagic mud (31-90 cm) | Fig. V-3 |
| MV0209-11GC | 3300 | 9°40.767 | 86°34.268 | 375 | Dark olive gray hemipelagic mud; white ash layer at 190 cm; local clay-rich bands | Fig. V-10 |
| MV0209-12GC | 3300 | 9°40.793 | 86°34.307 | 355 | Dark olive gray hemipelagic mud; thin layers of indurated material may be Mn oxide; sampled for physical properties | Fig. V-10 |
| MV0209-13GC | 3145 | 9°36.444 | 86°39.078 | 124 | Dark olive gray hemipelagic mud; homogeneous | Fig. V-10 |
| MV0209-14GC | 3160 | 9°36.395 | 86°39.144 | 390 | Dark olive gray hemipelagic mud; light gray ash layer at 338-340 cm; sampled for physical properties | Fig. V-10 |
| MV0209-15GC | 2810 | 8°29.942 | 85°58.173 | 130 | Dark olive gray hemipelagic mud; homogeneous | Fig. V-4 |
| MV0209-16GC | 2755 | 8°29.835 | 85°58.062 | 371 | Dark olive gray hemipelagic mud; homogeneous; sampled for physical properties | Fig. V-4 |
| MV0209-17GC | 2830 | 8°32.215 | 85°54.249 | 415 | Dark olive gray hemipelagic mud; homogeneous | Fig. V-4 |
| MV0209-18GC | 2844 | 8°31.819 | 85°54.895 | 93 | Grayish brown clay; indurated sediment in core catcher; altered basalt and Mn oxide at 36-50 cm | Fig. V-4 |
| MV0209-19GC | 2835 | 8°29.797 | 85°58.022 | 363 | Dark olive gray hemipelagic mud; thin layer of black volcanic ash at 348 cm | Fig. V-4 |
| MV0209-20GC | 2780 | 8°29.751 | 85°58.050 | 356 | Dark olive gray hemipelagic mud; homogeneous | Fig. V-4 |
| MV0209-21GC | 3035 | 8°44.202 | 87°12.749 | 209 | Light olive brown clay (0-72 cm); olive brown carbonate-bearing mud with light olive brown mottling (76-141 cm); dark olive gray hemipelagic mud (141-209); white ash layer at 76 cm | Fig. V-6 |
| MV0209-22GC | 3020 | 8°44.348 | 87°12.642 | 73 | Very light gray nannofossil chalk; Mn-oxide | Fig. V-6 |
| MV0209-23GC | 2875 | 8°37.006 | 87°16.799 | 10 | Core catcher only: Mn-oxide nodule | Fig. V-5 |
| MV0209-24GC | 2860 | 8°37.251 | 87°17.069 | 292 | Yellowish brown foraminiferal ooze; Mn-oxide nodule at 20-30 cm; light gray mottling | Fig. V-5 |
| MV0209-25GC | 3050 | 8°44.550 | 87°12.900 | 124 | Light olive brown nanno-bearing mud (22-79 cm); very light gray nanno ooze (79-124 cm); fragments of Mn oxide | Fig. V-6 |

Table V-1. Core locations, recovery, and figure cross-reference.

| Core Identification | Depth (m) | Latitude (°N) | Longitude (°W) | Length (cm) | Lithologic Summary | Location map |
|---|---|---|---|---|---|---|
| MV0209-26GC | 3140 | 8°44.518 | 87°12.820 | 342 | Light olive brown clay (18-25 cm); light gray nanno-bearing mud (25-210 cm); very light gray nanno ooze (210-342 cm); brown volcanic ash at 48-50 and 86 cm | Fig. V-6 |
| MV0209-27GC | 3030 | 8°44.445 | 87°12.749 | 101 | Very light gray nannofossil ooze; black gravel and granules at 52-56 | Fig. V-6 |
| MV0209-28GC | 3030 | 8°44.430 | 87°12.873 | 375 | Light brown nanno-bearing mud (13-34 cm); very light gray nanno ooze (43-375 cm) | Fig. V-6 |
| MV0209-29GC | 3020 | 8°44.236 | 87°12.709 | 165 | Olive brown clay; homogeneous | Fig. V-6 |
| MV0209-30GC | 3030 | 8°44.200 | 87°12.500 | 33 | Very light gray nannofossil ooze | Fig. V-6 |
| MV0209-31GC | 3060 | 8°44.161 | 87°12.440 | 353 | Very light gray nannofossil ooze; local burrows filled with greenish-black material | Fig. V-6 |
| MV0209-32GC | 3040 | 8°44.579 | 87°12.775 | 342 | Light olive brown clay (12-129 cm); light gray nanno-bearing mixed sediment (129-182); very light gray nannofossil ooze (182-343 cm) | Fig. V-6 |
| MV0209-33GC | 3030 | 9°05.252 | 87°05.777 | 380 | Dark olive gray hemipelagic mud; white volcanic ash layer at 58-64 cm | Fig. V-7 |
| MV0209-34GC | 3030 | 9°05.195 | 87°05.845 | 10 | Core catcher only: Mn oxide nodules | Fig. V-7 |
| MV0209-35GC | 3124 | 9°05.235 | 87°05.805 | 372 | Olive hemipelagic mud (15-30 cm); dark olive gray hemipelagic mud (30-372 cm); white volcanic ash layer at 54-57 cm | Fig. V-7 |
| MV0209-36GC | 3075 | 9°06.306 | 87°05.650 | 373 | Dark olive gray hemipelagic mud; white volcanic ash layer at 229-234 cm | Fig. V-7 |
| MV0209-37GC | 3110 | 9°05.215 | 87°05.826 | 379 | Olive clay-rich mud (13-47 cm); dark olive gray hemipelagic mud (47-379 cm); white ash patches at 17 cm, 27 cm; black ash layer at 280 cm | Fig. V-7 |
| MV0209-38GC | 3206 | 9°04.969 | 87°05.992 | 333 | Olive clay-rich mud (13-47 cm) becomes darker at top; dark olive gray hemipelagic mud (47-379 cm); Mn-oxide nodules and chips | Fig. V-7 |
| MV0209-39GC | 3182 | 9°05.012 | 87°05.957 | 123 | Light yellowish brown clay-rich mud; scattered Mn-oxide nodules | Fig. V-7 |
| MV0209-40GC | 3140 | 9°05.046 | 87°05.931 | 227 | Light yellowish brown clay-rich mud; scattered Mn-oxide nodules and Mn-coated rock fragments | Fig. V-7 |
| MV0209-41GC | 3102 | 9°05.085 | 87°05.907 | 5 | Core catcher only: fragments of basalt with Mn-oxide coating; dark brown mud | Fig. V-7 |
| MV0209-42GC | 3140 | 9°04.854 | 87°05.792 | 243 | Light olive brown clay-rich mud; scattered fragments of basalt and Mn-oxide; sampled for physical properties | Fig. V-7 |
| MV0209-43GC | 3140 | 9°04.884 | 87°05.771 | 143 | Light olive brown clay-rich mud; Mn-oxide nodule at surface; basalt fragments at 60, 105 cm, core catcher | Fig. V-7 |
| MV0209-44GC | 3306 | 9°40.797 | 86°34.309 | 300 | Dark olive gray hemipelagic mud; homogeneous | Fig. V-10 |
| MV0209-44PC | 3314 | 9°40.797 | 86°34.309 | 694 | Dark olive gray hemipelagic mud; homogeneous; sampled for physical properties | Fig. V-10 |
| MV0209-45GC | 4780 | 9°51.944 | 86°21.282 | 91 | Dark gray sand with indurated mudstone clasts, normal size grading; dark olive gray hemipelagic mud | Fig. V-11 |
| MV0209-45PC | 4780 | 9°51.944 | 86°21.282 | 712 | Dark gray sand with indurated mudstone clasts, normal size grading; dark gray debris flow and mudflow deposits; dark olive gray hemipelagic mud; volcanic ash layer with normal grading (500-510 cm); sampled for physical properties | Fig. V-11 |
| MV0209-46GC | 2840 | 8°29.810 | 85°58.001 | 425 | Dark olive gray hemipelagic mud; homogeneous | Fig. V-4 |

Table V-1. Core locations, recovery, and figure cross-reference.

| Core Identification | Depth (m) | Latitude (°N) | Longitude (°W) | Length (cm) | Lithologic Summary | Location map |
|---|---|---|---|---|---|---|
| MV0209-47GC | 2840 | 8°29.784 | 85°58.001 | 426 | Dark olive gray hemipelagic mud; thin black ash layer at 375 cm | Fig. V-4 |
| MV0209-48GC | 2820 | 8°29.799 | 85°58.009 | 290 | Dark olive gray hemipelagic mud; homogeneous | Fig. V-4 |
| MV0209-48PC | 2820 | 8°29.799 | 85°58.009 | 843 | Dark olive gray hemipelagic mud; homogeneous; sampled for physical properties | Fig. V-4 |
| MV0209-49GC | 3140 | 9°05.004 | 87°05.932 | 55 | Yellowish brown clay; scattered Mn-oxide and fragments of basalt | Fig. V-7 |
| MV0209-50GC | 3142 | 9°05.044 | 87°05.929 | 158 | Mottled mixture of dark brown clay-rich zeolitic mud and yellowish brown mud; dark yellowish brown zeolitic clay (122-158 cm); layers and patches of Mn-oxide; scattered fragments of glassy basalt | Fig. V-7 |
| MV0209-51GC | 3140 | 9°05.046 | 87°05.930 | 43 | Surface crust and scattered patches of Mn-oxide; dark yellowish brown to yellowish brown clay | Fig. V-7 |
| MV0209-52GC | 3150 | 8°49.175 | 87°10.106 | 369 | Dark olive gray hemipelagic mud; homogeneous | Fig. V-6 |
| MV0209-53GC | 3080 | 8°49.116 | 87°10.148 | 4 | Core catcher only: Mn-oxide in core cutter; top of core weight trapped fist-sized piece of basalt, hemipelagic mud | Fig. V-6 |
| MV0209-54GC | 3125 | 8°49.145 | 87°10.126 | 194 | Dark olive gray hemipelagic mud (37-53, 128-194 cm); olive brown clay-rich mud (53-128 cm); gradational contact | Fig. V-6 |
| MV0209-55GC | 3213 | 8°47.340 | 87°11.820 | 365 | Olive brown clay-rich mud; scattered Mn-oxide nodules | Fig. V-6 |
| MV0209-56GC | 3170 | 8°47.387 | 87°11.770 | 257 | Olive brown clay-rich mud; scattered Mn-oxide nodules, Mn crust in core catcher | Fig. V-6 |
| MV0209-57GC | 2750 | 8°47.418 | 87°11.737 | 2 | Core catcher only: Mn-oxide crust | Fig. V-6 |
| MV0209-58GC | 3000 | 9°26.601 | 87°03.047 | 180 | Dark olive gray hemipelagic mud; homogeneous; bottom of core cutter contains debris-flow deposit with fragments of indurated chalk | Fig. V-9 |
| MV0209-59GC | 3140 | 9°10.219 | 87°15.493 | 378 | Dark olive gray hemipelagic mud; foram sand (149-158 cm); patches of white volcanic ash (260-280 cm) | Fig. V-8 |
| MV0209-60GC | 3120 | 9°10.529 | 87°15.578 | 285 | Dark olive gray hemipelagic mud; white volcanic ash (156-162 cm), black volcanic ash (173 cm) | Fig. V-8 |
| MV0209-61GC | 3116 | 9°10.474 | 87°15.625 | 162 | Dark olive gray hemipelagic mud; white volcanic ash (132-136 cm) | Fig. V-8 |
| MV0209-62GC | 3340 | 9°40.890 | 86°34.445 | 358 | Dark olive gray hemipelagic mud; light gray volcanic ash at 190-196 cm; black ash layer at 284 cm | Fig. V-10 |
| MV0209-63GC | 3340 | 9°40.922 | 86°34.316 | 410 | Dark olive gray hemipelagic mud; light gray volcanic ash at 260-270 cm; black ash layer at 332 cm | Fig. V-10 |
| MV0209-64GC | 3320 | 9°40.840 | 86°34.200 | 337 | Dark olive gray hemipelagic mud; black volcanic ash at 314 cm | Fig. V-10 |
| MV0209-65GC | 3340 | 9°40.672 | 86°34.373 | 386 | Dark olive gray hemipelagic mud; homogeneous | Fig. V-10 |

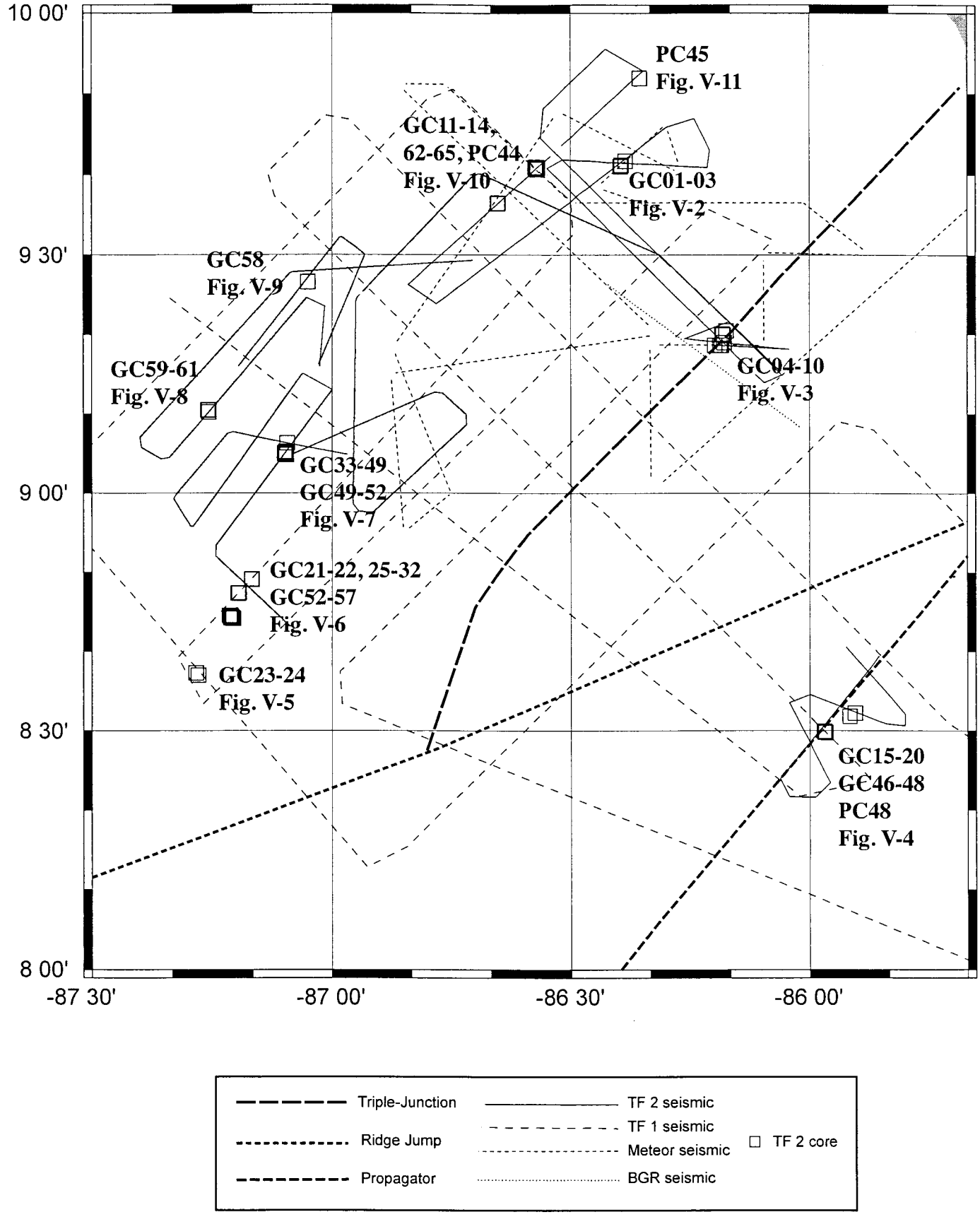
10 00'
9 30'
9 00'
8 30'
8 00'
-87 30'
-87 00'
-86 30'
-86 00'
PC45
Fig. V-11
GC11-14,
62-65, PC44
Fig. V-10
GC01-03
Fig. V-2
GC58
Fig. V-9
GC59-61
Fig. V-8
GC04-10
Fig. V-3
GC33-49
GC49-52
Fig. V-7
GC21-22, 25-32
GC52-57
Fig. V-6
GC23-24
Fig. V-5
GC15-20
GC46-48
PC48
Fig. V-4
Triple-Junction
Ridge Jump
Propagator
TF 2 seismic
TF 1 seismic
Meteor seismic
BGR seismic
TF 2 core

Figure V-1

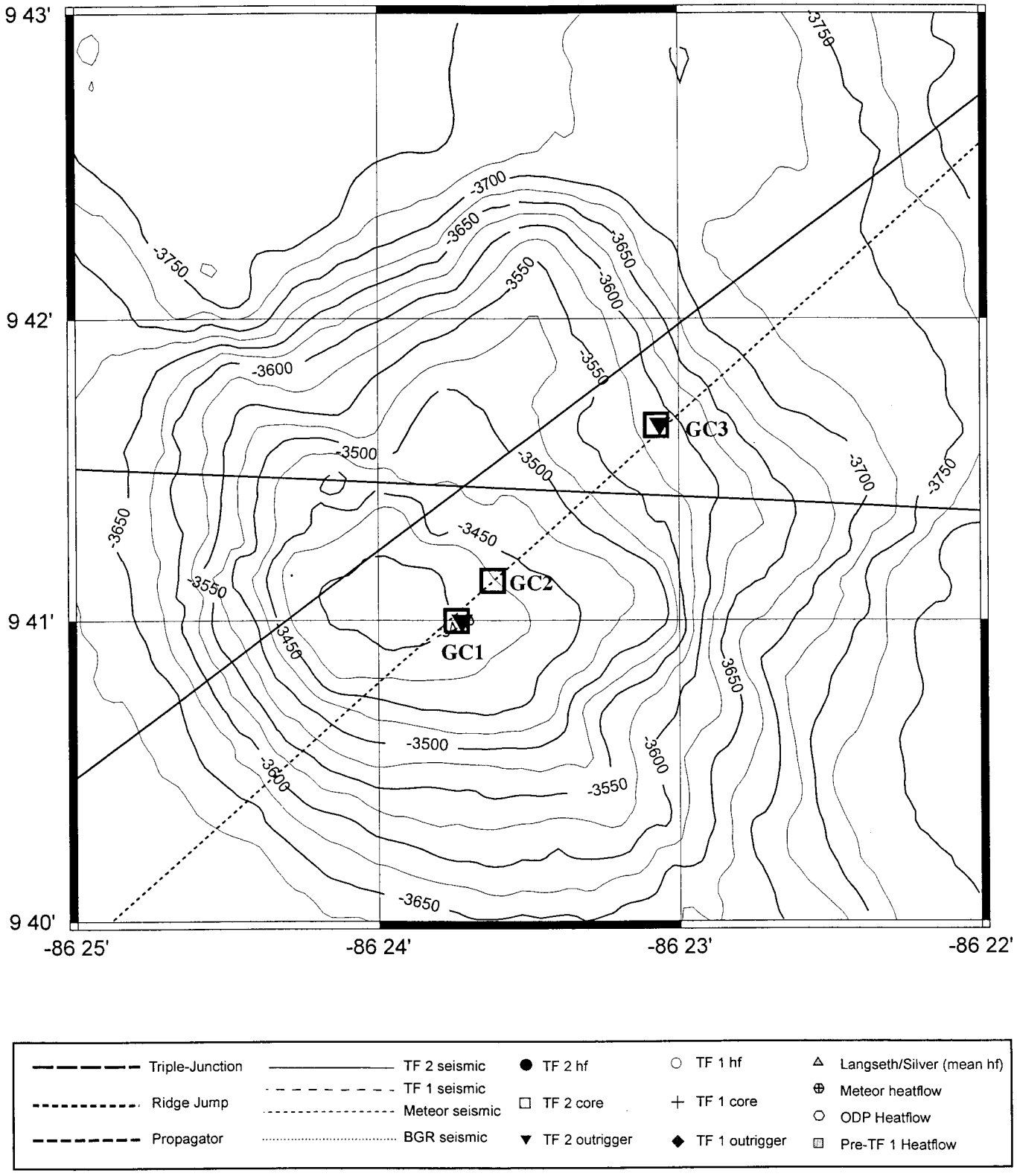
9 43'
9 42'
9 41'
9 40'
-86 25'
-86 24'
-86 23'
-86 22'
GC3
GC2
GC1
-3750
-3700
-3650
-3600
-3550
-3500
-3450
Triple-Junction
Ridge Jump
Propagator
TF 2 seismic
TF 1 seismic
Meteor seismic
BGR seismic
TF 2 hf
TF 2 core
TF 2 outrigger
TF 1 hf
TF 1 core
TF 1 outrigger
Langseth/Silver (mean hf)
Meteor heatflow
ODP Heatflow
Pre-TF 1 Heatflow

Figure V-2

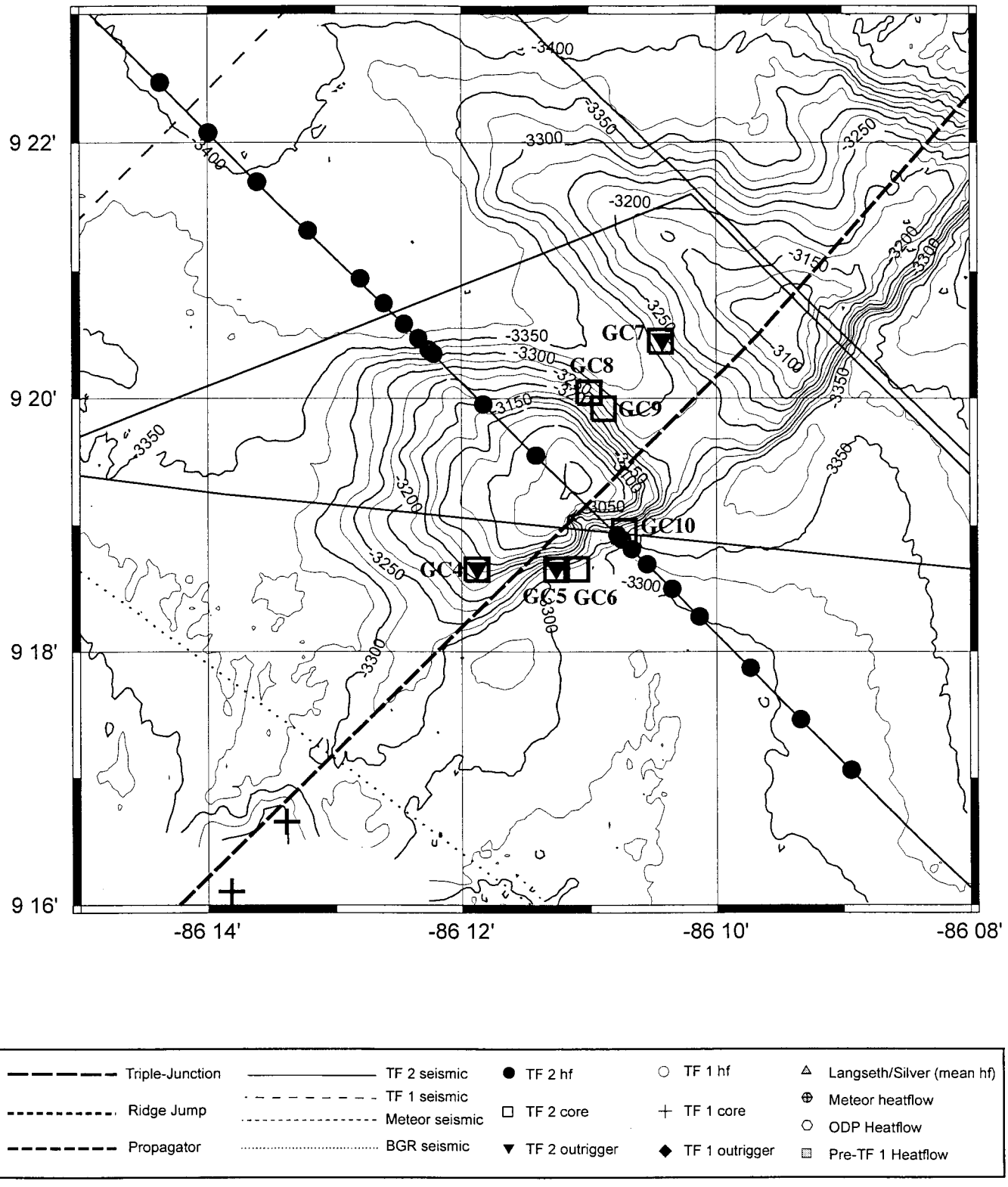
9 22'
9 20'
9 18'
9 16'
-86 14'
-86 12'
-86 10'
-86 08'
GC7
GC8
GC9
GC10
GC4
GC5 GC6
-3400
-3350
-3300
-3250
-3200
-3150
-3100
-3050
Triple-Junction
Ridge Jump
Propagator
TF 2 seismic
TF 1 seismic
Meteor seismic
BGR seismic
TF 2 hf
TF 2 core
TF 2 outrigger
TF 1 hf
TF 1 core
TF 1 outrigger
Langseth/Silver (mean hf)
Meteor heatflow
ODP Heatflow
Pre-TF 1 Heatflow

Figure V-3

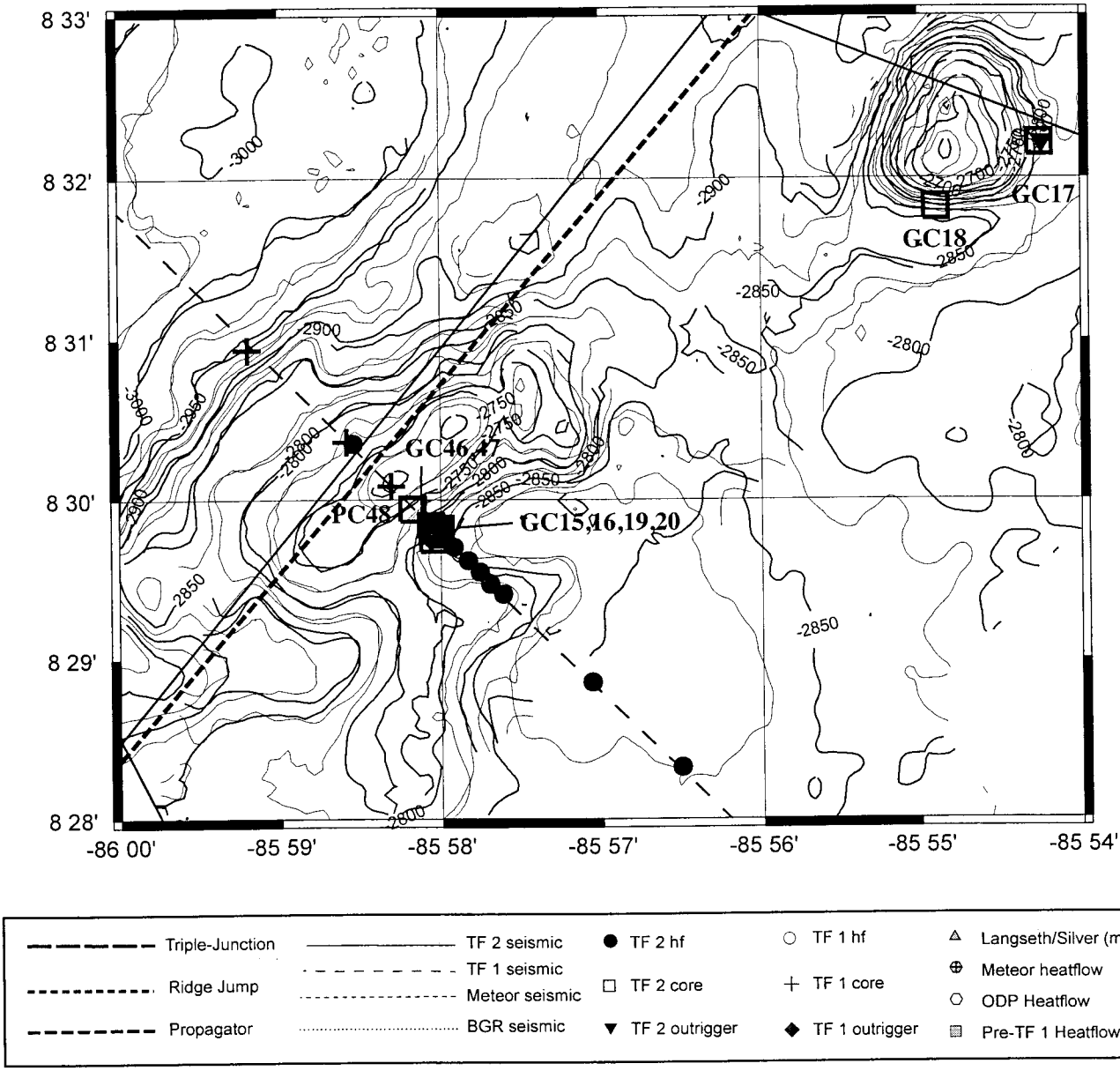
8 33'
8 32'
8 31'
8 30'
8 29'
8 28'
-86 00'
-85 59'
-85 58'
-85 57'
-85 56'
-85 55'
-85 54'
GC17
GC18
GC46,47
PC48
GC15,16,19,20
-3000
-2900
-2850
-2800
-2750
Triple-Junction
Ridge Jump
Propagator
TF 2 seismic
TF 1 seismic
Meteor seismic
BGR seismic
TF 2 hf
TF 2 core
TF 2 outrigger
TF 1 hf
TF 1 core
TF 1 outrigger
Langseth/Silver (mean hf)
Meteor heatflow
ODP Heatflow
Pre-TF 1 Heatflow

Figure V-4

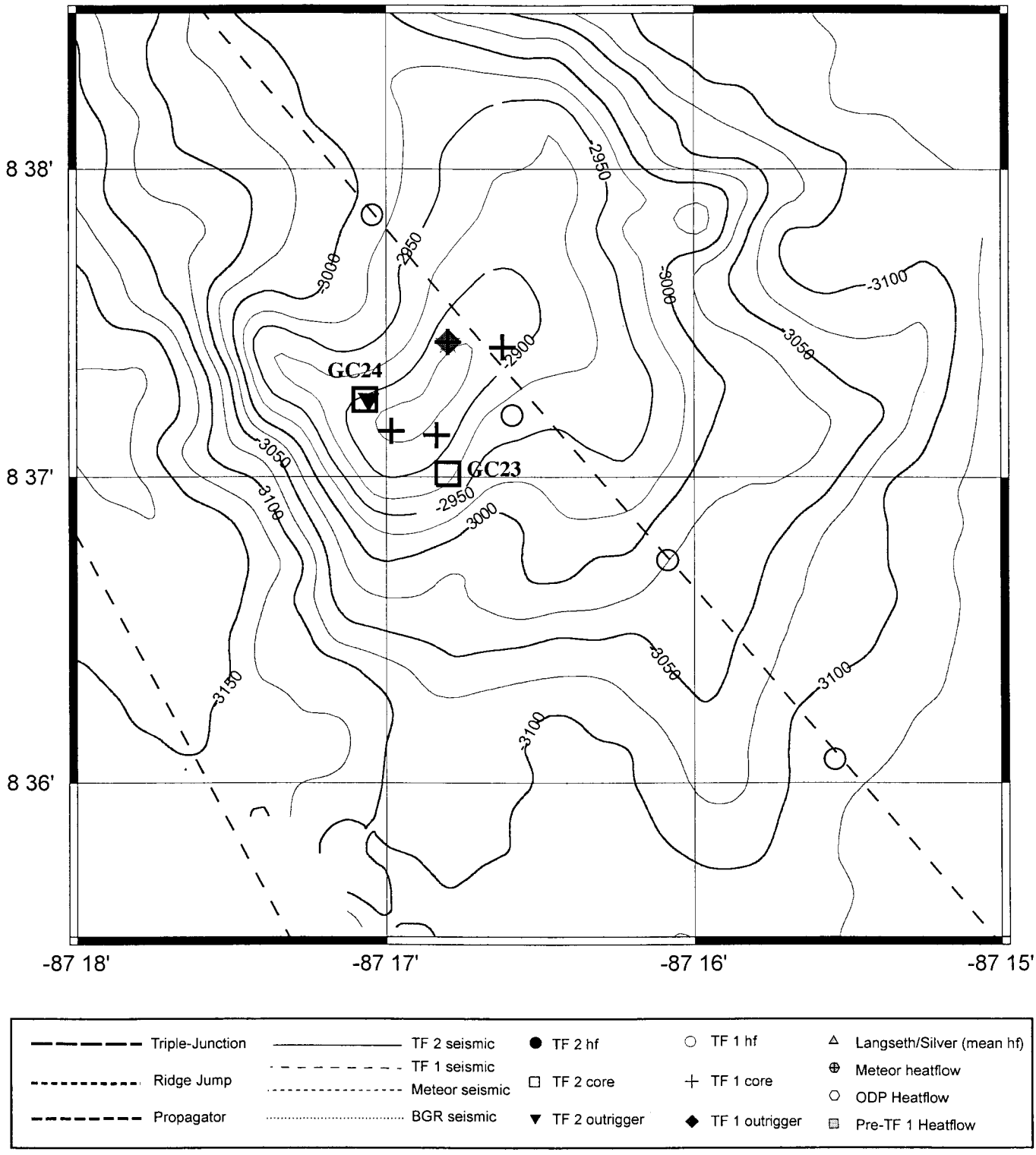
8 38'
8 37'
8 36'
-87 18'
-87 17'
-87 16'
-87 15'
GC24
GC23
2950
3000
3050
3100
3150
Triple-Junction
Ridge Jump
Propagator
TF 2 seismic
TF 1 seismic
Meteor seismic
BGR seismic
TF 2 hf
TF 2 core
TF 2 outrigger
TF 1 hf
TF 1 core
TF 1 outrigger
Langseth/Silver (mean hf)
Meteor heatflow
ODP Heatflow
Pre-TF 1 Heatflow

Figure V-5

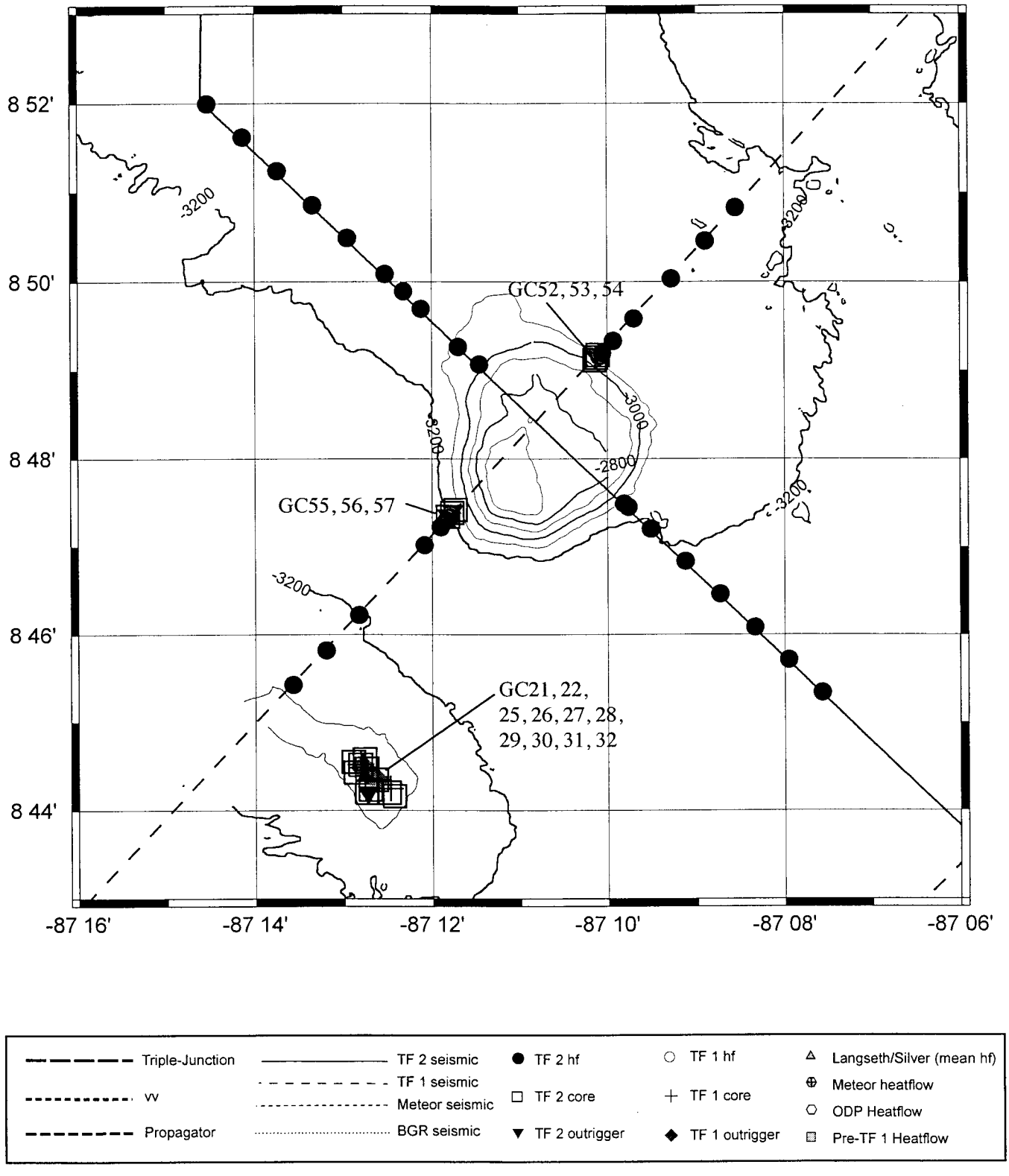
8 52'
8 50'
8 48'
8 46'
8 44'
-87 16'
-87 14'
-87 12'
-87 10'
-87 08'
-87 06'
-3200
-3000
-2800
GC52, 53, 54
GC55, 56, 57
GC21, 22,
25, 26, 27, 28,
29, 30, 31, 32
Triple-Junction
VV
Propagator
TF 2 seismic
TF 1 seismic
Meteor seismic
BGR seismic
TF 2 hf
TF 2 core
TF 2 outrigger
TF 1 hf
TF 1 core
TF 1 outrigger
Langseth/Silver (mean hf)
Meteor heatflow
ODP Heatflow
Pre-TF 1 Heatflow

Figure V-6

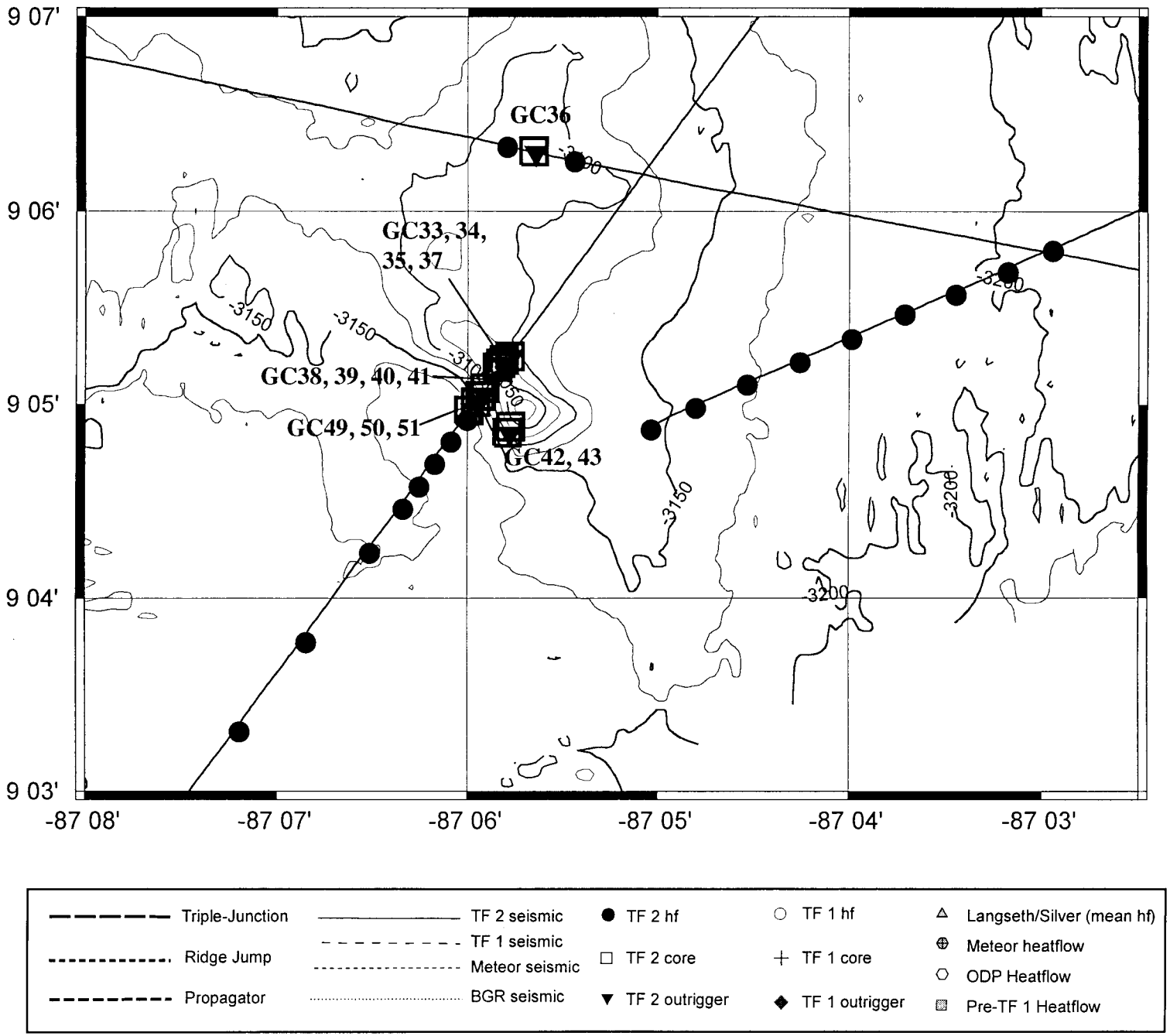
9 07'
9 06'
9 05'
9 04'
9 03'
-87 08'
-87 07'
-87 06'
-87 05'
-87 04'
-87 03'
GC36
GC33, 34, 35, 37
GC38, 39, 40, 41
GC49, 50, 51
GC42, 43
-3150
-3200
Triple-Junction
Ridge Jump
Propagator
TF 2 seismic
TF 1 seismic
Meteor seismic
BGR seismic
TF 2 hf
TF 2 core
TF 2 outrigger
TF 1 hf
TF 1 core
TF 1 outrigger
Langseth/Silver (mean hf)
Meteor heatflow
ODP Heatflow
Pre-TF 1 Heatflow

Figure V-7

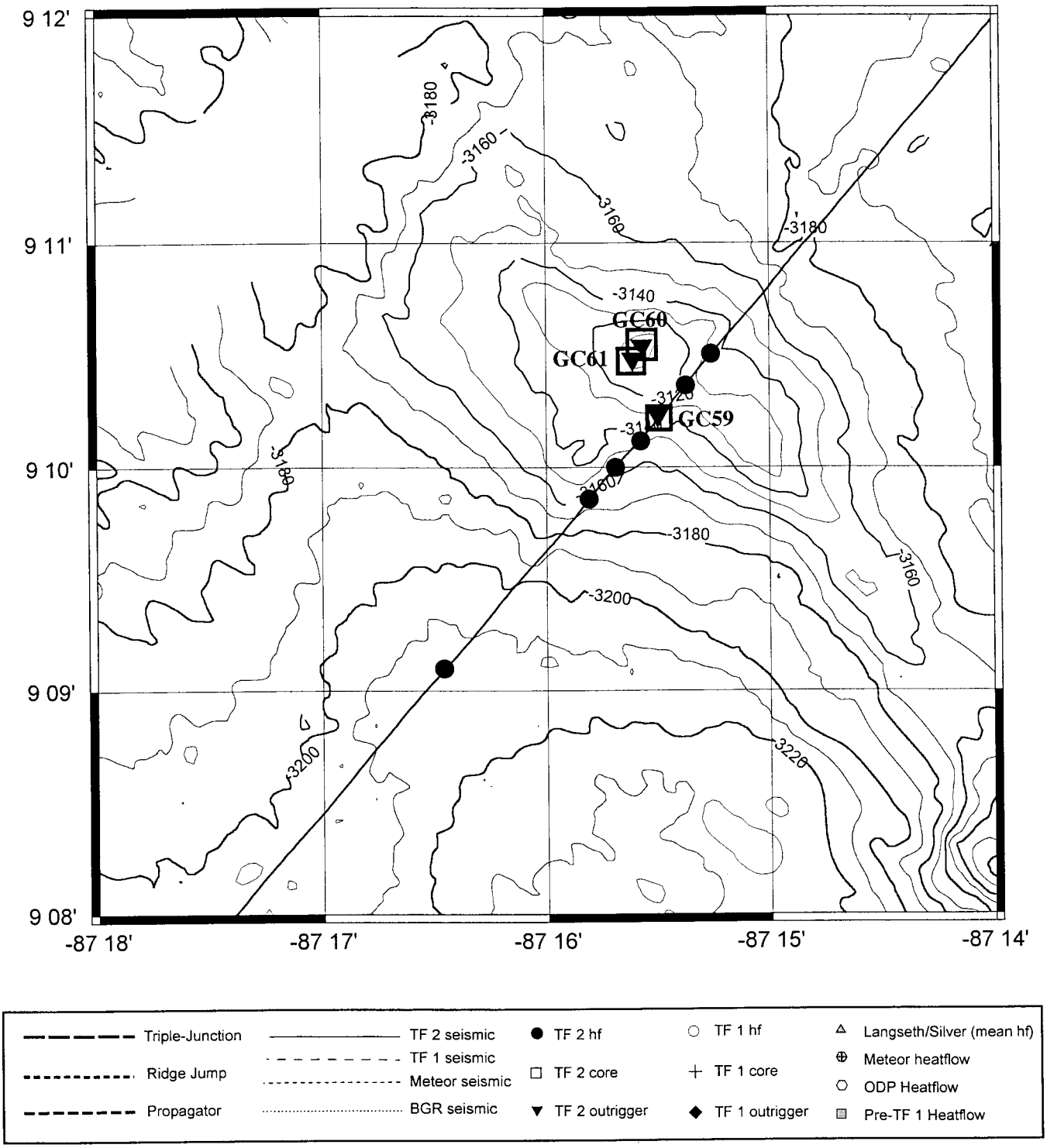
9 12'
9 11'
9 10'
9 09'
9 08'
-87 18'
-87 17'
-87 16'
-87 15'
-87 14'
-3180
-3160
-3140
-3120
-3200
-3220
GC60
GC61
GC59
Triple-Junction
Ridge Jump
Propagator
TF 2 seismic
TF 1 seismic
Meteor seismic
BGR seismic
TF 2 hf
TF 2 core
TF 2 outrigger
TF 1 hf
TF 1 core
TF 1 outrigger
Langseth/Silver (mean hf)
Meteor heatflow
ODP Heatflow
Pre-TF 1 Heatflow

Figure V-8

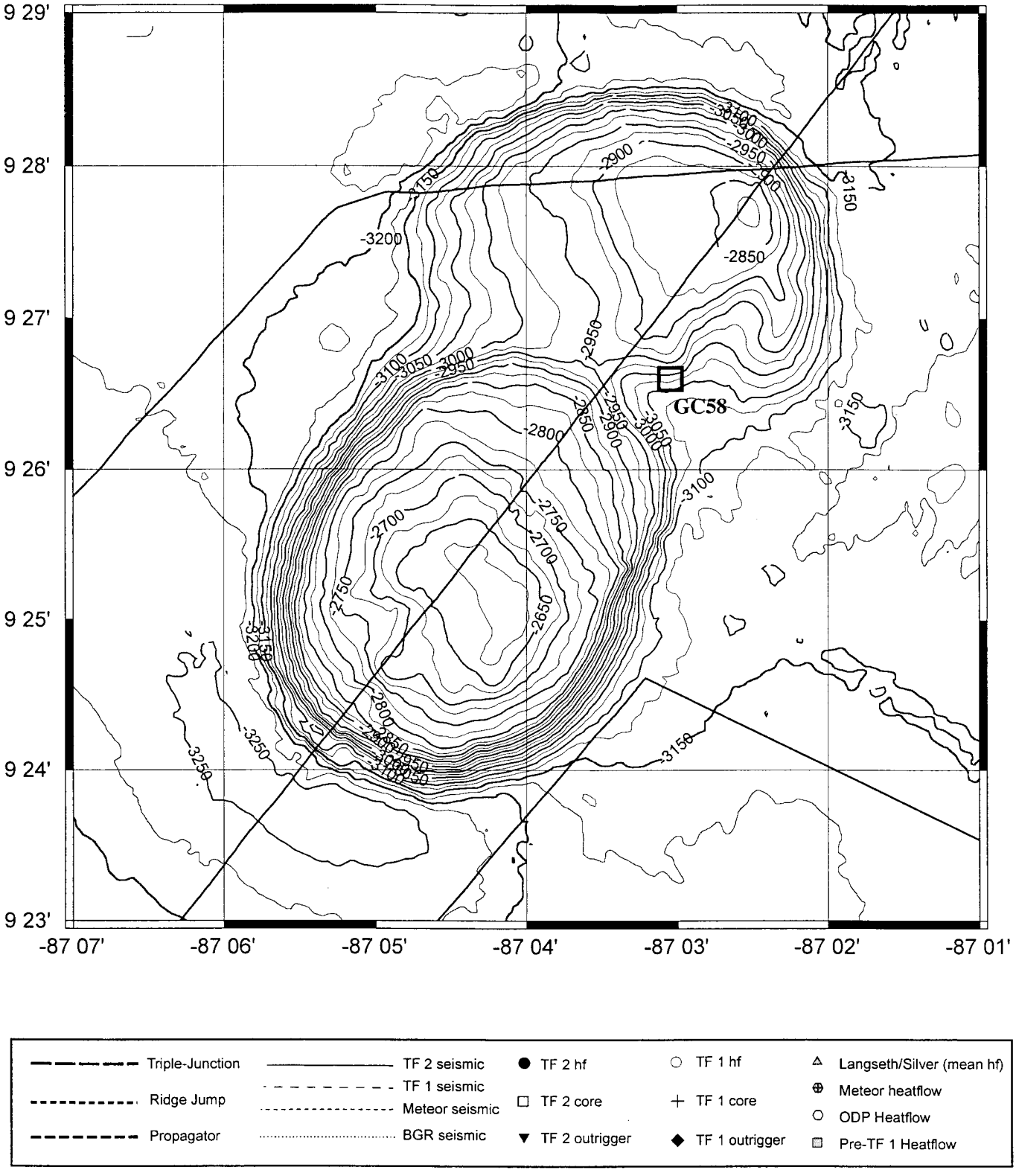
9 29'
9 28'
9 27'
9 26'
9 25'
9 24'
9 23'
-87 07'
-87 06'
-87 05'
-87 04'
-87 03'
-87 02'
-87 01'
GC58
Triple-Junction
Ridge Jump
Propagator
TF 2 seismic
TF 1 seismic
Meteor seismic
BGR seismic
TF 2 hf
TF 2 core
TF 2 outrigger
TF 1 hf
TF 1 core
TF 1 outrigger
Langseth/Silver (mean hf)
Meteor heatflow
ODP Heatflow
Pre-TF 1 Heatflow

Figure V-9

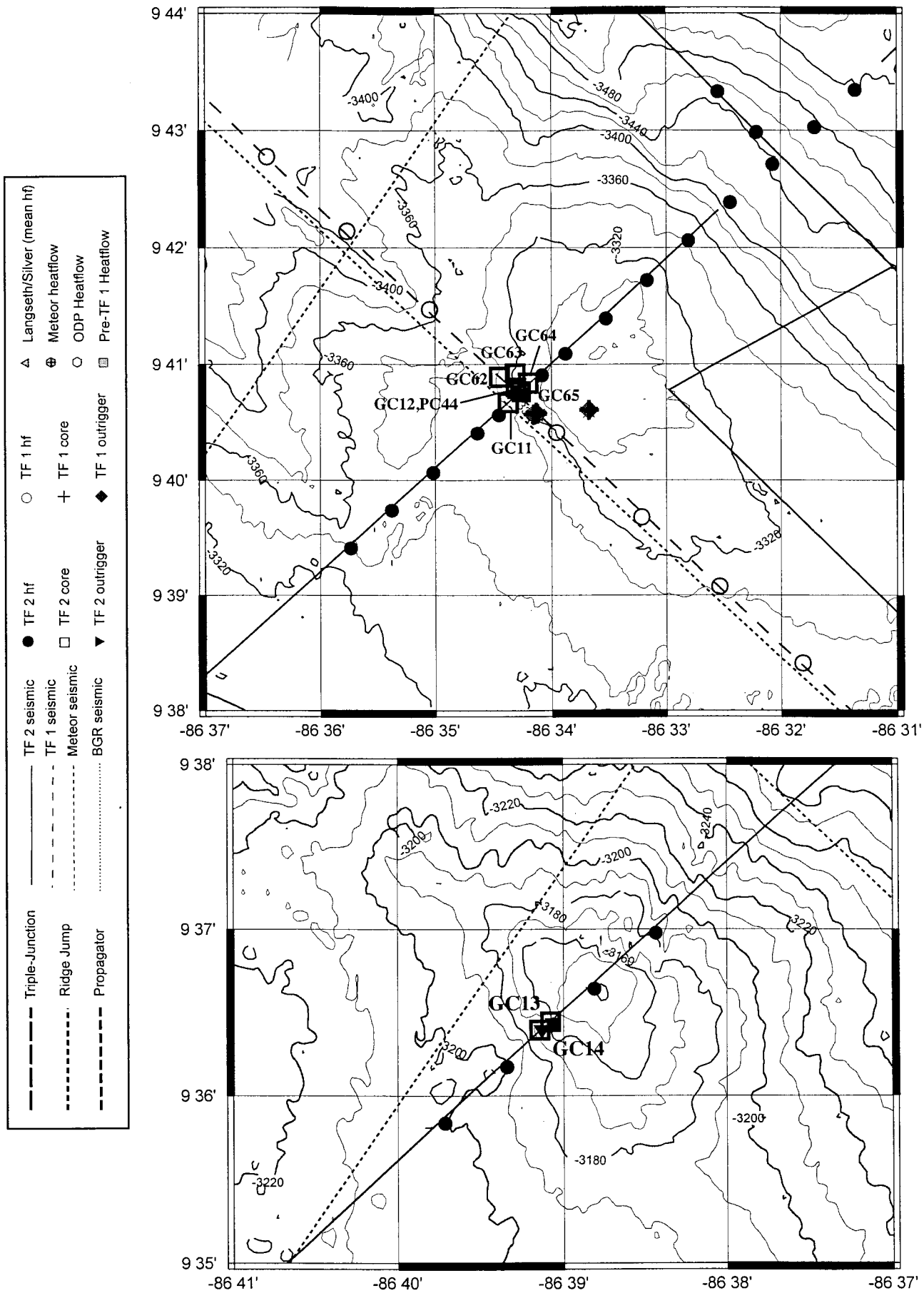
Triple-Junction
Ridge Jump
Propagator
TF 2 seismic
TF 1 seismic
Meteor seismic
BGR seismic
TF 2 hf
TF 2 core
TF 2 outrigger
TF 1 hf
TF 1 core
TF 1 outrigger
Langseth/Silver (mean hf)
Meteor heatflow
ODP Heatflow
Pre-TF 1 Heatflow
GC64
GC63
GC62
GC65
GC12,PC44
GC11
GC13
GC14
9 44'
9 43'
9 42'
9 41'
9 40'
9 39'
9 38'
9 37'
9 36'
9 35'
-86 37'
-86 36'
-86 35'
-86 34'
-86 33'
-86 32'
-86 31'
-86 41'
-86 40'
-86 39'
-86 38'
-3400
-3480
-3440
-3360
-3320
-3220
-3200
-3240
-3180
-3160

Figure V-10

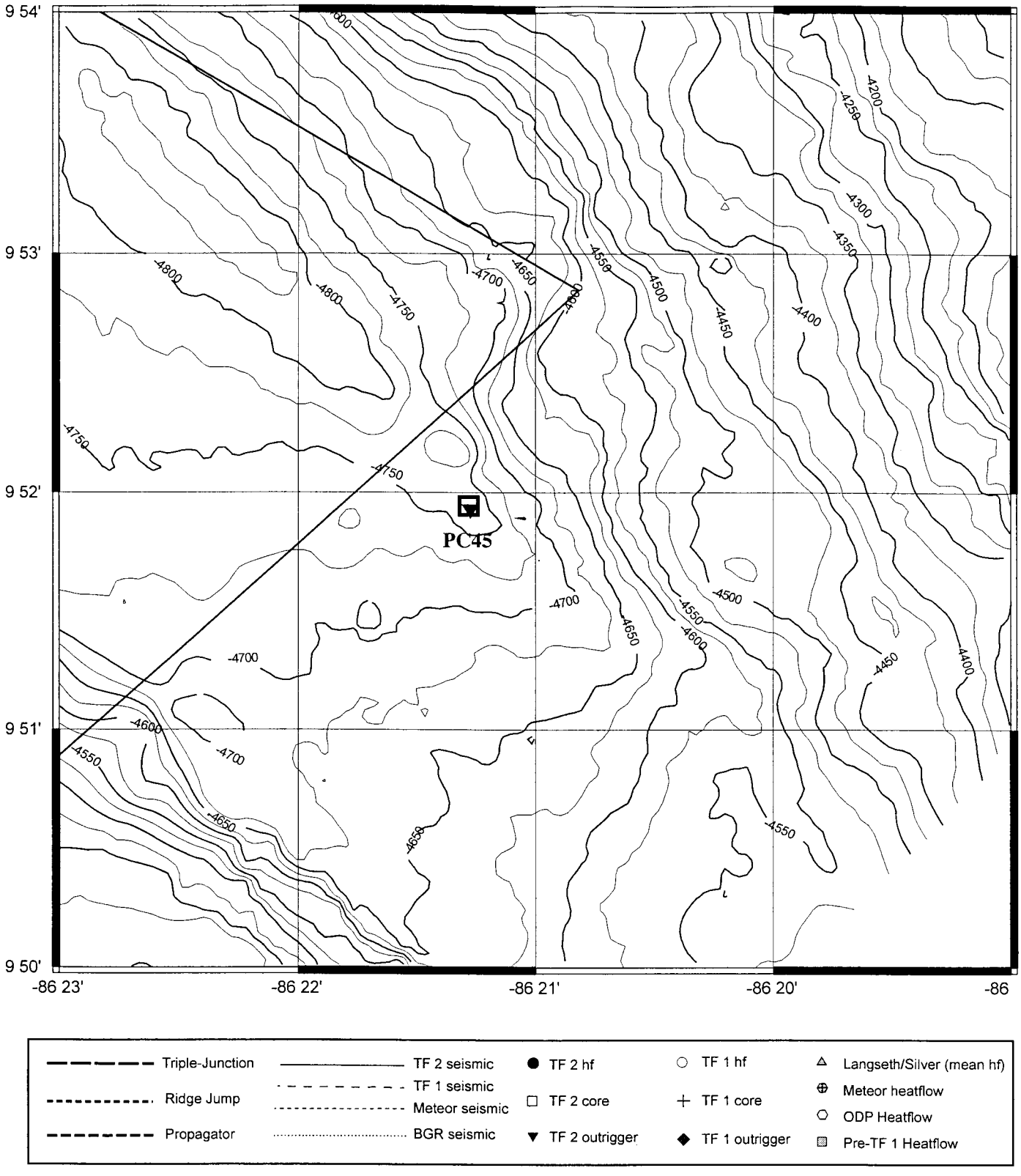
9 54'
9 53'
9 52'
9 51'
9 50'
-86 23'
-86 22'
-86 21'
-86 20'
-86
PC45
-4800
-4750
-4700
-4650
-4600
-4550
-4500
-4450
-4400
-4350
-4300
-4250
-4200
Triple-Junction
Ridge Jump
Propagator
TF 2 seismic
TF 1 seismic
Meteor seismic
BGR seismic
TF 2 hf
TF 2 core
TF 2 outrigger
TF 1 hf
TF 1 core
TF 1 outrigger
Langseth/Silver (mean hf)
Meteor heatflow
ODP Heatflow
Pre-TF 1 Heatflow

Figure V-11

01GC
02GC
03GC
04GC
05GC
06GC
07GC
08GC
09GC
void
void
core catcher only
core catcher only
core catcher only
KEY TO LITHOLOGY
Dark olive gray hemipelagic mud
Yellowish brown, brown, olive clay
Gravel, breccia
White volcanic ash
Black/gray volcanic ash
0
50
100
150
200
250
300
350
Depth (centimeters below seafloor)

Figure V-12

10GC
11GC
12GC
13GC
14GC
15GC
16GC
17GC
18GC
19GC
void
void
0
50
100
150
200
250
300
350
Depth (centimeters below seafloor)
KEY TO LITHOLOGY
Dark olive gray hemipelagic mud
Yellowish brown, brown, olive clay
White volcanic ash
Black/gray volcanic ash

Figure V-13

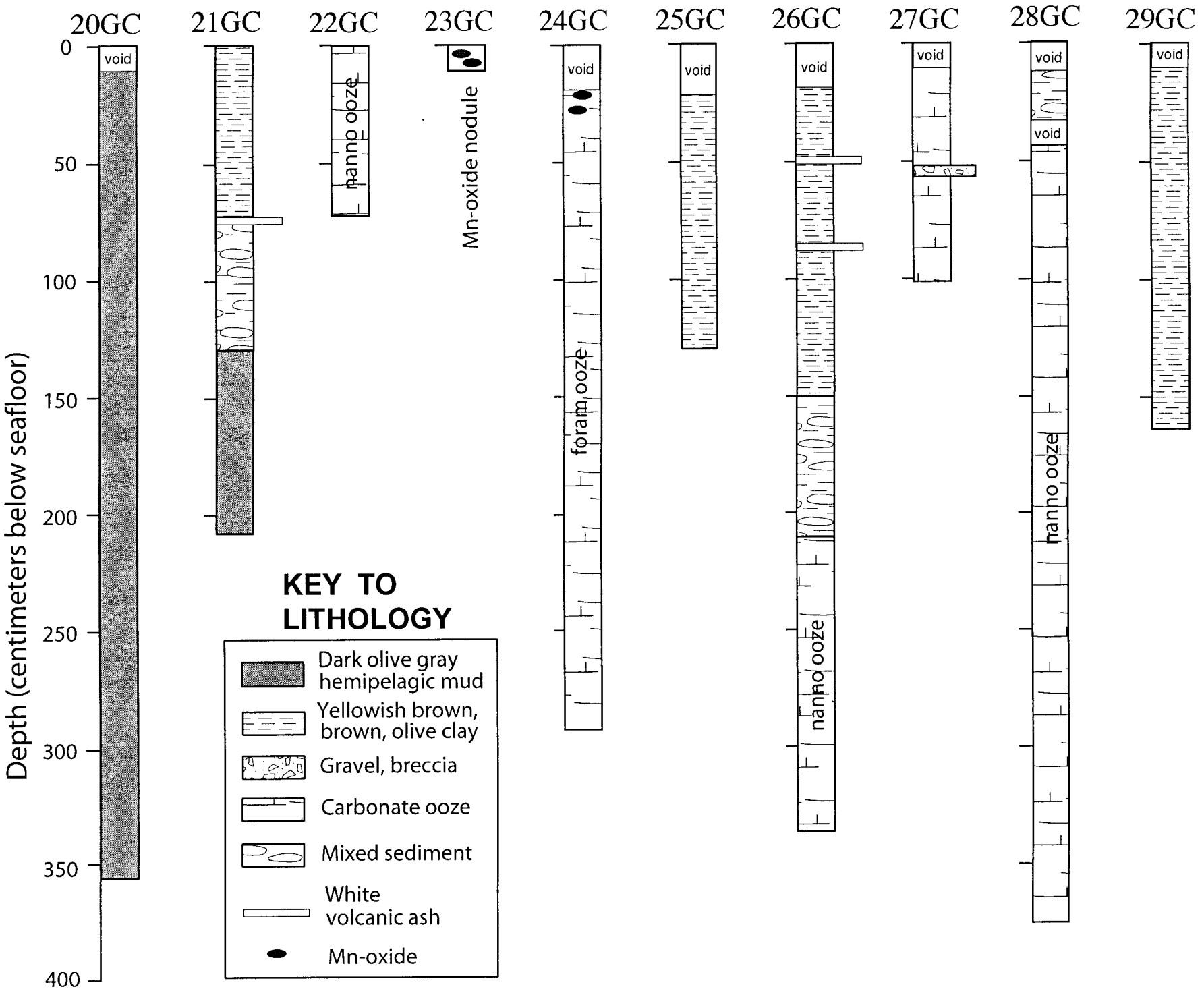
20GC
21GC
22GC
23GC
24GC
25GC
26GC
27GC
28GC
29GC
Depth (centimeters below seafloor)
0
50
100
150
200
250
300
350
400
void
nanno ooze
Mn-oxide nodule
foram ooze
KEY TO LITHOLOGY
Dark olive gray hemipelagic mud
Yellowish brown, brown, olive clay
Gravel, breccia
Carbonate ooze
Mixed sediment
White volcanic ash
Mn-oxide

Figure V-14

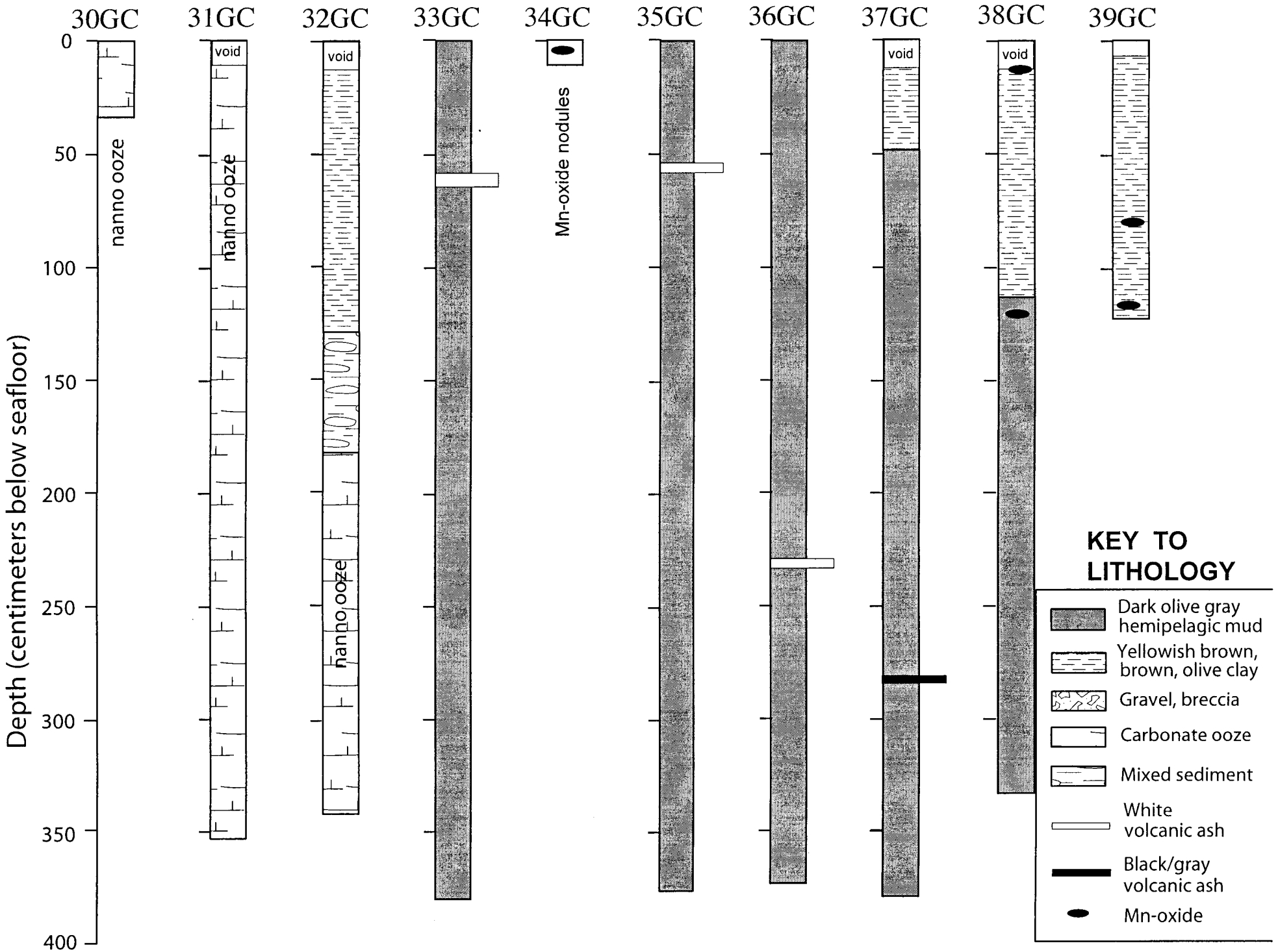
30GC
31GC
32GC
33GC
34GC
35GC
36GC
37GC
38GC
39GC
Depth (centimeters below seafloor)
0
50
100
150
200
250
300
350
400
nanno ooze
void
Mn-oxide nodules
KEY TO LITHOLOGY
Dark olive gray hemipelagic mud
Yellowish brown, brown, olive clay
Gravel, breccia
Carbonate ooze
Mixed sediment
White volcanic ash
Black/gray volcanic ash
Mn-oxide

Figure V-15

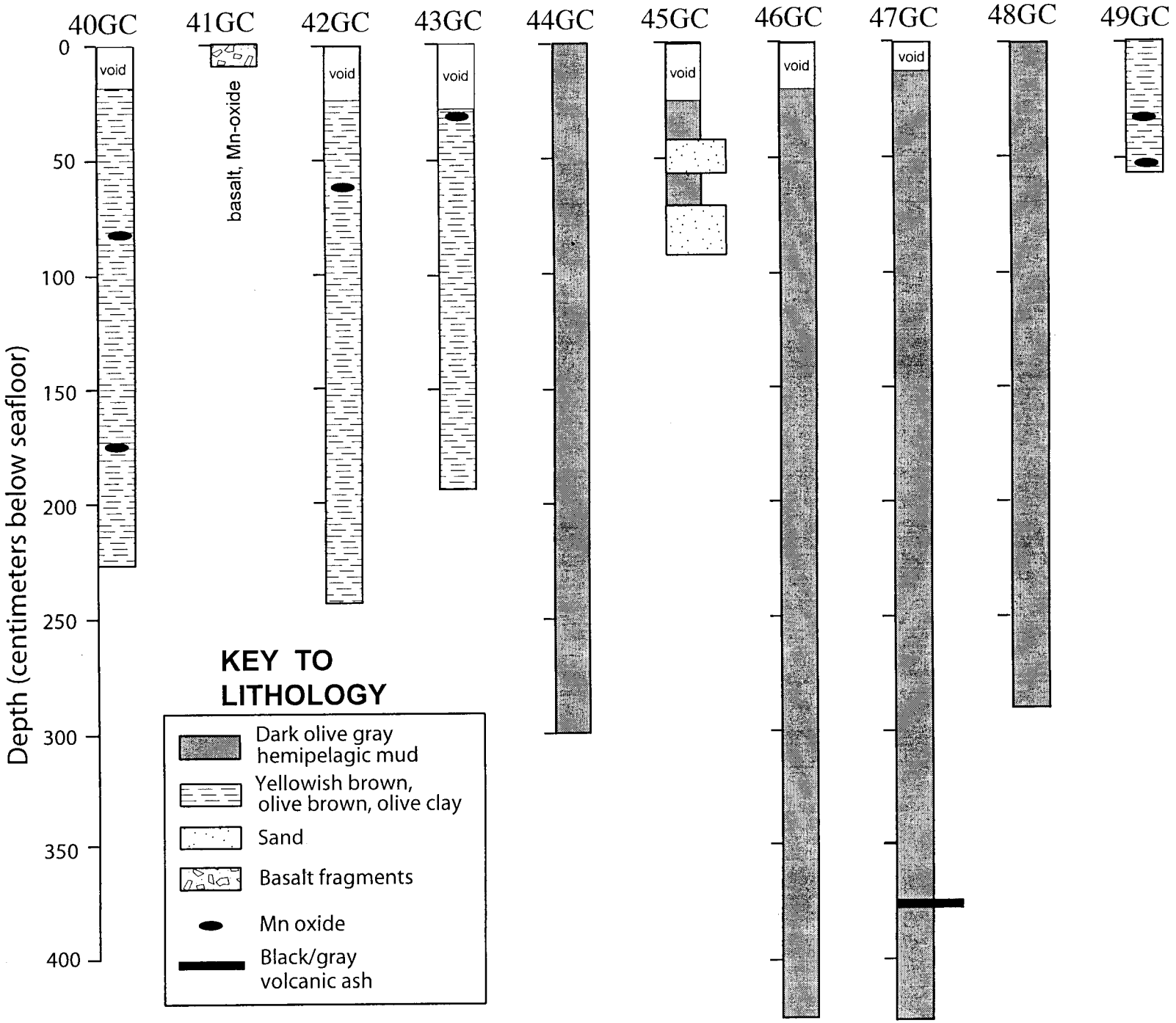
40GC
41GC
42GC
43GC
44GC
45GC
46GC
47GC
48GC
49GC
void
basalt, Mn-oxide
Depth (centimeters below seafloor)
0
50
100
150
200
250
300
350
400
KEY TO LITHOLOGY
Dark olive gray hemipelagic mud
Yellowish brown, olive brown, olive clay
Sand
Basalt fragments
Mn oxide
Black/gray volcanic ash

Figure V-16

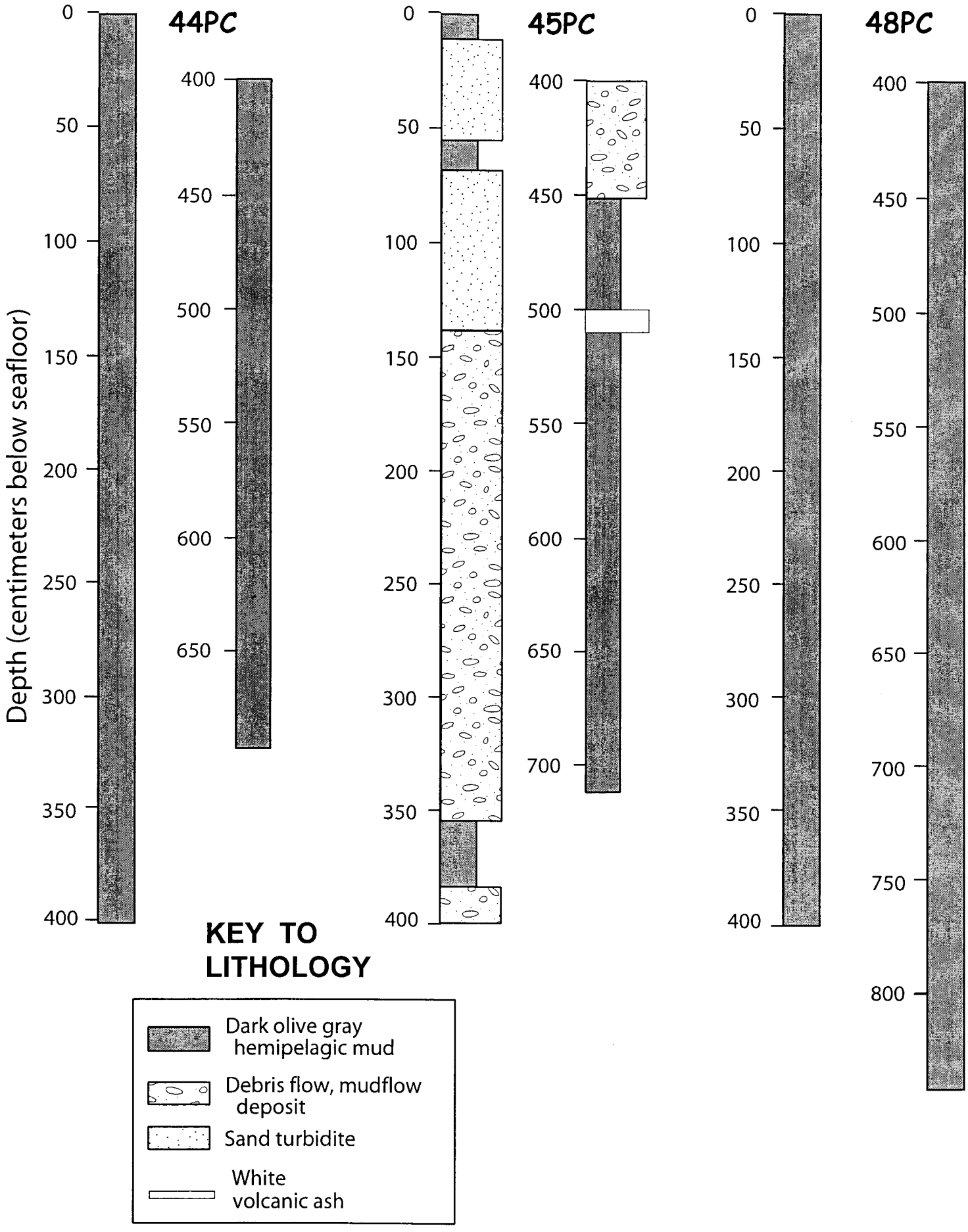
44PC
45PC
48PC
Depth (centimeters below seafloor)
0
50
100
150
200
250
300
350
400
450
500
550
600
650
700
750
800
KEY TO LITHOLOGY
Dark olive gray hemipelagic mud
Debris flow, mudflow deposit
Sand turbidite
White volcanic ash

Figure V-17

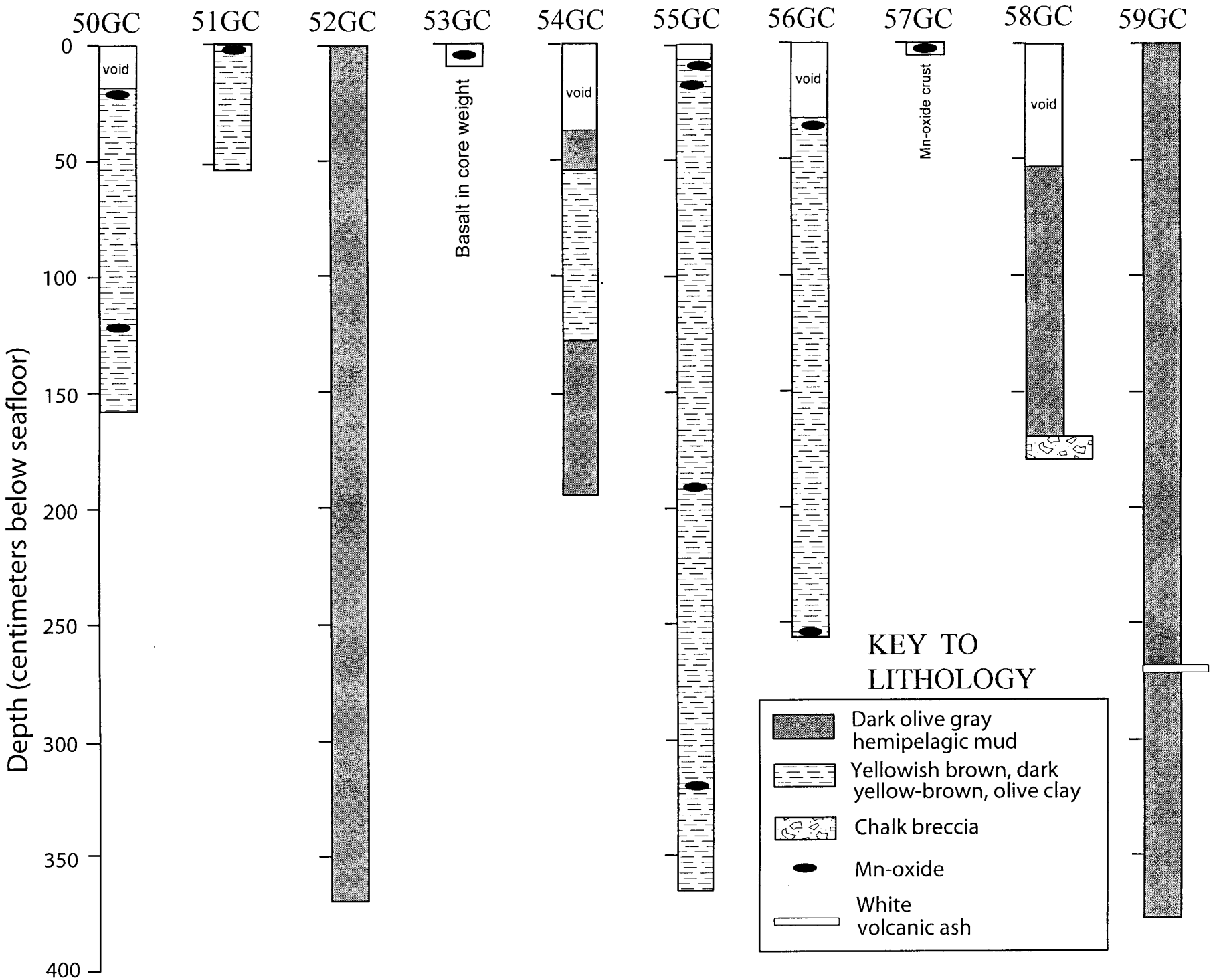
50GC
51GC
52GC
53GC
54GC
55GC
56GC
57GC
58GC
59GC
Depth (centimeters below seafloor)
0
50
100
150
200
250
300
350
400
void
void
void
Basalt in core weight
Mn-oxide crust
KEY TO LITHOLOGY
Dark olive gray hemipelagic mud
Yellowish brown, dark yellow-brown, olive clay
Chalk breccia
Mn-oxide
White volcanic ash

Figure V-18

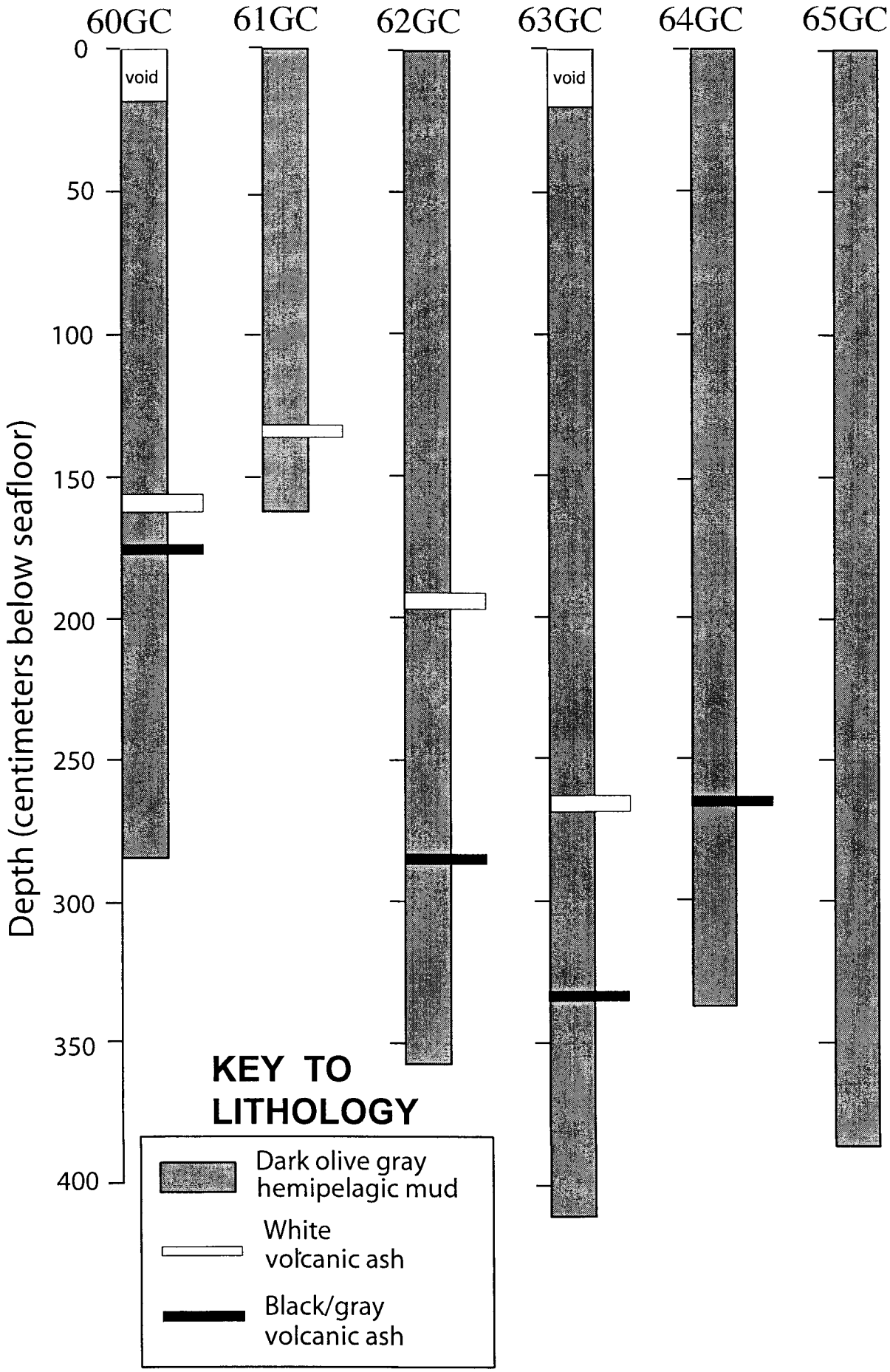
60GC
61GC
62GC
63GC
64GC
65GC
void
void
0
50
100
150
200
250
300
350
400
Depth (centimeters below seafloor)
KEY TO LITHOLOGY
Dark olive gray hemipelagic mud
White volcanic ash
Black/gray volcanic ash

Figure V-19

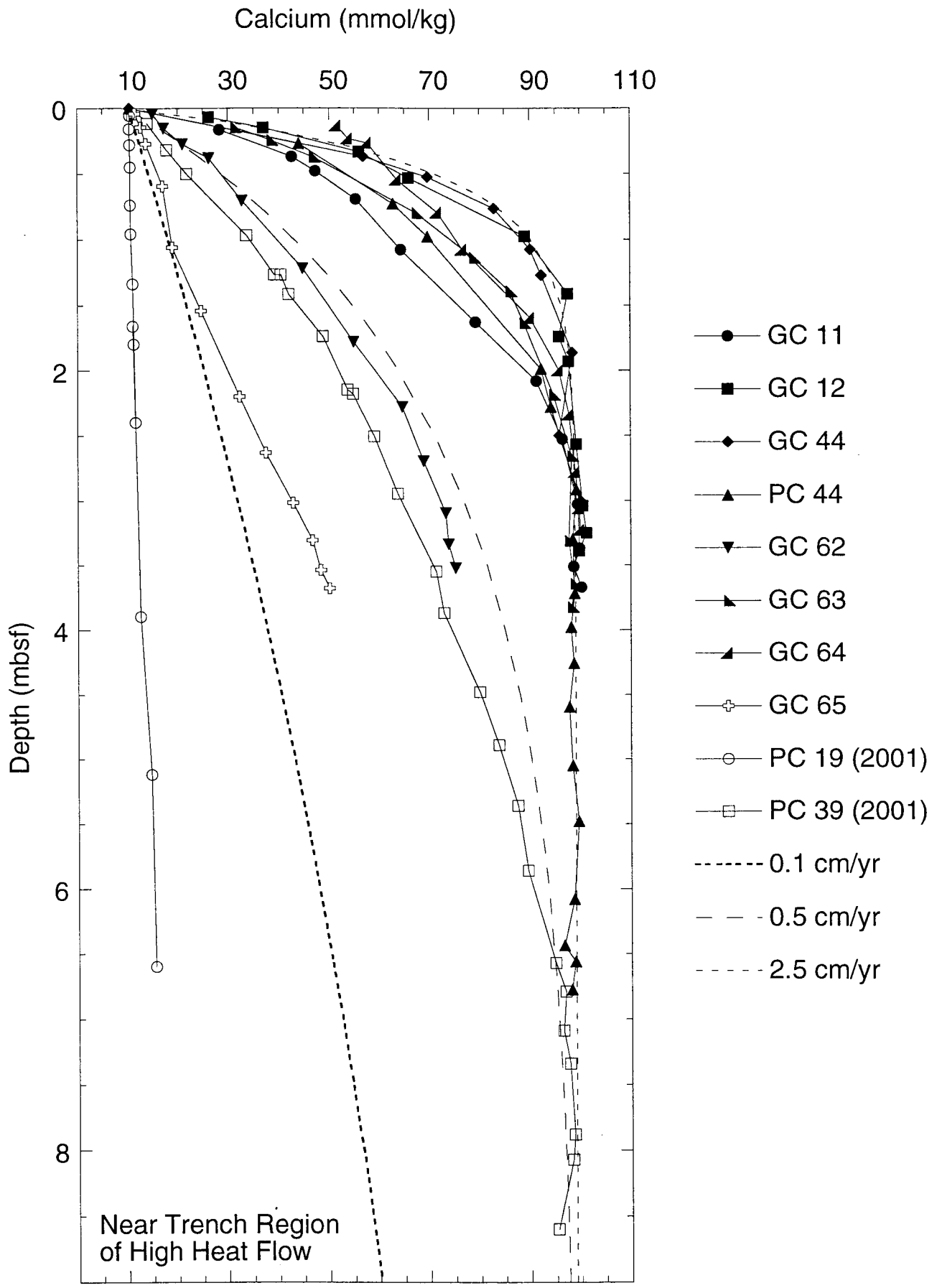
Calcium (mmol/kg)
10
30
50
70
90
110
0
2
4
6
8
Depth (mbsf)
Near Trench Region
of High Heat Flow
GC 11
GC 12
GC 44
PC 44
GC 62
GC 63
GC 64
GC 65
PC 19 (2001)
PC 39 (2001)
0.1 cm/yr
0.5 cm/yr
2.5 cm/yr

Figure VI-1

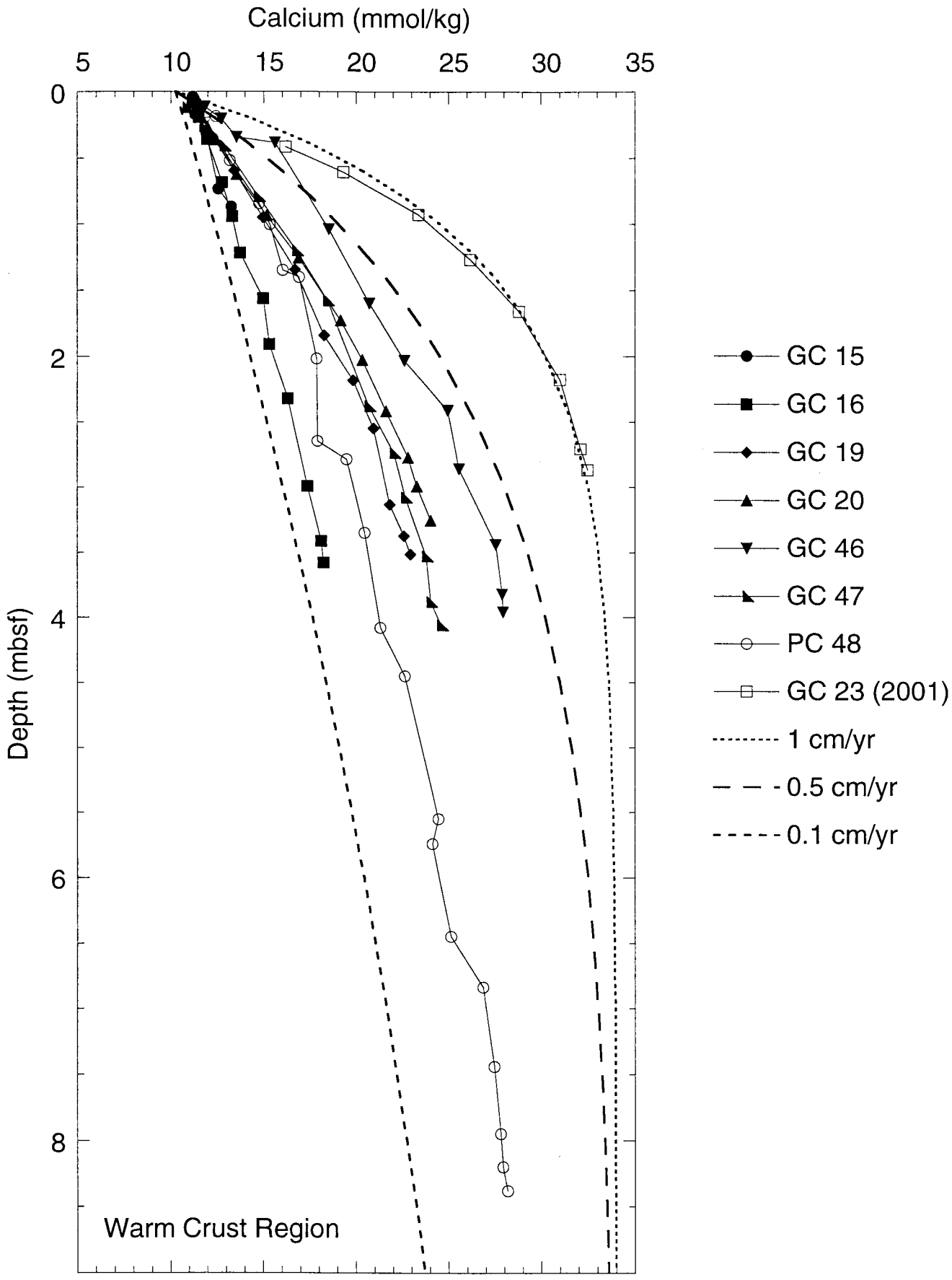
Calcium (mmol/kg)
5
10
15
20
25
30
35
0
2
4
6
8
Depth (mbsf)
Warm Crust Region
GC 15
GC 16
GC 19
GC 20
GC 46
GC 47
PC 48
GC 23 (2001)
1 cm/yr
0.5 cm/yr
0.1 cm/yr

Figure VI-2

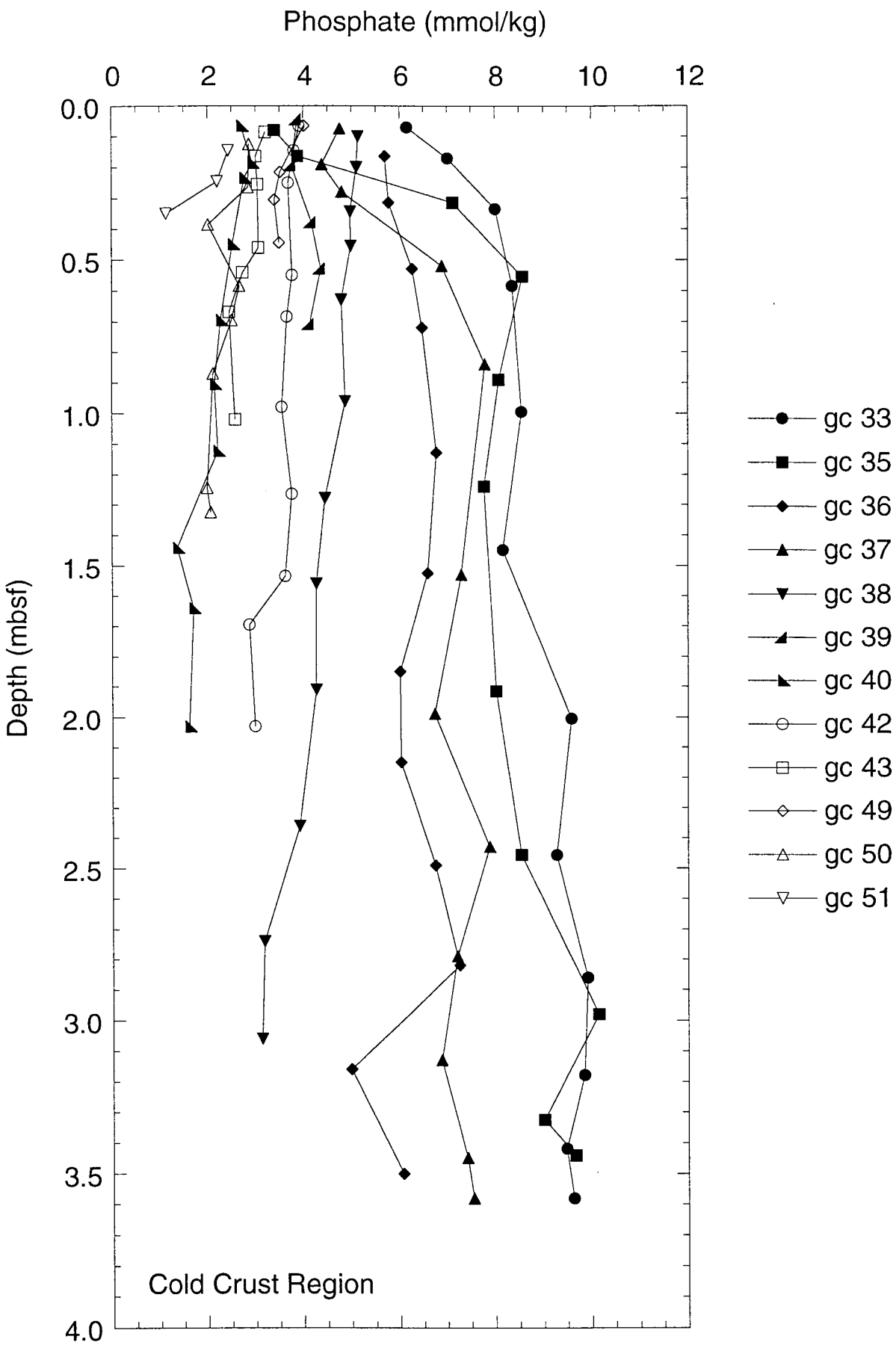
Phosphate (mmol/kg)
0
2
4
6
8
10
12
0.0
0.5
1.0
1.5
2.0
2.5
3.0
3.5
4.0
Depth (mbsf)
Cold Crust Region
gc 33
gc 35
gc 36
gc 37
gc 38
gc 39
gc 40
gc 42
gc 43
gc 49
gc 50
gc 51

Figure VI-3